



École Doctorale
d'Informatique,
Télécommunications
et Électronique de Paris

Thèse

Présentée pour obtenir le grade de docteur
de l'École Nationale Supérieure des Télécommunications

Spécialité : **Electronique et Communications**

Hassan TEIMOORI

Commutation de paquets dans les réseaux optiques transparents à partir de fonctions logiques tout optiques

Soutenue le 28 Septembre 2007 devant le jury composé de :

Bruno Thedrez	Président
Philippe Gravey	Rapporteurs
Guang-Hua Duan	
Michael J. O'Mahony	Examinateur
Dominique Chiaroni	Invité
Didier Erasme	Directeur de thèse
Cédric Ware	Co-directeur de thèse

Acknowledgments

The completion of this dissertation would not have been possible without the encouragement, help and friendship of many individuals. It is my privilege to thank the people who have supported and guided me throughout my pursuit of higher education, and my sincere apologies to the people I may miss.

I could not be thankful enough for having had professor Didier Erasme as my advisor, who is a true friend to me. Under his guidance, I have learnt to identify and approach research problems, and to develop and present the solutions in a comprehensible manner. Whenever I had a problem of personal, academic, reserach, of any nature, his door of help was always opened for me.

I would like to acknowledge and thank professor Philippe Gravey and Dr Guang-Hua Duan, Dr Bruno Thedrez, professor Michael J. O'Mahony and Dr Dominique Chiaroni for serving on my dissertation committee. Their insightful feedback and approval of my research goals and objectives have helped me to complete this thesis.

I would like to express my sincere gratitude toward Dr Cedric Ware for his help and friendship.

I am especially grateful to the members of the optical telecommunication group: Philippe Gallion, Guy Debarge, Yves Jaouen, Renaud Gabet, Christophe Minot and Catherine Lepers. I must appreciate for their helping attitude which was the constant motivating factor for me to complete this thesis.

My sincere thanks to Dr Horacio Soto Ortiz for his encouragements and his friendship.

My special thanks to Dr Joseph Desire Topomondzo for his valuable suggestions, critical comments, encouragements and friendship.

Special thanks to my colleagues at ENST, Ghalid Idir Abib, Kaïs Mabrouk, Francois Ziade, Mohammad Vahdani, Fausto Gomez Agis, Vincent Lanticq, Shifeng Jiang, Philippe Hamel, Mohammad Gharaei,Juan Petit, Qing Xu, Ihsan Fsaifes, Lydia Lourdiane, Manuel Sabban, Damien Fafchamps, Alireza Kazemipour, Hassan

Khotanlou, Saeid Homayouni, Judson Braga, Charif Mohamed, Steevy Cordette, Amel Farhat, Fabien Kéfélian, Fernando Rangel de sousa, Marcia Costa E Silva, Francisco Mendieta, Sebastien Agnoli and Bruno Bristiel for their moral support and for sharing my workload during my thesis period

I wish to express my sincere thanks to Professor Mahmoud Kamarei, vice-president for Academic Affairs, University of Tehran, for his encouragement, help and friendship.

I would like to thank Chantal Cadiat, Marie Baquero and Danielle Childz, Florence Besnard, Karim Ben Kalaia, Frederic Pauget and Alain Croullebois and all the other staff of COMELEC departement for their help and friendship.

I am very grateful to my wife, Atousa Assadi-haghi, for her love and patience during the PhD period. One of the best experiences that we lived through in this period was the birth of our daughter, Tania, who provided an additional and joyful dimension to our life mission.

Hassan Teimoori

Optical-logic-gate aided packet-switching in transparent optical networks

Abstract

The objective of this research is twofold; first, the optical packet label recognition using all-optical logic functions and second, the design and partially implementation of optoelectronic and all-optical packet switching systems.

The optoelectronic packet switch is composed of a 4-bit time-to-wavelength converter in order to slow down a 4-bit subset of the packet label. The slowed down bits are transformed in electronics via photo-detectors. Next, an analog-to-digital converter is employed for each bit to be amplified, equalized and digitized. Finally, the digitized bits are processed within a FPGA in order to provide the corresponding command signals of the optical switch.

In the all-optical packet switch a 3-bit of label is parallelized via the time-to-wavelength converter and is processed through an optical decoder in order to provide 8 command pulses. These command pulses are used to drive 8 optical flip-flops (to activate 8 distinct wavelengths). Thus, for each bit combination of the label a distinct wavelength will be generated.

New architectures for realization the optical logic gates at 10 Gbit/s using semiconductor optical amplifiers (SOA) are presented. Furthermore, some more advanced logic function such as half-adder, time-to-wavelength converter and decoder are demonstrated based on these logic gates. Non-linear effects in SOA such as four wave mixing, cross phase modulation, cross polarisation modulation are used for realisation these logic gates and functions.

Commutation de paquets dans les réseaux optiques transparents à partir de fonctions logiques tout optiques

Résumé

L'objectif de ce travail était double: d'une part la reconnaissance de label des paquets optiques en utilisant les fonctions logiques tout-optiques, et d'autre part la conception et la réalisation partielle des commutateurs (optoélectronique et tout-optique) de paquet. Le commutateur optoélectronique est composé d'un convertisseur de temps-longueur d'ondes de 4-bit. Les bits ont été ralentis, parallélisés, puis convertis en électronique via les photo-détecteurs. Un convertisseur analogique-numérique est utilisé pour chaque bit afin de le digitaliser et de l'égaliser. Les bits digitalisés du labelsont traités dans un FPGA afin de produire les signaux de commande correspondant pour le commutateur.

Dans le commutateur tout-optique, 3-bits du label, parallélisés via le convertisseur temps-longueur d'onde, sont traités par un décodeur tout optique afin de produire 8 impulsions différentes de la commande. Ces impulsions de commandes ont servi dans huit bascules optiques afin de générer huit longueurs d'ondes différentes. Ainsi, pour chaque combinaison de bits du label, une seule longueur d'ondes différente est produite.

De nouvelles architectures optiques permettant de réaliser les fonctions logiques à 10 Gbit/s avec l'amplificateur optique à semiconducteur (SOA) sont présentées. Des fonctions logiques complexes telles que le demi-additionneur, le convertisseur temps-longueur d'onde et le décodeur ont été démontrées à base de ces fonctions logiques. Les phénomènes non-linéaires dans un SOA tels que le mélange à quatre ondes, la modulation croisée de phase, la modulation croisée de la polarisation ont été utilisés pour réaliser ces portes et ces fonctions logiques.

Résumé en français

Introduction

Ces dernières décennies, la croissance de l'informatique a suscité un important développement des réseaux de télécommunications. Les techniques optiques pour la transmission se sont généralisées à l'ensemble des fonctions du réseau. En particulier la fonction de commutation par paquets utilisant des techniques optiques s'avère une des solutions prometteuses.

Un paquet est composé d'une part d'un en-tête (label d'après le protocole de MPLS) optique qui contient les informations de routage du paquet et d'autre part de l'information utile (payload). La reconnaissance et le traitement tout-optique des labels, des mémoires optiques pour stocker l'information de label et de payload, et la fonction de commutation pour transférer un paquet d'un port à un autre, sont les fonctions optiques nécessaires pour la commutation de paquet optique. Afin de réaliser certaines de ces opérations, des fonctions tout-optiques de base telles que des portes logiques et des commutateurs rapides fonctionnant à haut débit sont nécessaires.

Dans ce contexte, nous allons démontrer plusieurs fonctions tout-optiques nouvelles. Celles-ci sont réalisées en exploitant les non-linéarités dans un amplificateur optique à semiconducteur (SOA). On s'intéresse plus particulièrement aux fonctions telles que les portes logiques tout-optiques nécessaires pour le routage (AND, NOT, NOR, XOR et XNOR), les fonctions logiques avancées (demi-additionneur, convertisseur temps-à-longueur d'ondes et décodeur optique) et à la commutation des paquets et la reconnaissance des labels.

Amplificateur optique à semiconducteurs (SOA)

En raison de leur comportement non-linéaire, leur bande passante relativement large (120 nm) [1], leur dynamique rapide, leur gain et leur faible volume, les SOAs adressent (peuvent être utilisé dans) divers champs d'application dans la commutation optique à haute vitesse. La dynamique de porteurs dans le SOA est à l'origine de la non-linéarité observée. La variation de la densité totale de porteurs

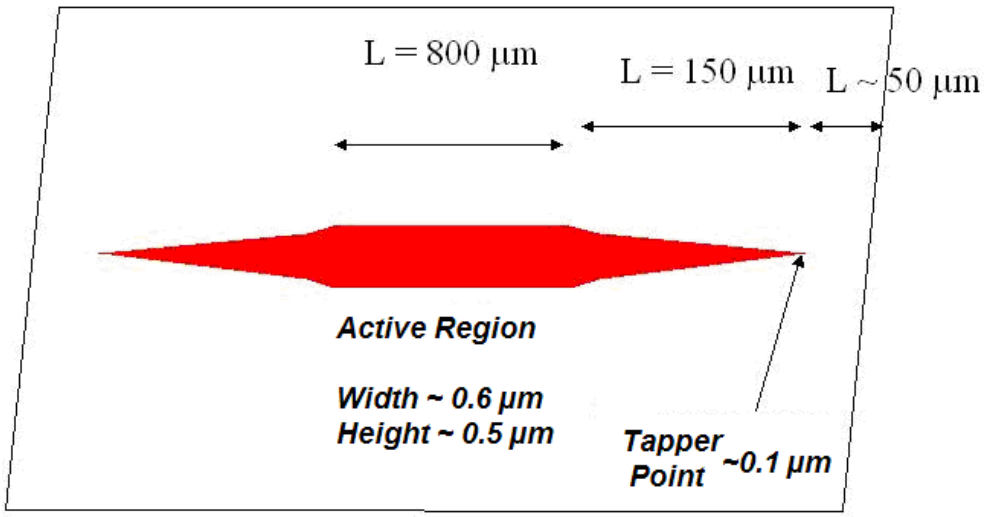


Figure 1: Vu schématique du SOA utilisé dans nos expériences

et de leurs distributions via la fonction de Fermi engendrent des transitions inter-bande et intra-bande. La transition inter-bande est produite par l'émission stimulée, l'émission spontanée, la recombinaison non- radiative. La modification de la densité totale de porteurs s'accompagne de la modification de la distribution de porteurs dans la même bande. Ce sont les transitions intra-bandes telles que Spectral Hole Burning (SHB) et Carrier Heating (CH) qui sont à l'origine de la dynamique rapide des SOA. Ces phénomènes se produisent au même moment mais ont des constantes de temps différentes.

Dans cette thèse, nous avons utilisé un SOA qui a été mis à notre disposition par Alcatel OPTO+. Il mesure 1.2 mm. Nous l'avons polarisé en inverse à 300mA. La figure 1 montre un vu schématique de ce SOA. En particulier, parmi les effets non-linéaires dans SOA, la modulation de phase croisée (XPM), mélange à quatre ondes (FWM) et la modulation croisée de la polarisation (XPolM) seront utilisées.

Porte logique optique

Des nombreuses fonctions optiques ont été démontrées en utilisant les portes logiques optiques tel que le cryptage et le codage des données [2], pattern matching [3], l'additionneur [4] [5], parity checking [6], bit-error monitoring [7] et le traitement de label de paquet optique [8]. Le tableau 1 résume les techniques signalées pour réaliser les portes logiques optiques. La plupart de ces méthodes sont basées sur les effets non-linéaires dans un SOA. Ces non-linéarités peuvent-être classifié en deux catégories;

- Les non-linéarités du SOA lui-même (tel que XPolM, XGM et FWM).
- L'interféromètre assisté par SOA (tel que un système UNI et MZ).

Table 1: Les techniques utilisé pour réaliser les portes logiques optiques.

	NOT	AND	NAND	OR	NOR	XOR	XNOR
SOA (NOLM) (TOAD)	[9]	[10] [12] [14]				[2][11] [10] [13]	[10]
SOA (MZI)		[15]	[16] [21]	[17] [16]	[16]	[18] [19] [22] [23] [24] [25] [16] [26]	[20]
SOA (FWM)	[27]	[28] [31]		[27]		[29] [30] [32] [33] [35]	[27] [34]
SOA (XGM)	[36]	[37] [41]	[36]	[38]	[39] [41] [42]	[40] [43]	[34]
Semiconductor microresonator structure		[44] [45] [47]	[45]		[46]		
Optical difrectional coupler	[48]	[48] [49] [50]	[50]	[48] [49] [50]		[49] [50]	[50]
Optical waveguides	[51]	[52] [54]	[52]		[53]		
Nonlinear fibers		[55] [56] [57] [61]		[57]	[57] [59]	[55] [58] [60] [3] [57]	[57]
Electro-absorption modulator	[62]	[63]					
Fabry-Pérot laser diode					[7]		
UNI	[64]	[64] [65]		[64]	[64]	[66] [67]	
SOA (XPolM)		[68] [69]		[70]	[71] [70]	[72]	[73]

Dans la partie suivante, nous allons présenter la réalisation des portes logiques XOR et XNOR et demi-additionneur à partir du système UNI (Ultrafast nonlinear interferometer).

Réalisation des porte XOR et XNOR à partir d'un système UNI

Le concept du système UNI est basé sur la rotation de polarisation du signal en présence du signal contrôle [74]. Le schéma du système UNI en configuration contra-propagation est schématiquement illustré dans la figure 2. Le laser 1

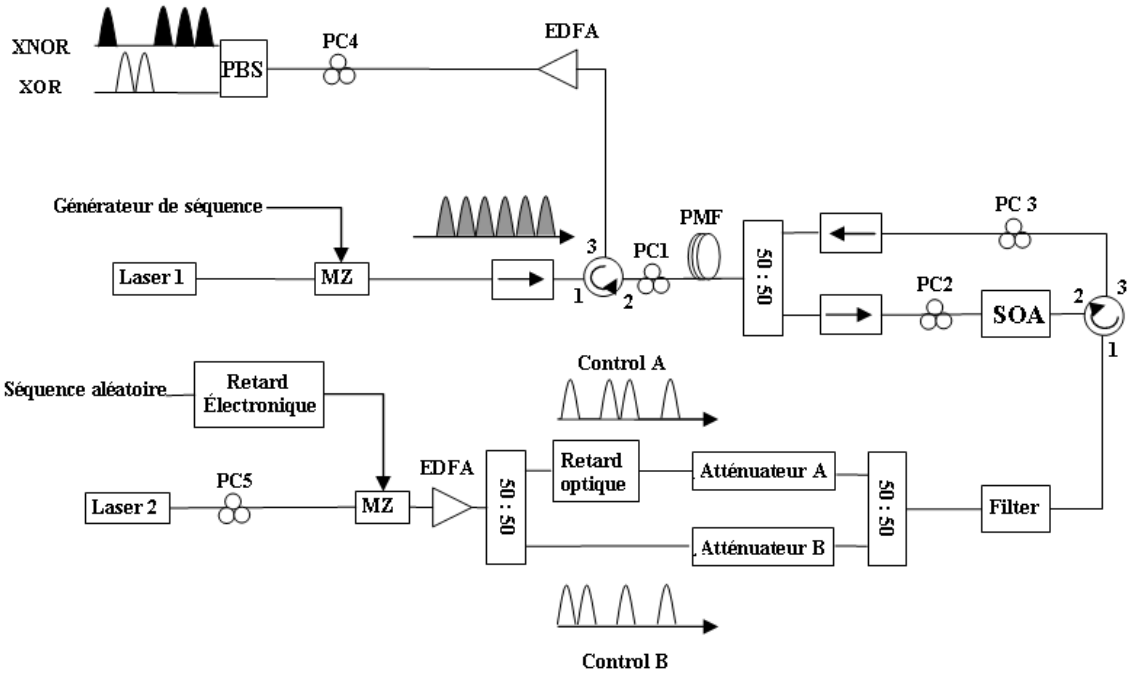


Figure 2: Montage expérimental des portes XOR and XNOR à base système UNI à 10 Gbit/s

(λ=1556.85 nm) modulé par une séquence à 10 Gbit/s servira de sortie logique. Il est divisé en deux composantes orthogonales et décalées dans le temps lors de son passage dans une fibre à maintien de polarisation (PMF) et est injecté dans un SOA. On choisit la longueur de la PMF de manière à obtenir un décalage entre les deux composantes du signal égal à la moitié du temps bit (40 m pour débits de 10 Gbit/s). Ces composantes du signal ont été synchronisées avec les signaux de contrôle. Deux signaux de contrôle modulés servent d'entrées logiques. Pour une certaine puissance du signal de contrôle injectée, la composante du signal synchronisée avec le signal de contrôle dans le SOA va subir un déphasage de π via la modulation croisée de phase.

A la sortie du SOA, le retard causé par le passage du signal dans le PMF est compensé par un second passage dans le même PMF. Les contrôleurs de polarisation (PC1 et PC3) permettent d'ajuster la polarisation à l'entrée de PMF. Le PC2 permet d'injecter les composantes orthogonales du signal dans les axes propres du guide d'onde du SOA. Le signal de contrôle est amplifié avec un EDFA, suivi d'un atténuateur optique variable. La ligne de retard permet de synchroniser le signal de contrôle avec une composante du signal. L'isolateur permet d'éviter des réflexions parasites. Le PC4 et le PBS (polarization beam splitter) permettent de réaliser la fonction de XOR et XNOR. Le taux d'extinction qui correspond à la différence entre l'état 1 et l'état 0 permet d'évaluer l'efficacité de cette technique.

Quand les signaux de contrôles sont éteints, le faisceau de laser 1 passe dans le SOA. Le contrôleur de polarisation (PC4) permet d'ajuster la polarisation de la sortie logique de telle sorte qu'elle soit sortie par une des portes de PBS (la sortie 1

Table 2: variation de la polarisation de la sortie en fonction des différents états des signaux de contrôle

Contrôle A	Contrôle B	Impulsion d'entrée	Sortie XOR	sortie XNOR
OFF (0)	OFF (0)	↗ (45^o)	0	1
OFF (0)	ON (1)	↖ (135^o)	1	0
ON (1)	OFF (0)	↘ (-45^o)	1	0
ON (1)	ON (1)	↙ (225^o)	0	1

pour la porte XOR et la sortie 2 pour la porte XNOR).

La présence des entrées logiques perturbe le milieu amplificateur, ce qui conduit à une modification de phase des impulsions du laser 1. Cette modification se traduit par une rotation de l'état de polarisation du signal à la sortie du SOA. Les tables de vérité des portes XOR et XNOR et l'état de polarisation de laser 1 ont été résumées dans le tableau 2.

Afin de vérifier la porte XOR, les séquences binaires à 10 Gbit/s suivantes ont été utilisées pour les entrées logiques ('0010011000' et '0001001100'), et couvrent toutes les combinaisons possibles des entrées mentionnées dans le tableau 2. La figure 3 montre ces entrées et la sortie de la porte XOR. Le taux d'extinction mesuré, est de 6.1 dB.

La figure 4 présente les résultats normalisés obtenus d'une porte XNOR pour les deux séquences d'entrée telles que '001100010' et '000110001'. Le débit est toujours 10 Gbit/s. Le taux d'extinction mesuré se situe entre 5.5 et 7.5 dB. La différence entre le niveau des '1's à la sortie de porte XNOR est causée par la saturation du gain dans le SOA en présence des entrées logiques et du laser 1. Ce phénomène n'apparat pas dans le cas de XOR car la valeur logique de sortie en présence de deux entrées logiques simultanées est '0'.

Proposition d'un demi-additionneur optique à partir des portes XOR et XNOR

L'architecture proposée pour les portes XOR et XNOR peut être modifiée pour réaliser un demi-additionneur. La table 3 montre la table de vérité d'un demi-additionneur. En comparant les tables 2 et 3, on constate que la sortie (Somme) est la même que celle de la porte XOR. Ainsi que pour sortie (retenu), à l'exception de la première ligne ([0,0]→0), identique à celle de porte XNOR. Alors, l'idée est d'éteindre la sortie de la porte XNOR quand les entrées logiques sont éteintes ([0,0]→1). Pour cela, une partie du laser 1 est retirée et est ajoutée à la sortie de XNOR. La figure 5 présente le schéma utilisé pour la simulation par la méthode des faisceaux propagés (BPM) du demi-additionneur. Les résultats de simulation sont montrés dans la figure 6.

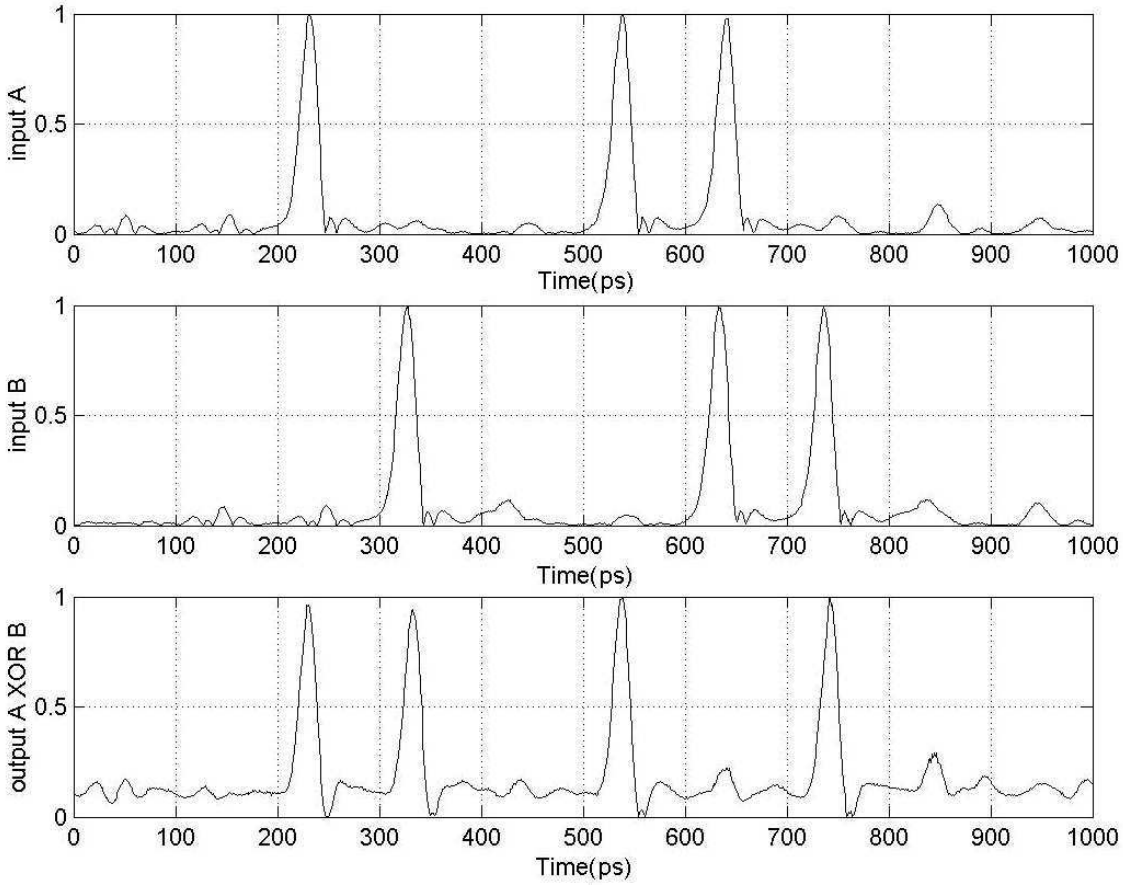


Figure 3: Les résultats normalisés de la fonction XOR

Table 3: La table de vérité d'un demi-additionnaire

Entrée 1	Entrée 2	Sortie (Retenu)	Sortie (Somme)
0	0	0	0
0	1	0	1
1	0	0	1
1	1	1	0

Proposition des commutateurs de paquets optiques à base des fonctions logiques

Parmi les stratégies de commutation, la commutation par agrégats (bursts) est plus compatible avec le niveau de la technologie d'optoélectronique actuelle. Cependant, la commutation par paquets est plus efficace pour la transmission de données, mais pour en raison de la vitesse limitée des composants électroniques (en comparaison de la bande passante optique présente dans les fibres optiques) et l'évolution insuffisante des alternatives de traitement de signal tout-optique, les réseaux optiques

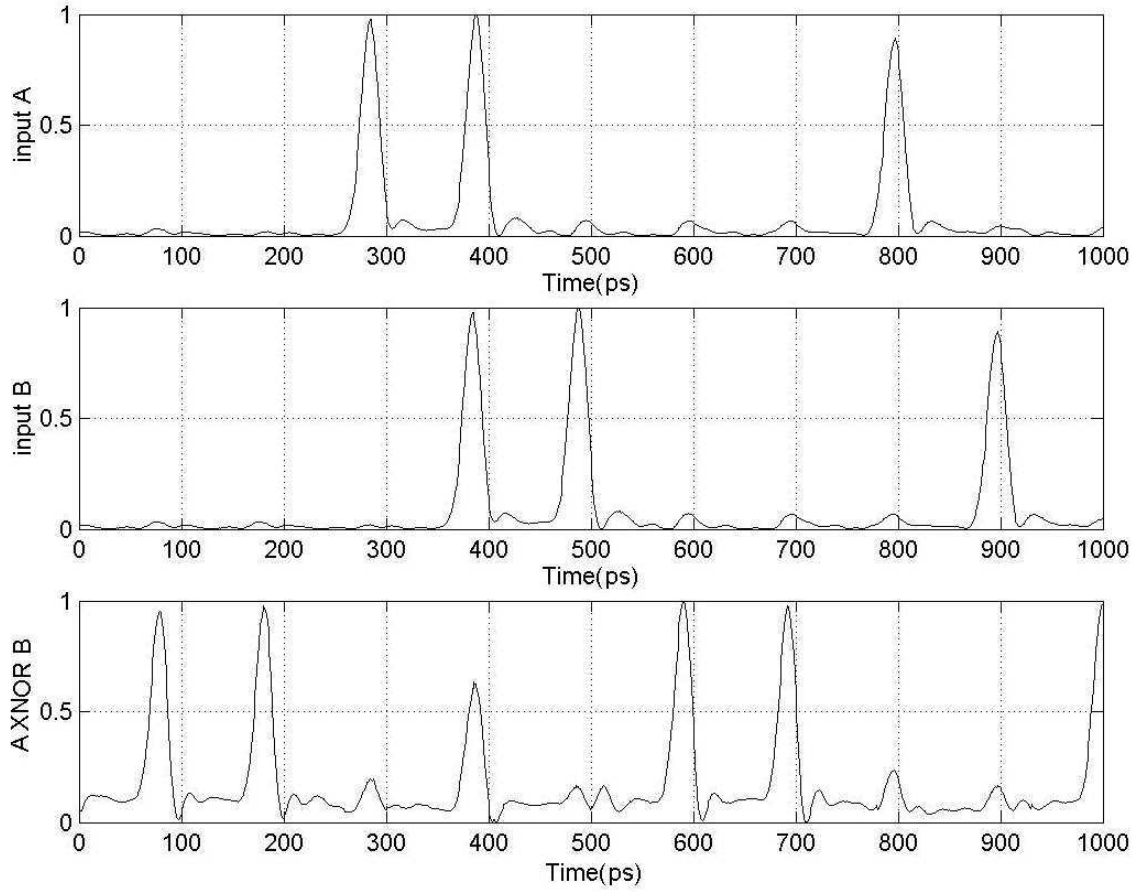


Figure 4: Les résultats normalisés de la fonction XNOR

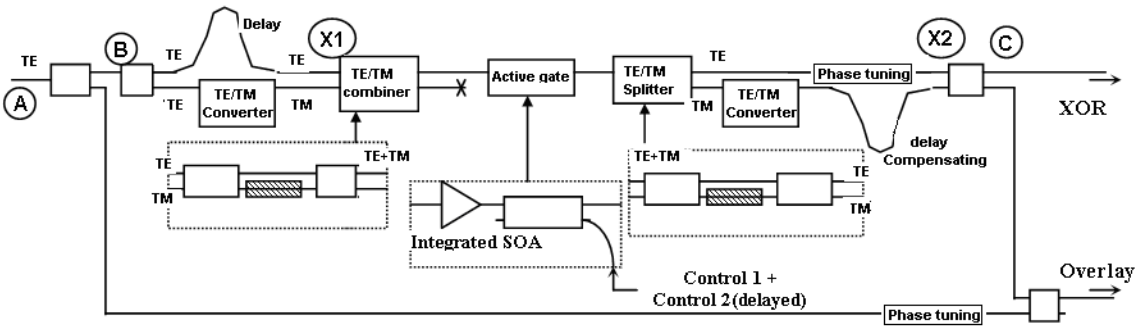


Figure 5: L'architecture d'un demi-additionneur à base d'un système UNI intégré

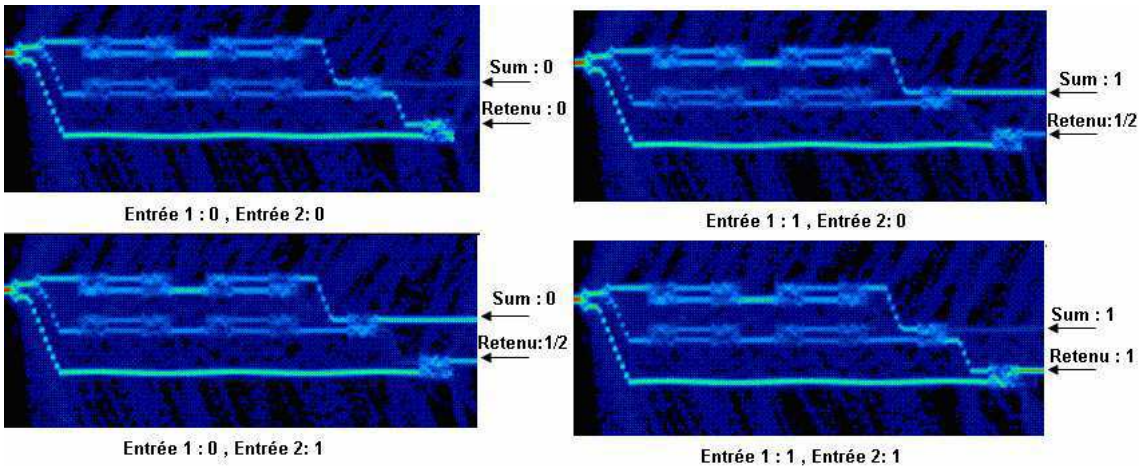


Figure 6: Les résultats de la simulation de demi-additionnaire (figure 5) avec BPM

basés sur la commutation par paquets ne sont pas encore une solution pratique pour implémenter un réseaux optique transparent.

Dans la commutation de paquets, les paquets sont dirigés vers leurs destinations en interrogeant leur adresse de destination enregistrée dans leurs en-têtes (qui sera appelé le label dans cette thèse en référence au protocole de MPLS). Le label de paquet doit être séparé, reconnu et récrit dans chaque routeur de réseaux. Dans le cas du réseau métropolitain, les routeurs ont quatre sorties pour les paquets, mais il est possible de déterminer la direction sortant du paquet en traitant simplement un sous-ensemble de l'adresse du label. De cette façon, le cot et la complexité de routeur va se réduire.

Quatre approches principales ont été proposées pour le codage de label optique; codage sur différentes longueur d'ondes [75], codage sur sous-porteuse (SCM) [76] [77] [78], la modulation orthogonale optique [79] et en série [80] [81]. Chaque méthode a ses avantages et ses inconvénients [82]. Mais elle doit être toujours compatible avec l'ensemble des sous-systèmes du routeur (commutateur). L'approche du codage en série est utilisée dans cette thèse afin de réduire non seulement la complexité du format de paquet, mais aussi pace qu'elle est adaptée avec d'autre sous-système dans les architectures proposées.

Les stratégies de reconnaissance de label des paquets optiques peuvent être classées dans trois catégories : la comparaison de la séquence (bit pattern matching) [83] [84] [85] [86] [87] [88][89][90] [91] [92] [93] [94][95] [96], le ralentissement de label [97][98][99][100] et la méthode tout-optique. Dans cette thèse, nous proposons deux méthodes de traitement des labels de paquets optiques (optoélectronique et tout-optique) fondées sur un convertisseur temps-longueur d'onde en utilisant l'effet du mélange à quatre ondes dans un amplificateur optique à semi-conducteur (SOA). Chaque méthode est composée de trois sous-systèmes principaux nommés;

- Synchronisation & stockage.
- Extraction et traitement du label.

- Réexpédition du paquet.

L'architecture optoélectronique d'un commutateur de paquet optique

Dans cette architecture, les bits parallélisés du label sont traités par des circuits électroniques à grande vitesse (figure 7). Ici, le convertisseur tempsvers-longueur d'ondes agit comme un pont entre le label du paquet optique à haut débit et un sous-système de traitement des signaux électroniques.

Ainsi, des photo-détecteurs simples peuvent être utilisés pour convertir le signal optique en signal électrique afin d'alimenter le processeur numérique du label. Un convertisseur analogique numérique (ADC) est utilisé pour échantillonner, amplifier et sauvegarder les bits transformés électroniquement à la sortie des photo-détecteurs et également produire un niveau de seuil variable. Les opérations du routage peuvent être effectuées à l'aide d'un FPGA.

Finalement, les opérations de "substitution du label" et conversion de longueur d'onde de paquet sera effectuées. Par la suite, nous allons détailler les sous-systèmes de cette architecture.

Synchronisation & stockage

La contribution de ce sous-système est double : d'une part, il préserve le payload du paquet dans le domaine optique pendant le traitement du label et de la commutation de paquet et d'autre part, il prépare des signaux de commande afin de synchroniser les sous-systèmes différents.

Les lignes à retard optique (FDL) représentent une technique simple pour stoker des données en optique [101]. La plupart des systèmes actuels de récupération d'horloge utilisent un photo-détecteur rapide suivi par un récupérateur d'horloge électrique. Dans notre conception, la présence d'une horloge n'est pas nécessaire. Il suffit simplement de connatre le commencement de chaque paquet. Un tel sous-système avec la précision exigée, peut fonctionner à partie de longueur d'onde [102], de la polarisation [103], de la période de bit [74] ou de l'amplitude [104].

Extraction et traitement du label

L'idée fondamentale est fondée sur la conversion série-parallèle (temps-longueur d'ondes) d'un sous-ensemble du label. Ensuite, les bits parallélisés vont être traités dans un soussystème électronique afin de produire les signaux de commande pour le commutateur et "substitution du label".

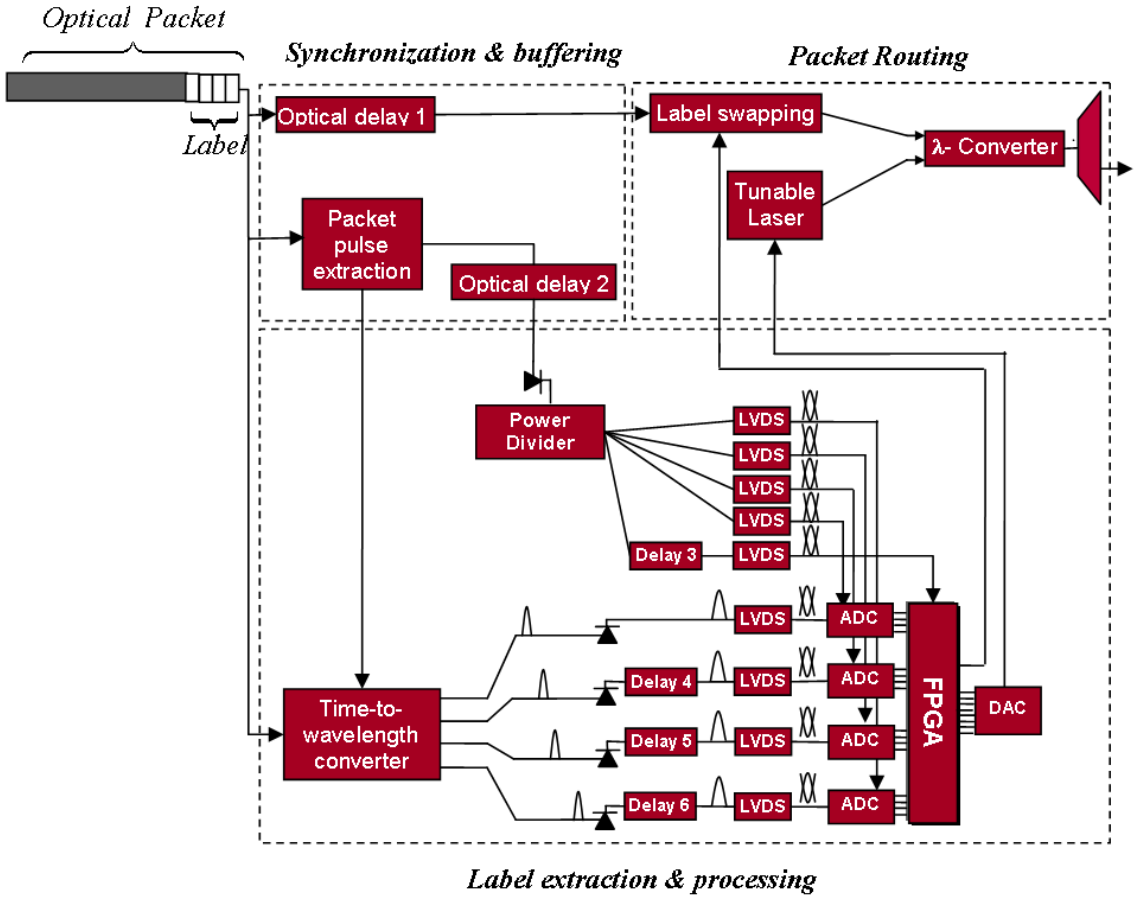


Figure 7: Le schéma d'architecture optoélectronique d'un commutateur de paquet optique

Convertisseur temps-longueur d'ondes

Le convertisseur temps-longueur d'ondes est un dispositif dont la fonction consiste à transférer les bits successifs du label sur des longueurs d'ondes distinctes. Pour cela, il faut synchroniser chaque bit avec une impulsion optique de longueur d'onde différente dans une porte logique AND (figure 8). La porte AND peut être réalisée par différentes méthodes, mais doit fonctionner simultanément pour plusieurs longueurs d'ondes. Dans nos expériences, le mélange à quatre ondes (FWM) et la modulation croisée de la polarisation (XPolM) ont été utilisés pour réaliser la fonction AND. Quatre lasers auxiliaires avec des longueurs d'ondes distinctes sont multiplexés, puis modulés par une impulsion de durée au plus égale au temps bit du label. Ensuite, ils sont séparés, temporellement, à l'aide d'un élément dispersif (ici une fibre compensatrice de dispersion (DCF)). Afin d'éviter le phénomène de recouvrement, le retard est égal au temps bit du label (100 ps pour un débit de 10 Gbit/s). La synchronisation entre les lasers auxiliaires et les bits de l'en-tête sont obtenus à l'aide de l'extraction d'une impulsion introduisant le début du paquet.

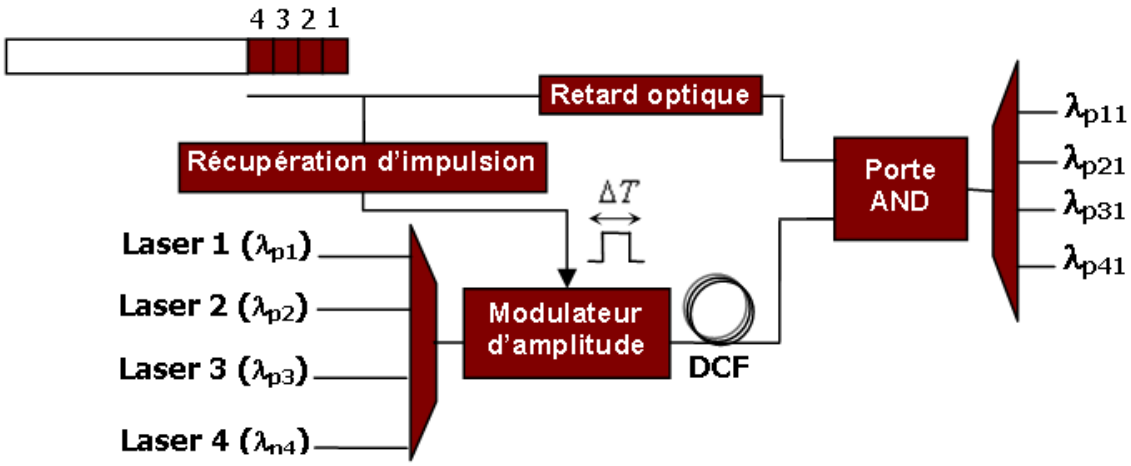


Figure 8: Schéma du principe d'un convertisseur de temps à longueur d'ondes.

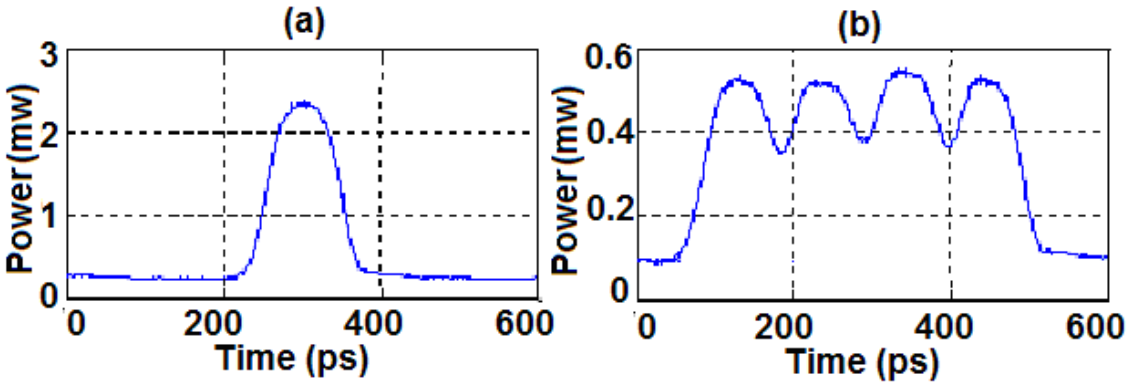


Figure 9: Les lasers auxiliaires modulés à 10 Gbit/s; (a) avant DCF, (b) après DCF.

La figure 9 montre les mesures des lasers auxiliaires modulés et multiplexés avant et après la DCF (à 10 Gbit/s) sur un oscilloscope à échantillonnage. Dans notre expérience, les longueurs d'ondes des lasers auxiliaires sont : 1551.95, 1551.15, 1550.35 et 1549.35 nm. La largeur d'impulsion modulant les lasers auxiliaires est de 100 ps (au format NRZ). Le modulateur est un Mach-Zehnder en LiNbO3 et la DCF mesure 2.4 Km et a un coefficient de dispersion mesuré égal à D = 503,44 - 0,29λ ps/nm/Km. Grâce à l'effet de mélange à quatre ondes, l'interaction entre les lasers auxiliaires et les bits du label (de longueur d'onde 1553.1 nm) dans le SOA va produire les longueurs d'ondes suivantes : 1554.45 nm, 1555.25 nm, 1556.05 nm et 1556.85 nm. La puissance des lasers auxiliaires et du label sont respectivement de -3.7 dBm et de -7.6 dBm. Le taux d'extension des signaux mesurés à la sortie de convertisseur varie entre 9 et 12.5 dB (figure 10).

Le gros problème de mélange à quatre ondes est la sensibilité de ces effets à la polarisation des signaux à l'entrée du SOA. Nous avons donc présenté une nouvelle méthode dans laquelle une source blanche filtrée est remplacée par les lasers de la pompe. D'après nos expériences dont les résultats ont été confirmés par la théorie

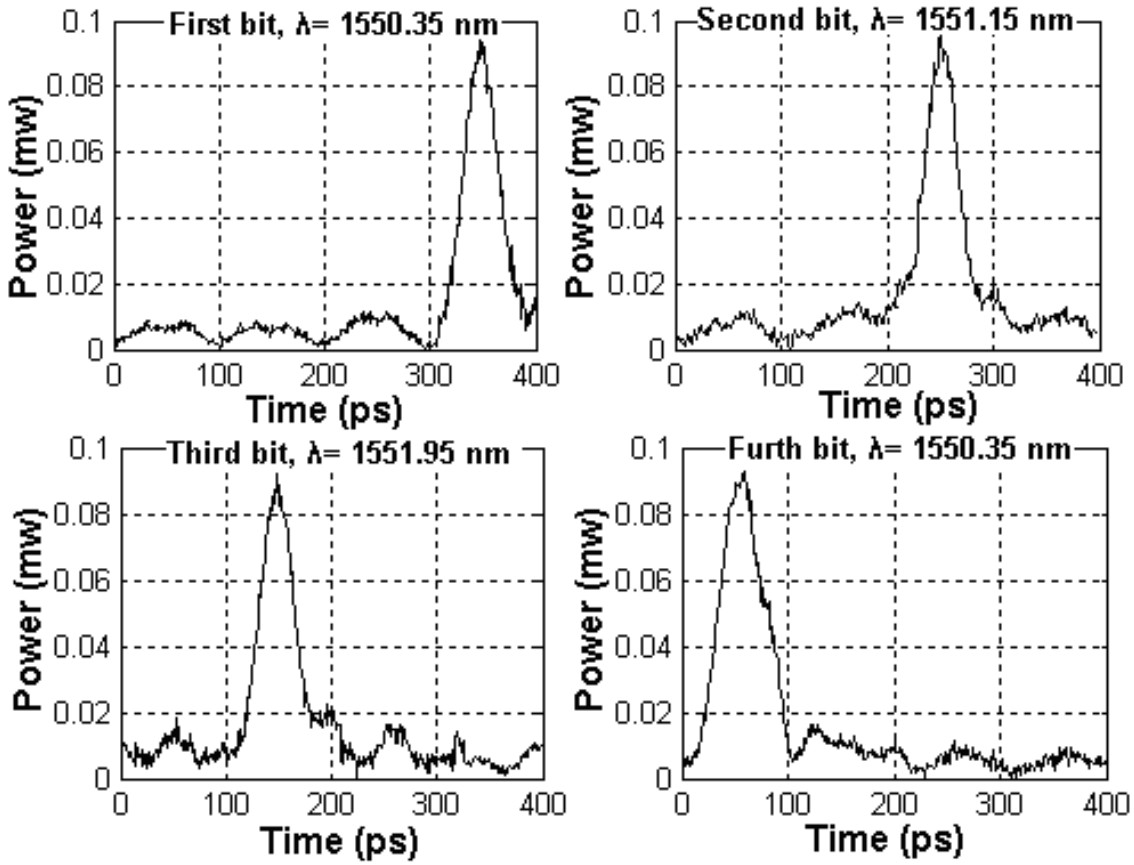


Figure 10: Les longueurs d'onde séparées à la sortie du démultiplexeur.

et la simulation, le convertisseur de temps-longueur d'ondes devient insensible à la polarisation des signaux à l'entrée de SOA. Par contre, le taux d'extinction va diminuer de 3 dB. La figure 11 montre les résultats expérimentaux de convertisseur temps-longueur d'onde à base de mélange à quatre ondes en utilisant la source blanche en tant que la pompe.

Traitement du label

à l'aide de quatre photo-détecteurs, les bits parallélisés sont convertis au format électrique. Ensuite, ils sont transformés en format de LVDS (Low Voltage Differential Signalling) avant le traitement. La compatibilité avec les sources d'alimentation à basse tension, la réduction du niveau de bruit, le débit élevé (jusqu'à 2 Gbit/s), et la capacité d'intégration sont d'autres avantages de la technologie de LVDS. Un convertisseur analogique-numérique de 8 bits (AD9480) optimisé pour le taux de conversion de 250 MSPS est utilisé pour le prélèvement, l'amplification et stockage des bits aussi bien que produire un niveau de seuil variable de détection.

Si on fixe la table de routage, on peut utiliser un circuit logique pour produire le signal exigé de commande. En dynamique, un algorithme adaptatif doit être exécuté. Une des solutions est l'utilisation d'un FPGA.

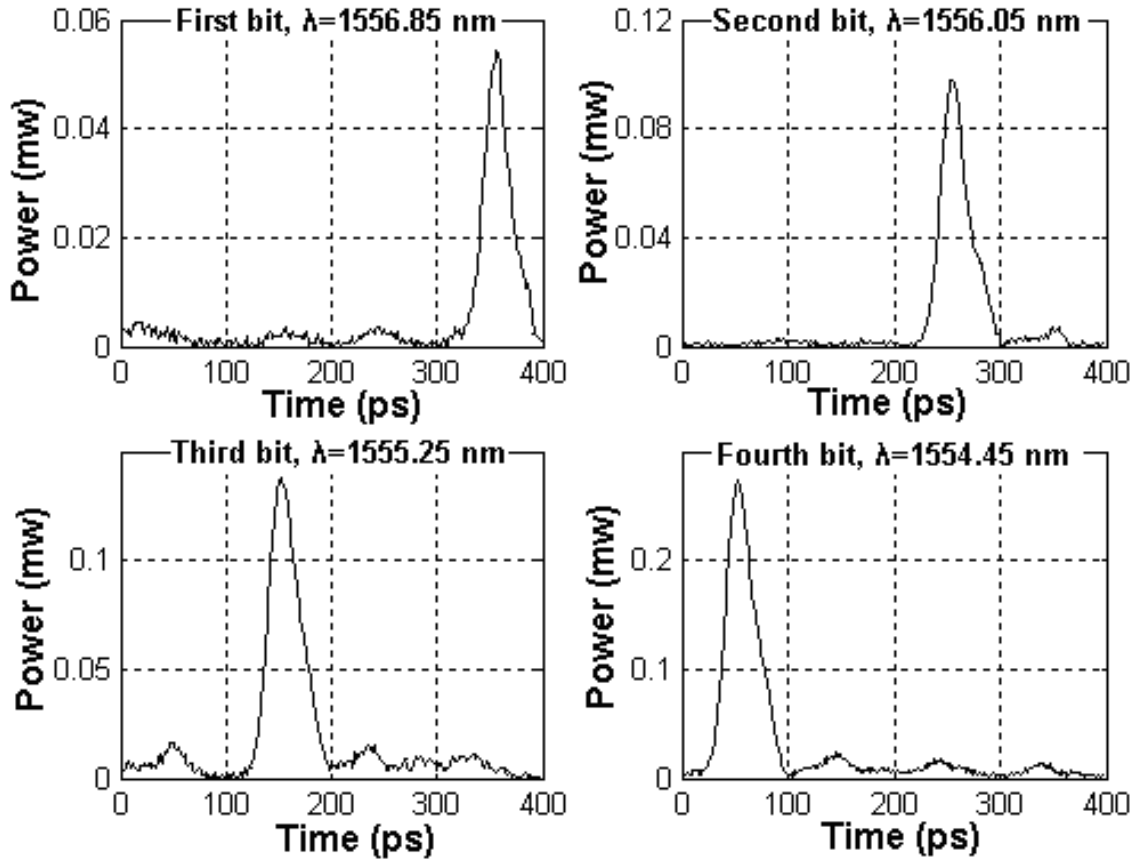


Figure 11: Les longueurs d'onde séparées à la sortie du démultiplexeur.

Réexpédition de paquet

La substitution du label par un nouveau label ensemble et la commutation de paquets sont des opérations essentielles de ce sous-système.

Substitution du label:

Dans le protocole de MPLS, selon le tableau de référence (look up table) présenté dans le sous-système de traitement de label, un nouveau label peut être produit et remplacé par le label actuel de paquet.

Commutateur optique:

La commutation des paquets optiques peut être réalisée dans le domaine spatial, temporel, de la longueur d'ondes, ou de la diversité de code. Nous avons choisi de réexpédier le paquet par la commutation en longueur d'ondes. La technique la plus simple pour réaliser un commutateur en longueur d'ondes, utilise un laser accordable et un convertisseur de longueur d'ondes. Les convertisseurs optiques de longueur d'ondes qui utilisent des effets non-linéarités dans les SOAs offrent

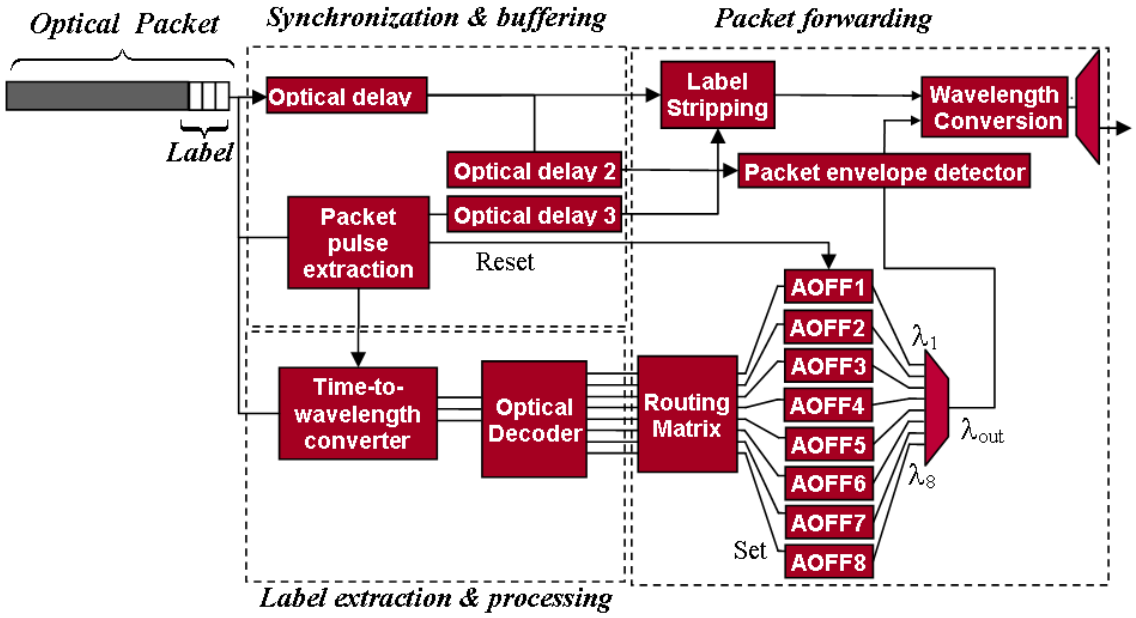


Figure 12: Représentation schématique d'un commutateur tout-optique.

quelques avantages sur le plan de la potentialité d'intégration, de la consommation d'énergie, et l'efficacité optique.

L'architecture tout-optique d'un commutateur de paquet optique

La deuxième approche permet de traiter le label de manière tout optique. Elle utilise un décodeur tout-optique afin de fournir un signal de commande nécessaire au routage des paquets. Des signaux de commande correspondent aux combinaisons binaires de sousensembles de labels (000, 001,..., et 111). Ces signaux peuvent servir à commander un convertisseur de longueur d'ondes ou un commutateur optique dont le rôle est d'expédier le paquet sur la destination désirée. Le décodeur est réalisé à base des portes logiques toutoptiques à 10 Gbit/s, exploitant la modulation croisée de polarisation dans le SOA (figure 12).

Extraction et traitement du label

Le convertisseur temps-longueur d'ondes est encore employé afin de paralléliser un sousensemble de 3 bits du label de paquet. Ensuite, les bits sont amplifiés, puis ils sont envoyés vers un module de décodeur optique qui produit huit impulsions optiques qui correspondent à chaque combinaison de ces 3 bits.

Le décodeur que nous allons présenter exploite la rotation non-linéaire de polarisation dans le SOA (XPolM). Cet effet consiste à modifier l'état de polarisation d'un faisceau optique par l'action d'un second faisceau optique se propageant si-

Table 4: La table de vérité d'un décodeur 3×8

Entrée a	Entrée b	Entrée c	Sortie 1	Sortie 2	Sortie 3	Sortie 4	Sortie 5	Sortie 6	Sortie 7	Sortie 8
0	0	0	1	0	0	0	0	0	0	0
0	0	1	0	1	0	0	0	0	0	0
0	1	0	0	0	1	0	0	0	0	0
0	1	1	0	0	0	1	0	0	0	0
1	0	0	0	0	0	0	1	0	0	0
1	0	1	0	0	0	0	0	1	0	0
1	1	0	0	0	0	0	0	0	1	0
1	1	1	0	0	0	0	0	0	0	1

multanément dans le SOA [105]. La valeur idéale pour la rotation de polarisation est de 90^o. A l'aide d'un polariseur et d'un contrôleur de polarisation le niveau de sortie souhaité peut être sélectionné. Suivant la fonction logique désirée, les configurations co-propagative ou contra-propagative seront utilisées. La seconde nous dispense d'un filtrage optique et permet d'éviter d'autres effets non linéaires tels que le mélange à quatre ondes. Dans tous les cas une des entrées logiques sert de sortie logique. Comme le montre la figure 13, la méthode proposée n'utilise qu'un seul SOA pour chaque sortie du décodeur. Chacune des 8 sorties du dispositif est égale à 1 pour seulement une combinaison des bits à l'entrée et égale à 0 pour toutes les autres combinaisons. En d'autres termes, la sortie est au niveau '1' pour i=i0 et '0' pour ii0 où i0 peut être déterminé à l'aide du tableau 1.

Différentes configurations sont proposées afin de réaliser les portes logiques tout-optiques nécessaires au décodeur. Pour trois entrées a, b et c, les portes logiques peuvent être obtenues à l'aide des 8 fonctions logiques suivantes : un NOR à trois entrées ($\overline{a+b+c}$) pour la sortie 1 (figure 13-a), trois fonctions AND-NOT (i.j.$\overline{k}$) pour les sorties 4, 6 et 7 (figure 13-c), trois AND-NOR (i.$\overline{j+k}$) pour les sorties 2, 3 et 5 (figure 13-b) et une porte AND à trois entrées pour la sortie 8 (figure 13-b) ; où les symboles '**.** 'et '+'représentent les opérations booléennes AND et OR, respectivement et i, j et k ∈ {a, b, c}. Les faisceaux optiques des entrées logiques sont modulés à 10 Gbit/s au format RZ. Les taux d'extension (efficacité) des fonctions logiques AND, AND-NOT et AND-NOR sont respectivement de 7.9, 12 et 10,4 dB. Par exemple, la figure 14 montre les résultats expérimentaux à 10 Gbit/s pour la fonction logique i.$\overline{j+k}$. Le taux d'erreur sur les bits est estimé à partir de l'histogramme de diagramme d'oeil et vaut 10^{-6} pour les symboles '1' et 10^{-7} pour les symboles '0' (PRBS 2^{15}-1). La porte logique NOR à trois entrées a été publiée récemment [71].

Réexpédition de paquets

La réexpédition du paquet inclut 4 opérations, nommées, la sélection adaptive des longueurs d'ondes, la détection de l'enveloppe de paquet, "label stripping" et conversion de longueur d'ondes, qui vont être discuté par la suite.

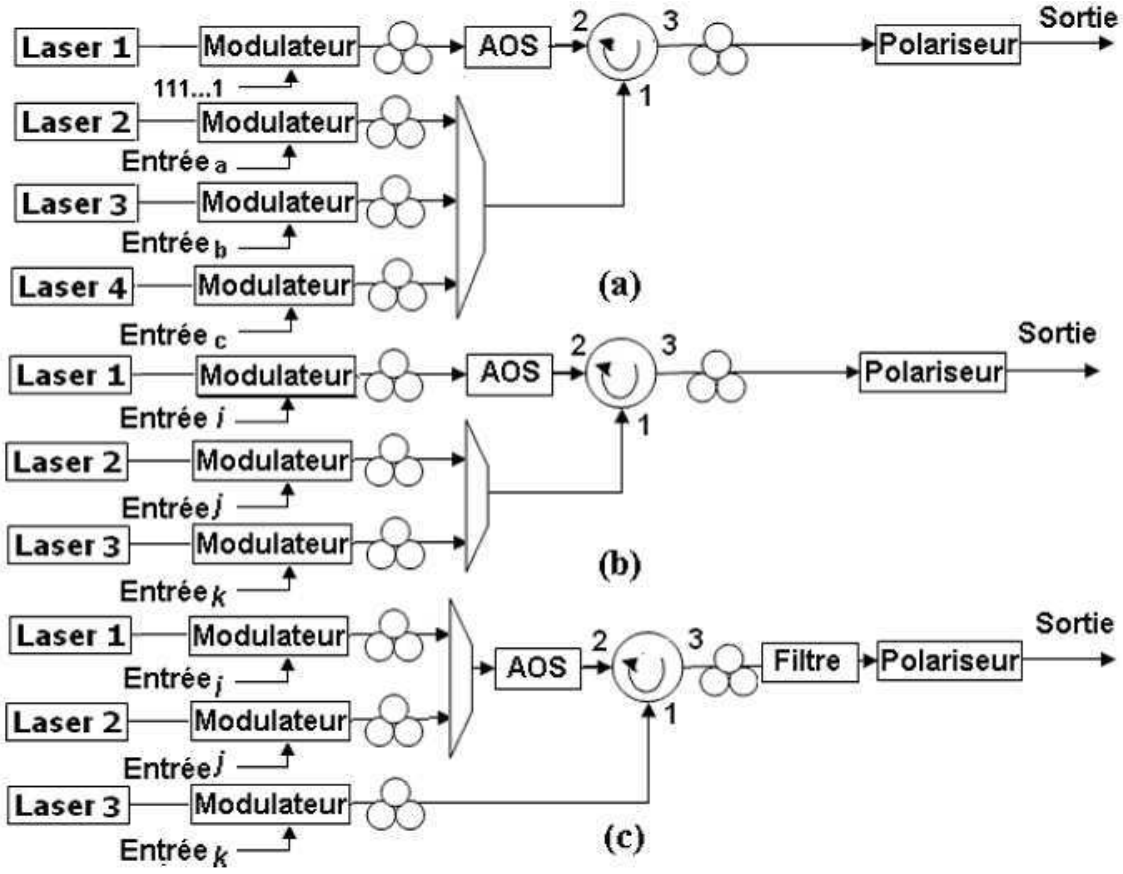


Figure 13: Configuration pour la réalisation du décodeur tout-optique à base de l'effet de XPolM.

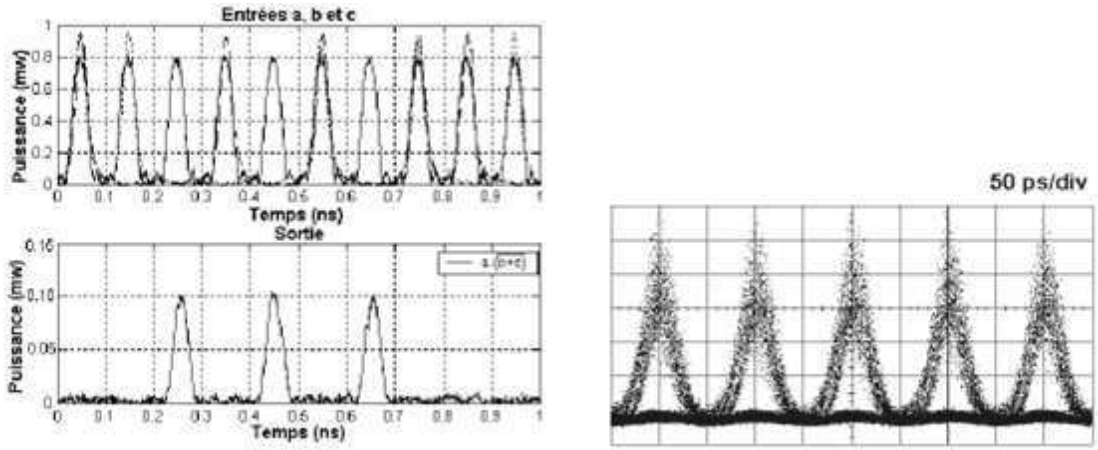


Figure 14: Résultats expérimentaux de la fonction logique a.b + c à 10 Gbit/s.

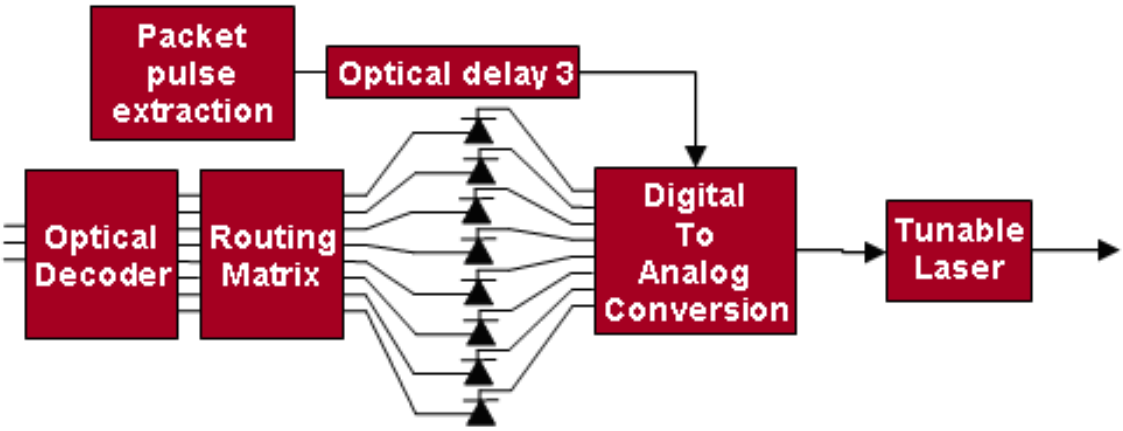


Figure 15: Sélection adaptive des longueurs d'ondes de manière optoélectronique.

Sélection adaptive des longueurs d'ondes

Pour choisir les longueurs d'ondes distinguées par rapport aux différentes combinaisons des bits du label, le choix optoélectronique est le plus simple. La figure 15 présente le schéma proposé. L'impulsion engendrée par le paquet est réutilisée une nouvelle fois pour activer l'échantillonnage d'un convertisseur numérique-analogique (DAC). Les sorties de décodeur (peuvent être réarrangé par une matrice de routage de manière active ou passive) passent dans 8 photo-détecteur parallèle. Finalement, le convertisseur numérique-analogique fournit huit niveau de tension (par rapporte des différent sorties du décodeur) afin de commander un laser accordable. Cette technique est utilisée par Chan et al. [106] pour sélectionner 100 longueurs d'ondes avec un pas de 0,4 nm et à 100 ns de temps de commutation en 2001.

Dans la méthode précédente, la limite est constituée par la vitesse du circuit de contrôle électronique et par le temps de commutation du laser accordable. Une solution plus avancée consiste à utiliser des bascules optiques afin de fournir un système de sélection de longueur d'ondes tout-optique. Le temps de commutation, la puissance et la largeur des impulsions "set" et "reset" des bascules et la possibilité d'intégration sont les paramètres principaux de celles-ci [107] [108] [84].

A la sortie de chaque bascule optique, il y a deux longueurs d'ondes concernant ces états '0' et '1' nommées λ_{ON} et λ_{OFF}. λ_{OFF} pour tout les bascules utilisé est identique (λ_0). Ce faisceau va être bloqué par le multiplexeur (figure 12). Huit longueurs d'ondes différentes (λ_1,... et λ_8) sont choisies pour les 8 états '1' (λ_{ON}). Le fonctionnement séquentiel du système est le suivant : premièrement, toutes les bascules sont remis à l'état initial (λ_0) suite à l'arrivée sur l'entrée "reset" de l'impulsion produite par l'extracteur d'impulsion ; ensuite l'impulsion issue de l'une des sorties du décodeur passe dans la matrice de routage et déclenche une des bascules ; finalement, cette bascule activée va transmettre sa longueur d'ondes propre vers le sous-système suivant (détection d'enveloppe de paquet).

Dans ce concept, la largeur des impulsions de "set" et "reset" sont importantes

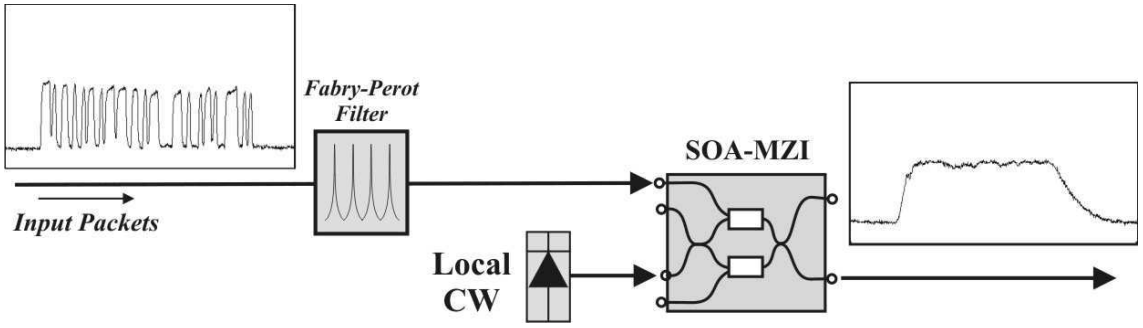


Figure 16: Détection de l'enveloppe des paquets à 10 Gbit/s en utilisant la technique SOA-MZI.

pour commander les bascules. Quand les bits du label soient modulés dans le format de RZ, la largeur des impulsions peut être insuffisante pour conduire (changeant) les bascules. Elargissement des impulsions [109] et la conversion RZ vers NRZ [110] sont deux techniques proposées pour élargir les impulsions optiques.

Détection de l'enveloppe des paquets

La détection d'enveloppe de paquet (PED) est utilisée pour effacer/récrire de label figure 16. Elle présente une nouvelle méthode tout-optique a base d'interféromètre Mach-Zehnder active.

Discussion

Toutes les deux techniques proposées pour la commutation des paquets optiques illustrés dans les figures 7 et 12 sont transparentes au niveau des données (payload). Elles présentent aussi d'autres avantages comme:

- Extensibilité (scalability) au niveau de taux de paquet: Le taux de signal concerne le sousensemble de label utilisé pour la commutation est critique seulement à l'entrée du convertisseur temps-longueur d'ondes. (Après le convertisseur temps-longueur d'onde les bits sont parallélisés et le taux n'est plus significatif). Pour modifier le taux d'opération de convertisseur temps-longueur d'onde il faut modifier la dispersion de l'élément dispersif ou le pas entre les longueurs d'ondes de la pompe afin de modifier le décalage entre les impulsions de la pompe. Cela n'est pas possible dans les convertisseurs temps-longueur d'ondes fondées sur la technique Bragg (FBG).

- Fonctionnement asynchrone : Le convertisseur temps-longueur d'onde proposé comme les autres sous-systèmes a seulement besoin d'informations indiquant le moment d'arrivée du label afin de fonctionner correctement. Cette information de synchronisation est fournie intérieurement par l'extracteur d'impulsion de paquet. Le retard entre les composants intermédiaires peut

être compensé avec précision. Par conséquent, les commutateurs de paquet peuvent faire face à l'opération asynchrone et indépendante de la longueur de paquet.

- Modularité : tous les sous-systèmes présentés sur les schémas 7 et 12 peuvent être optimisé séparément. Autrement dit, la réalisation et l'optimisation de chaque sous-système peuvent être faites indépendamment.

- Flexibilité : En augmentant l'ordre du convertisseur de temps- longueur d'onde, la longueur du sous-ensemble de label à traiter peut être augmentée. L'efficacité de mélange à quatre ondes (ou l'écart entre la pompe et le sonde soit grand) peut devenir critique. D'autre part, le décodeur tout-optique ne semble pas pouvoir faire face à un plus grand nombre de bits à l'entrée. La solution optoélectronique peut être meilleure pour de tels cas.

- Diversité de la polarisation : L'état de polarisation de paquet à l'entrée de commutateur est inconnu. Dans ce cas, utilisation des effets dépendant de la polarisation (FWM, XPolM) dans le convertisseur de temps-longueur d'onde ou le décodeur optique peut devenir problématique. Une des solutions consiste à utiliser un convertisseur de longueur d'onde qui soit insensible à la polarisation [111] à l'entrée du commutateur afin de fixer la polarisation à l'état désiré.

Conclusion

Nous avons proposé deux nouvelles méthodes modulaires tout-optiques de traitement des labels des paquets optiques à base d'un convertisseur temps-longueur d'onde exploitant la non-linéarité d'un amplificateur optique à semi-conducteur et un décodeur optique.

Cette opération permet de séparer chaque bit d'un sous-ensemble de label. Associé à un décodeur tout optique dont nous avons démontré la faisabilité à 10Gbit/s, cette architecture constitue une avancée vers la réalisation d'un système de commutation tout-optique de paquets. Alternativement, une partie du traitement peut être effectué de manière électronique.

TABLE OF CONTENTS

Acknowledgments I

Abstract III

Résumé V

Résumé en français 1
- Introduction . . . 1
- Amplificateur optique à semiconducteurs (SOA) . . . 1
- Porte logique optique . . . 2
  - Réalisation des porte XOR et XNOR à partir d'un système UNI . . . 3
  - Proposition d'un demi-additionneur optique à partir des portes XOR et XNOR . . . 5
- Proposition des commutateurs de paquets optiques à base des fonctions logiques . . . 6
- L'architecture optoélectronique d'un commutateur de paquet optique . . . 9
  - Synchronisation & stockage . . . 9
  - Extraction et traitement du label . . . 9
  - Réexpédition de paquet . . . 13
- L'architecture tout-optique d'un commutateur de paquet optique . . . 14
  - Extraction et traitement du label . . . 14
  - Réexpédition de paquets . . . 15
- Discussion . . . 18
- Conclusion . . . 19

List of figures 25

List of tables **31**

General Introduction **33**

1 Introduction to optical networks - a survey **35**
1.1 Introduction . . . 35
1.2 Telecommunication networks . . . 36
1.3 Optical transmission . . . 37
1.4 Evolution of optical networks . . . 38
1.4.1 First generation . . . 39
1.4.2 Second generation . . . 40
1.4.3 Third generation . . . 41
1.4.4 Fourth generation . . . 44
1.5 Optical networks node architecture (transparent vs. opaque networks) 49
1.6 Optical network protocols . . . 49
1.6.1 Open Systems Interconnection (OSI) networking hierarchy . . 50
1.6.2 Optical Transport Network (OTN) . . . 51
1.6.3 Multi-Protocol Label Switching (MPLS) . . . 53
1.6.4 Multi-Protocol Lambda Switching . . . 55
1.6.5 Generalized Multiprotocol Label Switching (GMPLS) . . . 55
1.7 Summary . . . 56

2 Semiconductor Optical Amplifiers **57**
2.1 Introduction . . . 57
2.2 SOA structure . . . 58
2.3 Operation principle of the SOA . . . 60
2.4 Wave equation and nonlinear effects of SOA . . . 62
2.5 Phenomenological description . . . 63
2.5.1 Interband processes . . . 64
2.5.2 Intraband processes . . . 64
2.6 Gain-transparent operation . . . 64
2.7 Nonlinear effects in the SOA . . . 65
2.8 FWM in SOA using spectrum-sliced incoherent source . . . 68
2.9 Summary . . . 74

3 All Optical Logic Gates **75**
3.1 Introduction . . . 75
3.2 XOR and XNOR realization with UNI technique . . . 76
3.3 Optical NOT gate using the XPolM effect in SOA . . . 82
3.4 A half-adder design based on the XOR-XNOR gates . . . 85
3.5 Summary . . . 88

4 Optical Packet Label Switching Systems **91**
4.1 Introduction . . . 91
4.2 Optical label structure . . . 92
4.3 Optical labelling techniques . . . 94
4.4 Clock recovery . . . 97
4.5 Optical switch . . . 98
4.6 Optical buffering . . . 101
4.7 Optical regeneration . . . 102
4.8 Packet label processing . . . 103
4.8.1 Label-payload separation . . . 103
4.8.2 Packet pulse extraction . . . 104
4.8.3 Label recognition . . . 104
4.8.4 Label swapping . . . 109
4.9 Summary . . . 111

5 Time-to-Wavelength Conversion **113**
5.1 Introduction . . . 113
5.2 Colored bit generation and synchronization . . . 114
5.3 AND logic gate . . . 116
5.4 Time-to-wavelength conversion using the XPolM effect . . . 117
5.5 Time-to-wavelength conversion using the FWM effect . . . 118
5.6 Time-to-wavelength conversion using spectrum-sliced incoherent source 121
5.7 Summary . . . 124

6 Demonstration of an Opto-Electronic Optical Packet Routing System **125**
6.1 Introduction . . . 125
6.2 Synchronization & buffering . . . 126
6.3 Label extraction . . . 127
6.4 Electronic packet label processing . . . 127
6.4.1 Photo-detection . . . 128
6.4.2 Analog-to-digital converter (ADC) . . . 131
6.4.3 Label processing (within FPGA) . . . 136
6.5 Packet forwarding . . . 137
6.5.1 Label swapping . . . 137
6.5.2 Optical switching . . . 139
6.5.3 Tunable laser source . . . 139
6.5.4 Wavelength conversion . . . 140
6.5.5 Integrating possibility . . . 140
6.6 Discussion . . . 140
6.7 Summary . . . 142

7 Design of an All-optical Packet Forwarding System **143**
7.1 Introduction . . . 143
7.2 All-optical decoder . . . 144
7.2.1 All-optical NOR gate using XPolM effect in SOA ($\overline{a+b+c}$) . . . 146

7.2.2 All-optical three-input AND logic gate ($a.b.c$) 147
7.2.3 All-optical AND-NOT logic gate ($i.j.\bar{k}$) 149
7.2.4 All-optical AND-NOR logic gate ($i.\overline{j+k}$) 151
7.3 Packet forwarding 155
7.3.1 Adaptive wavelength selection 156
7.3.2 Packet envelope detection 159
7.3.3 Packet label stripping 159
7.3.4 Wavelength conversion 160
7.4 Discussion 160
7.5 Summary 165

General Conclusion and Perspectives **167**

Bibliography **171**

List of Publications **205**

LIST OF FIGURES

1 Vu schématique du SOA utilisé dans nos expériences 2
2 Montage expérimental des portes XOR and XNOR à base système UNI à 10 Gbit/s 4
3 Les résultats normalisés de la fonction XOR 6
4 Les résultats normalisés de la fonction XNOR 7
5 L'architecture d'un demi-additionneur à base d'un système UNI intégré 7
6 Les résultats de la simulation de demi-additionnaire (figure 5) avec BPM 8
7 Le schéma d'architecture optoélectronique d'un commutateur de paquet optique 10
8 Schéma du principe d'un convertisseur de temps à longueur d'ondes. 11
9 Les lasers auxiliaires modulés à 10 Gbit/s; (a) avant DCF, (b) après DCF. 11
10 Les longueurs d'onde séparées à la sortie du démultiplexeur. 12
11 Les longueurs d'onde séparées à la sortie du démultiplexeur. 13
12 Représentation schématique d'un commutateur tout-optique. 14
13 Configuration pour la réalisation du décodeur tout-optique à base de l'effet de XPolM. 16
14 Résultats expérimentaux de la fonction logique a.b + c à 10 Gbit/s. . . 16
15 Sélection adaptive des longueurs d'ondes de manière optoélectronique. 17
16 Détection de l'enveloppe des paquets à 10 Gbit/s en utilisant la technique SOA-MZI. 18

1.1 Telecommunication network, after [112] 36
1.2 Evolution of optical transport methodologies, after [113]. 39
1.3 An n-channel point-to-point WDM transmission system 39
1.4 A wavelength add/drop multiplexer (WADM) 41
1.5 An 8×8 passive star architecture 42

1.6 A 4×4 passive router (four wavelengths) . . . 43
1.7 A 4×4 active switch (four wavelengths) . . . 43
1.8 Illustrations of optical packet switching node (OPS), after [114] . . . 46
1.9 The use of offset time in Optical burst switching, after [113] . . . 47
1.10 Illustrations of optical burst switching (OBS), after [114] . . . 47
1.11 Open Systems Interconnection (OSI) model . . . 50
1.12 Evolution of technology toward photonic networking, after [115] . . . 53
1.13 MPLS architecture; LER- Label edge router, LSR- Label switching router LSP- Label switched path . . . 55

2.1 Schematic cross-section and top view of a buried ridge stripe SOA, after [116] . . . 59
2.2 Schematic view of a DBR-SOA (GC-SOA), after [117] . . . 59
2.3 Simplified band structure of a direct-gap semiconductor in quasi-equilibrium, after [116] . . . 61
2.4 Light induced variation of the gain and the refractive index in an SOA (schematic picture) as a function of the light energy *Eprobe* relative to the band gap energy *Eg*, after [116]. . . . 65
2.5 Experimental scheme utilized for evaluating the FWM polarization sensitivity in the SOA . . . 68
2.6 FWM variations of polarization angle detuning between pump and probe beams (from 0^o to 90^o with a step of 5^o). . . . 70
2.7 Top view schematic of the used SOA . . . 70
2.8 FWM variations of polarization angle detuning between incoherent probe and coherent pump beams (0^o-90^o with a step of 5^o). . . . 71
2.9 Experimental result of FWM signal power as function of pump polarization angle; '□', up-conversion FWM (coherent probe), 'o', down-conversion FWM (coherent probe), '+', up-conversion FWM (incoherent probe), '*', down-conversion FWM (incoherent probe). . . . 74

3.1 Graphic representation of basic logic gates . . . 76
3.2 Block diagram of the UNI system; PC is the polarization controller, PMF stands for polarization maintaining fiber and BPF is band pass filter. . . . 78
3.3 The cross section of two types of PM fiber . . . 79
3.4 Schematic of UNI system in a loop . . . 80
3.5 Experimental setup for XOR and XNOR gates based on UNI technique; PBS is polarization beam splitter and MZ is Mach-Zehnder modulator . . . 80
3.6 The normalized XOR result of two input sequence . . . 82
3.7 The normalized XNOR result of two input sequence . . . 83
3.8 (a) XOR switching window, (b) XNOR switching window . . . 84
3.9 Experimental setup used for NOT logic gate based on XPolM in SOA; (a)Co-propagating, (b)Counter-propagating . . . 84

3.10 NOT logic gate realization using XPolM in SOA; (a)the control signal, (b)the input data signal and (c)the output NOT logic gate. 85
3.11 Integrated UNI scheme for the half-adder operation 86
3.12 BPM simulation of integrated UNI based scheme for the half-adder operation 88

4.1 The network architecture of an optical label switched network, WAN stands for wide area network, OLS for optical label switch, OXC for optical cross connection, after [82] 92
4.2 A generic architecture of an OLS core router. 93
4.3 MPLS label Format; S is the bottom of stack and exp is the reserved bits for experimental uses. 93
4.4 Label transmission schemes. (a) and (b) serial bit label with different and the same bit rate of the label in relation with payload, (c) Wavelength labelling, (d) Subcarrier multiplexed label (SCM), and (e) Orthogonal modulation label. 95
4.5 Two type of switching architecture: shared medium and interchanger, after [118] 98
4.6 Key functional blocks of 3R-regenration; reamplification, retiming and reshaping, after [119] 103
4.7 Experimental set-up to demonstrate SLALOM based serial all-optical header processor. τ_1−Delay Line for HPU1 (Header Processor Unit 1) ; τ_2−Delay Line for HPU2 (Header Processor Unit 2), after [120] . . 105
4.8 Conceptual diagram of an Internet core router with N output ports (typically two to four) assisted by a bank of M optical FBG-based correlators that are dynamically configured by a software algorithm, after [120] 106
4.9 Experimental set-up of packet header recognition module based on (a) wavelength shifting for time-to-wavelength mapping, (b) wavelength selective delay for optical correlation, and (c) electronic decoder. (SMF: single mode fiber, FBG: fiber Bragg grating, SOA: semiconductor optical amplifier, EDFA: erbium doped fiber amplifier.), after [100] 108
4.10 Schematic diagram of proposed all-optical SCM label-swapping system. EML represents integrated electroabsorption modulation laser, after [121]. 110

5.1 Schematic diagram of a 4-bit time-to-wavelength converter 114
5.2 Measured time delay generated between two synchronous input optical pulses as function of their wavelength detuning. 115
5.3 Four synchronous pulse-modulated auxiliary lasers; (a) before DCF, (b) after DCF 115
5.4 Four synchronous pulse-modulated incoherent sliced spectrum light, (a) before DCF, (b) after DCF. 116
5.5 XPolM based 4-bit time-to-wavelength converter 117

5.6 Four wavelength-separated bits at the output of the final demultiplexer by the XPolM effect . . . 118
5.7 Wavelength configurations for efficient FWM; (a) Wavelength configuration giving a maximum gain to the FWM signal, (b) Ideal wavelength configuration for to minimize pattern dependencies of FWM signal . . . 119
5.8 4-bit time-to-wavelength converter by the FWM effect . . . 119
5.9 Pump and probe spectrum; (a) SOA input, (b) SOA output (continuous beams), (c) SOA output (modulated beams) . . . 120
5.10 Four wavelength-separated bits at the output of the final demultiplexer. 121
5.11 Four-bit time-to-wavelength converter by FWM effect in SOA with a incoherent light source . . . 122
5.12 Simulation of the time-to-wavelength converter output spectrum after the SOA with a spectrum-sliced incoherent light source; (a) a broad band filter, (b) four narrow band filters . . . 122
5.13 Measured spectrum of the time-to-wavelength converter using a spectrum-sliced incoherent light source and serial-data modulated beam; (a) SOA input, (b) SOA output. . . . 123
5.14 Four wavelength-separated bits at the demultiplexer output created by sliced incoherent light source . . . 123

6.1 Conceptual diagram of the proposed optical packet label processing 126
6.2 Conceptual diagram of time-to-wavelength converter based optical packet label processing . . . 128
6.3 The pulse detected within the TIA-950 and TIA-525 photo-detectors 130
6.4 Functional block diagram and pin out diagram of ADC converter AD9480 . . . 131
6.5 ADT1-1WT wideband transformer insertion loss . . . 133
6.6 Schematic montage of ADC . . . 134
6.7 ADC test circuit . . . 135
6.8 ADC functionality test with a periodic 7-bit block sequence . . . 136
6.9 ADC functionality test with a periodic 13-bit block sequence . . . 137
6.10 Schematic diagram of the packet label swapping . . . 138
6.11 (a) First mask schematic proposed, (b) Mask lay out designed by TU/e 141

7.1 Conceptual diagram of time-to-wavelength converter based optical packet label processing . . . 144
7.2 Schematic of a 3×8 logic-gate decoder . . . 145
7.3 All-optical two input NOR gate setup . . . 146
7.4 Experimental result of two-input NOR gate (based on figure 7.3); (a)*input a*, (b) *input b* and (c) *input a NOR input b* . . . 148
7.5 All-optical three input AND gate setup using the XPolM effect in SOA 149
7.6 Three-input AND logic function based on figure 7.5; (a) *input a* (co-propagating), (b) and (c) are the *input b* and *c* (counter-propagating) and (d) is the output. . . . 150

7.7 All-optical three-input AND-NOT gate function ($i.j.\bar{k}$) setup 151
7.8 AND-NOT logic function ($i.j.\bar{k}$) based on figure 7.7; (a) and (b) are the *inputi* and j (co-propagating), (c) is the *input* k (counter-propagating) and (d) is the output. 152
7.9 AND-NOR logic function ($i.\overline{j+k}$) 154
7.10 Measured eye diagram of ($i.\overline{j+k}$) logic function. 155
7.11 Adaptive wavelength generator subsystem. 156
7.12 Arrangement of two coupled identical lasing cavities showing the possible states, after [107]. 157
7.13 All-optical wavelength selection system; AOFF represents all-optical flip-flop 158
7.14 10 Gbit/s packet envelope detector using SOA-MZI technique, after [122] 159
7.15 Label stripping strategy, after [107] 160
7.16 Schematic representation of an all optical label processing and routing system 161
7.17 Experimental verification of LASAGNE label swapper and packet router, after [107] 162
7.18 ARTEMIS network architecture and all-optical burst forwarding, after [123]. 163
7.19 Detailed schematic diagram of the header-processing/forwarding plane, after [123]. 164
7.20 ARTEMIS (a) 4×4 and (b) 8×8 switching matrices. In both cases, the elementary 1×2 switching elements are interconnected so as to form a strictly nonblocking switching fabric, after [123]. 164

LIST OF TABLES

1 Les techniques utilisé pour réaliser les portes logiques optiques. . . . 3
2 variation de la polarisation de la sortie en fonction des différents états des signaux de contrôle 5
3 La table de vérité d'un demi-additionnaire 6
4 La table de vérité d'un décodeur 3×8 15

1.1 Evolution of WDM to DWDM systems 40
1.2 Comparison between the different all-optical technologies; OCS is optical circuit switching, OPS is optical packet switching and OBS stands for optical burst switching 48
1.3 Tolerance levels by data type 52
1.4 SONET system hierarchy 53

2.1 Comparison of different state of the art SOAs 60

3.1 A summary of technique used for all-optical logic gate 77
3.2 Comparison between SOA based technique utilized for XOR logic gate producing 78
3.3 Variation of polarization of incoming pulse with control pulses . . . 81
3.4 Truth table of a half adder 86
3.5 Wave characteristics of the control beams 87

4.1 Comparison of four main coding approaches 97

6.1 Characteristics of TIA-950 and TIA-525 photo-detectors 130
6.2 Pin function descriptions 132
6.3 Comparison between addressing standards 133

7.1 Truth table of a 2×4 (in bold part) and 3×8 decoder 145
7.2 Representation of a 4×16 decoder truth table; O_i stands for *output i* 153

General Introduction

Optical networks become an important part of the global telecommunication due to the optical fiber capacity, which is the only medium capable of forwarding data at multi-Gbit/s. However, this huge capacity is not employed optimally because of the electronics bottleneck. Electronic devices take control of the switching and routing techniques. In all-optical networks the data along the fiber remain in optical channel all the way from source to destination in order to reduce the amount of electro/optic conversions.

The intention of this thesis is to investigate the complexity and technical feasibility of an optical packet switching (OPS) network. Different physical and technological propositions in an OPS network are investigated by considering available key technologies in optical packet switching systems. In this context, all-optical gates have been used as core elements performing a diversity of network functionalities such as time-to-wavelength convertion, optical decoder, wavelength converter, and so on. Semiconductor optical amplifiers (SOAs) are used for optical logic gate realization, since they exhibit a strong variation of the refractive index and a high gain. The thesis work is described in seven chapters. The outline of the thesis is as follows:

- In chapter 1, an overview of telecommunication optical network, their evolution, technological advances, and research issues in optical networks is given. Moreover, optical network node architectures are compared in transparent and opaque aspects. The evolution of optical network protocols is also reviewed in this chapter.

- Chapter 2 provides a discussion on the SOAs in terms of physical structure (e.g. bulk, multiple quantum well,$\cdots$), operating principle, dynamical processes, and resulted nonlinear effect (such as self gain modulation, cross phase modulation, four-wave mixing and etc.). Moreover, the experimental results together with the simulation and modelling of a new technique to decrease the polarization sensitivity of four-wave mixing in SOA by using an incoherent sliced-spectrum unpolarized beam is presented.

- Chapter 3 concerns the attempts for building up different optical logic gates. Majority of the presented methods use SOAs as the nonlinear element for

the realization of different logic functions. A simplified Ultrafast Nonlinear Interferometer (UNI) in a loop configuration is used for providing XOR and XNOR logic functions. Moreover, an all-optical half-adder scheme based on the proposed XOR and XNOR gates within only one UNI system is proposed. The BPM simulation of the integrated scheme is shown.

- Chapter 4 addresses the optical label switching (OLS) subsystems as a promising technique for high-speed optical packets in future packet-based WDM networks. Several labelling schemes and packet label recognition (processing) techniques are reviewed in this chapter.

- The all-optical time-to-wavelength converter concept is presented in chapter 5. The realization of AND logic gate thanks to the four-wave mixing and cross polarization modulation effects in the SOA is proposed for separating four serial bits onto four distinct wavelengths.

- Chapter 6 addresses the application of a 4-bit time-to-wavelength converter in an opto-electronic packet label processing architecture. The time-to-wavelength converter acts as a serial-to-parallel converter in order to slowed down label processing. In this method all the label processing and control signal to derive the optical switches are done in the electronic domain. However, the routing system is transparent for the packet payloads.

- Chapter 7 focuses on an all-optical self-routing scenario for optical packet label processing and packet forwarding system. The key element is an all optical 3×8 decoder for optical label subset processing. The entire implementation imposes specific requirements concerning the operation of the optical logic circuits involved.

Finally, general conclusions are presented where recommendations for future researches are proposed.

CHAPTER

1

Introduction to optical networks - a survey

1.1 Introduction

The growth of the Internet-related services has caused Internet protocol (IP) data traffic to overtake voice traffic faster than predicted by the well-known Moore's law [124]. To cope with the rapid growth of IP traffic, not only telecommunication link capacity must be increased (e.g. by using wavelength division multiplexing technology), but also the throughput of nodes must be improved (e.g. by introducing specific optical technologies). In addition, the entire network must be optimized at all levels (especially the backbone and metropolitan levels) for IP data traffic and the underlying IP support protocols. The optimization must take into consideration three fundamental requirements: flexibility of resource allocation and reallocation (traffic engineering, protection, rerouting, various services and etc.), scalability of network topologies and algorithms, and cost effectiveness.

The focus of this chapter is to present technological advances, promising, architectures, and research issues in optical networks. The next section provides an overview of access, metropolitan, and backbone telecommunication networks. Section 1.3 explains the advantages of optical transmission system in data telecommunication. Section 1.4 provides a brief discussion on the evolution and the generations of optical networks. Optical network node architectures are compared in transparent and opaque aspects in section 1.5. Finally, section 1.6 presents the evolution of optical networks protocols.

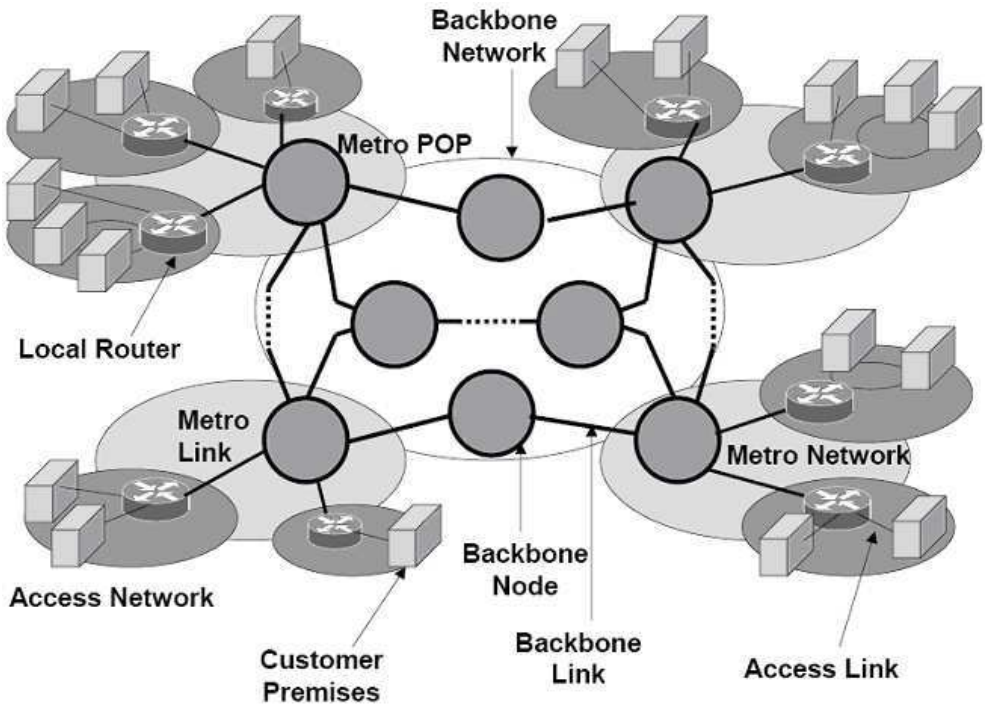


Figure 1.1: Telecommunication network, after [112]

1.2 Telecommunication networks

Generally, a telecommunication network can be divided into three sub-networks; access, metro and backbone. A schematic of these three sub-networks is illustrated in figure 1.1;

- The access networks connect the subscribers (e.g. home or business) to the service providers. It is typically a ring or star network. The links in an access network can be fibers, copper wires or even wireless. The next wave in access network deployment is bring the fiber to the building (FTTB) or to the home (FTTH), enabling Gbit/s speeds at costs comparable to other technologies such as digital subscriber line (DSL) and hybrid fiber coax (HFC) [125]. Three optical technologies are promising candidates for the next-generation access networks: point-to-point topologies, passive optical networks, and free-space optics.

  From the access network, the traffic is transported to the metro network through local routers. These routers are also known as access routers. Since each local router manages traffic from a relatively small community of clients who are connected to the local access router, its capacity is relatively low.

- Metro (metropolitan) or regional networks on the other hand bridge the gap between the access or edge and long-haul or backbone networks. They typically cover large metropolitan areas. Currently, SONET/SDH-based rings form

the physical-layer infrastructure in metro networks. Along with local routers, the metro network also has a metro point-of-presence (POP). The functions of the metro POP are,

  - Adding(dropping) traffic to(from) the metro network
  - Switching traffic from(to) local routers
  - Serving as a pass-through hub for backbone network traffic
  - Taking appropriate measures in the event of link failures
  - Having facilities to differentiate services.

  The access traffic is groomed into a higher capacity by the metro POP and is transferred to the backbone network.

- A backbone network (which also is called long-haul or core networks) spans greater regional and global distances, and provides interconnectivity between various regional and metropolitan domains and subnets. The key purpose of the backbone routers is to route IP packets to manage traffic from multiple local routers. So, the required capacity of these routers is higher than the local routers. In the most advanced telecommunication network, links in backbone and metro networks are generally fibers running WDM technology. A backbone network with fiber links is called an optical network.

1.3 Optical transmission

Optical networks are interesting for five reasons:

- **Cost-effective bandwidth:** Due to the potential bandwidth (50 THz or greater) of fiber optics, the price per unit of bandwidth is low. For example, for high bandwidths (~Gbit/second and higher) and even relatively short distances, optical fiber is usually the only practical choice. This threshold is constantly being driven down due to manufacturing economies and technological development.
- **Noise isolation:** Optical fibers are isolated against electrical noise-producing sources. They can be used in environments where adequate shielding of electrical cables would be difficult or impossible.
- **Security:** Since optical fiber does not emit electromagnetic radiation which can be intercepted, it is much more secure than many other types of wiring. Moreover, tapping optical fiber is also much more difficult than tapping most electrical wires.
- **Smaller physical presence:** A bulky cable with hundreds of wires can be replace with a single optical fiber cable with a diameter of less than 6 mm. This is critical in applications where space is at a premium, such as ships, aircrafts and in rewiring of buildings where space may also be limited.

- **Ready upgrade path:** Although there are continual improvements to fiber optic cable itself, in most cases increased bandwidth can be had simply by installing new optical multiplexing equipment (i.e., not replacing the fiber itself).

Moreover, there are five reasons which are forcing service providers and users to deploy optical networking technology:

- **Ever-increasing demand for bandwidth:** More Internet applications at all levels demand more bandwidth. Even in the home environment, video on demand and high definition TV quality video, is driving fiber to the curb (FTTC) and fiber to the home (FTTH).
- **Optical network component productions:** Mass production and standardization of components are enabling more powerful and economical networks. Moreover, their plug-and-play compatibility reduces the risks of deploying optical technology.
- **Reduced number of components:** Higher bandwidth per fiber together with development of all-optical components means network simplification and equipment consolidation. This improves reliability and reduces maintenance stores and costs.
- **Shorter service contracts:** The rapid rate of technology development implies faster depreciation and more rapid replacement of equipment with newer technology. Shorter equipment life time can translate into shorter service contracts, with accompanying lower risks to users, since service providers do not have to recover plant and equipment costs over long periods (e.g., decades).
- **Rapid provisioning:** Although not yet realized, widespread deployment of optical network hardware coupled with enormous amounts of in ground unused fiber will mean an era of bandwidth abundance, in which new service can be deployed with a few keystrokes at a computer terminal, rather than after months of cable laying.

1.4 Evolution of optical networks

The research phase of fiber-optic communication systems started around 1975. In 1992, the advent of the wavelength-division multiplexing (WDM) technique started a revolution that resulted rapidly increasing of system capacity which led to lightwave systems operating at a bit rate of 25.6 Tbit/s by 2007 (Alcatel-Lucent). In WDM systems, each fiber carries multiple communication channels, with each channel operating on a different wavelength. Such optical transmission systems have the potential to provide over 50 Tb/s on a single fiber. Figure 1.2 displays the evolution of the different optical transport methodologies [113]. Here, we investigate several generations of optical networks.

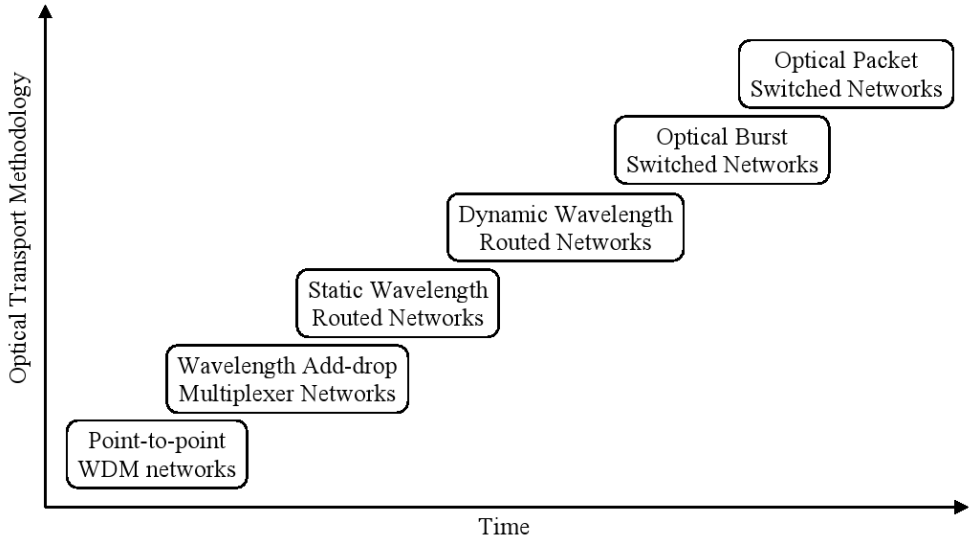


Figure 1.2: Evolution of optical transport methodologies, after [113].

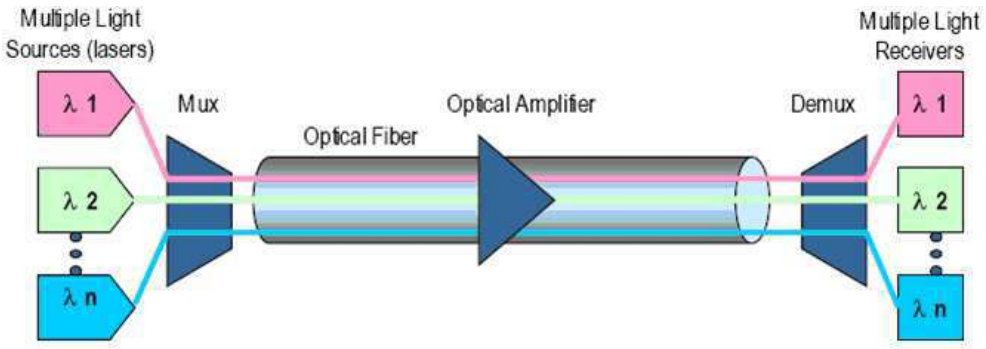


Figure 1.3: An n-channel point-to-point WDM transmission system

1.4.1 First generation

The first generation of optical networks consist of point-to-point WDM links (see figure 1.3). A WDM link involves

- Generation of multiple streams (channels) of light each at a different wavelength,
- Combination of the channels and coupling into an optical fiber (single mode),
- Amplification of the optical signals as required,
- Separation of the multiplexed stream into its substreams,
- Reception of the optical streams via wavelength specific receivers.

Table 1.1 illustrates the evolution of WDM to DWDM systems where c-band is centered at 1550 nm and L-band is centered at 1625 nm. The first generation of

optical networks was based on synchronous optical networking (SONET) and synchronous digital hierarchy (SDH) protocols [115]. Such networks are comprised of several point-to-point links at which circuit switching, traffic separation, routing, and protection functions are performed in electronic domain. This requires optical-to-electrical (O-E) and electrical-to-optical (E-O) conversions. The data switching at every network node incurs significant overhead in terms of switch complexity and electronic processing cost [126].

Table 1.1: Evolution of WDM to DWDM systems

Time frame	WDM type	channels	Wavelength	channel spacing
1980's	Wideband	2	1310 nm, 1550 nm	–
Early 90's	Narrowband	2–8	C–band	200 – 400 MHz
Mid 90's	Dense	16–40	C–band	100–200 MHz
Late 90's	Dense	64–160	C–band	25–50 GHz
Current	Dense	160–320	C/L band	12.5–25 GHz

1.4.2 Second generation

In the second generation of optical networks, several switching and routing functions are handled optically with electronic controls. The most important enabling component technologies in the second generation of optical networks are the optical add-drop multiplexers (OADMs) [113], optical circulators and advent of erbium dopped fiber amplifiers (EDFAs) [115].

Figure 1.4 shows a schematic of an OADM system. The OADMs can add and drop a specific predefined channel (or a group of channels). They can be fixed-tuned (static) or reconfigurable(dynamic). The technology for manufacturing the static OADMs is mature. In reconfigurable OADMs (ROADMs), add-drop wavelengths can be controlled by an external command (e.g., by software or based on optical switches and fiber bragg grating [127]). Arrayed waveguide grating (AWG) [128], optical filters (e.g. fiber bragg grating and thin film filters) [127] [129], thermo-optic (glass or silicon) [130], liquid crystal [131], electro-optic ($LiNbO_3$ [132], InGaAsP [133], Mach-Zehnder [134], injection locked Fabry-Pérot laser diodes [135]) acousto-optic [136], micro electro mechanical systems (MEMS) [137] are some of technologies proposed for wavelength add/drop multiplexer (WADM) applications. WADMs are primarily employed to build optical WDM ring networks, which are expected to deploy in metropolitan area markets.

Second-generation optical networks rely on such WDM technologies and constitute the optical-layer that provides the services such as light-path and circuit-switching;

- A light-path is used in order to transmit a message between the network nodes when the light is not encountering any electronic interface. A light-path must

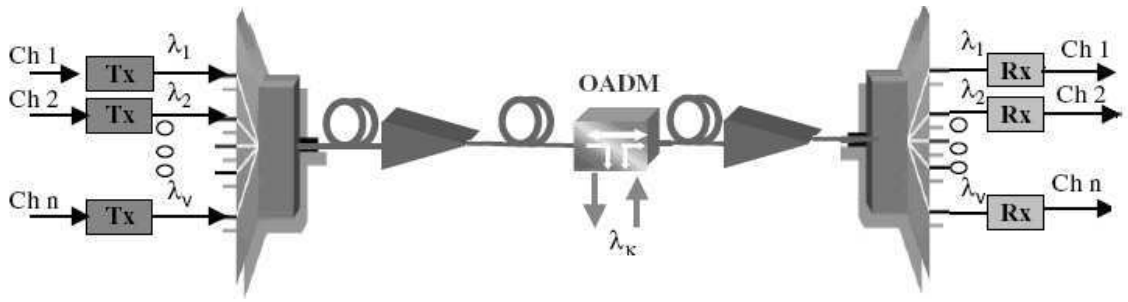


Figure 1.4: A wavelength add/drop multiplexer (WADM)

use the same wavelength on all the links along its physical route (wavelength continuity constraint)[138].

- A circuit switching network employs a dedicated circuit (or channel) between network nodes (terminals) before the users may communicate. Each dedicated circuit can not be used by other callers until the circuit is released and in order to set up a new connection. The data from a network node may be passed to a destination node over more than one switching circuit during the period of communication. However, the switching is hidden from the users.

1.4.3 Third generation

In order to build a network using multi-wavelength fiber links, appropriate fiber interconnection systems are needed [113]. Third-generation optical network architectures are based on all-optical interconnection devices. These devices fall under three categories, namely, passive star couplers, passive routers and active switches [139].

1.4.3.1 Passive star couplers

The passive star is a broadcast device to interconnect an optical network via optical fibers [140]. A signal with a given wavelength arrives on input fiber port of the star coupler. It will have its power equally divided among all output ports of the star coupler. There are several advantages to using an optical passive star network. First, it is very simple and is completely passive. Second, its scalability is very good up to a certain number of stations. Last, optical passive stars offer flexibility of topological embeddings [141].

As an example, in figure 1.5, a signal on wavelength λ_1 from input fiber1 and another on wavelength λ_4 from input fiber 4 are broadcast to all output ports. A "collision" will occur when two or more signals from the input fibers are simultaneously launched into the star on the same wavelength. A passive star coupler plays the role of hubs in LAN (local area network). Contrarily, arrayed waveguide grating (AWG) can be used in order to provide one wavelength channel to every

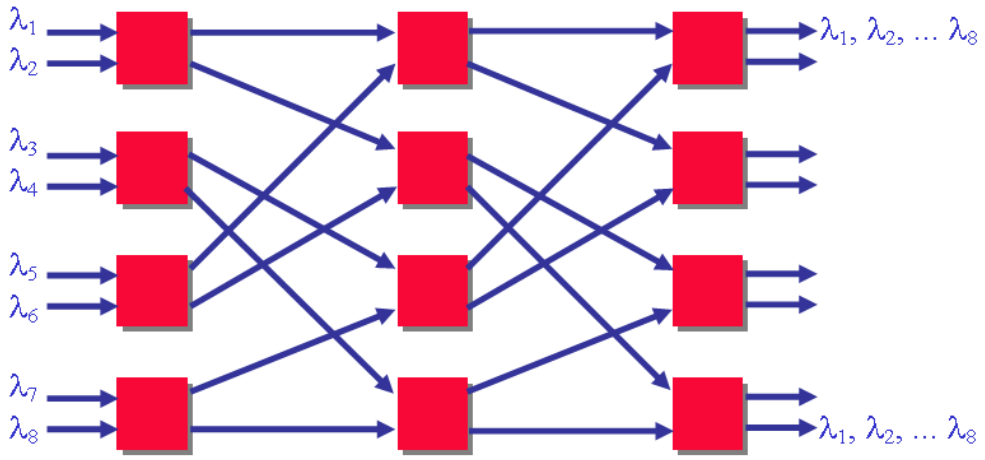


Figure 1.5: An 8×8 passive star architecture

input and every output [142] [143]. It can provide more wavelength channels than passive star coupler hubs [144].

1.4.3.2 Passive routers

Passive router separates each of input incident wavelengths to the same wavelength on separate output fibers. For example, λ_1, λ_2, λ_3, and λ_4 incident on input fiber 1 are routed to the same corresponding wavelengths to output fibers 1, 2, 3, and 4, respectively, in figure 1.6. This device allows wavelength reuse (the same wavelength may be spatially reused to carry multiple connections through the router) [145]. The wavelength on which an input port gets routed to an output port depends on a "routing matrix" characterizing the router; this matrix is determined by the internal "connections" between the demux (demultiplexer) and mux (multiplexer) stages inside the router (see figure 1.6). Such routers are also known as Latin routers [146], waveguide grating routers (WGRs) [147], wavelength routers (WRs) [148], etc. An N×N passive router can route N^2 simultaneous connections (compared to only N for the passive star). However, it lacks the broadcast capability of the star.

1.4.3.3 Active switches

The active switch is also called wavelength selective cross-connect (WSXC), wavelength-routing switch (WRS), or just cross-connect. They allow wavelength reuse and can support simultaneous connections as like as the passive router. In return, the routing matrix in the active star can be reconfigured on demand, under electronic control. However, the active switch needs to be powered. Although the active switch in figure 1.7 include the wavelength demux/mux devices, note that the mux/demux devices could be part of the (multi-wavelength) fiber transmission system.

The active switches are used in (wavelength-routed) wide-area networks, while the passive star is employed in local WDM networks. The passive router has

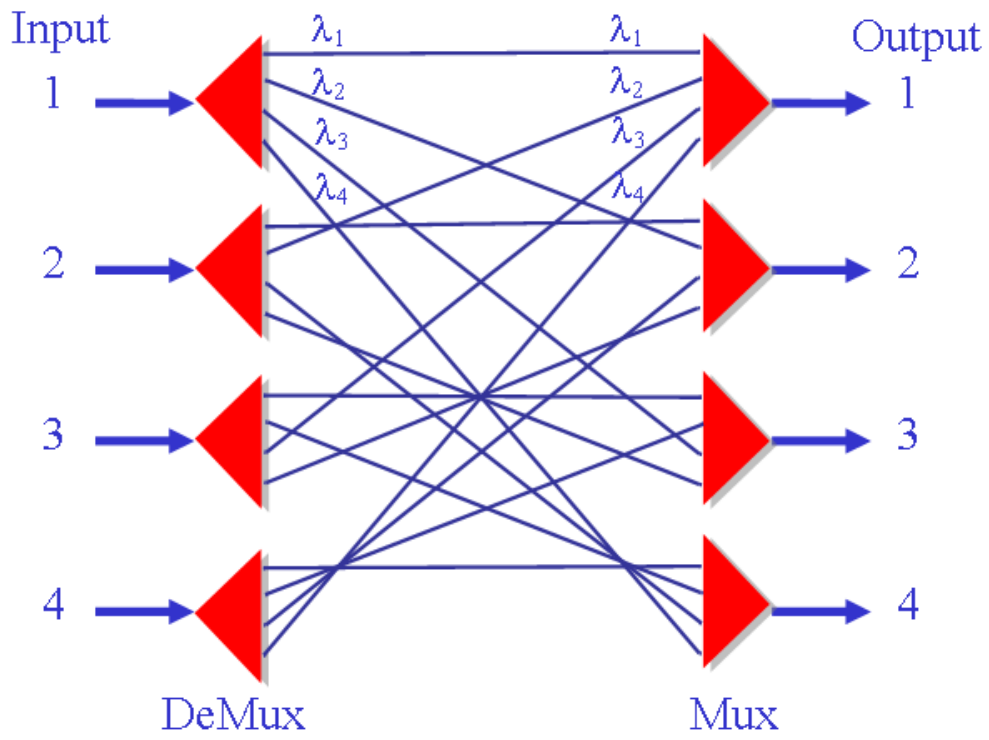


Figure 1.6: A 4×4 passive router (four wavelengths)

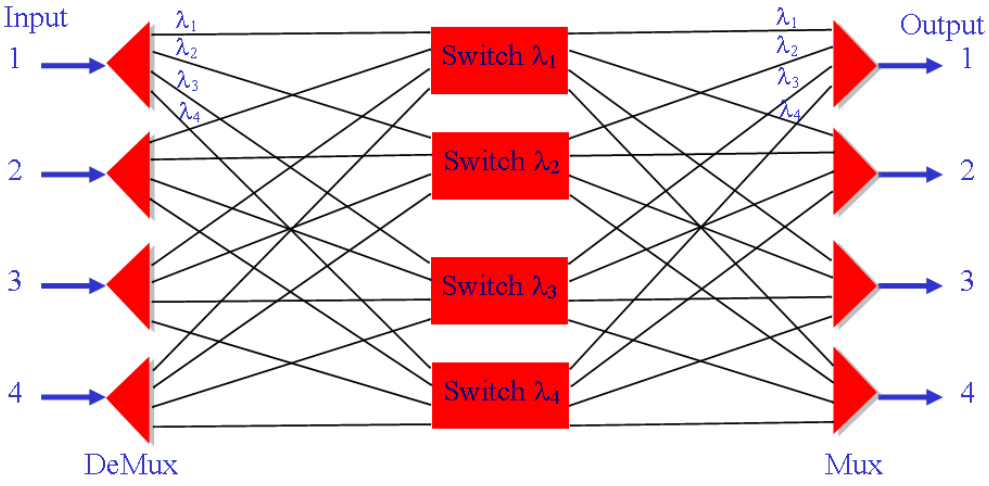


Figure 1.7: A 4×4 active switch (four wavelengths)

mainly found application as a mux/demux device. The WADM devices are mainly used in optical WDM ring networks which are expected to deploy mainly in the metropolitan area market. In the third-generation optical networks, data is allowed to bypass intermediate nodes without O/E conversion, thereby reducing the costs at each node.

1.4.4 Fourth generation

All-optical system developments are expected to provide optical circuit-switched connections, or light-paths, between the optical core network routers. However, since these circuit-switched connections are almost static, they may not be able to adapt with the bursty nature of Internet traffic in an efficient manner [149]. Ideally, in order to optimize the efficiency, nodes would need to exploit packet switching at the optical level. Such all-optical packet switching is not commercialized so far due to technological constraints. Otical burst switching is a possible near-term alternative to all-optical circuit switching and packet switching, where the packets are sent into transport units referred to as bursts.

Then, the bursts are switched through the optical core network. A greater degree of statistical multiplexing is available via the burst-switched networks. At the same time, optical burst-switched networks do not have as many technological constraints as all-optical packet-switched networks. In order to highlight the differences between optical circuit switching, optical packet switching, and optical burst switching, we discuss each approach in detail.

1.4.4.1 Optical circuit switching:

In optical circuit switching, all-optical wavelength paths (light-paths) are established between pairs of nodes. The establishment of light-paths involves several tasks including topology and resource discovery, routing, wavelength assignment, and signaling and resource reservation.

Topology and resource discovery involves the distribution and maintenance of network state information. Typically this information will include information on the physical network topology and the status of links in the network. In a wavelength-routed WDM network, this information may include the wavelength availability on a given network link. A common protocol for maintaining link state information in the Internet is the Open Shortest Path First (OSPF) protocol [150]. Typically, Routing, Wavelength Assignment and connection requests may be performed either static or dynamic.

- In the Static Light-path Establishment (SLE), the entire of the connection set is known in advance, and the problem is to set up light-paths for these connections in order to minimize the network resources such as the number of fibers or the number of wavelengths in the network. A review of approaches to the SLE problem may be found in [151].

- In the Dynamic Light-path Establishment (DLE), each light-path is set up for each connection request which will be released after some finite amount of time. The objective in the dynamic traffic cases is to set up light-paths and assign wavelengths in a manner which minimizes the amount of connection blocking or maximizes the number of established connections in the network at any time. DLE approaches are reviewed in [152].

1.4.4.2 Optical Packet switching:

Optical packet switching (OPS) became a viable candidate because of its flexibility, high-speed, fine-granularity switching, and its ability to use the resources economically. In general, optical packet-switched networks can be divided into two categories: slotted (synchronous) and unslotted (asynchronous) [153]. However, bit-level synchronization is required for packet header recognition and packet forwarding.

In a slotted network the packets have the same length (e.g. digitized voice packets). Each packet is enclasped inside a fixed time slot together with a header. The time-slot has longer duration than the packet and header to provide guard time. Slotted networks have been extensively studied, while optical fiber was being proposed as the buffer in store-and-forward contention resolution [82]. The European DAVID (data and voice integration over DWDM) project quoted synchronous slotted OPS, with a time slot in the order of $1\mu s$, as the most promising option for the WDM backbone network [81].

In unslotted networks the packets may not have the same length (e.g. IP datagrams). As the packets enter the router without any alignment, the packet switching can take place at any point in time. However, in unslotted networks, the chance of the packet contention is greater than slotted networks due to the unpredictable and less regulated behavior of the packets.

A disadvantage of using fixed-length packets is that the percentage of control overhead is higher (due to a relatively large header in each packet) and bandwidth utilization is lower (due to headers bits) than using variable-length packets. On the other hand, unslotted networks are more easier and more cheaper to build, more flexible, and more robust than slotted networks. [153].

A basic photonic packet-switch architecture is displayed in figure 1.8 [114]. Each node contains an optical switch fabric which is reconfigurable for each input packet. The switch fabric is reconfigured based on the packet header information. Resolving the issues in OPS networks will require many technical improvements in several areas [154]:

- Optical packet header (label) conceptions
- Optical header (label) processing (recognition/swapping)
- Optical packet contention resolution
- Clock extraction (bit/packet-level synchronization)

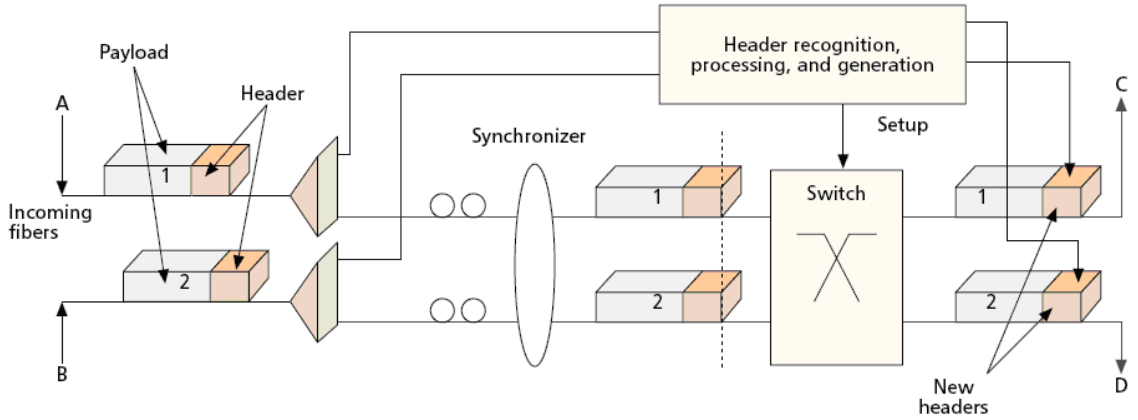


Figure 1.8: Illustrations of optical packet switching node (OPS), after [114]

- Optical packet compression/decompression
- Optical space switching
- Wavelength conversion
- 3R (reamplification, reshaping, retiming) regeneration
- Packet switching (routing) strategies
- Packet buffering.

These issues will be investigated in the forth chapter.

1.4.4.3 Optical Burst Switching (OBS):

Optical burst switching is proposed to fulfill a balance between optical circuit switching and optical packet switching [114]. In an optical burst-switched network, a data burst may consist of multiple IP packets. A control packet is transmitted in front of the burst so as to configure the switches along the burst's route. The offset time (see figure 1.9) allows for the control packet to be processed and the switch to be set up before the burst arrives at the intermediate node. Thus, neither electronic nor optical buffering is necessary at the intermediate nodes while the control packet is being processed. The control packet may also specify the burst duration in order to permit the node know when it may reconfigure its switch for the next arriving burst. Figure 1.10 illustrates a schematic of an optical burst switching node [114].

By resource reserving only for a specified period of time rather than reserving it for an indefinite period of time, the resources can be allocated in a more efficient manner and a higher degree of statistical multiplexing can be achieved. Since data is transmitted in large bursts, optical burst switching reduces the technological requirement of fast optical switches that is necessary for optical packet switching [113].

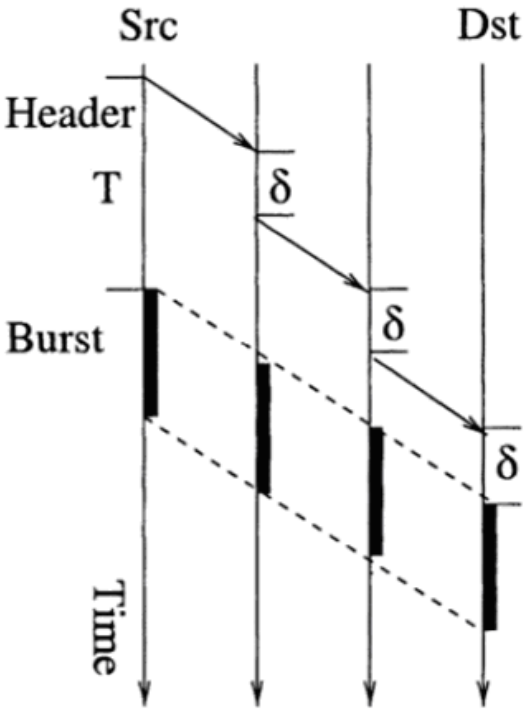


Figure 1.9: The use of offset time in Optical burst switching, after [113]

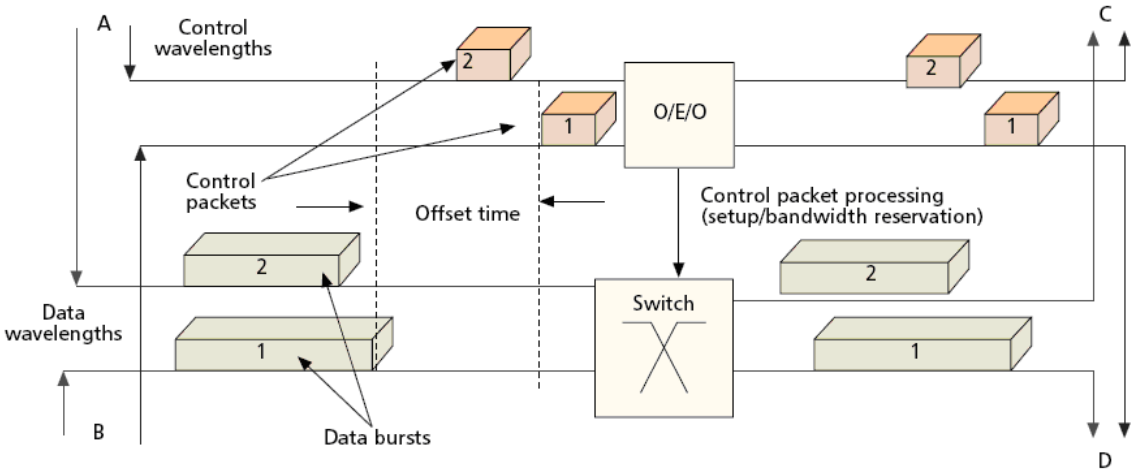


Figure 1.10: Illustrations of optical burst switching (OBS), after [114]

However, several issues in optical burst switching need to be addressed before it can be deployed in working networks. In particular, these issues include burst assembly, signaling schemes, contention resolution, burst scheduling, and quality of service;

- A burst scheme is required to determine the number and the type of the packets assembled into bursts. Issues include when to assemble a burst, how many packets to include in a burst, and what types of packets to include in a burst.

Table 1.2: Comparison between the different all-optical technologies; OCS is optical circuit switching, OPS is optical packet switching and OBS stands for optical burst switching

Optical switching paradigm	OCS	OPS	OBS
Bandwidth utilization	Low	High	High
Wavelength tuning speed vs. function	Slow	Fast	Medium
Setup latency	High	Low	Low
Switching speed request	Slow	Fast	Medium
Proc./synch. overhead	Low	High	Low
Traffic adaptively	Low	High	High

The burst assembly scheme will affect the burst length as well as the amount of time that a packet must wait before being transmitted [155].

- A signaling protocol is required for configuring switches and reserving resources for an arriving burst. Tell-and-go (TAG), tell-and-wait (TAW), and just-enough-time (JET) are some of the common signaling schemes for reserving resources in OBS networks [113].

- In the TAG and JET protocol, the sources do not wait for an acknowledgement before sending a burst. Thus, it is possible that the reservations fail at some node in the path. In this case, the burst will experience contention. Contention happens when multiple bursts contend for the same resource at the same time. It may be resolved in a number of ways;

  - Optical buffering: Storing the bursts until the appropriate resources become available [76].
  - Deflection routing: Deflect one of the bursts to a different output port [156].
  - Wavelength conversion: In this method, the appropriate wavelength for a burst on an outgoing link must be determine. This problem is referred as channel scheduling [157]. [158].

  When contention resolution techniques are not successful, the burst must be dropped. Burst segmentation is a method to reduce the dropped bursts during a contention. In burst segmentation, only those parts of a burst that overlap with another burst will be dropped [159].

- In order to provide quality of service for different classes of traffic, burst assembly, contention resolution, channel scheduling, and signaling protocols can be modified.

Table 1.2 summarizes the mentioned different optical switching paradigms.

1.5 Optical networks node architecture (transparent vs. opaque networks)

The network structure of existing core networks is currently transformed from rings (using SONET Add/Drop Multiplexers) to mesh topologies (using Optical Cross-connects (OXCs)) [160]. An OXC can be implemented either in the electronic (opaque) [161] or in optical (transparent) domain [162].

In an opaque architecture, the optical signal carrying traffic experiences an optical to electronic and an electronic to optical (O-E-O) conversion at different nodes in the network. The electronic signals are then switched in electronic and are converted back into optical signals in order to be multiplexed via optical multiplexers onto outlet optical fibers. The opaque network offers the following key factors to build a large-scale manageable core mesh network [163]:

- No cascading of signal impairments. The network size can be large since signal regeneration is present in every network node.
- Multi-vendor inter-operability.
- Wavelength conversion. All of the network capacity can be utilized for service without any restrictions and additional significant cost saving in a mesh architecture.
- Support the management and control functions of the network. This allows full flexibility in the signal routing.

However, a bottleneck is the electronic circuits maximum bandwidth. A transparent architecture, in the strict sense, means that the optical signal carrying traffic stays in the optical domain end-to-end communication of data (from the time it is generated at the edge of the network until it leaves the network), independent of bit rates and signal modulation formats. Such a network node is often called a transparent OXC or photonic cross-connect (PXC) [164]. A variety of technologies (such as micro electro mechanical systems (MEMS) [165], liquid crystals [166], bubbles [167], holograms [168], and etc.) can be used in PXC applications.

Translucent OXC is proposed as an accommodation between opaque and transparent OXC's [169]. It consists of an optical switch and an electronic switch modules. When the optical switches are busy or an signal regeneration is required, the electronic module is used [170].

However, the transparent network is still a hot research subject because of the technical problems such as computational power, storage capacity, real-time processing, inflexibility of configuration and network-level cost.

1.6 Optical network protocols

In packet based telecommunication networks, the layered architecture permits to assign the different functions to each layer as appropriate. This simplifies the design,

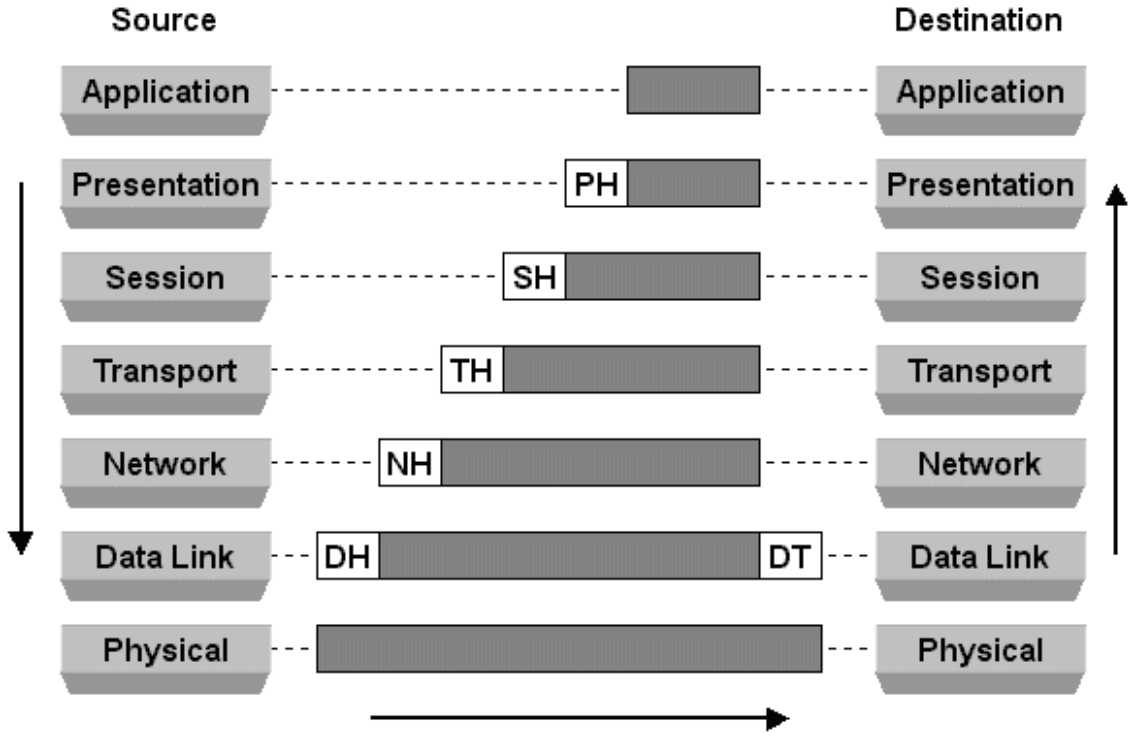


Figure 1.11: Open Systems Interconnection (OSI) model

development, and operation of the network, and allows smooth network evolution. Each network layer can evolve independently with either different protocols or different technologies. In this section, firstly, we review the classic networking model and afterwards the evolution of optical networks protocols will be presented.

1.6.1 Open Systems Interconnection (OSI) networking hierarchy

In the late 1970s, the International Organization for Standardization (ISO) began to develop its Open Systems Interconnection (OSI) networking model [171]. This model of networking is composed of seven layers (see figure 1.11);

Layer 1-Physical layer: It contains all the physical devices, such as physical cabling (copper, fiber optic, a radio link and etc.), Hubs, repeaters and network adapters, for data telecommunications. It is responsible to transfer the bit stream between the network nodes.

Layer 2-Data link layer: This layer furnishes data packets encoding and decoding into bit streams, ransmission protocol management, errors handling in the physical layer, and frame synchronization. The data link layer is divided into two sub-layers: The Media Access Control (MAC) and the Logical Link Control (LLC). The MAC layer controls the the data access and transmission. Frame synchronization, flow control and error checking are controled by LLC layer.

Layer 3-Network layer: The network layer transfers variable length data sequences via one or more networks while maintaining the quality of service requested by the transport layer. Routing, error cheking, congestion control and packet sequencing are the major functions of this layer. Routers operate at this layer.

Layer 4-Transport layer: It offers transparent transfer of data between end users. The transport layer controls the reliability of a given link through flow control, segmentation/desegmentation, and error control. The well known example of a layer 4 protocol is the Transmission Control Protocol (TCP).

Layer 5- Session layer: It establishes, manages and terminates the connections between the end-point nodes.

Layer 6-Presentation layer: It transforms data to provide a standard interface for the application layer. Data compression and data encryption are done at this layer.

Layer 7-Application layer: The application layer permits the user to access information on the network through a protocol such as File Transfer Protocol (FTP), applications which use Simple Mail Transfer Protocol (SMTP) and applications which use HyperText Transfer Protocol (HTTP).

As shown in figure 1.11, each layer adds its associated header information. This addition of a header to the higher layer data unit is also called encapsulation. For example, the presentation layer adds a presentation header (PH), the session layer a session header (SH), and so on. Note that the data link layer adds both a header (DH) and a trailer (DT); the DT header contains CRC (Cyclic Redundancy Check) and the frame boundary identifications. Finally, the physical layer transfers the data (frame) over the physical medium. At the receiver, the above steps are followed in reverse order.

1.6.2 Optical Transport Network (OTN)

The physical layer, as shown in the previous sections, has to handle the transmission over the physical media which includes the representation of the bytes, line-coding, modulation, signal power, etc. From the perspective of the data transmission network each optical channel behaves like a physical medium, therefore one could refer to an optical channel as a "virtual physical medium" on a optical fiber, which is capable to transport hundreds of optical channels. Moreover, optical channels (wavelengths) can be transported across a whole country and can be bridged from one operator to another operator. These relationships between operators and the size of the network require additional functionalities to configure and protect channels, to measure the signal quality of each channel, to detect failures and to isolate the different areas of responsibility between different operators [172].

The concept of the optical transport network (OTN, standardized by the ITU-T) covers these operator specific functionalities. The OTN is structured in a hierarchical

Table 1.3: Tolerance levels by data type

Data type	Tolerance packet loss	Level delay sensitive
Voice	Low	High
Video	Moderate	High
Data	High	Low

order and is used either as an end-to-end networking entity or as point-to-point structure for operations, administration, and maintenance (OAM) purposes. Optical data networks are typically constructed with four stacked layers [154]:

Internet Protocol (IP) layer: The Internet Protocol (IP) is a network-layer (layer 3) protocol that contains the routing information of packets as well as carrying applications and services.

Asynchronous Transfer Mode (ATM) layer: It is responsible for traffic engineering and quality of service. The ATM is a Connection-Oriented protocol in which connection setup is performed before transferring information. ATM was designed with a view to transmitting voice, video, and data on the same network. These different types of data are different in terms of packet loss and end-to-end delay, as shown in table 1.3. For instance, packets containing voice have to be delivered on time so that the play-out process at the destination does not run out of data. On the other hand, the loss of some data might not necessarily deteriorate the quality of the voice delivered at the destination. At the other extreme, when transporting a data file, loss of data cannot be tolerated since this will compromise the file's integrity, but there is no stringent requirement that the file should be delivered as fast as possible.

SONET/SDH layer: Synchronous Optical NETworking (SONET) and Synchronous Digital Hierarchy (SDH) standards were proposed for the transmission of time division multiplexing (TDM) of digital signals over fiber in the 1980s. Using TDM, a data stream at a higher bit rate is generated by multiplexing the lower bit rate channels. SONET defines Optical Carrier (OC) levels and electrically equivalent synchronous transport signal (STSs) for fiber-optic based transmission hierarchy [126]. High-capacity SONET/SDH systems now operate up to 10 Gbit/s (OC-192). The architecture is reliable for the transport of voice services. Table 1.4 shows the SONET hierarchy.

DWDM layer: Wavelength division multiplexing (WDM) systems employ different colors of light in the same fiber to carry the different channels of information. Each channel (wavelength) of the WDM signal can handle up to 160 sub-channels and can thus expand a basic 10 Gbit/s fiber system to a theoretical total capacity of over 1.6 Tbit/s over a single fiber optic [173]. Narrower channel spacing (50 GHz) permits to increase total dense wavelength division multiplexing (DWDM) system capacity [174].

Table 1.4: SONET system hierarchy

Transmission standards	Bandwidth (Bit per second)
STS-1, OC-1	51.840 Mbps
STS-3, OC-3	155.520 Mbps
STS-12, OC-12	622.080 Mbps
STS-48, OC-48	2,488 Gbps
STS-192, OC-192	9.953 Gbps
STS-768, OC-768	39.813 Gbps

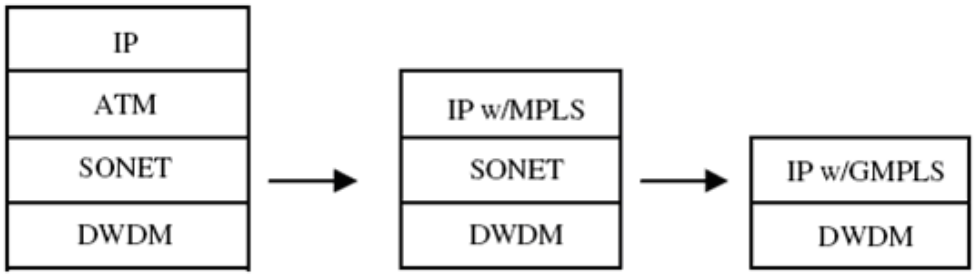


Figure 1.12: Evolution of technology toward photonic networking, after [115]

Although this layered architecture provides some benefits, it also leads to inefficiencies and increases the latencies of connections. Furthermore, there is some duplication of transport protocols and management tasks [175]. Therefore, optimizing the network in order to achieve flexibility, scalability, and cost effectiveness will require a simplified layer configuration.

MPLS networks are the alternatives for high throughput, low packet loss probability, short delay, high signal quality of outgoing packets, transparency to data rate and format, small power consumption, and compactness. It can be used to carry many different kinds of traffic, including IP packets, as well as ATM, SONET, and Ethernet frames. Figure 1.12 shows the evolution of optical network technologies.

1.6.3 Multi-Protocol Label Switching (MPLS)

MPLS accumulates some properties of circuit-switched network over packet-switched network. It is standardized by the Internet Engineering Task Force (IETF) to enhance the speed, scalability, and service provisioning capabilities in the Internet. As a technology for backbone networks, MPLS can be used for IP as well as other network-layer protocols. It has become the prime candidate for IP-over-ATM backbone networks [176], [177]. MPLS is based on the following concepts [178], [179], [180]:

- It is a connection-oriented protocol which appears between the data link layer and the network layer (OSI Model).
- It uses the distributed control protocols for path setting up.

- IP router's function is separated in two parts: forwarding and control.
- It uses labels in the place of IP addresses to eliminate IP header interrogating of each packet at every intermediate router.
- It uses label swapping technique to support multiple-routing paradigms.
- It supports the IP, ATM, and frame-relay layer 2 protocols.
- It supports the delivery of services with QoS guarantees and thereby facilitates voice, video, and data service integration.
- It provides flexibility in the delivery of new routing services.
- It facilitates scalability through traffic aggregation.
- It allows the construction of virtual private network (VPN) in IP networks.

In a conventional IP network, streams of traffic between two network nodes are divided into many IP packets with each packet having its own header. Along the way, each router inspects every packet header in order to route it. The less time routers spend inspecting packets, the more time they have to forward them. It is a waste of resources to inspect every IP packet header when transferring a large number of packets destined for the same destination from the same source. MPLS recognizes such packets and adds a special label identifying them as a unified flow of information. Intermediate routers would then see the labels and forward them rapidly toward their destination. Optical burst switching techniques facilitate the extension of the MPLS framework [181], [114].

At the ingress point (the point at which traffic enters the network) of an MPLS network, the label edge router (LER) adds a label to each incoming IP packet according to its destination and the state of the network. The label is embedded in the layer 2 protocol header of the packet. Each intermediate router needs information on the topology and status of the network, and where the egress of the respective destination is located. Label switching relies on the setup of switched paths through the network known as label switching paths (LSPs). In other words, LSP is an established logical MPLS connection, which links an LER via a label switched router (LSR) to another LER, as illustrated in figure 1.13.

Thus, an MPLS network consists of MPLS nodes called label switch routers (LSRs) connected by circuits called label switched paths (LSPs). The main component of MPLS architecture is the label distribution protocol (LDP), which is a set of protocols by which an LSR communicates with an adjacent peer by means of exchanging labels. To establish an LSP, a signaling protocol such as LDP is needed. Each LSP has a forwarding equivalent class (FEC) associated with it. The classification of packets into specific FECs identifies the set of packets that will be mapped to a path through the network. At the ingress of an MPLS domain, all incoming packets will be assigned to one of these FECs. Once a packet gets to the end of the last egress edge router, the labels are popped and the packet is routed according

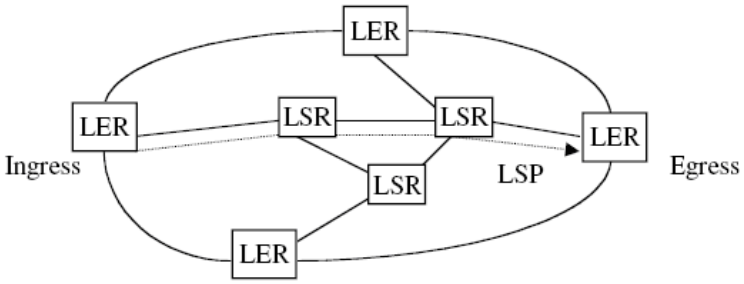


Figure 1.13: MPLS architecture; LER- Label edge router, LSR- Label switching router LSP- Label switched path

to the conventional IP rules. The European IST-DAVID (data and voice integration over DWDM) project investigates in optical packet switching with MPLS control plane for MANs/WANs [81].

1.6.4 Multi-Protocol Lambda Switching

In 1999, and MPλS was designed for intelligent usage of optical resources. It builds on top of the existing traffic-engineering tools found in MPLS to provide a common platform for managing both the IP and the optical layers [182]. The main idea was to facilitate provisioning and reconfiguration of lightpaths in optical cross-connects (OXCs) [183]. MPλS utilizes the following components of MPLS traffic engineering control plane:

- Resource discovery
- State information dissemination
- Path selection
- Path management.

The basic assumption of MPλS is that OXCs as network elements are capable of reconfiguring optical circuits. This differs from OLS where the assumption is that optical-label switching routers (OLSR) are capable of packet, circuit, or burst switching directly in the optical layer. While MPLambdaS was successful in combining MPLS with WDM, the integration between data networking and optical networking was insufficient. MPLambdaS maintains a master-slave relationship between MPLS and OXCs whereas optical-label switching will seek a seamless integration between data and optical networking by means of optical-labels. Another key difference is that MPLambdaS will perform wavelength conversion only if wavelength-interchanging cross-connects are utilized.

1.6.5 Generalized Multiprotocol Label Switching (GMPLS)

Although MPLS was designed exclusively for packet services, the primary goal of GMPLS is to provide a single suite of protocols that would be applicable to all kinds

of traffic. GMPLS permits simplification of networks and improves their scalability in ways unheard of until now. The basic features of GMPLS include the following [115]:

- It is a set of traffic engineering to existing MPLS routing and signaling protocols.
- It is an optical networking standard that represents an integral part of next-generation data and optical networks.
- It provides the necessary bridge between IP and optical layers.
- It brings more intelligence to optical networks (better restoration and better bandwidth utilization).
- It is designed to allow edge networking devices such as routers and switches to request bandwidth from the optical layer.
- It is designed to support multiple switching layers such as packet switching, time-division switching (SONET/SDH, PDH), wavelength switching and spatial switching.

1.7 Summary

This chapter attempts to briefly discuss the optical network issues. Network evolutions have always been induced by various technologies, as we have seen with synchronous optical network (SONET), asynchronous transfer mode (ATM), and MPLS. It seems that the all-optical packet switching will eventually emerge as one such technology, which will significantly impact on next-generation networks. The optical packet networks' building blocks, and more specifically, packet label processing methods and routing algorithms will be investigated in chapter 4. Moreover, all-optical signal processing and in particular optical packet label processing alternatives are investigated in the following chapters.

CHAPTER

2

Semiconductor Optical Amplifiers

2.1 Introduction

The history of Semiconductor Optical Amplifiers (SOAs) goes back to the beginning of the 1980s where linear amplification in point-to-point systems was needed. With the arrival of the erbium doped fiber amplifier (EDFA) around 1990 the SOA were out-competed as a linear amplifier. But the nonlinear behaviors of SOA together with high gain make it a good choice for nonlinear optic functionalities [27]. In addition, the SOAs have several advantages such as:

- Fast gating and switching [184]
- Fast carrier dynamics
- Compact size
- Potential for photonic integration with other device structures [185]
- Relatively broad optical bandwidth (120 nm) [1]
- Moderate to low power consumption [186]

However, SOAs have some disadvantages such as relatively high noise, susceptibility to electrostatic shock and high cost for early devices. Moreover, a serious restriction on the operation of SOAs is caused by the gain saturation effect caused by carrier depletion. This results in an optical gain reduction at high input powers

and serious waveform distortion known as the patterning effect [187]. In this chapter, a brief introduction on the SOAs, their operation principle and their nonlinear effects are reviewed. Next, a new method for polarization sensitivity reduction of the four-wave mixing in SOA thanks to a spectrum-sliced incoherent light source is presented.

2.2 SOA structure

An SOA is basically a semiconductor laser operated as a broadband single-pass device for amplification. SOAs are classified into two main types:

- The Fabry-Pérot SOA (FP-SOA) where reflections from the end facets are significant (i.e. the signal undergoes many passes through the amplifier).
- Traveling-wave SOA (TW-SOA) where the reflections are negligible (i.e. the signal undergoes a single-pass of the amplifier).

The FP-SOA is biased under its threshold current and provides significant amplification, but it is more sensitive to fluctuations in bias current, temperature and signal polarization compared than the TW-SOA [188]. In addition, due to the end facet reflections of the FP-SOA, its gain spectrum is frequency dependent. Therefore, the traveling-wave SOA has replaced the Fabry-Pérot SOA in almost all practical applications. To achieve a stable amplification in a traveling-wave SOA (which will simply be called SOA from now on), the facet reflectivity must be reduced ($\sim 10^{-5}$). A number of methods such as anti-reflection coating [189], angled facets [190], buried facets (windows) [191] or a combination of them [192] can be used for facet reflectivity reduction. Figure 2.1 shows the schematic of a typical InGaAsP/InP SOA architecture.

There are several structures proposed for the SOA active region;

Bulk: These SOAs have only one single active layer.

Multiple quantum well (MQW): A MQW structure consists of a sandwich of different layers. The MQW-SOA has generally a larger gain bandwidth, a higher output saturation power and low polarization dependence than the bulk SOA devices [193].

Quantum dot (QD): A quantum dot is a semiconductor nanostructure in which the electrons are confined with respect to motion in all three dimensions. A high unsaturated optical gain can be obtained from QD-SOA at a low device current [194].

Gain-Clamped (GC): In GC-SOA, the SOA gain is clamped by an internal laser in order to prevent gain saturation. The gain clamping is achieved by forcing the SOA to lase at a wavelength λ_{laser} lying outside the desired bandwidth of the SOA (for instance λ_{laser}=1580 nm for λ_{signal}=1550±20 nm) [195]. The carrier

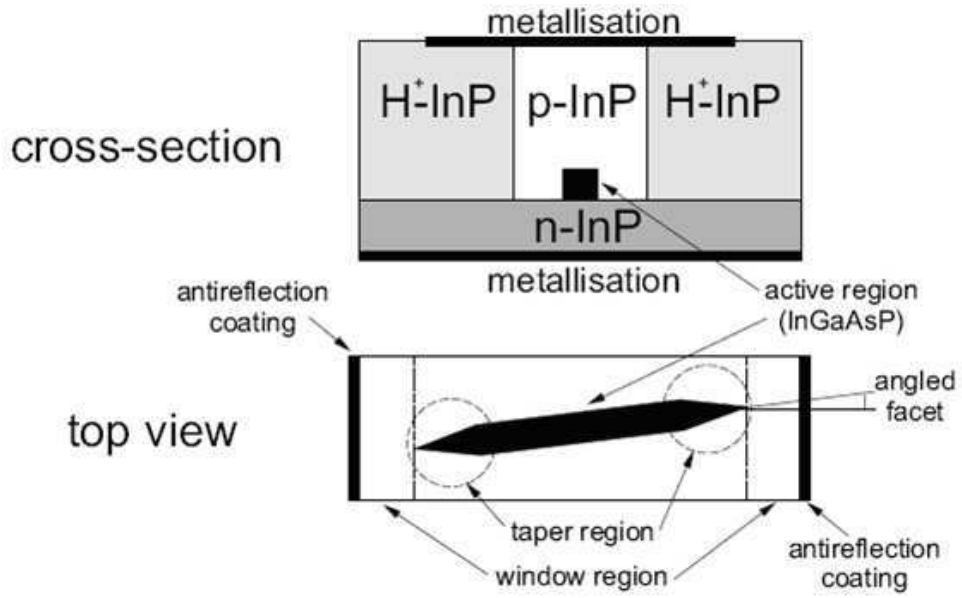


Figure 2.1: Schematic cross-section and top view of a buried ridge stripe SOA, after [116]

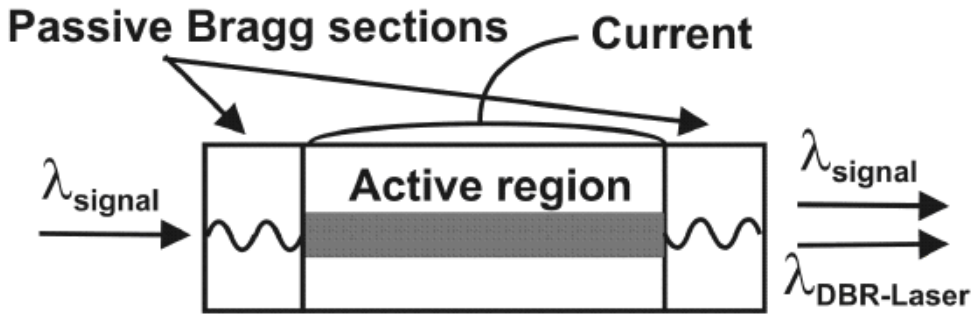


Figure 2.2: Schematic view of a DBR-SOA (GC-SOA), after [117]

density in a laser is constant when it operates above threshold. Hereby, a signal coupled to the device will show a constant gain (only the laser power will decrease by increasing the injected beam). Therefore, the SOA gain is stabilized at a lower level compared to the conventional SOA. For example, the GC-SOA fabricated by Avanex is accomplished by adding the passive distributed Bragg reflector (DBR) for each end of a conventional SOA in which the lasing is achieved at the Bragg wavelength [196]. Figure 2.2 illustrates a schematic view of a DBR-SOA.

Reflective SOA (R-SOA): The R-SOA utilizes a high reflectivity coating on one facet, along with a curved waveguide, and ultra low reflectivity coating on the other facet to produce a highly versatile reflective gain medium. It is proposed either as detector or signal modulator in the fiber-to-the-home networks [197] [198].

Table 2.1: Comparison of different state of the art SOAs

Technique	Gain (dB)	NF (dB)	P_{Sat}(dBm)	Current (A)	Bandwidth (nm)
Bulk [202]	> 29		> 9	0.2	50
Bulk [203]	> 15	< 6	> 17.6	0.5	C band
MQW[204]	> 26		17	0.24	85(1500−1585)
MQW [205]	> 26	< 9	> 7.5	0.15−0.25	C-band
QD [206]	> 20	< 7	> 19	1−2.5	120(E&S-band)
QD [207]	> 10	< 9	> 19	1−2	C-band
GC [208]	> 9	< 12	> 10	0.15 − 0.2	
GC [209]	> 12	< 8.2	13	0.2−0.25	C-band
R-SOA [210]	> 18	< 10	> 10	0.08−0.12	C-band

In table 2.1, a brief comparison between the SOAs fabricated by different companies using different techniques for the SOA active area are shown. The operation of SOAs at high speed (upper than 10 Gbit/s) is limited by their inherent recovery time (100-300 ps). There are different approaches to speeding up this recovery time, like use of a holding beam [199], long SOAs, and quantum dot based SOAs [200] [201]. It has been shown theoretically that in SOAs having quantum dots as their active medium can operate at 40 Gbit/s or even higher with recovery times on the order of 20 ps [200].

2.3 Operation principle of the SOA

The operation principle of the SOA lies in the creation of an inversion in the carrier population used to amplify the input optical signal via stimulated emission. The population inversion is achieved by electric current injection into the SOA. Figure 2.3 displays the simplified band structure of a direct-gap semiconductor. The conduction band and the valence band are separated by the band-gap energy E_g.

The current injection leads to free electron-hole pairs generation in the conduction band and valence band, respectively. In quasi-equilibrium the relaxation times for transitions within either of the bands are much shorter than the relaxation time between the two bands. So, the carrier distribution within each band can be described by two quasi-Fermi levels (denoted as E_{fc} and E_{fv}). The position of the quasi-Fermi levels is determined by the current injection (pumping rate).

If the current injection is sufficiently large the separation between the quasi-Fermi levels exceeds the band-gap energy ($E_{fc} - E_{fv} > E_g$) and the semiconductor acts as an amplifier for optical frequencies (ν) with

$$E_g < h\nu < E_{fc} - E_{fv} \tag{2.1}$$

The medium is transparent for photons which their energy is below the band gap ($h\nu < E_g$), whereas absorption dominates over stimulated emission for photon

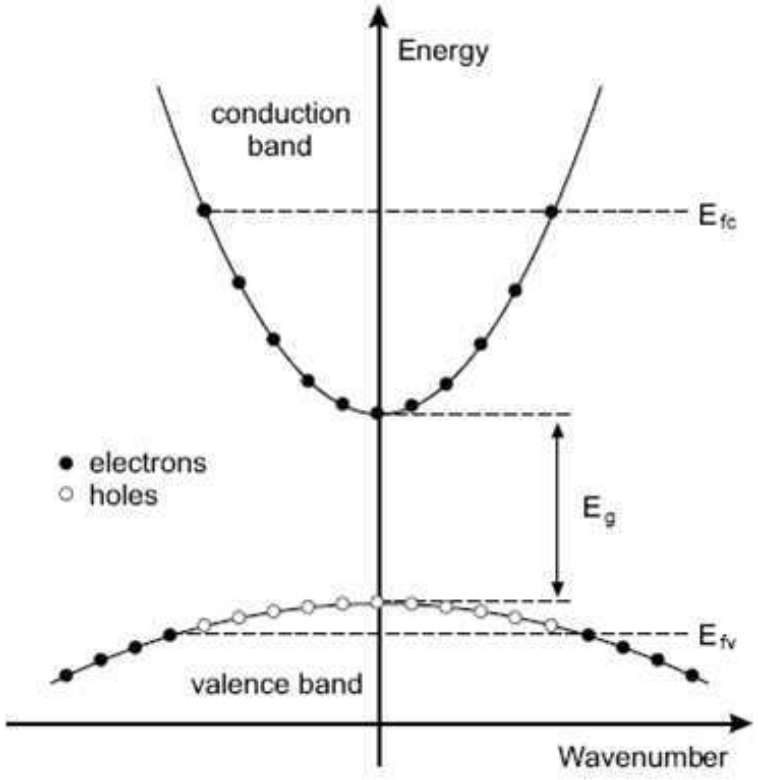


Figure 2.3: Simplified band structure of a direct-gap semiconductor in quasi-equilibrium, after [116]

energies larger than $\Delta E_f = E_{f_c} - E_{f_v} (h\nu > \triangle E_f)$ and the material acts as an attenuator. The propagation of light power along the z axis in an amplifying medium can be described by [116],

$$\frac{d}{dz}P(z) = [\Gamma g(z) - \alpha_s]P(z) \tag{2.2}$$

where $P(z)$ is the optical power at the longitudinal coordinate of the SOA (z), α_s denotes the scattering losses, Γ is the confinement factor which describes the gain reduction due to the spreading of the optical mode beyond the active region of the SOA, and $g(z)$ is the local gain coefficient. The single-pass gain G of an SOA is defined as the ratio of the output optical power, $P(L)$, to the SOA input optical power, $P(0)$. It is obtained by integration of equation (2.2) over the length L of the active region:

$$G = \exp\left(\int [\Gamma g(z) - \alpha_s]\, dz\right) \tag{2.3}$$

In the small-signal regime, $g(z)$ can be replaced by the spatially uniform, unsaturated gain coefficient g_0, which gives $G = \exp[(\Gamma g_0 - \alpha_S)L]$. The unsaturated gain coefficient is a function of optical frequency (or wavelength) and the carrier density. In general, the confinement factor Γ for the two fundamental modes TE and TM in the SOA is different [188].

2.4 Wave equation and nonlinear effects of SOA

The propagation of optical fields can be explained by Maxwell's equations. In a nonmagnetic, charge free and dielectric media (e.g. optical fiber), the wave equation is written as [211],

$$\nabla^2\overline{E} - \frac{1}{c^2}\frac{\partial^2}{\partial t^2}\overline{E} = \frac{1}{\varepsilon_0 c^2}\frac{\partial^2}{\partial t^2}\overline{P} \tag{2.4}$$

where ε_0 is the electric permittivity of free space and c is the speed of light in vacuum.$\overline{E}$ is the electric field vector of the optical field and $\overline{P}$ is the polarization density vector inside the medium due to the optical field. The wave equation in frequency domain is written as

$$\nabla^2\tilde{E}(\omega) + \frac{\omega^2}{c^2}\tilde{E}(\omega) = -\frac{\omega^2}{\varepsilon_0 c^2}\tilde{P}(\omega) \tag{2.5}$$

where $\tilde{E}(\omega)$ and $\tilde{P}(\omega)$ are the Fourier transform of the electric field $\overline{E}(t)$ and the polarization density $\overline{P}(t)$ respectively. In general $\tilde{P}(\omega)$ is a function of $\tilde{E}(\omega)$ which can be separated into linear and nonlinear parts;

$$\tilde{P}(\omega) = \underbrace{\tilde{P}^{(1)}(\omega)}_{linear} + \underbrace{\tilde{P}^{(2)}(\omega) + \ldots + \tilde{P}^{(n)}(\omega)}_{nonlinear} \tag{2.6}$$

with

$$\begin{aligned}\tilde{P}^{(n)}(\omega) = \varepsilon_0 \int_{-\infty}^{+\infty}\cdots\int_{-\infty}^{+\infty}\chi^{(n)}(-\omega_\sigma;\omega_{a1},\cdots,\omega_{an})|\tilde{E}(\omega_{a1})\cdots \\ \tilde{E}(\omega_{an})\,\delta(\omega-\omega_\sigma)\,d\omega_{a1}\cdots d\omega_{an}\end{aligned} \tag{2.7}$$

and

$$\omega_\sigma = \omega_{a1} + \omega_{a1} + \ldots + \omega_{an} \tag{2.8}$$

$\chi^{(n)}$ is the n$^{\text{th}}$-order susceptibility tensor which is independent of the electric field $\bar{E}$. The nonlinearity is called resonant, if the optical frequencies are close to transition frequencies in the medium. Therefore, specific susceptibilities are enhanced (resonance enhancement). So, the small-perturbation made by the non-resonant cases may be ignored. It is therefore not useful to write $\bar{P}$ as a power series in $\bar{E}$. A "field corrected" susceptibility (as $\bar{\chi}(\omega,\bar{E})$) is introduced instead, so that $\bar{P}$ can be expressed as [212],

$$\bar{P} = \varepsilon_0\bar{\chi}(\omega,\bar{E})\,\bar{E} \tag{2.9}$$

The susceptibility $\bar{\chi}(\omega,\bar{E})$ is in general complex and describes a number of different nonlinear effects. Due to the resonant nature of the nonlinearity, the SOA has a strong nonlinear behavior, despite its short interaction length. Thus, the Maxwell's equation is modified as,

$$\nabla^2\tilde{E}(\omega) + \frac{\omega^2}{c^2}\left[1 + \frac{j\sigma}{\varepsilon_0\omega}\bar{\chi}(\omega,\tilde{E})\right]\tilde{E}(\omega) = 0 \tag{2.10}$$

Compared to (2.5) the wave equation for the SOA has an additional term to include the conductivity σ of the SOA. The SOA susceptibility ($\bar{\chi}(\omega, \bar{E})$) is treated as a scalar quantity which can be decomposed in two parts:

$$\bar{\chi}(\omega, \bar{E}) = \bar{\chi_0} + \bar{\chi_p} \tag{2.11}$$

where $\bar{\chi_0}$ is the medium susceptibility in the absence of external current pumping and $\bar{\chi_p}$ is the additional contribution to the susceptibility related to the external current pumping. The refractive index (n) and the absorption coefficient (α) are the real and imaginary part of $\bar{\chi}(\omega, \bar{E})$, respectively [212];

$$\begin{aligned} n^2 &\approx n_b^2 + \Re\left\{\bar{\chi}_p\right\} \\ \alpha &\approx \frac{\omega}{cn}\left[\Im\left\{\bar{\chi}_0 + \bar{\chi}_p\right\} + \frac{\sigma}{\varepsilon_0 \omega}\right] \end{aligned} \tag{2.12}$$

where $n_b^2 \approx 1 + \Re\{\bar{\chi}_0\}$ is the background refractive index of the unpumped material. The refractive index n depends on the electric field ($\bar{E}$). This leads to a number of nonlinear effects, including the nonlinear refractive index changes used in interferometric devices. The absorption coefficient in 2.12 has three contributions arising from different sources. The term $\Im\{\chi_0\}$ accounts for the material absorption, while $\Im\left\{\chi_p\right\}$ is responsible for its reduction with the external pumping. Their combined effect is generally described as the net optical gain [212].

$$\Gamma g = -\frac{\omega}{cn_b}\Im\left\{\bar{\chi}_0 + \bar{\chi}_p\right\} \tag{2.13}$$

Here, g is the optical gain and Γ is the confinement factor. The net optical gain g depends on the electric field, which leads to nonlinear behavior of the optical gain in the SOA. The last term in 2.12 accounts for other internal losses which are summarized by

$$\alpha_{in} = \frac{\sigma}{c\varepsilon_0 n} \tag{2.14}$$

By using 2.13 and 2.14, the standard formula for the net absorption coefficient of the SOA can be derived [212].

$$\alpha = -\Gamma g + \alpha_{int} \tag{2.15}$$

2.5 Phenomenological description

The gain of the SOA results from transitions between the conduction and valence bands. These transitions depend on the carrier density and distribution in both bands. There are two classes of dynamical processes in the SOA; interband and intraband processes. So, the gain coefficient can be expressed by

$$g = \underbrace{g_{cdp}(N)}_{interband} + \underbrace{g_{ch}(N,T) + g_{shb}(N,T)}_{intraband} \tag{2.16}$$

where $g_{cdp}(N)$ is due to interband processes (e.g. spontaneous emission, stimulated emissions and absorption) depended on the carrier density whereas $g_{ch}(N,T)$ and $g_{shb}(N,T)$ are because of the intraband processes (e.g. carrier heating and spectral hole burning).

2.5.1 Interband processes

The interband dynamic refers to the exchange of carriers between the conduction band and the valence band which affects the carrier density. The interband energy gap implies the recovery of the carrier density (N) which is a slow process (with a time constant in the range of several tenths of picoseconds). This time constant depends on the SOA geometry and the operating conditions [116]. The recovery time is reduced by an assist light beam in the SOA [213]. Interband mechanism dominates the SOA dynamics when long optical pulses are used.

2.5.2 Intraband processes

When the SOA is operated using pulses shorter than few picoseconds, intraband effects become important. They change the electron distribution within the conduction band and the hole within the valence band. The two main intraband processes are spectral hole burning (SHB) and carrier heating (CH);

- When an short optical pulse arrives to the SOA, it interacts only with a certain part of the carrier distribution, depended on the photon energy and the spectral width of the pulse. This effect is called the spectral hole burning. The pulse causes a reduction (hole) in the carrier distribution at the particular photon energy (a deviation from the Fermi distribution). The time τ_{shb}, which is the time needed to restore the Fermi distribution by scattering processes (mainly carrier-carrier scattering), is typically several tens of femtoseconds.

- CH tends to increase the temperature of the carrier distribution above the lattice temperature. The distribution cools down to the lattice temperature through phonon emission. These processes include stimulated emission and absorption [214]. The CH recovery time τ_{ch} is several hundreds of femtoseconds to a few picoseconds.

The CH and SHB lifetimes have been measured experimentally by Zhou et al. [215] and it is believed that carrier-carrier scattering occurs at a time scale of 50-100 femtoseconds.

2.6 Gain-transparent operation

As mentioned before, the SOA gain coefficient and refractive index can be described as a function of the carrier density (see equation 2.12 and 2.16). They change by the injection of an optical pump beam into the SOA. When another light beam (probe

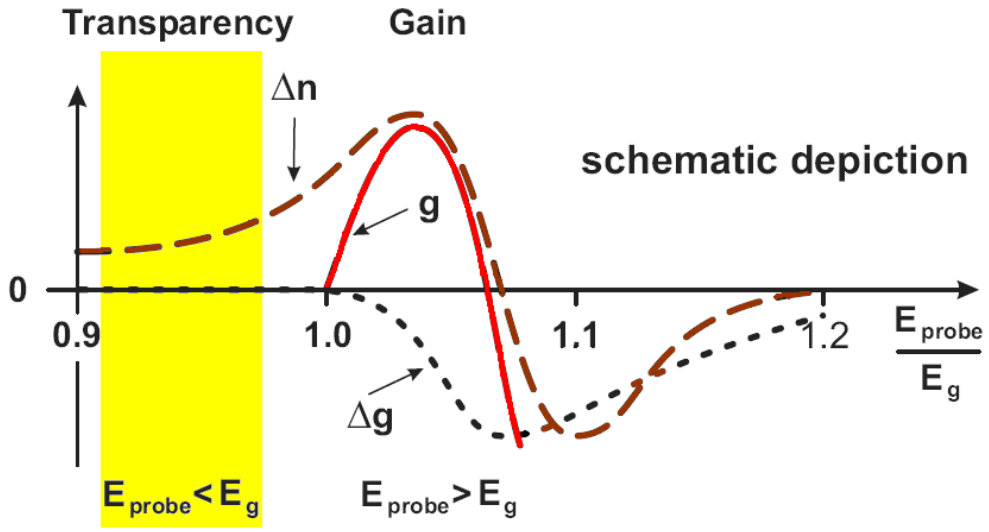


Figure 2.4: Light induced variation of the gain and the refractive index in an SOA (schematic picture) as a function of the light energy *Eprobe* relative to the band gap energy *Eg*, after [116].

beam) is injected in the SOA simultaneously with the pump signal, it experiences the variation of carrier density (ΔN) which results in a modification of the SOA gain Δg.

Figure 2.4 presents a schematic representation of the gain change Δg and refractive index change Δn as a function of the probe signal with photon energy $E_{probe} = \hbar\omega$ [116]. It is assumed that the photon energy of the optical pump is larger than the band gap energy E_g and lies within the range of a positive gain coefficient ($g > 0$).

The Δg curve in figure 2.4 illustrates that for short wavelengths (large E_{probe}) the carrier density variation results in a large gain variation, while there is no gain change below the band gap, as the SOA is transparent in this wavelength range [216]. The gain transparency denotes that the pump signal is in the gain region of the SOA, while the probe signal is in the transparency region [116]. Figure 2.4 also shows that the refractive index variation (Δn) is high within the whole amplification band of the SOA. Moreover, there is still a non-zero phase change below the band gap ($\Delta\Phi = 2\pi L\Delta n/\lambda$). This phase change of the data signal in transparency region can be used for interferometric switching [217].

The carrier density in the conduction band (N) is almost instantaneously reduced by interband processes (e.g. stimulated emission). On the other hand, if an optical pulse having a narrow pulse width (≈)1 ps is injected into the SOA. This causes an almost instantaneous change of Δg and $\Delta\Phi$.

2.7 Nonlinear effects in the SOA

SOA nonlinear effects can be classified via two different aspects; The first aspect includes new frequency components generation inside the medium (e.g. produced

by four-wave mixing). In the second aspect, the polarization, phase or amplitude of the data signal propagating through the medium is altered by nonlinear refractive index or gain changes induced either by itself (e.g. self-polarization modulation, self-phase modulation, and self-gain polarization) or by other optical control signals (e.g. cross-polarization modulation, cross-phase modulation and cross-gain modulation). Here, the main types of nonlinearity are reviewed;

Self-Phase Modulation (SPM): It occurs as a result of index nonlinearities induced by gain saturation. Time-dependent variations in the carrier density, and hence the refractive index are responsible for SPM. Likewise, it is the physical mechanism behind the spectral shift and distortion (spectral broadening). When the input pulse-width is much shorter than the carrier lifetime, the amplified pulse shape and spectrum is asymmetric (the spectrum exhibits a red shift). In return, the pulse-spectrum, when the input pulse-width longer than the carrier lifetime, is broadened on both the red and blue sides. The spectral and temporal changes also depend on the shape and the frequency chirp of the input pulses [218]. Pulse extinction in OTDM (optical time division multiplexing) system [219], all-optical NRZ-to-PSK modulation conversion [220], optical clock recovery [221], waveform shaping [222] and optical header-payload separation [223] are some applications of the SPM effect in the SOA.

Self Gain Modulation (SGM): It represents the modulation of the signal gain induced by the variation of the signal input power [224]. It can be used in waveform distortion compensation [225].

Cross Phase Modulation (XPM): XPM is related to a potentially fast process, which is the phase shift caused by fast changes in the refractive index [226] [227]. A change in the refractive index is always referred to a power change which causes the cross gain and chirp. Amplitude modulation can be performed by XPM via interferometric configurations [228]. Nonlinear Sagnac interferometer or nonlinear optical loop mirror (NOLM) [2], SLALOM [229], Michelson interferometer, Ultrafast Nonlinear Interferometer (UNI) [66] and Mach-Zehnder Interferometer (MZI) [230] are some proposed configurations. Time domain demultiplexing [231], add-drop multiplexing [232], optical sampling [233], wavelength conversion [234], clock recovery [235], pulse regeneration [236] and logic gates [16] are some of the applications of XPM.

Cross Gain Modulation (XGM): The process is based on the gain saturation characteristics. Due to the limited current distribution and availability of carriers, an increment of the SOA input power results a decrement of the SOA available gain. So, if an optical beam (probe) passes through the device, it will experience gain modulation (and suffer amplitude modulation) imposed by any other signal flowing also inside the device which makes a copy of this signal on the inserted probe [228]. XGM has been used for wavelength conversion [237] [84], OTDM to WDM trans-multiplexing [238], all-optical label swapping [239], format conversion from RZ to NRZ and vice versa [240] and

logic operations [41]. This process is limited in terms of speed. Although some techniques allow the expansion of the dynamic operational bandwidth of the devices [241].

Self-Polarization Rotation (SPolR): This effect occurs because of the polarization-dependent gain saturation in SOA. The phase difference between the TE and TM modes is created by the signal itself. When an optical bit with sufficient optical power arrives at the SOA, the leading edge of the bit introduces gain saturation in the SOA. Since the SOA gain saturation is polarization dependent, the TE component of the data bit experiences different gain saturation than the TM component. Thus, the leading edge of a data bit can introduce a rotation of the polarization state. SPolR has been previously used in optical packet header processing [242] and asynchronous all-optical label extraction [243] applications.

Cross Polarization Modulation (XPolM): This effect denotes the polarization rotation of a beam propagating in a SOA affected by the polarization and the power of a relatively strong control beam introduced simultaneously into the amplifier. When two signals are injected in the SOA, an additional birefringence and gain compression affects the SOA. The two signals affect one another by producing different phase and gain compression on TE and TM components (because the gain saturation of the TE and TM modes is different). This results in a rotation of the polarization state for each signal. The SOA bias current, and the input signal powers are the parameters that determine the magnitude of the polarization rotation.

Four Wave Mixing (FWM): In the four-wave mixing process, three input optical waves interact in a medium (e.g. SOA) and generate a fourth wave. It is generated at a further frequency whose intensity is proportional to the product of the interacting wave intensities [244] [245] [246]. A number of physical mechanisms have been proposed to account for the process of four-wave mixing in semiconductor media. Beating between two input waves results in carrier population pulsations which modulate the carrier density at the beat frequency [247]. This is referred to as an interband process, because it is the total carrier population in the conduction band which is modulated. There are also two intraband modulation processes which are commonly associated with four-wave mixing in semiconductors (carrier heating (CH) and spectral hole burning (SHB)). However, intraband processes are less efficient sources of four-wave mixing than carrier population pulsations, which dominate the mixing process for input waves separated by up to a hundred gigahertz [248] [249]. FWM in SOAs has been used for applications such as demultiplexing, wavelength conversion [250], and clock-recovery [251] [252].

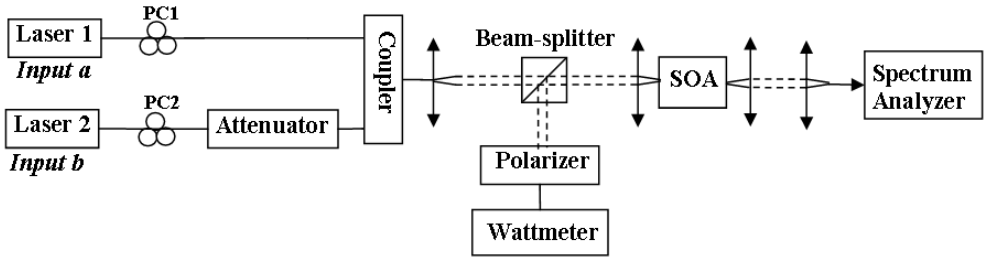


Figure 2.5: Experimental scheme utilized for evaluating the FWM polarization sensitivity in the SOA

2.8 FWM in SOA using spectrum-sliced incoherent source

Polarization sensitivity and wavelength dependency are the major inconveniences of the FWM effect in SOA. The dual pump FWM in SOAs has been proposed as a promising method to achieve high efficiency, signal to background noise ratio (SBR), and polarization and wavelength independency. In [253], a comparison between three polarization-insensitive wavelength converters based on FWM in SOAs (using two copolarized pumps, two orthogonal pumps, and polarization diversity) is presented.

Here, we propose another method in order to decrease the FWM polarization sensitivity in which an incoherent sliced-spectrum unpolarized beam is replaced by one of the two coherent beams contributing in FWM into the SOA. This solution, which is originally derived to fulfil the application described in chaper 5, is attractive since it provides a low-cost and highly scalable alternative with flexible wavelength selection [254]. The FWM effect using incoherent light has been studied on dispersion-shifted fiber [255] and experimentally presented on SOA [256].

Figure 2.5 displays the experimental scheme used for evaluating the FWM polarization dependency in SOA. Two coherent lasers with a detuning wavelength of 3.88 nm are used as the probe and pump beams (1547.96 nm and 1551.96 nm, respectively). The objective is the SOA output beam spectrum measurement for different polarization angle between laser 1 and laser 2. The polarization controllers, PC1 and PC2, are responsible for varying the polarization states of SOA input beams. Both of laser beams are transferred on a single fiber optic via a 3-dB coupler in order to be injected through a beam-splitter.

A part of the splitted power is injected in the SOA which provides new frequency components (due to the FWM effect). They are observable in a MS9710B Anritsu spectrum analyzer. The other output of beam-splitter passes through a free-space polarizer and can be measured via a wattmeter.

At first, the relative SOA input polarization states are optimized (via PC1 and PC2) whereby the maximum of FWM power will be displayed. It corresponds with two co-polarized input beams (a relative polarization angle of zero). Now, the attenuator is set to maximum and the polarizer is rotated to maximize the measured optical power on the wattmeter. The polarizer angle in the latter situation

is considered as the origin polarization angle ($\theta = 0$). For a relative polarization angle of $\Delta\theta$ between SOA input beams;

- The polarization angle of the polarizer is rotated (about $\Delta\theta$) from the origin polarization angle,
- The attenuator is set to maximize (the polarization angle of laser 2 will be fixed up to the end of experiment)
- Using PC1 (see figure 2.5), the polarization state of the laser 1 is rotated so as the measured power on the wattmeter is maximized.
- The attenuation is reduced and the spectrum of SOA output beam is measured with the spectrum analyzer.

Figure 2.6 displays the evolution of the FWM components when the mutual polarization match is tuned off. As expected the FWM process can be severely impaired (20 dB extinction). The experiment uses a 1.2 mm long SOA driven with a 300 mA current (with inverse bias polarity). It was fabricated by Alcatel OPTO+. A schematic top view of this SOA is shown in figure 2.7. Unfortunately, we do not have any more information about the parameters of this SOA. The probe and pump powers in the SOA input are -3.66 dBm and 0 dBm, respectively.

In the second part of the experience, a spectrum-sliced incoherent light source at 1547.96 nm (with 0.4 nm of bandwidth) replacs the probe beam. This is depicted in figure 2.8 that can be compared with figure 2.6. The pump and probe beams' optical power are identical in both experiments. The variation of FWM power is about 2 dB.

FWM process in SOA when one of the beams is an incoherent sliced-spectrum unpolarized beam has not been investigated theoretically. The FWM process (due to a coherent and a spectrum-sliced incoherent beam contribution in a SOA) will generate numerous frequency components via degenerate or non-degenerate processes. A simple theoretical analysis of the process is proposed here.

Suppose a monochromatic unpolarized and incoherent probe and a coherent pump beams as,

$$\begin{aligned} \overrightarrow{E_S} &= \overrightarrow{A_S} e^{j\omega_S t + \phi_S(t)} \overrightarrow{a_S} \\ \overrightarrow{E_P} &= \overrightarrow{A_P} e^{j\omega_P t + \phi_P} \overrightarrow{a_P} \end{aligned} \tag{2.17}$$

where ω_P and ω_S are the pump and probe frequencies. $A_P\overrightarrow{a_P}$ and $A_S\overrightarrow{a_S}(t)$ denote the pump and probe field vectors, respectively. The pump beam phase,ϕ_P , is a desired deterministic value and the probe phase,$\phi_S(t)$, is considered as a random function. The field vectors can be decomposed onto the TE and TM axis of the SOA called $\overrightarrow{x}$ and $\overrightarrow{y}$ axis respectively:

$$\begin{aligned} A_p\overrightarrow{a_p} &= A_{p_{TE}}\overrightarrow{x} + A_{p_{TM}} e^{j\theta_p}\overrightarrow{y} \\ A_s\overrightarrow{a_s}(t) &= A_{s_{TE}}(t)\overrightarrow{x} + A_{s_{TM}}(t) e^{j\theta_s(t)}\overrightarrow{y} \end{aligned} \tag{2.18}$$

Here, the pump and probe fields have been considered with elliptical polarization with phase-shift angle of θ_p and $\theta_S(t)$, respectively. The SOA can be modelled as a

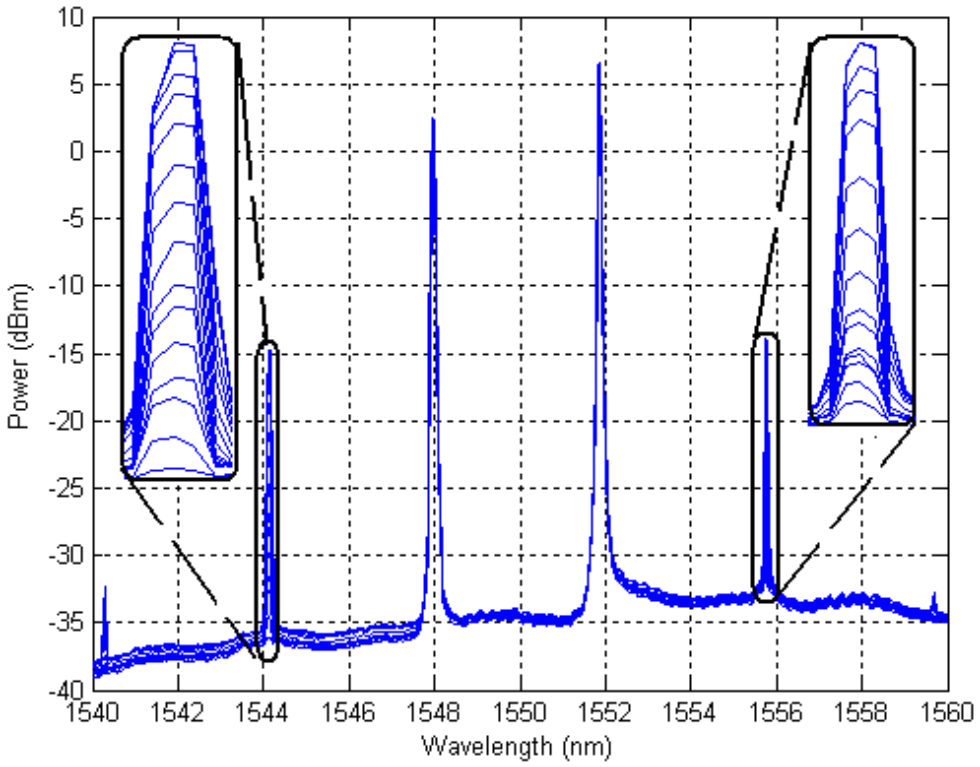


Figure 2.6: FWM variations of polarization angle detuning between pump and probe beams (from 0^o to 90^o with a step of 5^o).

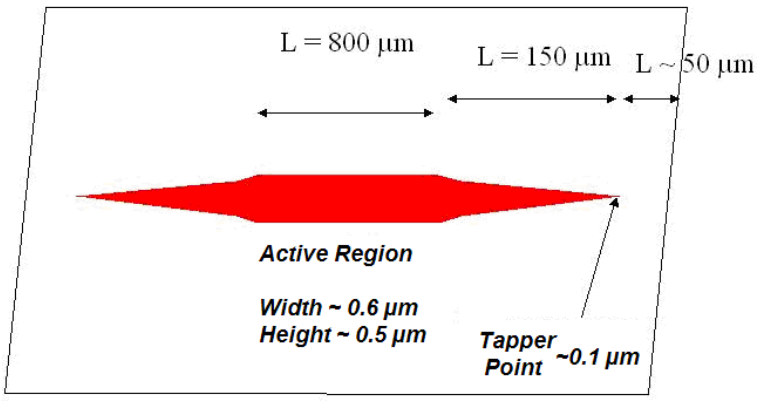


Figure 2.7: Top view schematic of the used SOA

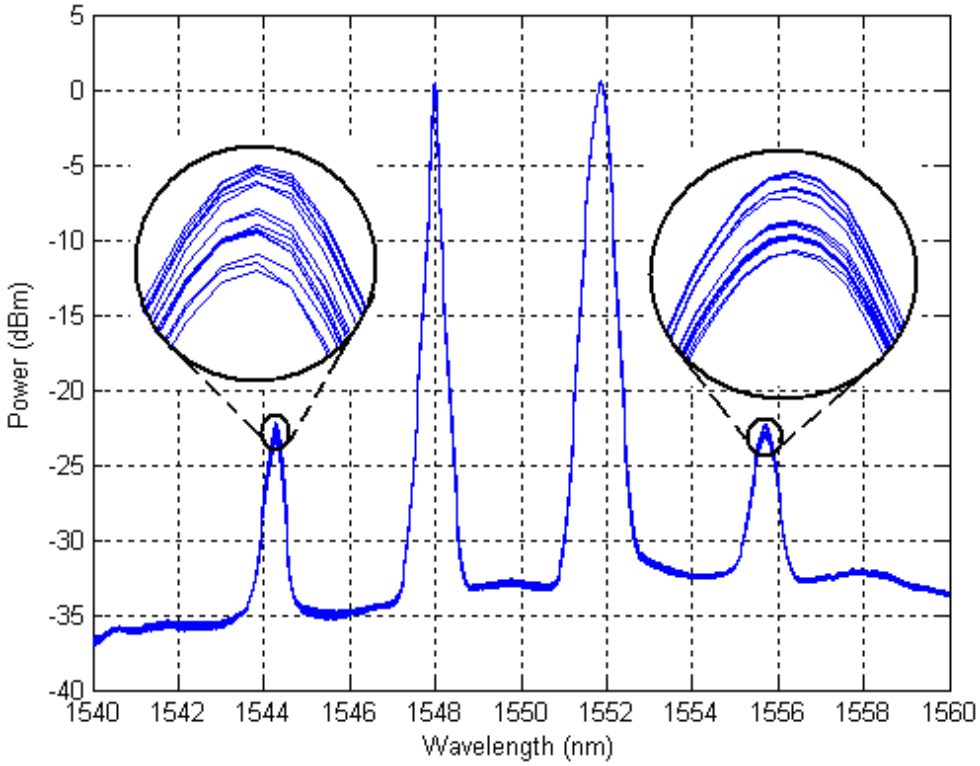


Figure 2.8: FWM variations of polarization angle detuning between incoherent probe and coherent pump beams (0^o-90^o with a step of 5^o).

lumped, saturable gain, followed by lumped third-order nonlinearity [253]. So, the SOA output beams will become as,

$$E_P^{out} = \left(\sqrt{G_{TE}} A_{P_{TE}} \overrightarrow{x} + \sqrt{G_{TM}} A_{P_{TM}} e^{j(\theta_P + \Delta\theta_P)} \overrightarrow{y} \right) e^{j(\omega_P t + \phi_P)} \tag{2.19}$$

$$E_S^{out}(t) = \left(\sqrt{G_{TE}} A_{S_{TE}}(t) \overrightarrow{x} + \sqrt{G_{TM}} A_{S_{TM}}(t) e^{j(\theta_S + \Delta\theta_S(t))} \overrightarrow{y} \right) .e^{j(\omega_P t + \phi_S(t))} \tag{2.20}$$

$\Delta\theta_P$ and $\Delta\theta_S(t)$ account for the birefringence of the pump and probe beams into the SOA, respectively. G_{TE} and G_{TM} represent the TE and TM gain of SOA. Here, we consider the up-conversion of FWM components. Using the SOA bulk model, the FWM electrical field is [253],

$$\overrightarrow{E}_{FWM} = A_P^2 A_S \left(\overrightarrow{a_P} . \overrightarrow{a_S} \right) r(\omega_P - \omega_S) e^{j[(2\omega_P - \omega_S)t + (2\phi_P - \phi_S)]} \overrightarrow{a_P} \tag{2.21}$$

where $r(\omega_P - \omega_S)$ is called the relative conversion efficiency function and is independent of gain and input power over some range of both [257]. The FWM field for

incoherent probe source can be modelled as follow:

$$\begin{aligned}\overrightarrow{E}_{FWM}(\omega_S,t) &= \left(G_{TE}A_{S_{TE}}(t)A_{P_{TE}} + G_{TM}A_{S_{TM}}(t)A_{P_{TM}}e^{j\gamma(t)}\right)\\ &.\left(\sqrt{G_{TE}}A_{P_{TE}}\overrightarrow{x} + \sqrt{G_{TM}}A_{P_{TM}}e^{j(\theta_P+\Delta\theta_P)}\overrightarrow{y}\right)\\ &.r(\omega_P-\omega_S)e^{j[(2\omega_P-\omega_S)t+(2\phi_P-\phi_S(t))]}\end{aligned} \tag{2.22}$$

where $\gamma(t) = \theta_P + \theta_S(t) + \Delta\theta_P + \Delta\theta_S(t)$. The FWM power can be calculated (using 2.22),

$$\begin{aligned}P_{FWM}(\omega_s,t) &= E_{FWM}(\omega_s,t)E^*_{FWM}(\omega_s,t)\\ &= (G^2_{TE}A^2_{S_{TE}}(\omega_s,t)A^2_{P_{TE}} + G^2_{TM}A^2_{S_{TM}}(\omega_s,t)A^2_{P_{TM}}\\ &+2G_{TE}G_{TM}A_{S_{TE}}(\omega_s,t)A_{P_{TM}}\cos\gamma(t))\\ &.R(\omega_P-\omega_S).(G_{TE}A^2_{P_{TE}} + G_{TM}A^2_{P_{TM}})\end{aligned} \tag{2.23}$$

in which $R(\omega_P-\omega_S) = |r(\omega_P-\omega_S)|^2$. Incoherent light is composed of numerous independent frequency components, in which the complex envelope of each frequency component is described by a circular complex Gaussian random variable [258]. The probe beam is an incoherent light which is a stationary random function of time and position. It means constancy of the average properties. For a stationary random function, the statistical averaging can be determined by time averaging over a long time duration (instead of averaging over many realizations of the wave). So, we can calculate the statistical average value of $P_{FWM}(\omega_S)$ as below:

$$\begin{aligned}\overline{P}_{FWM}(\omega_S) &= \langle P_{FWM}(\omega_S)\rangle\\ &= < \left(G^2_{TE}A^2_{S_{TE}}(\omega_S,t)A^2_{P_{TE}} + G^2_{TM}A^2_{S_{TM}}(\omega_S,t)A^2_{P_{TM}}\right)\\ &.\left(G_{TE}A^2_{P_{TE}} + G_{TM}A^2_{P_{TM}}\right) > .R(\omega_P-\omega_S)\end{aligned} \tag{2.24}$$

The symbol $\langle\bullet\rangle$ denotes an ensemble average over many realizations of the random function ($\langle\bullet\rangle = \lim_{T\to\infty}\frac{1}{2T}\int_{-T}^{T}\bullet dt$). As the incoherent light is described by circular complex Gaussian random variable it may be considered that

$$\begin{aligned}A_{S_{TE}}(\omega_S,t) &\cong A_{S_{TM}}(\omega_S,t)\\ &or\\ P^{TE}_{probe}(\omega_S,t) \cong P^{TM}_{probe}(\omega_S,t) &= \frac{P_{probe}(\omega_S,t)}{2}\end{aligned} \tag{2.25}$$

So, the average FWM power expression can be simplified once again:

$$\overline{P}_{FWM}(\omega_S) = \frac{1}{2}\left(G_{TE}^2 A_{P_{TE}}^2 + G_{TM}^2 A_{P_{TM}}^2\right) \cdot\left(G_{TE}^2 A_{P_{TE}}^2 + G_{TM}^2 A_{P_{TM}}^2\right) R(\omega_P - \omega_S) \left\langle P_{probe}(\omega_S, t)\right\rangle \tag{2.26}$$

Equation 2.26 shows the drawback of SOA birefringence on FWM components' power variation. It is due to unequal amplification of TE and TM components of signals ($G_{TE} \neq G_{TM}$). These variations are visible in figure 2.6. Now, if $G_{TE} = G_{TM} = G$ for the SOA, we can simplify the equation (2.26) as follow:

$$\overline{P}_{FWM}(\omega_S) = \frac{G^3}{2} R(\omega_P - \omega_S) P_{pump}^2 \overline{P}_{probe}(\omega_S) \tag{2.27}$$

where $P_{pump} = A_{P_{TE}}^2 + A_{P_{TM}}^2$. The P_{FWM} generated by coherent laser beams with identical polarization and the same settings (equal probe and pump power, SOA gain and detuning) [253] is,

$$\overline{P}_{FWM}(\omega_S) = G^3 R(\omega_P - \omega_S) P_{pump}^2 \overline{P}_{probe}(\omega_S) \left(\overrightarrow{a_P}.\overrightarrow{a_S}\right)^2 \tag{2.28}$$

Thus, the maximum of FWM efficiency (when pump and probe have identical polarization states) is 3 dB greater than when the probe beam is unpolarized (2.27). In return, the FWM sensitivity against polarization is alleviated.

The calculation above uses an extremely narrow spectrum incoherent light. Incoherent light typically has a broad spectrum, notably sliced incoherent light source. Therefore, the total FWM signal power could be calculated by integrating on the incoherent probe light spectrum.

$$\overline{P}_{FWM}^{Total} = \int_{\Delta\omega} G^3 R(\omega_P - \omega) P_{pump}^2 \overline{P}_{probe}(\omega) d\omega \tag{2.29}$$

where $\Delta\omega$ is the spectrum bandwidth of incoherent light source. Figure 2.9 shows the experimental measurement of P_{FWM}^{Total} as a function of pump polarization angle for up-conversion and down-conversion FWM components. The difference between the meandered FWM components power value between figure 2.6, 2.8 and 2.9 is due to the imperfect utilized optical filters. Although the FWM process between a coherent and an unpolarized spectrum-sliced incoherent light source is bounded to be less efficient than when two coherent lasers are used. The former situation leads to quasi-polarization insensitive operation (provided that the modulator and the SOA are polarization insensitive also).

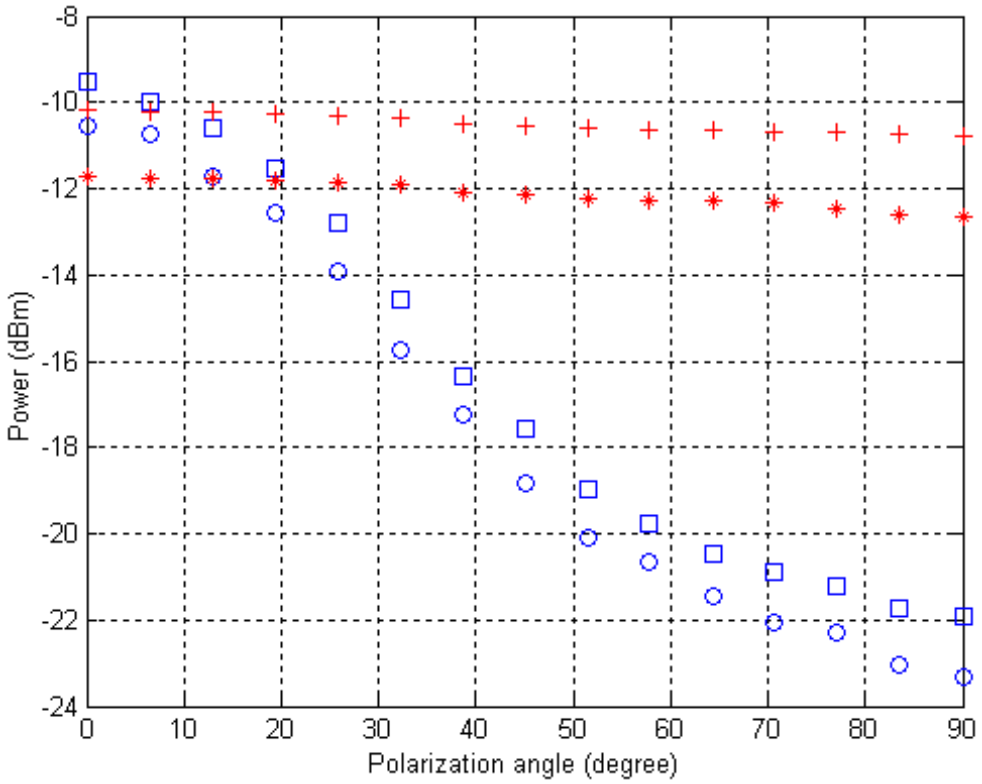


Figure 2.9: Experimental result of FWM signal power as function of pump polarization angle; '□', up-conversion FWM (coherent probe), 'o', down-conversion FWM (coherent probe), '+', up-conversion FWM (incoherent probe), '*', down-conversion FWM (incoherent probe).

2.9 Summary

A brief review on the SOA in terms of their different structures, their operation principles and their dynamical processes as well as interband and intraband processes is given. Moreover, the main types of nonlinear effects in the SOA (such as FWM, XPM, XPolM,$\cdots$) which are exploited in all-optical signal processing schemes, are addressed.

In order to reduce the sensitivity of FWM to input signal polarization, the use of a modulated spectrum-sliced incoherent light source is included in the setup. This expectation has been experimentally checked by performing FWM for two cases of the pump beam; coherent and incoherent. Despite a 3 dB efficiency reduction in the best case with respect to an equivalent coherent light launching, the use of unpolarized, incoherent light allows polarization insensitivity as demonstrated theoretically and experimentally. The application is in time-to-wavelength converter presented in chapter 5.

CHAPTER

3

All Optical Logic Gates

3.1 Introduction

In the first chapter, the potential of the optical network, and in particular transparent network capacities, were discussed. Clearly, an all-optical network can not be realized yet due to the lack of technology. During the last few years, nonlinear optics has stimulated increased interest towards the development of fundamental optical gates and functions. Optical logic gates are essential for implementing various all-optical signal processing in future high speed optical networks to overcome the electronic bottleneck. A variety of all-optical functions have been demonstrated using optical logic gates such as encryption and data encoding [2], pattern matching [3], binary addition/counting [4] [5], parity checking [6], bit-error monitoring [7] and in particular optical packet label processing. The last term will be discussed precisely in the next chapter. In this chapter, different methods and techniques for realization of SOA-based all-optical logic gates are compared. Furthermore, the application of optical gates in an optical half adder will be proposed. Figure 3.1 displays a graphic representation of the basic logic gates with their truth tables. Various optical logic gate schemes have been demonstrated in different materials (e.g. optical fibers, in semiconductor devices [259] and waveguides [260]). In particular, semiconductor optical amplifiers (SOAs) are attractive nonlinear devices, since they exhibit both a strong variation of the refractive index and a high gain. Table 3.1 presents some techniques that have been reported for the optical logic gate.

As mentioned in table 3.1, most of the reported optical logic gates have employed SOAs as the nonlinear elements. The SOA nonlinearities used in logic gate functions can be classified into two categories;

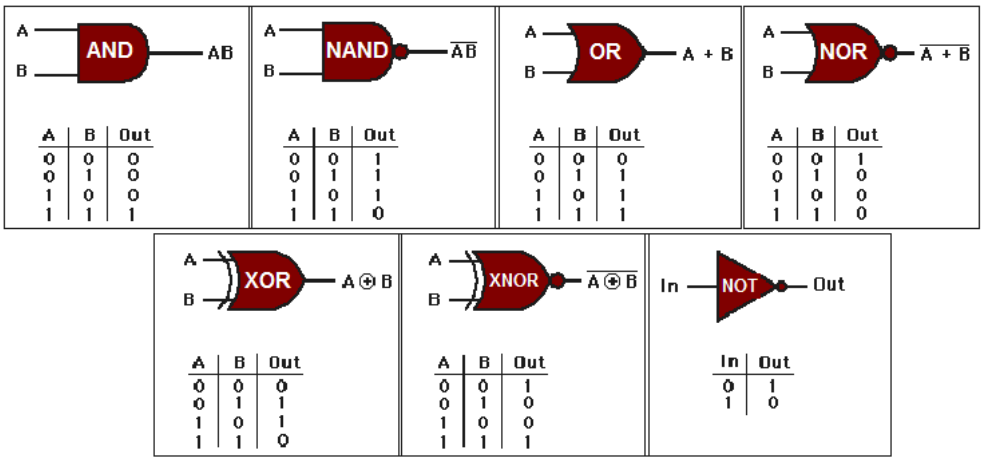


Figure 3.1: Graphic representation of basic logic gates

- Nonlinear effects in SOA itself such as XPolM, XGM, and FWM based devices.
- The SOA-assisted interferometers.

Among the optical logic gates, the all-optical XOR is considered to be a fundamental one. It can perform a set of critical functionalities such as label or packet switching, decision making, regenerating, basic or complex computing, pseudorandom number generating, parity checking, and so on. Here we propose a new design for of XOR and XNOR logic gates based on ultrafast nonlinear interferometer (UNI) system.

3.2 XOR and XNOR realization with UNI technique

An optical interferometer splits a single light beam in two and sends them by two different paths and recombines them again. The optical light at the output of the interferometer depends on the relative phase differences between the recombined beams:

$$\Delta\Phi = 2\pi \frac{|n_1 d_1 - n_2 d_2|}{\lambda} \tag{3.1}$$

where λ is the light wavelength, d_1 and d_2 are the path length of each separated beam and n_1 and n_2 denote the refractive indices of the materials they traveled through. The interferometers used in optical logic gate applications are almost exclusively two beam interferometers. Sagnac or cyclic interferometer (SI), Michelson interferometer (MI), Mach-Zehnder interferometer (MZI) and ultrafast nonlinear interferometer (UNI) are some of the well known interferometers. In the SI, MI and MZI, partially reflecting beam-splitters or fused fiber couplers (evanescent field couplers) divide and recombine the two beams. In the UNI, this is done by a polarizer. The UNI is also called a polarization interferometer. Table 3.2 compares some methods proposed for optical XOR logic gate realization. The main advantages of the method based on UNI, proposed here, are the low power consumption, speed and stability.

Table 3.1: A summary of technique used for all-optical logic gate

	NOT	AND	NAND	OR	NOR	XOR	XNOR
SOA (NOLM) (TOAD)	[9]	[10] [12] [14]				[2][11] [10] [13]	[10]
SOA (MZI)		[15]	[16] [21]	[17] [16]	[16]	[18] [19] [22] [23] [24] [25] [16] [26]	[20]
SOA (FWM)	[27]	[28] [31]		[27]		[29] [30] [32] [33] [35]	[27] [34]
SOA (XGM)	[36]	[37] [41]	[36]	[38]	[39] [41] [42]	[40] [43]	[34]
Semiconductor microresonator structure		[44] [45] [47]	[45]		[46]		
Optical difrectional coupler	[48]	[48] [49] [50]	[50]	[48] [49] [50]		[49] [50]	[50]
Optical waveguides	[51]	[52] [54]	[52]		[53]		
Nonlinear fibers		[55] [56] [57] [61]		[57]	[57] [59]	[55] [58] [60] [3] [57]	[57]
Electro-absorption modulator	[62]	[63]					
Fabry-Pérot laser diode					[7]		
UNI	[64]	[64] [65]		[64]	[64]	[66] [67]	
SOA (XPolM)		[68] [69]		[70]	[71] [70]	[72]	[73]

Figure 3.2 shows a schematic of a UNI system which employs a semiconductor optical amplifier in traditional single arm interferometer (SAI) geometry [261]. An input signal pulse is split in two orthogonal polarizations via a polarization controller (PC 1) and a polarization maintaining fiber (PMF 1). The polarization planes of light waves launched into a PMF are maintained during propagation with little or no cross-coupling of optical power between the polarization modes.

In the PMF, the two orthogonally polarized components are separated by a temporal delay which is given by the length of PMF and the refractive index difference

Table 3.2: Comparison between SOA based technique utilized for XOR logic gate producing

Parameter	Kerr effect (Fiber)	XPolM (SOA)	FWM (SOA)	XGM (SOA)	TOAD (SOA)	UNI	MZI (SOA)
Extension ratio at 10 Gbit/s	10 dB	10 dB	20 dB	11 dB	11 dB	8 dB	13–15.5 dB
Reported speed (Gbit/s)	100	5, 10, and 20	2.5, 10, and 20	5, 10	10	20, 40	10, 20, and 40
Switching power	High	Moderate	Moderate	High	Moderate	Low	Low
Number of SOAs	0	1	1	1 or 2	1	1	2
Bit pattern dependence	Very low	High	Low	Low	Moderate	Low	Low
Polarization sensitivity	No	Yes	Yes	Limited	Yes	Yes	Limited
Integration potential	-	+	+	+	-	-	+

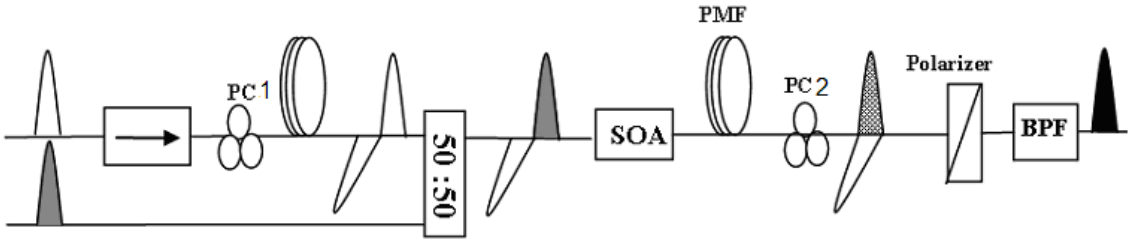


Figure 3.2: Block diagram of the UNI system; PC is the polarization controller, PMF stands for polarization maintaining fiber and BPF is band pass filter.

between its fast axis and its slow axis;

$$\Delta t = |n_x - n_y|L/c \tag{3.2}$$

where n_x and n_y are the refractive indices along the PMF axis (fast and slow axis). Figure 3.3 shows the cross section of two examples of PMF.

Two signal components travel through the SOA in which a control pulse, coupled in via a 3-dB coupler, is temporally coincident with one of the signal pulse components. The control imparts a differential phase and amplitude modulation between both of signal components in the SOA due to the ultrafast refractive index and gain nonlinearities such as two-photon absorption, carrier heating and other instantaneous virtual electronic processes [262]. Both signal components coming

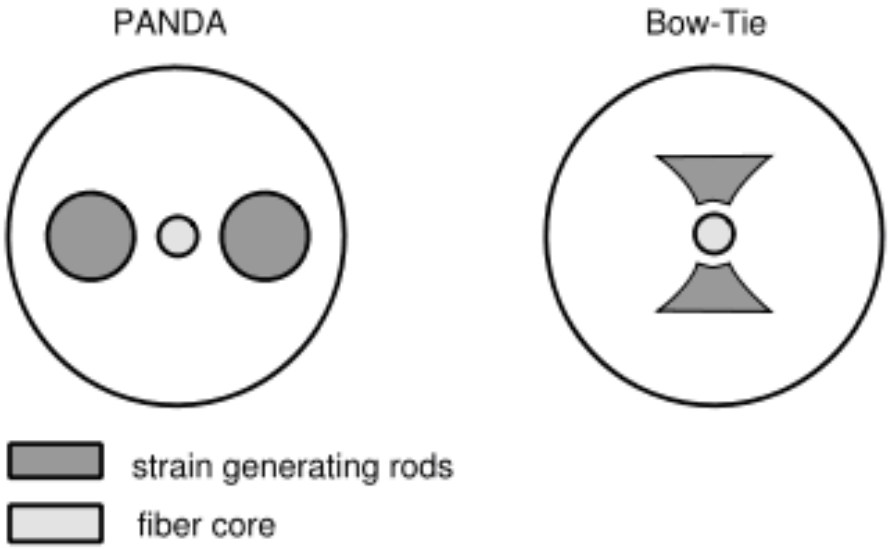


Figure 3.3: The cross section of two types of PM fiber

out of the SOA are retimed to overlap again by using a second polarization sensitive delay (PMF 2 with reversed fast and slow axis) and subsequently interfere using a polarizer. The control pulse is filtered out at the output of the device. The control signal can be injected either in co-propagating or counter-propagating configurations. In the counter- propagating geometry, the control and signal wavelengths can be identical [262]. The SOA refractive index upon saturation by a strong optical pulse and the associated phase shift (phase dynamics) is of major importance. The theoretical speed of the gate is directly related to the SOA's XPM response and can reach several tens of GHz [64].

The UNI configuration shown in figure 3.2 can be modified by means a loop configuration in which the control pulse affects the corresponding input pulse component in counter-propagation. So, the UNI system is demonstrated using a single PMF. The latter is used both for delaying the orthogonal polarization components of the incoming signal at the input of the SOA and for compensating this delay after the SOA via a loop geometry (Figure 3.4). This scheme is more stable and simpler. However, the counter-propagating configuration requires that the SOA interaction length be less than or equal to the pulse width so that the control pulse does not interact with more than one signal pulse. Thus, for higher bit rate operation, either the SOA length must decrease or a co-propagating geometry must be adopted.

The realization of a XOR and XNOR logic gates is illustrated schematically in Figure 3.5 where an UNI is used in loop configuration [263]. Each input pulse (incoming pulse in figure 3.5) passes into a 40 m long PMF in order to be splitted in two orthogonally polarized pulses separated by a time delay (Δt=45 ps). The polarization controller 1 (PC 1) adjusts the polarization of the incoming pulses in order to inject the linearly polarized light at 45^o off the fiber axis at the PMF. The control pulses (control A and B) represent the logic gate input data. They are counter-

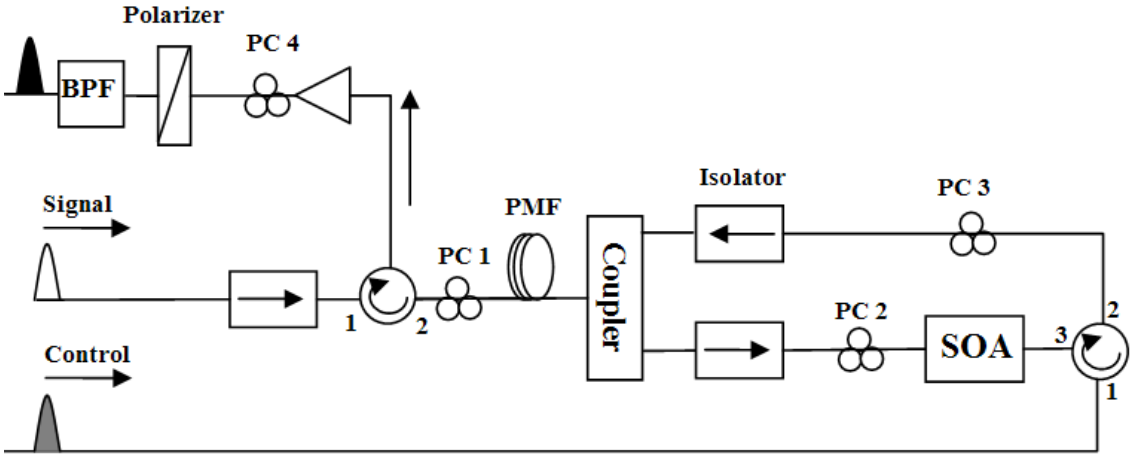


Figure 3.4: Schematic of UNI system in a loop

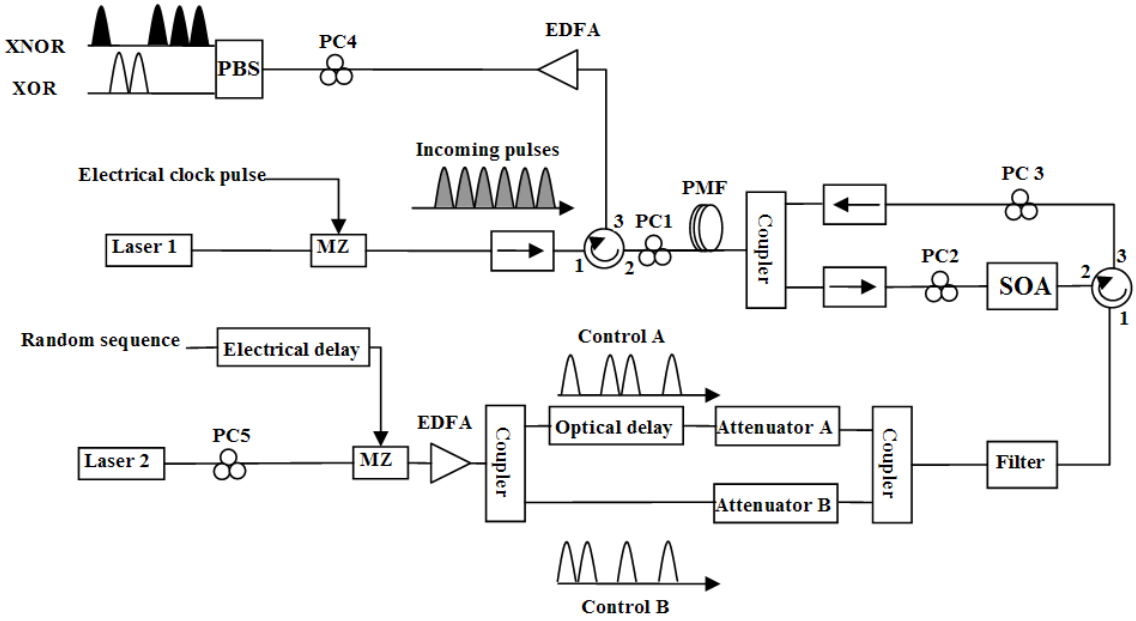


Figure 3.5: Experimental setup for XOR and XNOR gates based on UNI technique; PBS is polarization beam splitter and MZ is Mach-Zehnder modulator

propagating with respect to the incoming signal pulses and enter the SOA via a circulator. The control pulses induce the refractive index and the gain nonlinearities in the SOA. Depending on the intensity and synchronization of the control pulses with respected component of the incoming pulses, the polarization rotation of the incoming pulse occurs. In ideal conditions, each control pulse exactly synchronizes with one of the incoming pulse components and induces a phase shift of π to this component. When the relative delay between components is compensated in the PMF, the incoming pulse polarization will rotate by either 90^o or 180^o (depending on the availability of one or both of the control pulses, respectively).

Table 3.3: Variation of polarization of incoming pulse with control pulses

Control Pulse A	control Pulse B	Incoming Pulse Polarization	XOR Output	XNOR Output
OFF (0)	OFF (0)	↗ (45^o)	0	1
OFF (0)	ON (1)	↖ (135^o)	1	0
ON (1)	OFF (0)	↘ (-45^o)	1	0
ON (1)	ON (1)	↙ (225^o)	0	1

The experiment uses a 1.2 mm long SOA driven with a 300 mA current. The input signal consists in a laser (operating at λ=1556.85 nm) modulated with a 10 Gbit/s pulse sequence. The modulation format is RZ (Return to Zero). A random sequence is utilized in order to modulate laser 2 (operating at λ=1555.27 nm) at 10 Gbit/s through a Mach-Zehnder modulator. It will serve as both input data streams (control A and B in figure 3.5). The tunable optical delay line together with the different fiber length (between control A and B branches) provides two independent data sequences as two control signals. The data sequence and the optical delay are selected so as, to generate the different logic bit combinations between input signals in order to demonstrate the XOR and XNOR operations.

The synchronization of pulse trains is obtained by both an electrical delay on the laser 2 modulating signal and an optical delay line in one arm of the control beams (figure 3.5). For synchronization, a sequence of '1' bits are used instead of a random sequence. At first, the attenuation of the attenuator A is maximized. Then the control B's pulse is synchronized with one of the separated components of incoming pulse by using the electrical delay. Then, the attenuation of the attenuator B is maximized and the variable optical delay line is used for synchronizing the control A's pulse with the other component of incoming pulse. Moreover, the attenuators equalize the control pulses' power. The polarization controller 3 (PC 3) sets the polarization of the delayed incoming pulse along the fast axis of the PMF and the un-delayed component along the slow axis, obtaining a compensation of the delay as a result. At the exit of the PMF the output signal is separated in a circulator. Finally, the axes of the fiber are spliced 45^o with respect to the axis of the polarization beam splitter (PBS) to allow interference. Table 3.3 represents the polarization variation of the incoming pulse signal with respect to the control signal activation. To validate XOR gate operation, the control (input) binary streams are set as "0010011000" and "0001001100". Figure 3.6 shows the control sequences and their normalized XOR result ("0011010100"). The 7.45 dB extinction ratio is achieved at 10 Gbit/s data rate.

Figure 3.7 illustrates the normalized XNOR output waveform for two input sequences "0011000100" and "0001100010". The extinction ratio of the output signal ("1101011001") is between 5.5 dB and 7.5 dB. This is due to the gain saturation of SOA when both the control signals are available at the same time (cross-gain

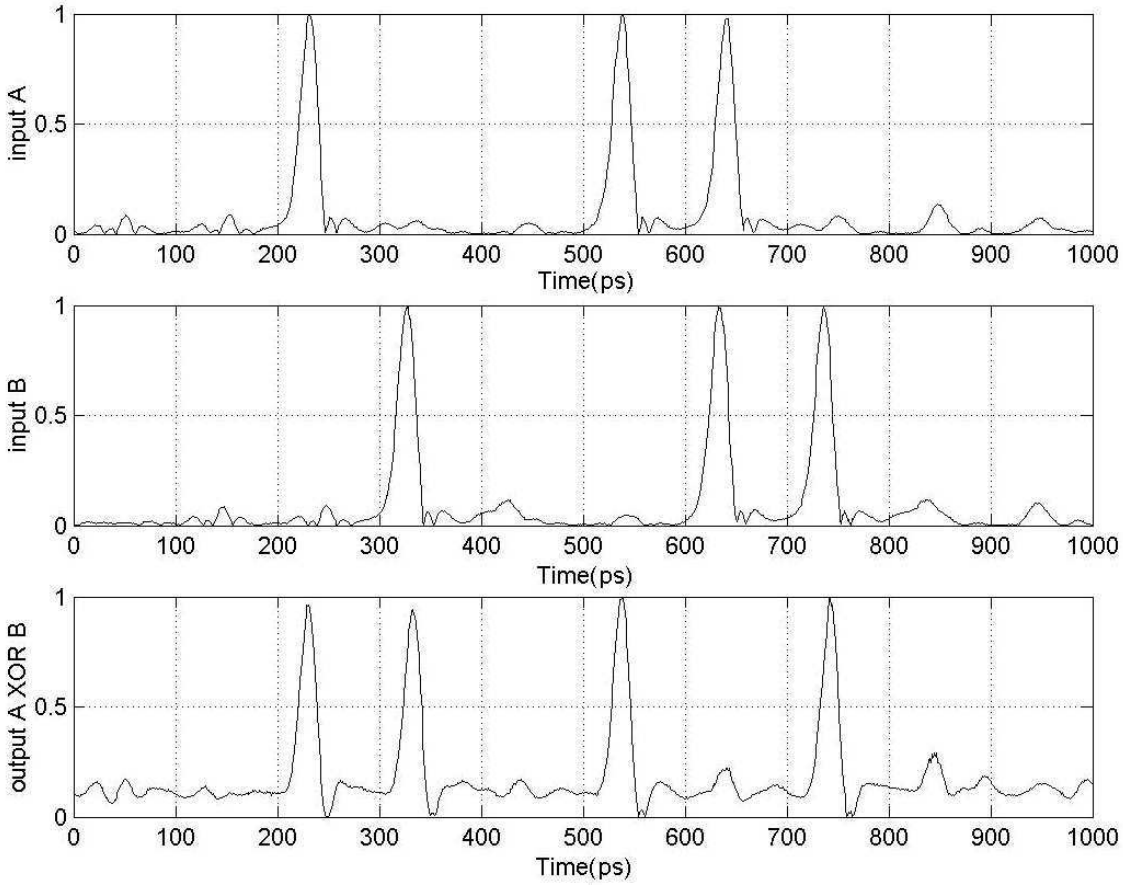


Figure 3.6: The normalized XOR result of two input sequence

modulation). In this case the output signal amplitude is lower than in the other states. This phenomenon disappears in XOR case because this state is not allowed.

In order to evaluate the precision of the synchronization of the optical signals and the degradation that could be induced by timing jitter, the temporal window of the gate is measured. The gate is adjusted, firstly, for the exact synchronization between the input signals and then a variable time-detuning is provided by using the delay lines. Figure 3.8 shows the variation of XOR and XNOR outputs as a function of detuning-time between the input signals. It indicates that the temporal window in which the amplitude of the output signal reduces by less than -3 dB is about 25 ps for XOR operation and 20 ps for XNOR operation at bit-rate of 10 Gbit/s.

3.3 Optical NOT gate using the XPolM effect in SOA

A NOT logic gate can be used in some complicated all optical logic functions or in all optical switching systems. Here, we present a new method for realizationg an all-optical logic NOT gate based on XPolM in SOA which will be employed in an all optical decoder design (chapter 7). The XPolM is not the only method for NOT logic

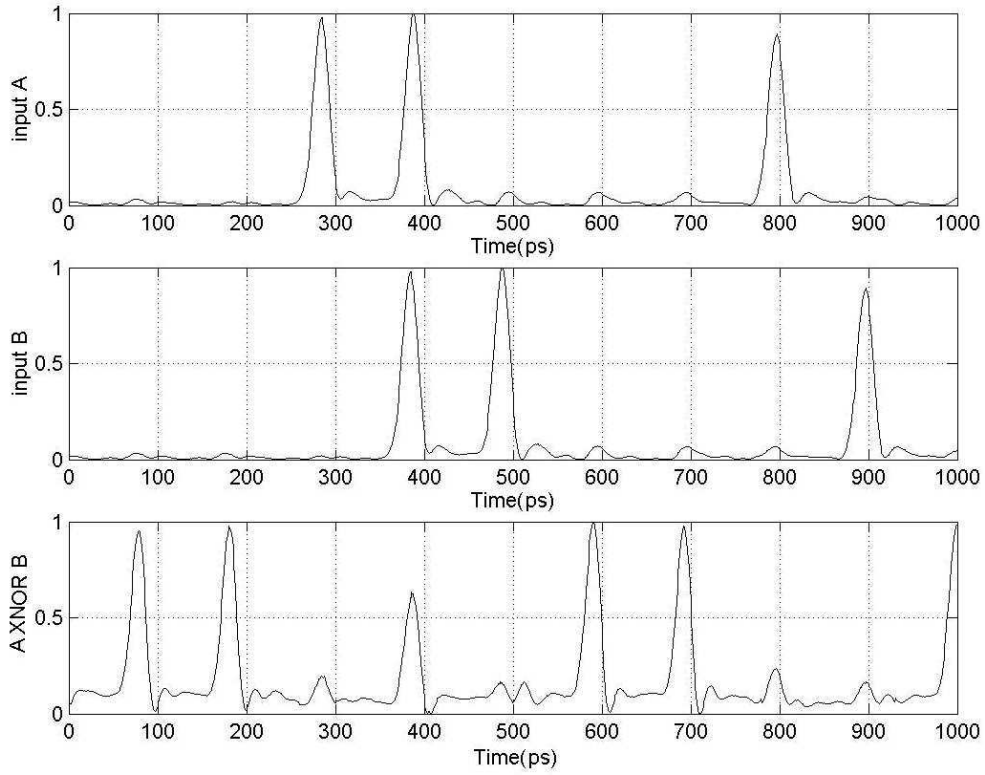


Figure 3.7: The normalized XNOR result of two input sequence

gate generation. For example, in [36] and [27], the XGM effect in SOA is employed to produce a NOT logic gate. For that, we need a strong auxiliary laser source so as to work in saturation regime of the SOA while our method is simpler and more efficient.

Figure 3.9 illustrates a schematic of the experimental setup used for NOT logic gate realization at 10 Gbit/s. The control laser is modulated in a Mach-Zehnder modulator at the same bit rate as the input sequence. It can be injected in SOA either in co- or in counter-propagation. In the co-propagating case an extra filter is used after the SOA to filter away the control pulses. Moreover the FWM effect is reduced in counter-propagating configuration. Besides, the co-propagating scheme has the drawback of leading to a wavelength conversion. In counter-propagating configuration, the control signal serves as the output signal. When the input bit is '0', the control pulse signal can be amplified and passed into SOA with a certain angle of polarization rotation. In the presence of input signal pulses ('1' bits), the polarization state of the control signal rotates through the SOA (XPolM). So, for a rotation of the polarization of 90^o, the control pulse can be completely blocked by the polarizer in the output of the SOA.

Figure 3.10 shows the result of the related experiment. A 1.2 mm long SOA (driven with a 300 mA of current) is used. The control and input signals are 1557.72 nm and 1550.62 nm respectively. The sequence "0101101010" is chosen as the input signal. The modulation format of input signals is RZ. RZ modulation format offers

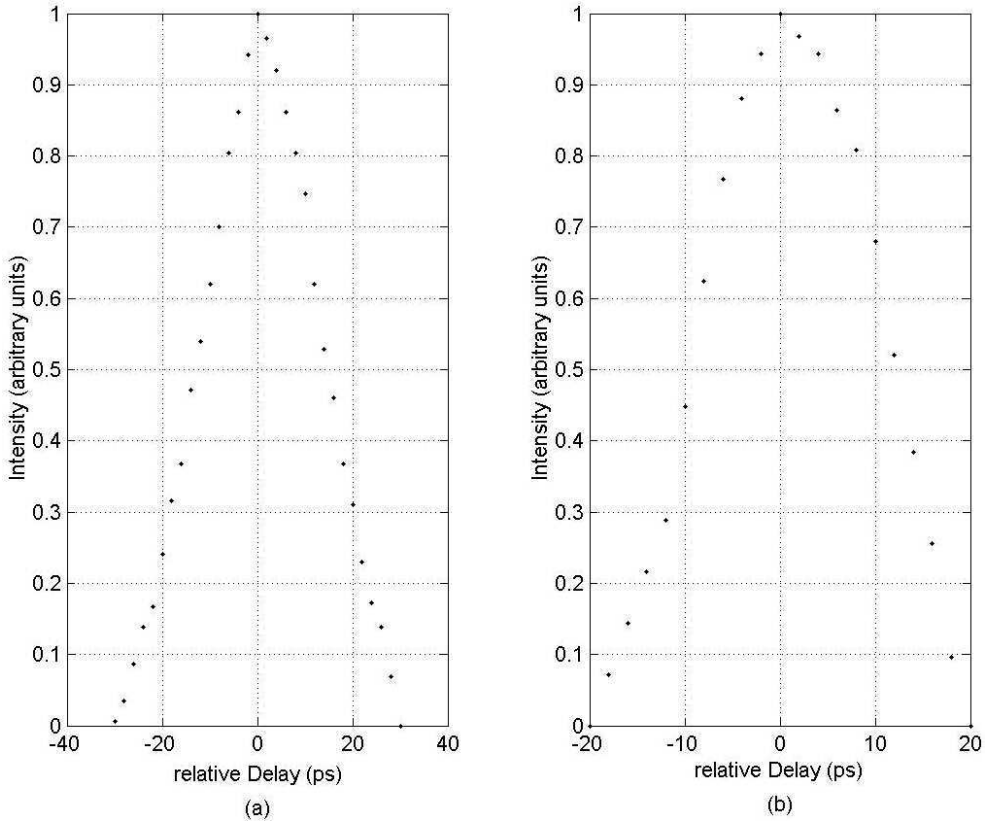


Figure 3.8: (a) XOR switching window, (b) XNOR switching window

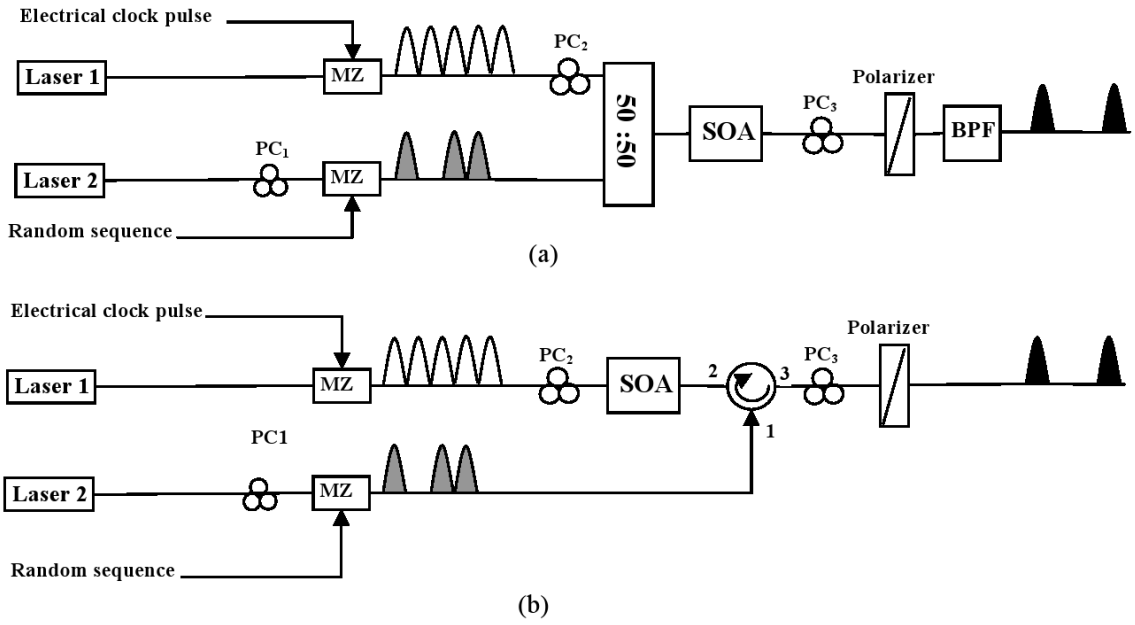


Figure 3.9: Experimental setup used for NOT logic gate based on XPolM in SOA; (a)Co-propagating, (b)Counter-propagating

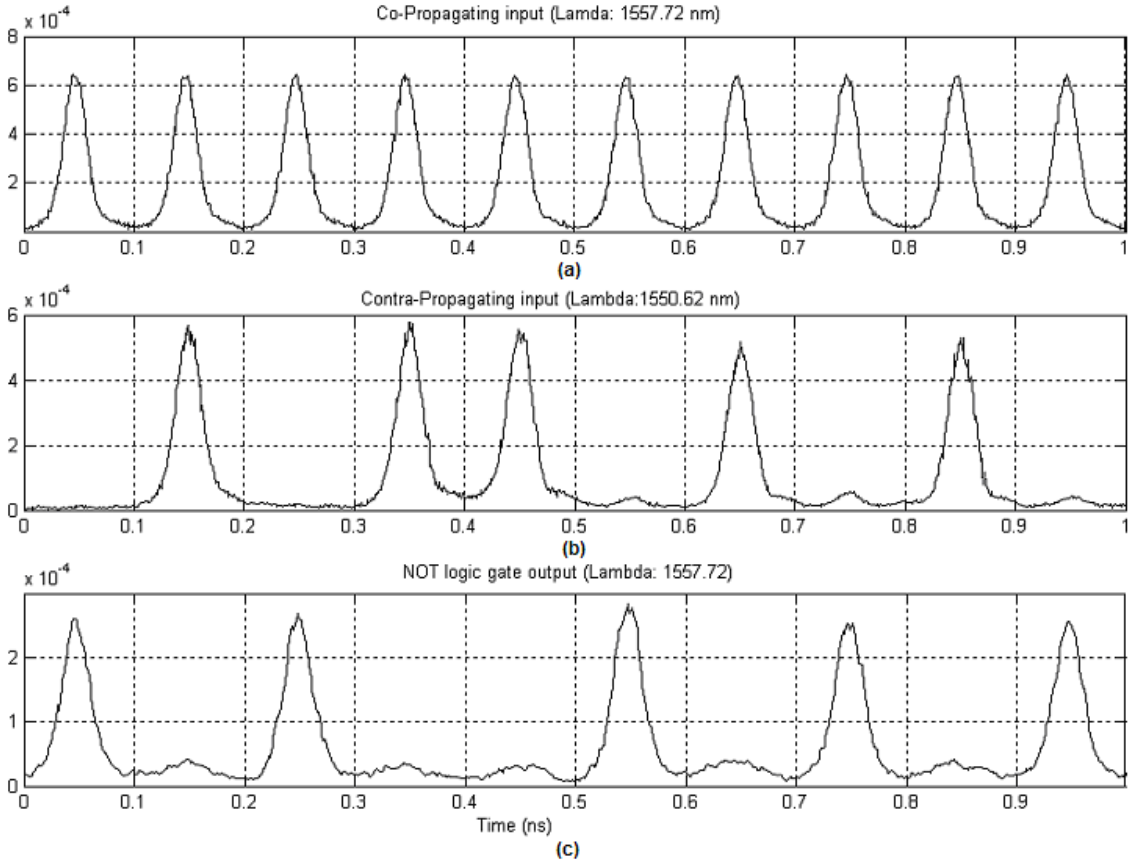


Figure 3.10: NOT logic gate realization using XPolM in SOA; (a)the control signal, (b)the input data signal and (c)the output NOT logic gate.

a number of advantages over NRZ (Non Return to Zero) modulation schemes. For example, RZ modulation is better suited to long haul and ultra long haul applications because it can maintain the integrity of the signal over longer distances as it travels through the network. Moreover, RZ formatting has a lower bit error rate and is less susceptible to fiber nonlinearities and dispersion effects, which can cause the signal to spread as it travels through the fiber and render it unintelligible. The output signal extinction ratio measured in this experience was 8.2 dB. For the NRZ modulation of input signals, the modulation of control laser is not required.

In the following section the SOA based logic gates are employed to perform a more complicated logic functionality (optical half adder).

3.4 A half-adder design based on the XOR-XNOR gates

The previous XOR design based on UNI system can be modified in order to fulfill half adder operation. The half adder is an example of a simple functional logic circuit built from two logic gates as minimum. The half adder adds two one-bit binary numbers (e.g. *input 1* and *input 2*). The output is the sum of the two bits (S)

Table 3.4: Truth table of a half adder

Input 1	Input 2	Output (C)	Output (S)
0	0	0	0
0	1	0	1
1	0	0	1
1	1	1	0

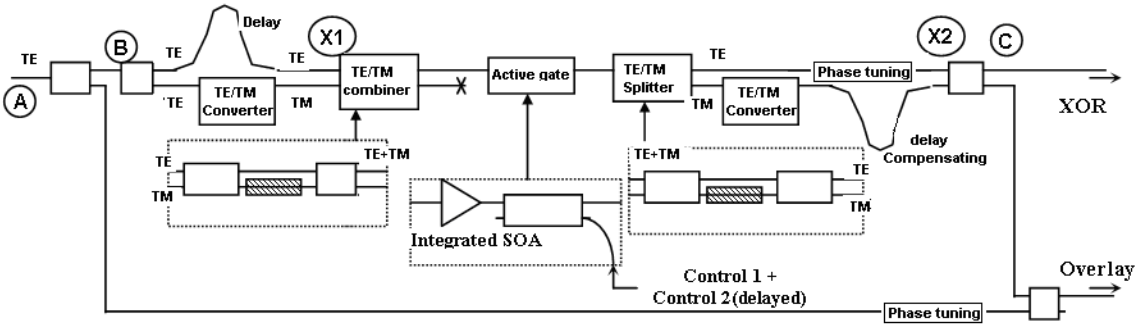


Figure 3.11: Integrated UNI scheme for the half-adder operation

and the carry (C). Table 3.4 illustrates the truth table of a half adder.

PPLN waveguide and an SOA [264], two cascaded UNI gates [265] [266], SLALOM [267], XGM in SOA [268] and [269] are some of the methods presented previously for optical half adder realization. The advantage of our method is the simplicity and the use of a single SOA in a high speed configuration (UNI) for half adder realization. As shown in table 3.4, the sum (S) and carry (C) output truth tables are the same as XOR and *AND* logic gates (see figure 3.1).

Here, we serve the XNOR logic gate in the place of carry in the half adder. The basic idea consists in making use of the π-phase difference for the XNOR output for [0,0] and [1,1] inputs. In order to exploit this phase shift in an interferometric structure, we propose the integrated UNI scheme as illustrated in figure 3.11.

The UNI gate itself is included between point B and C (figure 3.11). A TE wave entering the device in B is splitted into equal parts. One is delayed using a long waveguide where the second is converted into TM mode. Several TE/TM conversion scheme have been published in the literature [270]. The TE/TM combiner that follows is designed using an overlay layer over the waveguide that modifies strongly the TM effective index without effect on the TE one. The active part of the UNI gate is just an integrated version of the one studied in 3.2.

The TE/TM splitter is identical to the combiner. The TM wave is back converted into TE and delayed whereas a phase tuning on the TE wave allows the interferometer adjustment. The last MMI recombines the 2 waves that have been re-synchronized and have the same polarization. It has an identical effect as the polarizer in the previous UNI gate. Compensation of the polarization conversion losses may be obtained through a polarization sensitive amplification in the SOA.

Table 3.5: Wave characteristics of the control beams

Control 1 (Input 1)	Control 2 (Input 2)	XOR Amplitude(Phase)	XNOR Amplitude(Phase)	Overlay
0	0	0(·)	1(0)	0
1	0	1(0)	0(·)	1/2
0	1	1(π)	0(·)	1/2
1	1	0(·)	1(π)	1

In addition to the UNI-gate a new arm is added, which divert some input light and use it for recombination with the XNOR output. When ON, the control beams affect the signal pulses traveling in the SOA at the same instant by inducing an extra π-phase-shift to its phase as demonstrated, previously. The table 3.5 describes the wave characteristics with/without the control beams.

A BPM simulation has been performed to illustrate the operation of the device. Our 2D BPM cannot treat simultaneously TE and TM wave and can only feature CW wave. Thus the TE and TM path have been splitted into 2 different branches between point X1 and X2. The paths are strictly identical except for the TE/TM-combiner/splitter: in one branch the Mach-Zehnder interferometer includes the overlay layer on one arm to feature the TM wave propagation. The active SOA have been simulated by way of the addition of a π-phase-shift. Figure 3.12 illustrates the 4 possible situations.

As shown in table 3.5 for the inputs of [0, 1] and [1, 0] inputs the overlay output is not equal to zero but the half the maximum intensity obtained in the [0, 0] case. In order to eliminate this unwanted signal, Non-linear fiber [271] or nonlinear Bragg grating [272] can be used as the optical limiter.

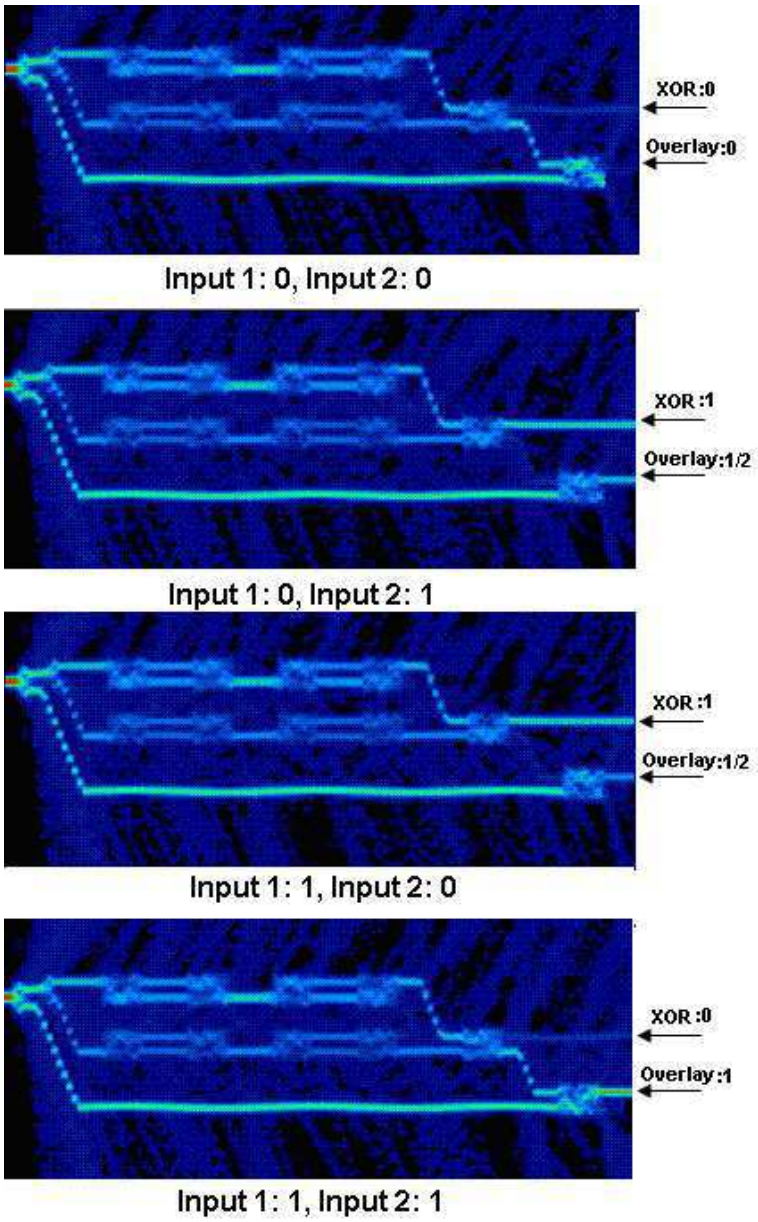


Figure 3.12: BPM simulation of integrated UNI based scheme for the half-adder operation

3.5 Summary

A review on the all-optical logic gate realization methods is given in this chapter. Next, the XOR and XNOR operations at 10 Gbit/s based on a new scheme of an UNI (ultrafast nonlinear interferometer) methods have been demonstrated experimentally. The main difference between our scheme with the UNI structure proposed before, is to employ a counter-propagation geometry that avoid the use of a filter and wavelength converter for the elimination of the control signal at the output of the system. Likewise in this scheme only one PMF is used for creating and compen-

sating the delay between two orthogonal polarization components of the incoming signal in traditional UNI structure. The attempts concerning to the all-optical label processing thanks to optical logic gates (e.g. in time-to-wavelength converter an all-optical decoder) are presented in the next chapters.

CHAPTER

4

Optical Packet Label Switching Systems

4.1 Introduction

As discussed in chapter 1, the optical packet switched (OPS) networks employing optical label switching (OLS) is one of the candidates to enable an all-optical Internet in which packets remain in the optical domain throughout the entire network and optical labels are used to route the data. The basic OLS network architecture is shown in figure 4.1.

In optical label switching the packets with a short length enters the core network from the client network through the 'ingress' edge node. The packet header is read and encapsulated in an optical label containing the information of the packet. From this point onwards, throughout the core network, the optical payload (consisting of packet payload and packet header) remains in optical format and is not examined again. The label is smaller and simpler than the payload and hence can be transmitted at a slower data rate and still arrive in the same time slot as the payload. This allows the labels to be processed using relatively simple electronic or optical processing. When the packet has reached the other side of the core network (destination node), the label is erased and the packet passes back into destination client network to be routed normally.

The realization of optical packet router requires many technological obstacles to be overcome such as optical packet label processing and optical packet routing protocols. The routing protocols are outside the scope of this thesis. In this chapter, we investigate the optical packet label processing methods. In the following sections the essential requirements for the realization of an optical packet router, and in particular in optical label switching core are addressed. New propositions for

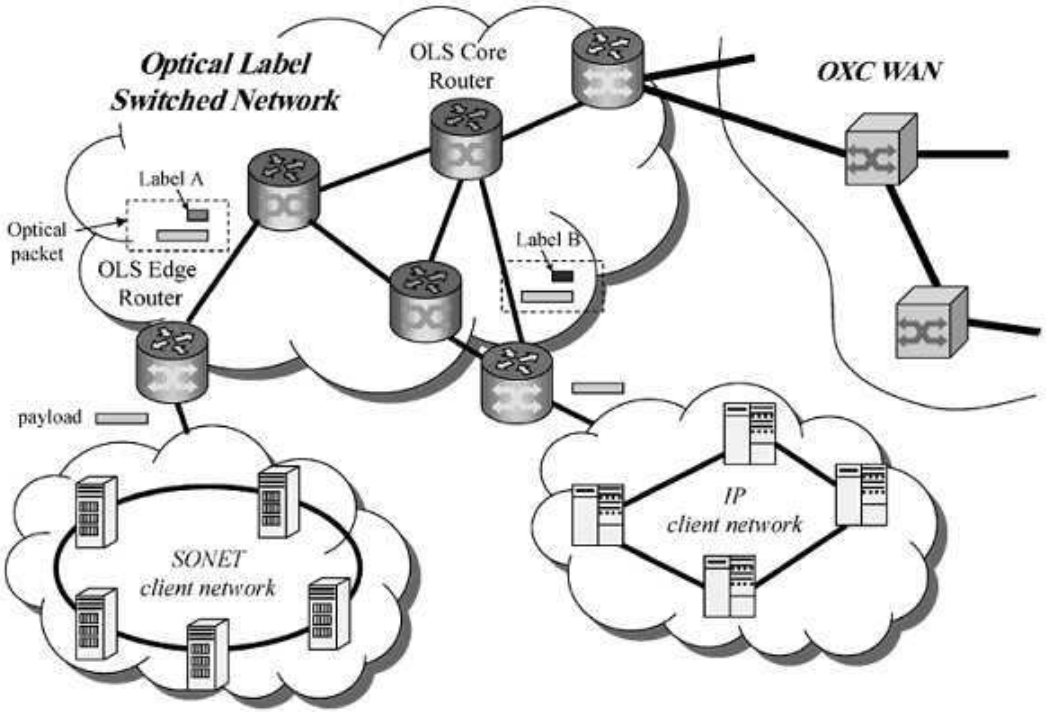


Figure 4.1: The network architecture of an optical label switched network, WAN stands for wide area network, OLS for optical label switch, OXC for optical cross connection, after [82]

optical label processing through optical networks will be presented in the following chapters.

The basic function of the OLS router is to route the packets to the proper destinations which typically involves the following steps:

1. Extraction of the label from the packet
2. Processing of the label in order to obtain routing information
3. Rewriting of the label and recombining it with the payload
4. Routing of the payload and resolve contention if necessary.

A generic architecture of a core OLS router that can perform these functions is shown in figure 4.2. The main challenges for optical label switching are in the areas of optical labelling, label swapping, optical buffering, optical high-speed switch, clock recovery and data regeneration. These will be discussed in detail in the following subsections.

4.2 Optical label structure

A label is a short, fixed-length (e. g. four-byte in MPLS), locally-significant identifier which is used to identify a forwarding equivalence class (FEC). FEC is a group of IP

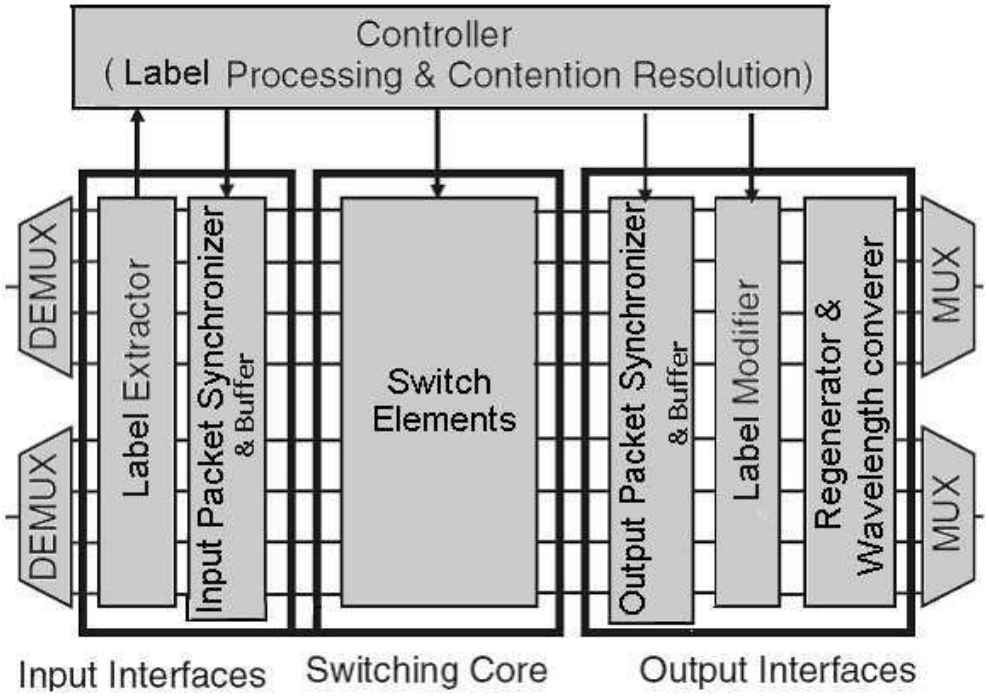


Figure 4.2: A generic architecture of an OLS core router.



Figure 4.3: MPLS label Format; S is the bottom of stack and exp is the reserved bits for experimental uses.

packets which are forwarded in the same manner, over the same path, and with the same forwarding treatment. An FEC might correspond to a destination IP subnet, but it also might correspond to any traffic class that the edge-LSR (label switch router) considers significant. Figure 4.3 presents the simple scheme of the optical label within the MPLS protocol.

The MPLS label consists in:

- Label: locally significant 20-bit label instead of 128 bit in IP protocol,
- Exp: 3 bits reserved for experimental use (currently used as a Class of Service (CoS) field such as DS (delay sensitive) information or per-hope behaviour (PHB)),
- S: 1 bit as the bottom of Stack (set to one for the oldest entry in the stack and zero for all other entries),
- TTL: 8 bits used to encode a hop count, or time to live, value.

4.3 Optical labelling techniques

A key issue in the OLS approach is the method of coding the optical label onto a data payload. It affects not only the architecture of the OLS router, but also the performance of the OLS system. The key requirements for label generation are efficiency, scalability, and flexibility; the label generation process should not introduce extra latency and impose restrictions on the bit rate and modulation format of both the label and the payload. The label rewriting process must also satisfy these requirements. Moreover, the label and payload will be subjected to signal impairments such as crosstalk, fiber nonlinearities, and amplified spontaneous emission (ASE) noise in the optical network. So, the selected labelling scheme should not make the packet more susceptible to such impairments.

The label and the payload transmission parameters (in terms of bit rate, wavelength and modulation format) are not necessarily the same since they can be processed separately. There are four main approaches proposed for optical label coding; bit serial (time-division multiplexing), label wavelength (wavelength division multiplexing), optical Sub-Carrier Multiplexing (SCM), and optical orthogonal modulation [75]. Figure 4.4 illustrates a schematic of these label transmission techniques;

- **Bit serial labelling:** Similar to SONET/SDH overhead, in this technique, the label information is attached in the time domain, by putting it in front of the payload and header. The payload and the attached label are encoded on the same wavelength carrier (which simplifies the bookkeeping in the routing node.) together with an optical guard time. The guard time not only facilitates the label extraction and processing but also reduces the buffer time for the payload data during the packet label processing operations. Precise timing control is thus required during the label processing and rewriting operations.

  The bit rates of the label and the payload can be the same or different. Commonly, a low bit-rate for the label is chosen to allow the use of low speed electronics for label processing and synchronization at the packet rate. KEOPS (Keys to Optical Packet Switching) and DAVID (data and voice integration over DWDM) projects use fixed-size packets with headers transmitted at a lower bit rate and transparent payload [80] [81]. For exmple, in the KEOPS project the following packet format was used: fixed time slot of 1.64 μs and a payload of 1.35 μs, and 14 bytes for header information [273]. To increase the header processing efficiency, methods such as serial-to-parallel conversion and an optical digital-to-analog conversion are proposed.

- **Wavelength-labelling:** It transmits the optical label on one [274] or multiple [275] wavelength channels apart from the payload wavelength. The label extracting and swapping is easily achieved using separate optical transceivers for the label and the payload onto the separate wavelengths. The primary drawback results from the chromatic dispersion of the optical fiber (different propagation speed of different wavelength channels in the optical fiber). It

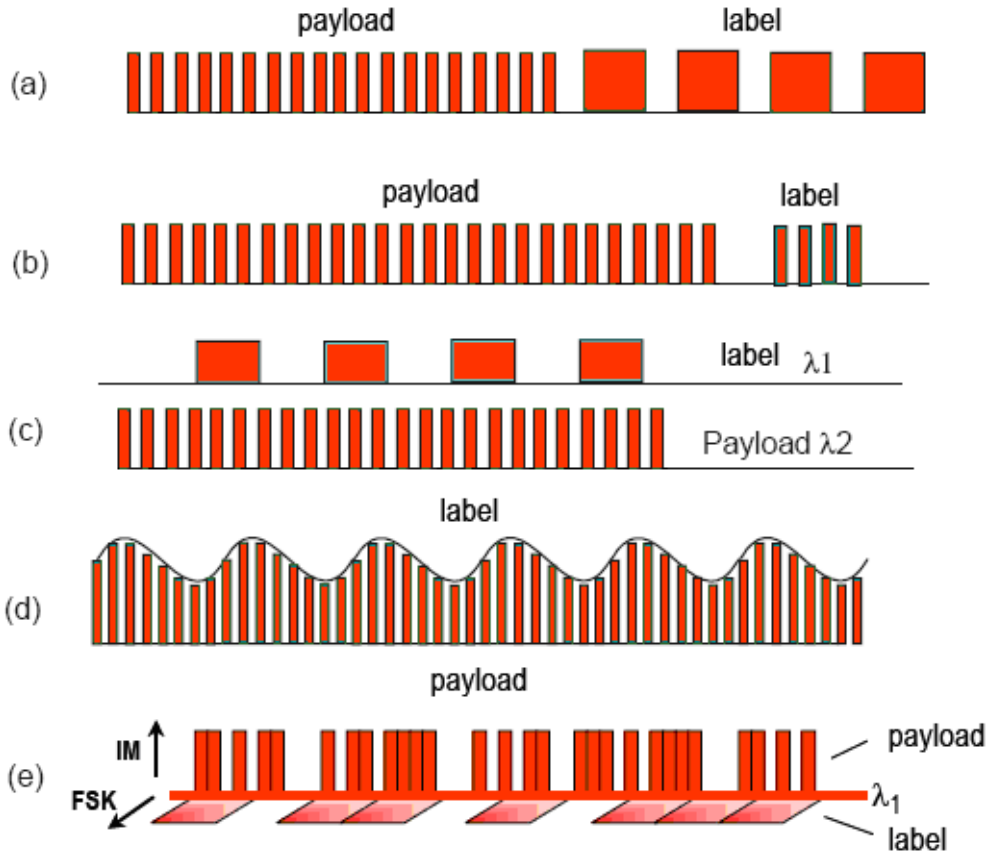


Figure 4.4: Label transmission schemes. (a) and (b) serial bit label with different and the same bit rate of the label in relation with payload, (c) Wavelength labelling, (d) Subcarrier multiplexed label (SCM), and (e) Orthogonal modulation label.

results in walk-off between the label and the payload which limits the transmission distance and the limited network scalability, unless each link incorporates dispersion management. Allocating one label wavelength for each payload channel will clearly require a far greater optical bandwidth than required by the information on the label and the data. Likewise, using one label wavelength for all of the multiple payload channels [274] could cause collisions between labels when the traffic becomes heavy. Furthermore, this method greatly underutilizes the label channel capacity since the optical labels are relatively short and low speed compared with the data payloads [75].

- **Sub-Carrier Multiplexing (SCM):** The optical SCM technique accommodates both the label and the data payload on the same optical wavelength. In return, the payload is treated as a base band signal while the label is modulated on the subcarrier channels. Therefore, the label and the payload travel simultaneously through the network and maintaining tight synchronization at any node is not required (achieving simplified network control). Furthermore, the SCM labelling is relatively efficient in terms of wavelength channel utilization

where the SCM labels do not occupy any additional time slots or wavelength channels. In return, they occupy a small portion of additional bandwidth in the optical spectrum (100 MHz - 1 GHz). The additional bandwidth required is usually well within what can be accommodated between the channel spacing of the dense-wavelength-division-multiplexing (DWDM) networks. In CORD (Contention resolution by delay lines) [76], OPERA (optical packet experimental routing architecture) [78], and HORNET (Hybrid Opto-electronic Ring Network) [77] projects, the SCM labelling are used. For example, in the HORNET project the payload data rate is 2.5 Gbit/s, and a subcarrier at 3 GHz carries FSK modulated header data.As another example,In the WASP-NET (wavelength switched packet network) project [276], a hybrid technique of utilizing out-of-band and mixed-rate formats (SCM and frequency- division multiplexing (FDM) of short SCM channels) are proposed in order to minimize the duration of the label.

- **Orthogonal Modulating:** The orthogonal modulation technique encodes the optical-label information using the optical carrier itself [277]. Here, the modulation format diversity for label and payload allows the label and payload to be processed asynchronously, but does not require them to exist on separate wavelengths.

  Different combinations of modulation formats have been reported: intensity modulated (IM) of the payload with frequency shift keying (FSK) modulation for label [278], IM for the payload with differential phase shift-keying (DPSK) modulation for label [279], dc-balanced-line-coded ASK payload modulation with ASK modulation of label [280], FSK payload and IM label [281], and polarization shift-keying modulated label and ASK modulation for the payload [282]. For example, in the European FP5-IST STOLAS project (Switching Technologies for Optically Labelled Signals) project, the packet consist of 155 Mbit/s FSK modulated label together with intensity modulation for the 10 Gbit/s payload [79].

  The label extraction method is uniquely different for each combination but usually additional signal processing is required to remove the label before the payload can be extracted. A common problem with modulation format labelling schemes is the compromise between the extinction ratio of the label and the bit rate and/or extinction ratio of the payload. Moreover, crosstalk between label and payload is also a problem that needs to be addressed. Table 4.1 summarizes overall discussions on the label-coding schemes in terms of timing requirement, cross talk and label processing techniques. Techniques for labelling of optical signals in burst switched networks are reviewed in [283].

Packet delay is an important issue for some types of payload. With an SCM label, the routing decision can be done after an entire packet time slot has elapsed, and the delay introduced by the node is equal to the packet duration plus the label processing time. This delay can be large if long packets are being routed across many nodes. However, the mixed-rate packet format only introduces a delay equal to the

Table 4.1: Comparison of four main coding approaches

Label coding method	Timing requirement	Cross-talk	Label processing
Bit serial	Tight	Very low	All-optical label processing is feasible
Label wavelength	Loose	Very low	Label Separation is easy
Optical SCM	Loose	Low, but it may suffer RF fading effect	Label swapping and contention resolution are demonstrated
Orthogonal Modulation	Loose	High	Complicated

header length plus the processing time. If the header length can be minimized, the processing time can fall within the remaining time period of the payload. Consequently, with minimal label time and fast processing, the network delay imposed on the payload can be kept very low. Among the coding schemes, bit-serial approach is the least restrictive approach in terms of packet bit rate and modulation extinction ratio.

4.4 Clock recovery

The input packet clock recovery is the first stage in packet label processing (in particular, in bit serial labelled packets) as well as in optical time division multiplexed (OTDM) systems. In order to detect and process the label, the receivers (even in burst mode) usually need sufficient clock information. Most of the current clock recovery systems use a fast photo-detector followed by an electrical clock recovery circuit to synchronize the clock with the incoming data. The limitation of these methods includes the speed of photo-detectors and electrical circuits. Optical clock recovery systems can overcome this limitation using ultrafast nonlinearities in the place of high-speed electronic components. One way to overcome the limited speed of electronic clock recovery systems is to measure the timing between the data and optical clock using a nonlinear optical process and utilize a phase-locked loop (PLL) to synchronize the two signals. Several nonlinear processes have been exploited for this purpose including four-wave mixing in fiber [284] or semiconductor waveguides [252], phase-modulation in SOA [235], cross-absorption modulation in an electro-absorption modulator [285], two photon absorption in a silicon photodiode [286] and three wave mixing in periodically poled lithium niobate (PPLN) crystals [287].The PLL based optical clock recovery systems can not be applied in burst mode receivers (in particular in optical packet label processing applications) due to the PLL locking time for detecting the burst mode packets. Burst-mode clock recovery circuit for 40-Gbit/s optical packet communications (with clock synchronization

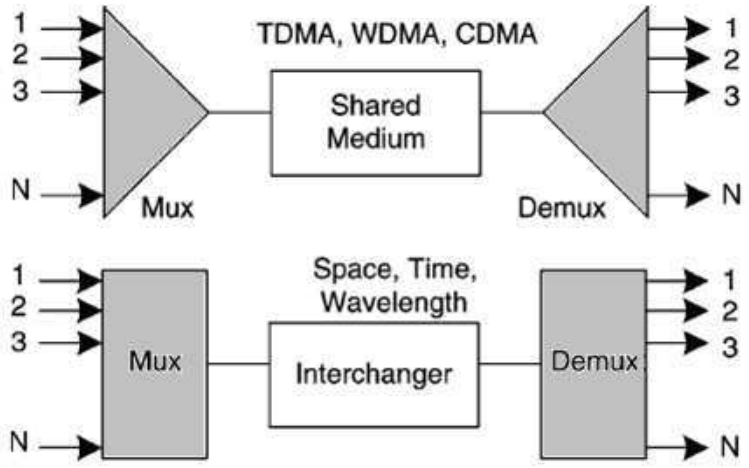


Figure 4.5: Two type of switching architecture: shared medium and interchanger, after [118]

time of 0.3 ns) is presented in [288].

Quantum-dots self-pulsating semiconductor laser [289] and optical carrier suppression and separation (OCSS) technique [290] are recently presented for instantaneous clock recovery. For example, in [290], the continuous clock information is always added onto the optical label or payload generated by OCSS technique at the transmission node. Therefore, a conventional receiver containing a high-Q filter extracts the clock at the receiving node.

4.5 Optical switch

Significant advances have been made in designing switching fabrics using different technologies including space, time, wavelength, and code division multiplexing. Photonic switching architectures can be classified in two categories; shared medium (shared links) and interchanger (dedicated links) [118]. Figure 4.5 depicts a generic example of these two classes.

In a shared medium, the input signals are multiplexed into a shared channel (using a star, bus, or ring topology) and are broadcast to the output stage. An input port signal is demultiplexed at the appropriate output port using a multiple access protocol (TDMA, WDMA and CDMA). In interchanger switching architecture, switching is performed by a mapping operation, using separate links. Both categories can use four types of techniques as follow:

Space-division switches, where physically disjoint input signals are mapped to physically disjoint outputs. The purpose is the ability of connecting every input to every output with minimum control and cross-points. Space-division switches can be classified according to their connectivity and blocking property. They include blocking, rearrangeably non-blocking [291], wide-sense non-blocking [292], and strictly non-blocking [293] switches.

Time-division switches, where inputs from the same link are mapped by interchanging time slots. Photonic Time-Division involves the sharing of a cross-point for a specific period of time. Thus, individual cross-points are assigned to multiple users and each user uses the resources for its assigned period of time. The main features are scalability and small physical size. However, time domain multiplexed (TDM) signals in the optical fiber transmission line requires significantly rapid operating speed and memory manipulation to accurately align and order data signals in the appropriate time slots.

Wavelength-division switches, where inputs from the same link are mapped by interchanging wavelengths. The purpose of wavelength-division switching is to interchange channels (wavelengths) from inputs to outputs. Signal interchanging from one path to another path may be with or without wavelength conversion. Here, high-speed multiplexing and synchronization are not required. In return, the wavelength tuning mechanisms are relatively slow, the WD switches are more appropriate for circuit-oriented switching.

Code-division switches, where inputs from the same link are mapped by interchanging orthogonal codes. Code-Division Multiple Access (CDMA) is a technique that originated from spread spectrum communication and is conventionally used in wireless communications. Recently, it has been applied to fiber optic networks to provide asynchronous access [294]. Because of its asynchronous access and star topology, OCMDA was originally developed for local area networks. Since the mid-90's, OCDMA has been considered for future telecommunications applications. OCDMA includes transparency to the overlaid transport protocols, the ability to support asynchronous access, the potential for improved security and capacity and support for QoS.

A switching solution may include one or multiple types of these switching techniques. For instance, a combination of temporal and spatial techniques might be both used to create an optical switch. Several technologies are used in photonic switching devices including;

Fiber Bragg grating (FBG): FBGs are most commonly used in WDM demultiplexers and optical add/drop multiplexers. Recently, they have been used in optical routing functions [89] [90] as well as in optical code division multiple access applications [295].

Wavelength converters: All optical wavelength converters may be used in the implementation of switches in WDM networks. The main features of a wavelength converter are its transparency to bit rate and signal format, operation at moderate optical power levels, low electrical power consumption, small frequency chirp, cascadability of multiple stages of converters, and signal reshaping [296].

Micro-Electro-Mechanical Systems (MEMS): The MEMS technology uses tiny mechanical mirrors that reflect light using the surface of a semiconductor. These

surfaces move by applying a current to an array of mirrors. The speed at which the mirrors move is relatively slow (in the order of miliseconds). They can be moved faster by applying more current, but they are limited by the basic control of the mechanical mechanism that moves the mirrors. By changing the mirror design, it is possible to achieve faster switching speeds (in the order of nanoseconds) [297].

Electro-holographic switches: They are based on controlling the reconstruction of holograms by applying an electric field beam. The application of electric field is to activate a pre-stored hologram that determines the routing of light beams. Salient characteristics of holographic switch are scalability (in the order of thousands of ports), high-speed switching (nanoseconds), and reliability since there are no-moving parts [298].

Interferometric SOA-based optical switches: They are based upon SOA nonlinearities combined with interferometric devices to perform switching in a very short time (around ps). Sagnac, Mach-Zehnder, UNI, and Michelson interferometers are some of proposed interferometric devices that can be used in the switch architecture [299]. The switching time on the order of a picosecond, was introduced by the device known as terahertz optical asymmetric demultiplexer (TOAD) [300], [301].

Thermal optical switches: They are based on waveguide thermo-optic effect or thermal phenomena of materials. Their main advantages are polarization insensitive operation and switching speed on the order of a millisecond. Switches based on waveguide thermo-optic effect are called thermo-optic switches (TOSW), which can use well-established planar lightwave circuit (PLC) technology [302]. They are divided into two basic types: digital optical switches (DOSs) and interferometric switches. Another kind of thermo optic switch is based on thermal effects of materials, such as thermo-capillarity optical switches [303], thermally generated bubble-type switches, and thermo optic switches using coated microsphere resonators [304].

Electro-optical switches: Their operation depends on the refractive index variation with control electric field. This characteristic makes them intrinsically high-speed devices (with relatively fast switching speed) and low power consumption. $LiNbO_3$ [305], SOA [306] and liquid crystal [307] are some technologies utilized in electro-optical switch fabrications.

Acousto-optical switches: They are based on acousto-optic effect in crystals (e. g. TeO_2) in which ultrasonic waves is used to deflect light [297]. Acoustic waves are generated in the crystal by a piezoelectric transducer driven by a RF signal source. The spatially periodic density variations in the crystal (corresponding to compressions and rarefactions of the travelling acoustic wave) are accompanied by corresponding changes in the refraction index for light propagation in the medium. Finally, the variation of the refraction index diffracts the incident.

Insertion loss, switching speed, crosstalk, polarization-dependent loss, wavelength dependency, stability/reliability, power consumption, operation bandwidth, and cost are some of performance parameters of optical switching technologies. A comparison of some switching performance parameters is reported in [297]. Moreover, multicasting possibility, physical switch dimension, optical integration possibility and scalability are other network swich requirements which must be noticed in optical network applications.

4.6 Optical buffering

One of the key challenges in the implementation of all-optical routers lies in packet buffering. Whenever two or more data packets arrive at a network node at the same time and contend for the same output, external blocking occurs. It is referred to as a contention among the packets. The contention resolution strategies can be categorized into three basic designs:

- Buffering, where there is packet buffered at each input (input buffering), each output (output buffering) or both of them (shared buffering) [308].
- Scheduling, where a frame of packets is examined at each input before being launched into the switching fabric [309]
- No buffering, where contention is resolved by either dropping or misrouting packets (e. g. deflection routing and wavelength conversion).

The optical buffer stores the data packets for a desired amount of time during destined output switch fabric port contentions and releases the data packets while the destined output port is cleared. A fiber delay lines (FDL) is a simple solution for optical buffering through which the departing times of packets are time-shifted. However, they can only provide limited buffer capacity and coarse delay granularity due to the bulky size of fiber delay lines [101]. Slow light in semiconductor nanostructures are also proposed for optical buffering applications. The basic idea centers on making a medium that can controllably slow down optical transmission such that it acts effectively as an optical memory. By controlling the group velocity reduction factor, the memory storage time can be adjusted to desired values [310]. The capabilities and limitations of slow light based optical buffers are studied in [311].

In deflection routing, for two or more packets which must be delivered to the same output, only one of them is sent along the link, while the others are sent along other available outputs, even though the other links are not preferred by the packets (e. g. those which do not yield shortest paths). Depending on the rate of incoming packets and the capacity of the outgoing links, deflection routing can work without any packet buffering. Advantages of implementing deflection routing in an optical network are a simpler and less expensive infrastructure implementation, network congestion reduction, and adaptability to mesh topologies. Disadvantages consist

of network synchronization issues that yield out-of-order packet arrival, no control over maximum number of hops through the network, difficult quality of service implementations, and possible localized bandwidth inefficiency.

Another alternative to contention resolution is the packet wavelength conversion which can be used for variable length and asynchronous optical packet routing [312]. By means of a wavelength converter, a packet or burst can be sent on a different wavelength channel to the designed output fiber. Thus, all wavelength channels of an output fiber can be considered as a single shared bundle of channels. EPSRC-funded project WASPNET (wavelength switched packet network) did some extensive work using multiple wavelengths to help resolving packet contention and to reduce the size of necessary optical buffers [276]. The contention resolution techniques can also be applied in optical burst switching networks [24], [313]. Vokkarane et al. [314] proposed a notion called the burst segmentation. Several mechanisms have been proposed on how to efficiently use the segmentation approach to achieve efficient contention resolution in optical burst switched networks, e.g., using burst segmentation combined with other approaches like the deflection routing.

4.7 Optical regeneration

Optical network cascadability faces a major limitation due to noise accumulation from optical amplifiers, chromatic dispersion, crosstalk, jitter, nonlinearities, and other imperfections in transmission and cross-connects. All these impairments degrade significantly the optical signal to noise ratio, resulting in restriction of the number of nodes through which signal can pass without fatal degradation. Typically, different levels of optical regeneration can be envisaged;

1R- amplification: The erbium-doped fibre amplifiers (EDFAs) are fully mature, commercially available, and are implemented in actual systems to provide amplification.

2R- amplification and reshaping: It can be used in long-haul high-speed optically amplified systems to maintain a high optical signal-to-noise ratio (OSNR) and avoid the accumulation of amplified spontaneous emission (ASE) noise in cascades of EDFAs. Alternatively, the excess noise produced in optical fibers by nonlinear transmission effects, such as four wave mixing (FWM), can be mitigated.

3R- amplification, reshaping and retiming: By combining 2R regeneration with retiming of the data to remove jitter impairments, full 3R regeneration of the optical signals is achieved. For 3R regeneration, a clock recovery technique is used to determine the frequency and phase of the incoming degraded data. 3R regenerators in burst-mode operation must be done for every burst packets separately [315], [316]. Figure 4.6 illustrates an example of the 3R principal operations.

A brief discussion on the optical regeneration is available in [317].

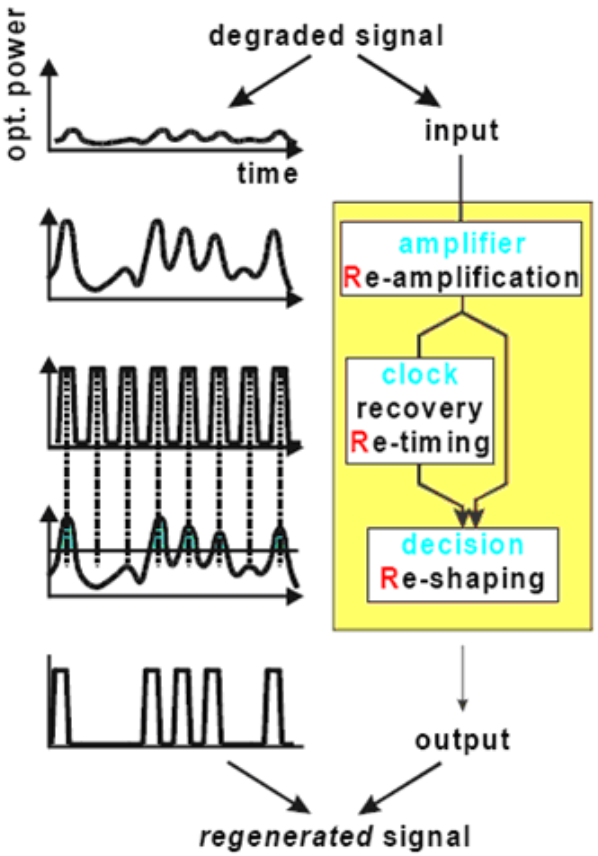


Figure 4.6: Key functional blocks of 3R-regenration; reamplification, retiming and reshaping, after [119]

4.8 Packet label processing

Packet label (header) processing is the fundamental operation in every packet based telecommunication network in order to dispatch the packets onto its desired destination. The packet label (header) must be separated, recognized and maybe rewritten in every core router. Due to the ever increasing line bit rate of data transmission over WDM links, the bottleneck is moving towards the electronic devices that processes the packet label at the core nodes of the network. Label and payload separation, packet pulse extraction, label recognition, and label swapping are some of the basic operations proposed for packet label processing.

4.8.1 Label-payload separation

The optical label is usually separated from the payload for the corresponding signal processing at the core nodes. The label separation technique is strictly dependent on the labelling format method described in section 4.3. Accordingly, several techniques has been proposed to separate the label and payload information such as fiber Bragg grating [223] [100], SOA [243], [318] and nonlinear optical loop mirror

(NOLM) [319].

In these methods, the packet timing information is extracted first. Afterwards, based on the labelling format of the packet, a decoding method is applied to separate packet label. However, the complexity of the involved circuits increases rapidly as the number of label bits increase. A header separation implementation in which the circuit complexity is independent of the header length was proposed in [320] but this circuit also requires a packet clock recovery circuit for correct operation. The implementation proposed in [223] does not require any clock extraction for header separation, but it still requires a specific modulation format (Manchester encoding of payload) to operate.

4.8.2 Packet pulse extraction

These techniques are essential for packet-level controlling and routing and are responsible for extracting a single pulse per incoming packet. This extracted pulse is then used in subsequent node sub-systems for powering or controlling additional optical gates. Several schemes for first pulse extraction have been demonstrated, mainly employing a marker pulse at the beginning of the packet at a different state relative to the rest of the packet, in terms of either, wavelength [102], polarization [103], bit period [74] or amplitude [104]. More recently, SOA based self synchronization methods are proposed whereas all the pulses of the packet share the same physical state [221] [321] [322] [242] [323].

4.8.3 Label recognition

During the past few years a number of header recognition strategies towards optically packet switching have been proposed. The different methods reported in literature can be categorized as below:

- **Interferometric methods:** They are based on auto-correlation of the packet label (header) bits. Semiconductor laser amplifier in a loop mirror (SLALOM) [83] and Terahertz Asymmetric Optical Demultiplexer (TOAD) [85] are the interferometric configuration with a SOA placed in a loop where the SOA is operated in a gain-transparent (GT) mode [324]. Figure 4.7 illustrates the conceptual diagram of an SLALOM based serial all-optical header processor [120].

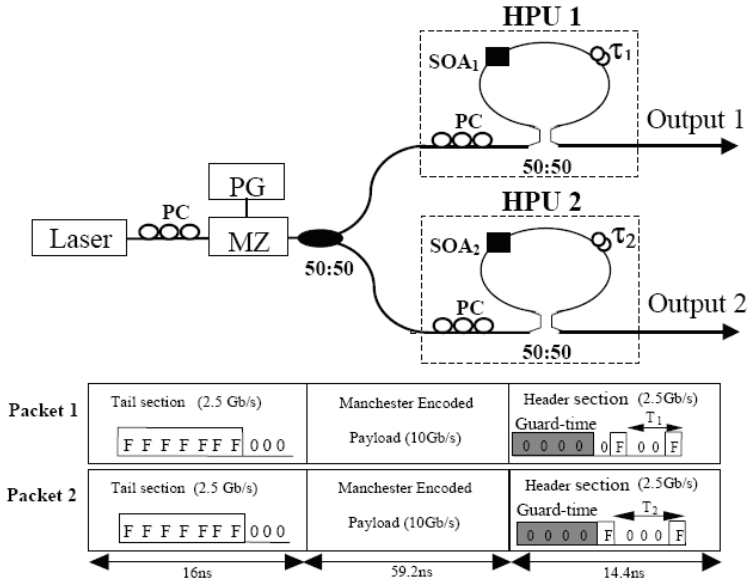


Figure 4.7: Experimental set-up to demonstrate SLALOM based serial all-optical header processor. τ_1−Delay Line for HPU1 (Header Processor Unit 1) ; τ_2−Delay Line for HPU2 (Header Processor Unit 2), after [120]

Dorren et al. proposed an all-optical header processing method based on two-pulse correlation in SLALOM [84]. The header of the data packets that were used in the experiments was at a lower bit-rate (2.5 Gbit/s) than the packet payload (10 Gbit/s). It does not require optical clock recovery, which reduces the complexity of the header recognition system. Moreover, Manchester encoding of the payload is necessary to guarantee that the header pattern is not repeated in the packet's payload.

Assigning the position of a signal in the time axis is also proposed using nonlinear optical loop mirrors (NOLMs) for optical header (label) processing aims [325]. These methods can be used to recognize low-power optical headers. However, header recognition by using this structure is limited to recognize specific bit patterns. Besides, they are too large to allow photonic integration.

- **Optical bit pattern matching** These methods are generally based on comparing every input packet label (header) with some pre-stored bit patterns. spectroholographic filtering [86] [87], Compact fiber-optic matched filters [88], fiber Bragg grating [89] [90] [326] [91] [295] [327], injection-locked Fabry-Pérot laser diode (FP-LD) [92], optical AND logic gate [74], [28] [93] [94], Optical XOR logic gate [95], Optical NAND logic gate [96] [328] are some of the proposed techniques for optical bit pattern matching. Figure 4.8 shows an FBG-based optical packet header pattern matching system [90]. In this architecture, if all the correlators fail to match the incoming packet address, then the packet is switched to an auxiliary port and processed by conventional electronics.

  Spectroholographic filtering requires free space optics. Moreover, compact

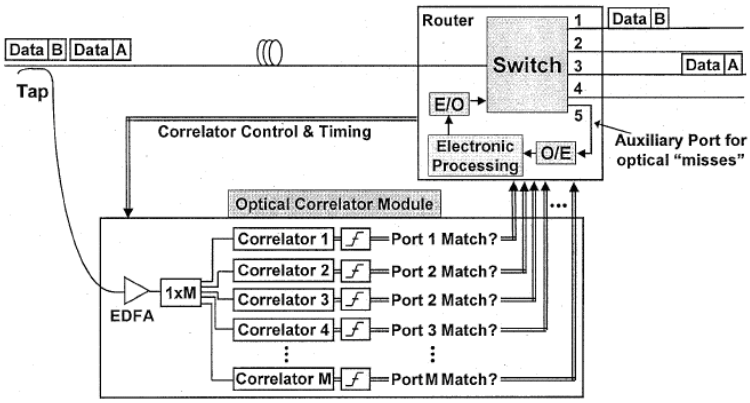


Figure 4.8: Conceptual diagram of an Internet core router with N output ports (typically two to four) assisted by a bank of M optical FBG-based correlators that are dynamically configured by a software algorithm, after [120]

fiber optic matched filters are fabricated by directly depositing metal thin films on fiber delay-line ends. Fiber optic delay line matched filters are proposed for the detection of an 8-bit optical packet address [88] where the incoming optical packet is split to make several identical packets (depending the number of header bits) and delayed by the fiber delay lines which determine the address code stored in the filter. However, this method is not tunable.

The other well-known alternative for the optical match filters is the fiber Bragg gratings (FBGs). Tunable FBGs are used in optical packet header (label) recognition performing optical bit sequence correlator. Since thin-film heaters can be fabricated with lithographic precision, spacing down to hundreds of micrometers are achievable with this technology, enabling for the higher bit rates [90]. The label (header) recognition can be done based on bit pattern correlation either in the same wavelength [89] [90] or in several wavelengths [100] [326] [91]. An advantage of operating at higher bit rates is that the realization of the FBG is simpler and the optical delay in the all optical correlator will be reduced. These would allow the photonic integration of the device. Moreover, the header recognizer operates at low power and asynchronously.

Optical Code Division Multiplexing (OCDM) is another FBG based technique proposed for optical header recognition [295]. The main attractive feature of OCDM is that the same time slots and the same wavelength bands are shared by many channels and its simple constitution [327].

Optical logic gate aided techniques are proposed for bit pattern recognition as well. For example, Cotter et al. [74] defined a corresponding 'keyword' for each header (label) which is simply its Boolean complement. An aligned bitwise AND operation (using FWM in SOA) carried out between the input packet header (label) and the keyword. By restricting the set of valid headers, it is possible to ensure that the output sequence from the aligned bit-wise AND operation between a header and a valid non-matching keyword will

always contain at least one 1. Therefore, an optical receiver monitoring the AND output with its threshold set just above the noise level can be used to determine if at least one 1 occurs during the header, indicating whether the header and keyword are matched. Although this method operates at low power and allows photonic integration, synchronization between the label and the keyword and the complexity of the receiver are its main disadvantages. Moreover, by increasing the header length, the number of required AND gates increases exponentially.

In IST-LASAGNE project (All-optical LAbel SwApping employing optical logic Gates in NEtwork nodes), the extracted optical label is fed to a bank of optical correlators based on all-optical logic XOR gates [26], where the comparison between the label and a set of local addresses is performed. After comparison between the label and a set of local addresses (using optical delay lines (ODLs)), a high intensity pulse will appear at the output of the XOR correlator with the matching address. This pulse feeds a control block that drives a wavelength converter [107].Thus, comparing the incoming label to the local addresses implies that for each possible incoming label a separate ODL and a correlator have to be installed [107].

Pulse-position modulation (PPM) format is used for coding of the packet header address and node routing table, making address-matching task much simpler where a single comparison is required [94]. The matching process is simply carried out by using a pair of all-optical symmetric Mach-Zehnder (SMZ) based AND gates by comparing the input packet label with routing table entries.

Martinez et al. [95] investigated a scalable scheme based on the principles of optical logic XOR gates (via SOA-MZIs [19]). The device acts as an all-optical correlator for bit-pattern matching applications. However, the Boolean one's complement (it is done by changing all the bits that are 1 to 0 and vice versa) of header to be compared must be introduced.

Hoanca et al.[93] presents a wavelength recognizing switch (WRS) device for all-optical control and routing. Routing addresses are encoded with the presence and absence of light in predetermined wavelength slots, and the address is processed in optical format, with sub-GHz resolution. The routing is based on optical filtering using four-wave mixing (FWM). Finally, the input packets are tapped out or blocked, based on the optical matching between the packet address wavelength and a local control wavelength (internal to the switching node). It allows the self-routing of optical packets in a dynamically reconfigurable way, but introduces new challenges for the network architecture in terms of crosstalk, noise performance and cascadability.

- **Slowed down label processing** In these methods, the packet label is separated and slowed down so that it could be processed within the high speed electronic devices. Optical digital-to-analog conversion [97], $N \times N$ arrayed waveguide Gratings (AWG) [98], serial-to-parallel conversion [99][100] are proposed in

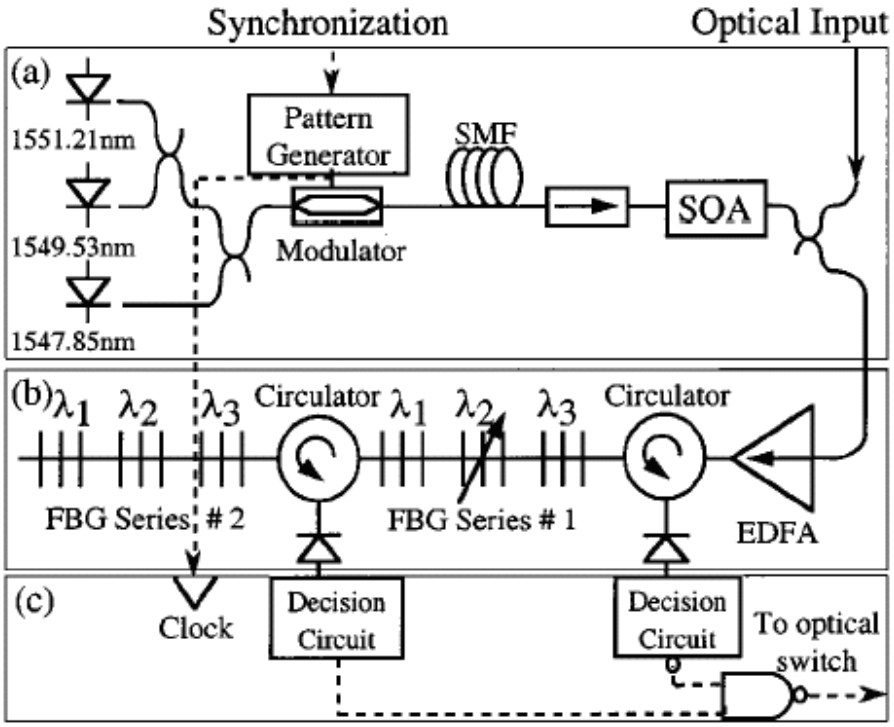


Figure 4.9: Experimental set-up of packet header recognition module based on (a) wavelength shifting for time-to-wavelength mapping, (b) wavelength selective delay for optical correlation, and (c) electronic decoder. (SMF: single mode fiber, FBG: fiber Bragg grating, SOA: semiconductor optical amplifier, EDFA: erbium doped fiber amplifier.), after [100]

order to slowed down label processing. Figure 4.9 displays an example of packet header recognition module based on header slowing down method [100].

In the optical digital to analog conversion based wavelength label switch (WLS) proposed in [97], the optical header (label) is converted to the analog pulse with different amplitude to discriminate the difference of the header pattern. The discriminated signal is used to select the wavelength of the electrically tunable laser for wavelength conversion.

Boyraz et al. [98] proposed the method of time stretch header recognition, where the header is optically extracted and slowed down using an optical true time delay (TTD) circuit, consisting $N \times N$ arrayed waveguide Gratings (AWG). Due to serial nature, the complexity of this approach does not increase for long headers.

Kit et al. [99] propose an all-optical ultrafast packet header recognition scheme for self-routing switch based on all-optical serial-to-parallel conversion. Each bit in the packet header is converted to a distinct wavelength, which is then separated by a 1×N wavelength demultiplexer. Thus, a parallel header bit

sequence, each at a lower bit-rate, can be obtained and it will be used to perform packet routing.

The multimode injection locking property and the bistable characteristic of injection-locking in an injection-locked FP-LD for all-optical header processing and switching of the control packet is utilized in this technique [92]. The header processing is based on the observation that the presence of a signal at a wavelength λ_d of a FP-LD can lower the injection-locking threshold at another wavelength λ_c. The switching of the control packets makes use of the bistable nature of injection-locking in FP-LDs, that is, it takes less power to maintain injection-locking than to initiate one.

A new label processing method based on time-to-wavelength converter (TWC) in order to slowed down label processing is proposed in chapter 5 and 6. Non-linear effects in SOA such as XPolM and FWM are employed in the proposed TMC architecture. Packet bit rate scalability, burst mode operation and modularity are some of the advantages in the proposed architecture [5].

- **All-optical label processing** In this method, the entire packet label processing is done optically. A new all-optical packet label processing and routing architecture is presented in chapter 7 [329]. In this method, in opposition to bit-pattern matching methods, regenerating the labels or saving them in the router nodes is not required.

4.8.4 Label swapping

Label swapping allows the current label to be erased and replaced by a new label which may contain local significant information [330]. For example, the new label may contain information which is specific to a certain section of the network. Similar techniques exist in IP, ATM and MPLS protocols; In IP the header contains a hop counter which gets continuously updated to prevent routing loops, ATM uses certain bits as locally significant information which has different meanings in different parts of the network and MPLS uses both of the above techniques. Label swapping allows much greater network scalability at a cost of greater required complexity at each node. The performance of the label-swapping operation is highly dependent on the labelling scheme [82].

Olsson et al. showed bit-serial label swapping by synchronous operation and fiber-loop mirror-based wavelength conversion, which required relatively accurate timing control, high-power operation, and bulky fiber spools [331].

In [279] and [332], the amplitude-shift keying payloads were modulated on the differential phase-shift keying/frequency-shift keying labels. Such schemes typically sacrifice the extinction ratio [279] or bandwidth efficiency [332] to sustain reasonable label performance.

The SCM label-swapping techniques involved a relatively complex single-sideband modulation method [333], an over-modulating scheme with intermodulation crosstalk

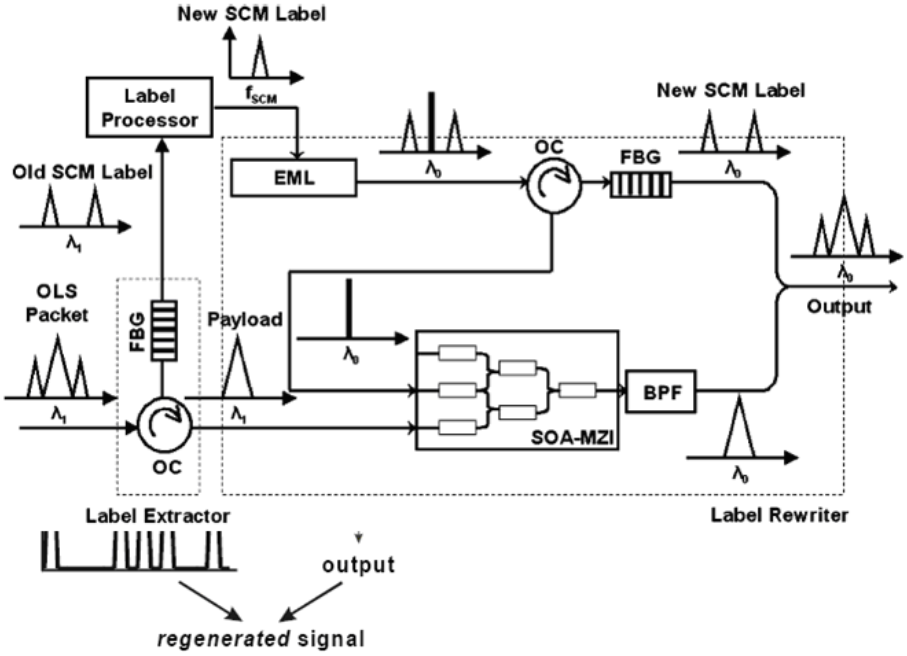


Figure 4.10: Schematic diagram of proposed all-optical SCM label-swapping system. EML represents integrated electroabsorption modulation laser, after [121].

[334], a bulky setup with external LiNbO modulators [335], or a relatively low-speed method (2.5 Gbit/s) limited by dynamic characteristics and intermodulation crosstalk of the components [336].

Recently, a compact all-optical subcarrier-multiplexed (SCM) label-swapping system employing an integrated electro-absorption modulation laser and a semiconductor optical amplifier based Mach-Zehnder interferometer wavelength converter [121]. Figure 4.10 shows the principle of the proposed label-swapping technique. This technique could be applied for bit-serial label swapping (chapter 6).

4.9 Summary

Optical label switching (OLS) is a promising technique for enabling low-latency forwarding of high-speed optical packets in future packet-based WDM networks. Most of the OLS subsystems are investigated in this chapter. Several labelling schemes, including bit-serial, sub-carrier multiplexing (SCM) and orthogonal modulation schemes have already been proposed and demonstrated. Among these schemes, bit-serial approach is the least restrictive approach in terms of packet bit rate and modulation extinction ratio.

Moreover, different all-optical packet label (header) recognition techniques as well as label slowing down, bit pattern matching, interferometric methods, and label processing are addressed in this chapter. New slowing down label processing and all-optical label processing methods will be presented in chapter 6 and 7, respectively.

CHAPTER

5

Time-to-Wavelength Conversion

5.1 Introduction

Optical telecommunication systems employ the wavelength domain to compensate the time domain inflexibility. Particularly, the enhanced connectivity required for performing intelligent optical networking in the metropolitan or backbone domains can be strongly boosted from the exploitation of the wavelength agility. A time-to-wavelength converter (TWC) can serve as a mapping element for transferring time domain optical data into the wavelength domain thus providing for OTDM/WDM functionalities [337], [338] and allowing optical header processing [100], [154], [339], and [340].

Time-to-wavelength conversion can be performed by means of SOAs. Nonlinear polarization rotation in SOA [341], cross-gain compression in SOA [100] have been proposed for TWC applications. This chapter addresses new SOA based methods for time-to-wavelength conversion in which the FWM and XPolM effects are employed. This operation can be dedicated to an optical label processing unit whose design is described in the following chapters.

The major element of the time-to-wavlength converter concept is the use of an optical AND logic gate. Each input data bit in the original time domain is transferred onto a specific wavelength. Nonlinear effects in SOA such as cross gain modulation (XGM), cross phase modulation (XPM), four wave mixing (FWM) and cross polarization modulation (XPolM) can be used for performing an all-optical AND logic gate.

Figure 5.1 illustrates a 4-bit time-to-wavelength converter. Each consecutive bit of an optical serial data sequence interacts with a single bit pulse carried on

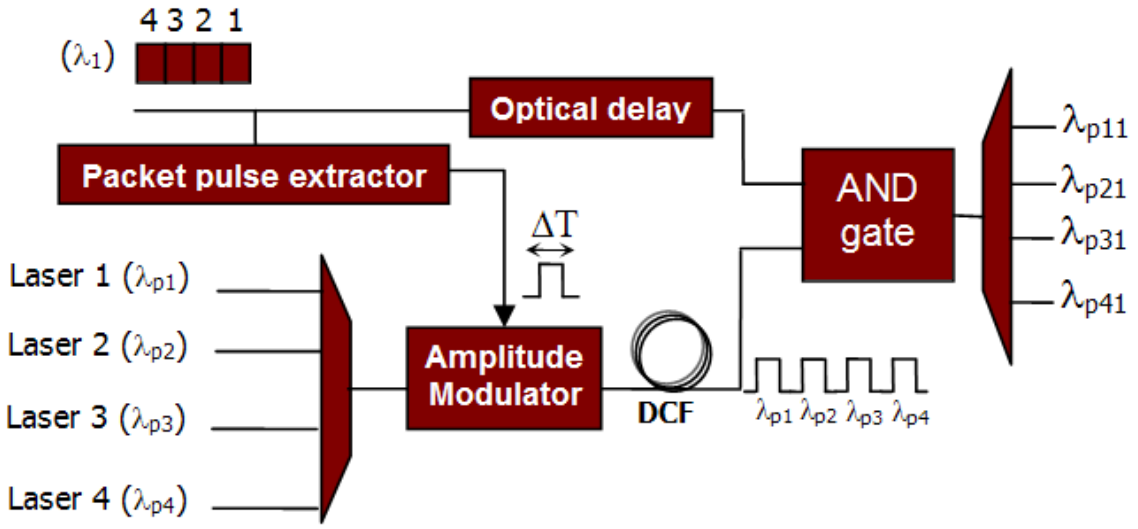


Figure 5.1: Schematic diagram of a 4-bit time-to-wavelength converter

one of 4 distinct auxiliary wavelengths. In order to obtain the required overlap, the amplitude of four auxiliary lasers multiplexed on a single optical fiber, are modulated by a single pulse of duration smaller than or equal to the label bit-time and delayed with respect to one another in a dispersive element (here a dispersion compensating fiber (DCF)).

5.2 Colored bit generation and synchronization

In order to avoid the interference effects, the required delay between the four wavelength bits is equal to the label time-bit. For synchronization of colored bits and data sequence, a clock recovery system must be used. Due to the lack of clock recovery in our experiment, it is replaced by a consecutive "1000" bit sequence. Therefore, every 4 bits in the serial data corresponds to a single electrical pulse used in order to modulate the pump laser beams.

In our experiment, the laser wavelengths are 1552.75 nm, 1551.95 nm, 1551.15 nm and 1550.35 nm. The maximum modulating pulse width is 100ps for a data sequence of 10 Gbit/s. The modulator is a Mach-Zehnder $LiNbO_3$ device and the DCF has 2.4 km long. Figure 5.2 displays the time delay generated by the DCF between two synchronous input optical pulses as a function of their wavelength difference. Figure 5.3 shows the time response measured on a sampling oscilloscope of the multiplexed modulated auxiliary laser signals before and after the DCF.

The auxiliary lasers can be replaced by a spectrum-sliced incoherent light source. In part 2.8, the advantage of using a spectrum-sliced incoherent light source has been explained in terms of cost and scalability. Figure 5.4 shows the spectrum-sliced incoherent light source modulated by a single pulse before and after the DCF. The light source is the amplified spontaneous emission of an erbium-doped fiber sliced by cascading a 1×4 wavelength demultiplexer and a 4×1 multiplexer centered on

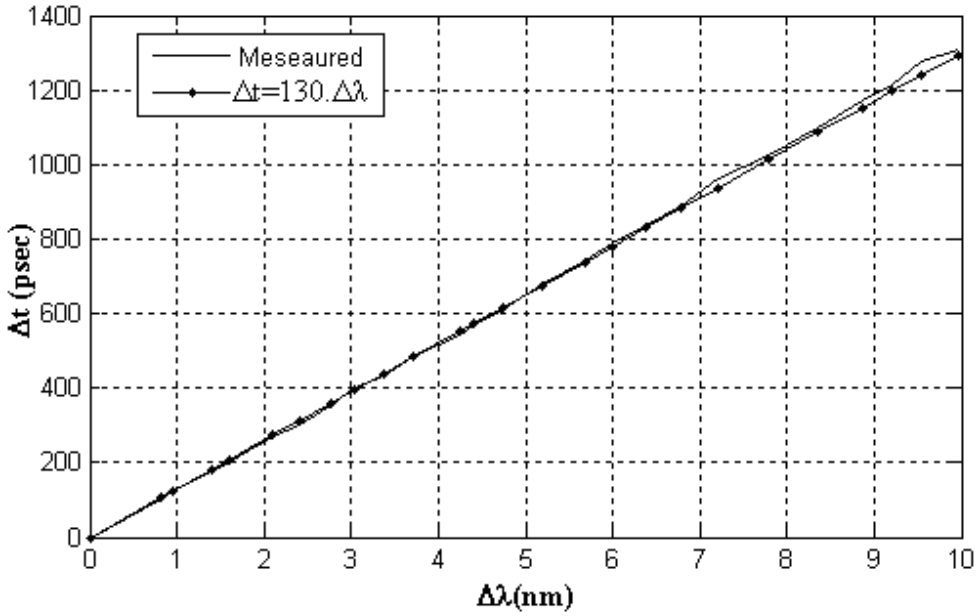


Figure 5.2: Measured time delay generated between two synchronous input optical pulses as function of their wavelength detuning.

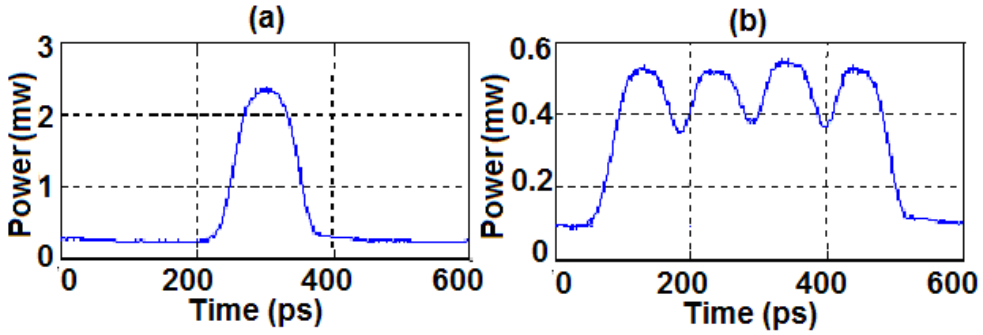


Figure 5.3: Four synchronous pulse-modulated auxiliary lasers; (a) before DCF, (b) after DCF

four wavelengths 1552.75 nm, 1551.95 nm, 1551.15 nm and 1550.35 nm with channel band width of 0.4 nm. Obviously, the pulse broadening occurs due to the pulse line-width (0.4 nm) which is visible in figure 5.4. A solution is to increase the finesse of filters (Multiplexer-Demultiplexer) of the sliced spectrum incoherent light (by using every other channel of a 50 GHz spacing Multiplexer-Demultiplexer channels instead of a 100 GHz channel spacing as used here). However, in our experiment, as the input data have RZ (return-to-zero) modulation format (with small pulse width of about 25 ps for bit rate of 10 Gbit/s), the overlap between the broadened incoherent pulses (figure 5.4) is not critical.

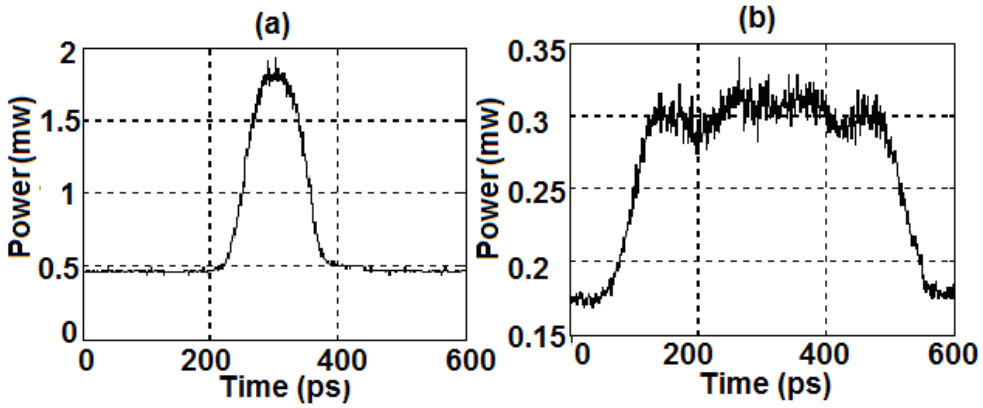


Figure 5.4: Four synchronous pulse-modulated incoherent sliced spectrum light, (a) before DCF, (b) after DCF.

5.3 AND logic gate

The four consecutive pulses carried on four different wavelengths are now ready to interact in the AND logic gate with the 4-bit of the serial data sequence (e.g. a part of a packet label) in order to transfer the label information onto the 4 different wavelengths which can be wavelength demultiplexed onto 4 different outputs. It must be noted that the requirements for increasing the operating bit rate of the time-to-wavelength converter are as follows: reducing the pulse duration which means using an appropriate modulator, reducing the delay introduced by the dispersive element (which is very straightforward) and using a fast AND gate. Furthermore, taking care of an increasing number of bit in the address sequence to adding auxiliary lasers in the first case (5.1) and very simply using extra channels of the multiplexer-demultiplexer in the second case (using the sliced spectrum incoherent light). The latter solution appeares as highly scalable and cost effective (as well as being polarization insensitive).

Different approaches have been proposed for optical AND logic gates (see table 3.1). The technique used for the AND gate in the time-to-wavelength converter must operate for all the auxiliary wavelengths, simultaneously. This excludes the methods such as PPLN, micro-resonator structures, NOLM and Sagnac interferometers. The SOA-based nonlinear techniques namely XGM, XPM, XPolM and FWM proposed for AND-gate realization. The XGM effect is limited by the speed of free carrier recovery, a low extinction ratio and limited input signal power range [37]. XPM is related to a potentially fast process: i.e. rapid variations in the refractive index of the SOA. The XPM is satisfactory in terms of speed and extinction ratio of the signal; in order to exploit the XPM, gates such as Mach-Zehnder and NOLM have been proposed [337], [15], [56]. However the former requires several (monolithically integrated) SOAs whereas the latter is rather bulky. Both are sensitive to the magnitude of the signal input power. The FWM and XPolM are methods which employ only a single SOA. Here we experimentally compare XPolM and FWM techniques for the required time-to-wavelength conversion application.

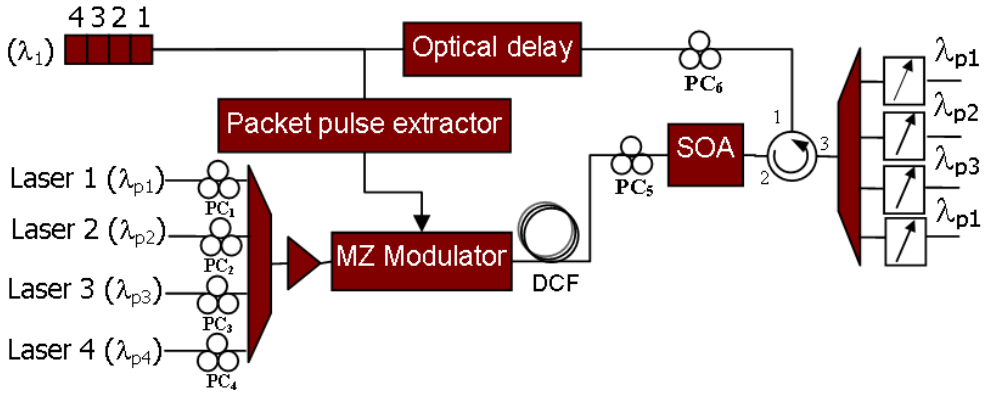


Figure 5.5: XPolM based 4-bit time-to-wavelength converter

5.4 Time-to-wavelength conversion using the XPolM effect

As mentioned in chapter 2, the XPolM effect in SOA is directly related to the TE/TM mode discrepancy of XPM and XGM. The SOA bias current, input signal powers and polarizations are the parameters that determine the magnitude of the polarization rotation. Figure 5.5 shows the scheme proposed for a time-to-wavelength converter based on the XPolM effect. A counter-propagating configuration is used in order to reduce the unwanted FWM effect in the SOA. The experiment described uses the four auxiliary lasers but could be just as well use the spectrum-sliced light source.

The polarization states of four auxiliary lasers are controlled by PC 1, 2, 3, and 4 in order to have the same polarization status before injection into the SOA (this is easy to verify by temporarily inserting a polarizer and oscilloscope at the end of DCF). PC 5 and PC 6 together with the laser1, 2, 3, and 4 power levels are tuned for optimizing the XPolM effect in SOA. After demultiplexing, a polarizer is set at each output so as to block the laser beam when the corresponding label bit is equal to zero (this setting is simply done by totally suppressing the input label sequence). By injecting the data sequence, the auxiliary laser beam polarizations rotate in the SOA because of XPolM effect, when the corresponding label bit equals to 1. Corresponding to the four bit label subsequence, there are 16 combinations ('0000', '0001',..., '1111'). For the zero bits, it is clear that the SOA output will be zero due to absence of light in the SOA input. The worst experimental case is the '1111' sequence which we have used to exhibit the time-to-wavelength converter functionality (figure 5.6). The data bit rate is 10 Gbit/s with RZ modulation format and the auxiliary (pump) laser wavelengths are 1552.75 nm, 1551.95 nm, 1551.15 nm and 1550.35 nm modulated by a Mach-Zehnder modulator using a RZ clock sequence generated by signal generator.

The maximum pulse-width of clock sequence (ΔT) is 100 ps corresponded to data sequence bit rate ($\Delta T \leq$ time-bit). Each data bit (λ=1556.7 nm) will coincide temporally with one of the "colored" auxiliary bits inside the SOA. The wider the

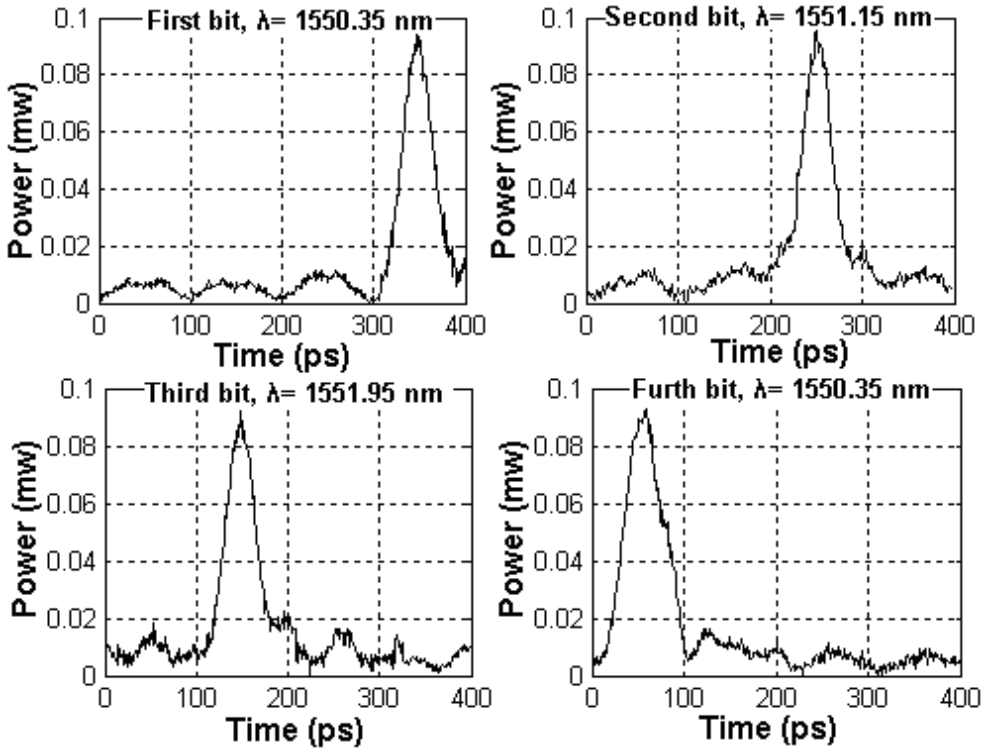


Figure 5.6: Four wavelength-separated bits at the output of the final demultiplexer by the XPolM effect

clock pulse width the weaker the synchronization sensitivity will be. The used SOA is fabricated by Alcatel OPTO+. It has 1.2 mm long biased (inversely) with a 300 mA current. Figure 5.6 shows the separated bits after demultiplexing. The extinction ratio is between 8 and 9 dB. By using a fast SOA with small recovery time, this technique could be used at 40 Gbit/s [342]. Generally, the input signal polarization state is unknown.

5.5 Time-to-wavelength conversion using the FWM effect

As mentioned in chapter 2, each SOA has a gain peak, which is determined by the composition of the material and the structure of the active layer. In the gain peak, the SOA has a maximum amplified spontaneous emission (ASE), but the input signal at that wavelength also experience a the maximum gain. A maximum amplification of the conjugated signal generated in the FWM process (idler) is obtained by placing the FWM signal at the gain maximum of the SOA (as depicted in figure 5.7-a). In order to minimize pattern dependencies a wavelength configuration as depicted in figure 5.7-b is the best configuration [343]; The wavelength of the data signal is chosen far away from the gain peak. The FWM signal also introduces a small pattern dependency and should thus slightly detuned from the center of the gain

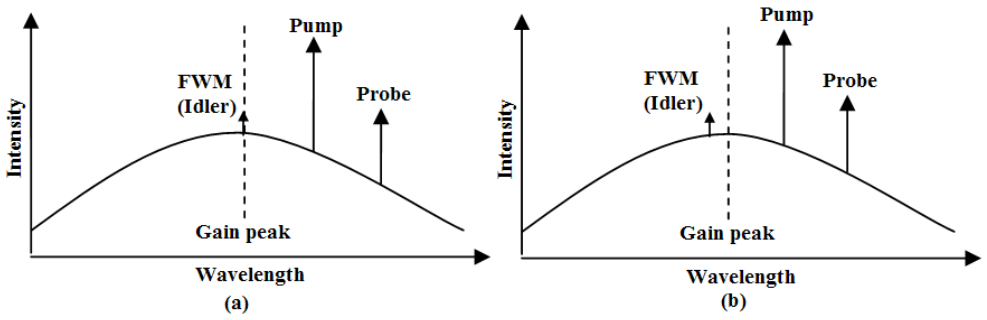


Figure 5.7: Wavelength configurations for efficient FWM; (a) Wavelength configuration giving a maximum gain to the FWM signal, (b) Ideal wavelength configuration for to minimize pattern dependencies of FWM signal

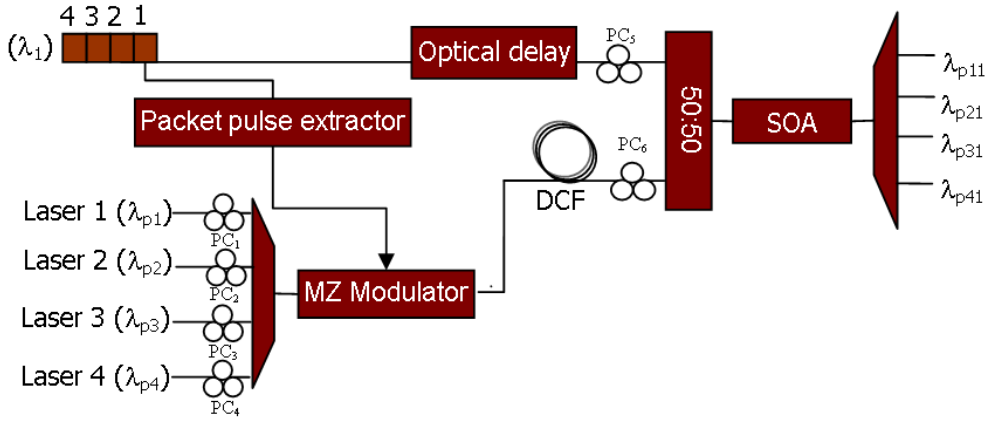


Figure 5.8: 4-bit time-to-wavelength converter by the FWM effect

peak. Therefore the configuration depicted in Fig. 5.7.b is the optimal configuration in which the FWM channel is not placed exaltly at the gain peak (but closed to it) while the data channel is placed far away from the gain peak [343].

Due to the experimental limitations, in our experiences, the pump and probe wavelengths are not chosen on the optimal configuration. Figure 5.8 presents a 4-bit time-to-wavelength converter based on FWM in SOA. A data sequence at λ=1553.1 nm is launched into a SOA together with 4 auxiliary modulated beams at λ=1551.4 nm, 1550.95 nm, 1550.15 nm and 1549.35 nm. In the SOA, each colored auxiliary bit coincides with a bit of the data sequence. The role of polarization controllers (PCs in figure 5.8) is to rotate the polarization state of laser beams so as to optimize the FWM in SOA for all bits, simultaneously.

Figure 5.9-a illustrates the spectrum of laser beams at the input of the SOA. The SOA output is shown in figure 5.9-b when the auxiliary beams are not modulated. One can observe the original wavelengths together with the FWM generated wavelength. The presence of more than two input wavelengths simultaneously in SOA is visible through the presence on many unwanted FWM components. These are removed in figure 5.9-c when the auxiliary laser is modulated with the method pre-

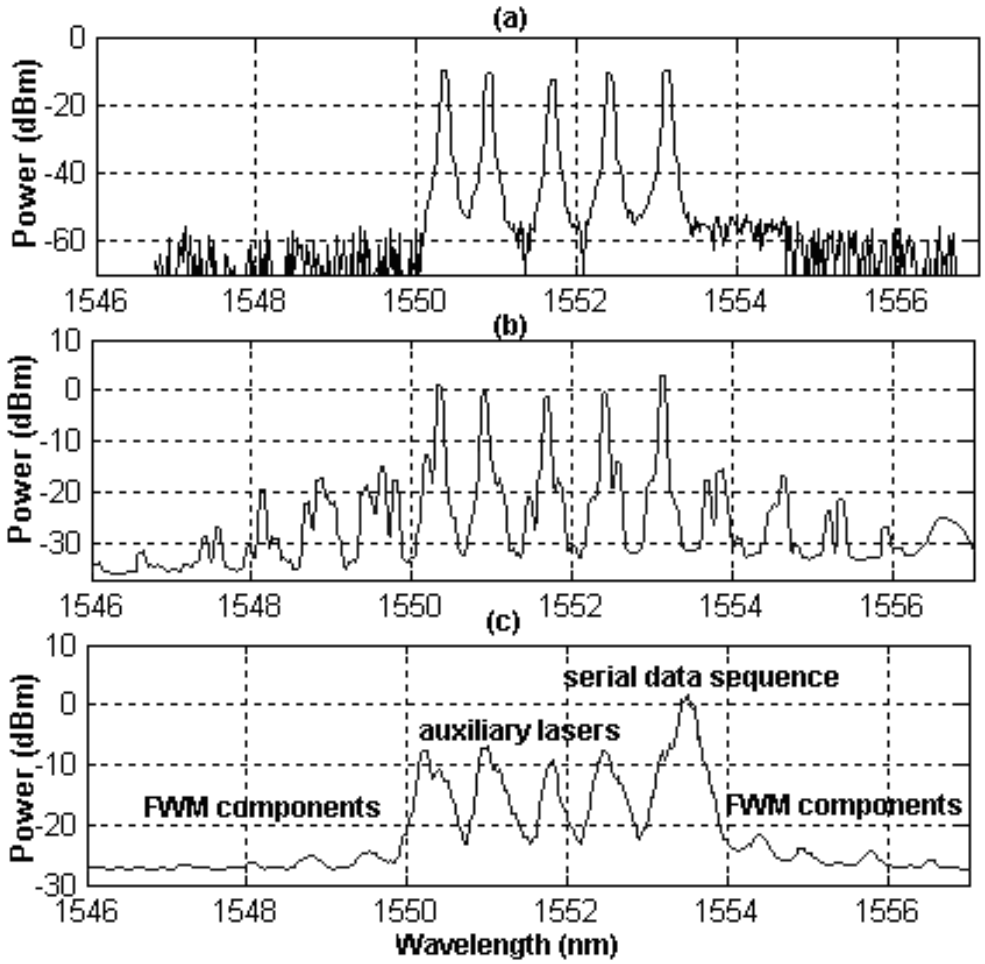


Figure 5.9: Pump and probe spectrum; (a) SOA input, (b) SOA output (continuous beams), (c) SOA output (modulated beams)

sented previously which prevents overlap due to the time spreading of the pulses.

In order to avoid the overlap of the generated and original components, the label sequence acts as the pump of the FWM process. The generated FWM wavelengths are 1554.45 nm, 1555.25 nm, 1556.05 nm and 1556.85 nm. Figure 5.10 shows the de-multiplexer outputs for the input sequence "1111" after transferring onto the different wavelengths. The probe and pump powers in the SOA input are -7.6 dBm and -3.7 dBm, respectively. The extinction ratio is between 9 and 12.5 dB. In all 4 cases, the signal amplitudes are different for each wavelength due to different FWM frequency detuning.

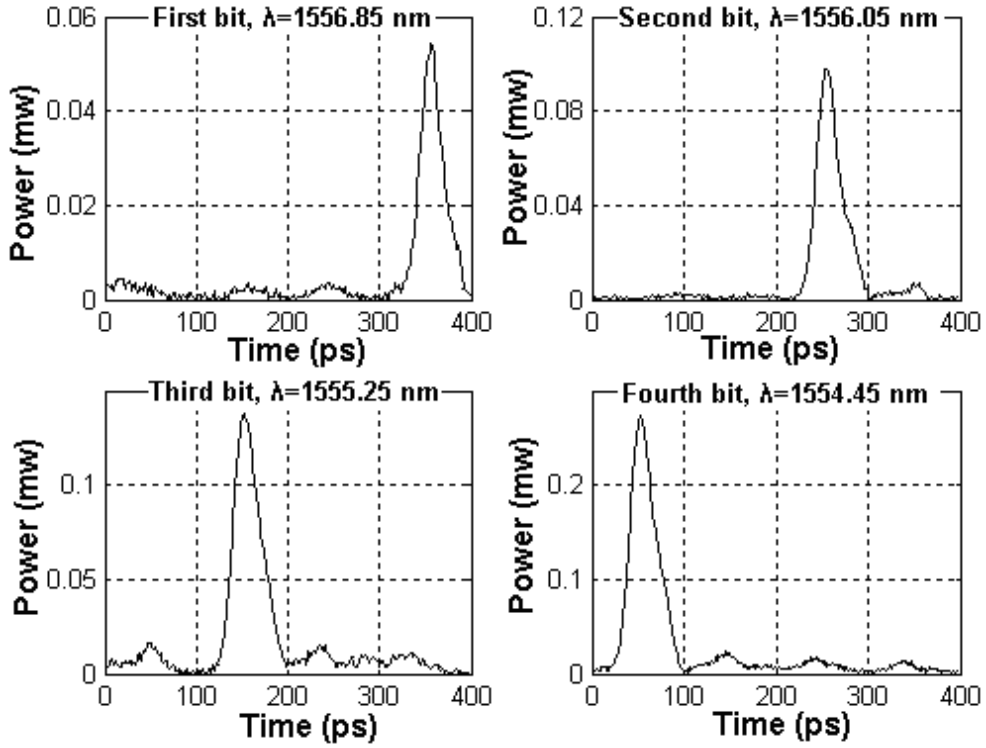


Figure 5.10: Four wavelength-separated bits at the output of the final demultiplexer.

5.6 Time-to-wavelength conversion using spectrum-sliced incoherent source

In part 5.2, the advantage of using a spectrum-sliced incoherent light source has been explained in terms of cost and scalability. Another major advantage relies on the potentiality for polarization insensitivity. As seen in chapter 2, although the FWM process between the data signal and the unpolarized spectrum-sliced light source is bounded to be less efficient than when the laser is used, the former situation leads to quasi-polarization insensitive operation (provided that the modulator and the SOA are polarization insensitive also). This expectation has been experimentally checked by performing FWM between a spectrum-sliced source at 1547.96 nm (with 0.4 nm of bandwidth) and the coherent laser beam (λ=1551.96 nm) in part 2.8.

Figure 5.11 shows the configuration of time-to-wavelength converter based on FWM in SOA with spectrum-sliced incoherent light source as probe beams. The four spectrum slices of the incoherent source are created by a multiplexer-demultilpexer pair (four channels at 1550.35, 1551.15, 1551.95 and 1551.75 nm with 0.4 nm channel bandwidth). The spectrum width of incoherent source can modify the FWM amplitude. Figure 5.12 depicts the simulated optical spectrum after the SOA in two cases; four spectrum-sliced incoherent light source ($\Delta\lambda$=0.4 nm) and a broadband filtered incoherent light source ($\Delta\lambda$=2.4 nm).

The FWM efficiency in four filtered thin slices is greater than a single wide sliced

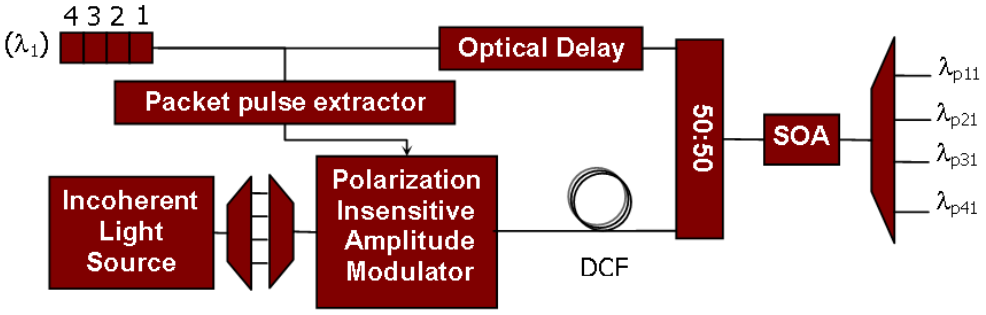


Figure 5.11: Four-bit time-to-wavelength converter by FWM effect in SOA with a incoherent light source

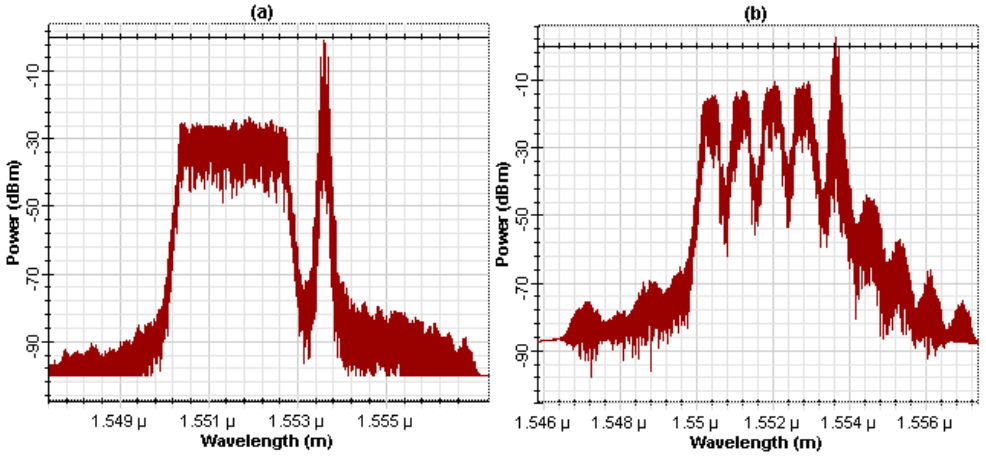


Figure 5.12: Simulation of the time-to-wavelength converter output spectrum after the SOA with a spectrum-sliced incoherent light source; (a) a broad band filter, (b) four narrow band filters

incoherent light source. In such a way, the unwanted interferences may be reduced. Figure 5.13 shows the measured SOA output spectrum where the FWM conjugated components are clearly visible. The four colored time-separated bits at the output of the demultiplexer are shown in figure 5.14. The probe and pump powers in the SOA input are -7.6 dBm and -3.7 dBm respectively (they are the same as the FWM and 4 auxiliary lasers). The extinction ratio is between 7 and 9 dB.

In the presented time-to-wavelength converter configurations, the bit rate can be easily modified by reducing the cumulative dispersion of the line and reducing the pulse duration. Moreover, the use of a spectrum-sliced incoherent light source instead of the lasers greatly reduce cost and improve the scalability in terms of the number of consecutive bits that can be converted.

The experimental demonstration of part 5.4 and 5.5 shows that both techniques can be used for performing the AND-gate of the time-to-wavelength sub-system. In both cases the extinction ratio of the transferred bit is similar and around 10dB. XPolM is known to be rather sensitive to input conditions: input power and input

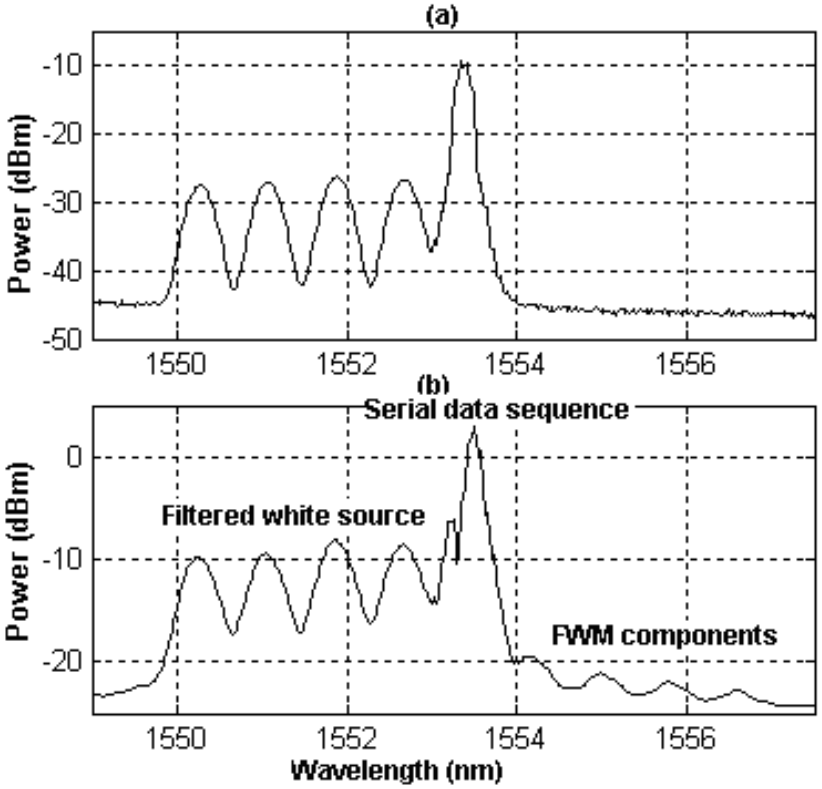


Figure 5.13: Measured spectrum of the time-to-wavelength converter using a spectrum-sliced incoherent light source and serial-data modulated beam; (a) SOA input, (b) SOA output.

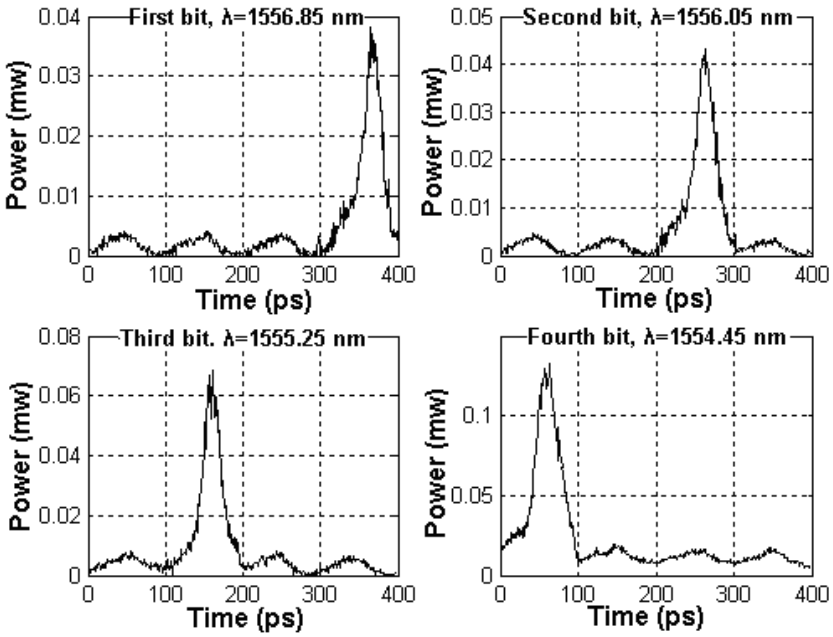


Figure 5.14: Four wavelength-separated bits at the demultiplexer output created by sliced incoherent light source

polarization. This can be solved by first launching the label sequence into an extra (and costly) polarization insensitive wavelength converter whose output polarization and power can be controlled [344]. XPolM based functionalities are difficult to realize in integrated optics. FWM is also polarization sensitive whereas the tuning of the input power is less critical. The effect suffers from a limited efficiency although the amplifier gain can partially compensate this. On the other hand, FWM can accommodate variable signal bit rates and operates up to very high rates. Polarization sensitivity can be overcome by using dual pump launching [345]. Another method for dealing with polarization sensitivity is the use a spectrum-sliced light source. In addition to the scalability, this solution solves the polarization problem as demonstrated theoretically and experimentally. The obvious drawback of the time-to-wavelength conversion technique using incoherent light source is the large degree of inherent intensity noise, which can be reduced using the non-linear gain compression characteristics of saturated semiconductor optical amplifiers (SOA) [346], [347].

5.7 Summary

Both XPolM and FWM in SOAs have been used for demonstrating the operating principle of time-to-wavelength converter at 10 Gbit/s. In order to reduce the sensitivity of FWM to input signal polarization, the use of a modulated spectrum-sliced incoherent light source is included in the setup. Despite a 3dB efficiency reduction in the best case with respect to an equivalent coherent light launching, the use of unpolarized, incoherent light allows polarization insensitivity as demonstrated theoretically and experimentally. New optical packet label processing system incorporating a time-to-wavelength converter by means of nonlinear effects in a SOA is proposed in two next chapters whereby each bit of a packet label subset is transmitted towards a separate output after wavelength conversion onto a dedicated wavelength.

CHAPTER

6

Demonstration of an Opto-Electronic Optical Packet Routing System

6.1 Introduction

As mentioned in chapter 4, in the MPLS protocol, packets are steered towards their destinations by interrogating their 20-bit destination label addresses. This can be time consuming given that core router must forward more than 100,000 entries. As a result, an all-optical router would need to be capable of dispatching this rate of packets. Such capability is below current optical technologies, but some recent developments leads to the feasibility of partial solutions. Given that most core routers of backbone or metro networks have only four to eight outgoing ports, it may be possible to determine a packet's outgoing port by looking at only a small subset of the label bits in the destination address. For example, IST-LASAGNE project targets to reduce the label length and thus the cost and complexity of individual components of the all optical label switching node [107].

Figure 6.1 illustrates the schematic diagram of opto-electronic label processing and routing system. The basic idea relies on time-to-wavelength conversion (TWC) whereby a subset of packet label is exploited onto distinct wavelengths. In other words, the time-to-wavelength converter serves as a serial-to-parallel converter. The parallelized bits are processed within an electronic signal processing subsystem. Burst-mode functionality of the proposed packet label processing module depends directly on the performance of clock recovery sub-system.

For an n-bit long packet label with a bit-rate of T, the parallelized label bit-rate

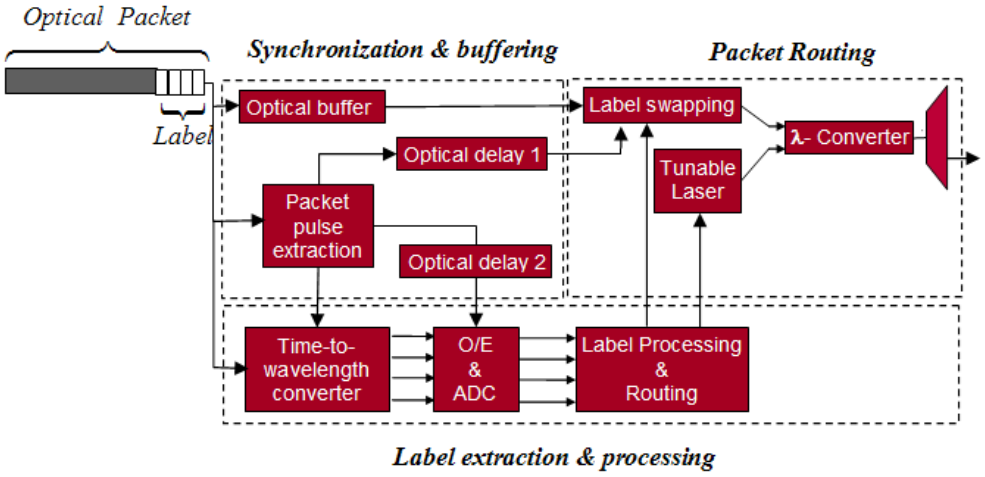


Figure 6.1: Conceptual diagram of the proposed optical packet label processing

at the time-to-wavelength converter output is T/n. So, the TWC acts as a bridge between high bit-rate optical packet label and an electronic signal processing sub-system working at a lower clock rate (e.g. given the actual electronic high speed circuit bit-rate of 40 Gbit/s, a packet bit rate of 160 Gbit/s is conceivable by using a 4-bit time-to-wavelength converter). Moreover, as the payload information is not ineresting for the packet routing procedure, the optic/electronic/optic (O/E/O) conversion of packet payload is not necessary, leading to payload transparent network nodes. So, all the packet duration can be dedicated for the label processing and packet routing operations in network router. In the following parts of this chapter, the opto-electronic packet label processing and packet routing system shown in figure 6.1 will be presented in detail. The evaluation and compatibility (between the input and output) of the various sub-systems should be assessed.

6.2 Synchronization & buffering

In the proposed architecture, the packet label processing could be accomplished either synchronously or asynchronously. It means that a true clock recovery sub-system is not necessary. However, the beginning bit of each packet must be known. A packet pulse extractor sub-system can serve for extracting a single pulse per incoming packet. The packet pulse extraction methods are discusted in part 4.8.2.

The packet pulse extractor output is used in order to modulate the auxiliary lasers in the time-to-wavelength sub-system (chapter 5). Moreover, it can serve into the packet routing subsystem (e.g. the chip-enable of analog-to-digital converter (ADC)). The optical delay 2 is responsible for compensating the delay provided by the label extraction & processing sub-systems. Moreover, optical buffering method and technologies have been studied previously in chapter 4 (see 4.6). The packet payload can be passively buffered within the optical delay line 1 and 2 during the routing procedure (figure 6.1).

6.3 Label extraction

In IST-LASAGNE project, the packet payload (40 Gb/s) and label (10 Gb/s) are separated due to a UNI (ultrafast nonlinear interferometers) system [107]. The UNI performs an AND operation between the properly delayed clock and packet signals [320].

Here, the proposed label extraction and processing system includes an optical (time-to-wavelength converter) and an electronic (packet label processing) subsystems. The time-to-wavelength converter is employed in order to parallelize the packet label subset [100]. Other serial-to-parallel conversion techniques proposed previously such as surface-reflection optical switch [348], surface-emitted second harmonic generation (SHG) in a waveguide [349], or lithium niobate intensity modulators [350] can be replace with the time-to-wavelength converter. But, the main advantage of this time-to-wavelength converter is the packet length and bit-rate flexibility. The parallelized bits are transformed onto an electrical format and amplified in order to feed into the label processing subsystem.

6.4 Electronic packet label processing

Figure 6.2 displays the schematic diagram of the electronic packet label processing in details. In time-to-wavelength converter methods presented in chapter 5, the parallelized (output) bits are not synchronous. A delay of the packet label time-bit exists between two successive bits (100 ps at bit rate of 10 Gbit/s). So, the role of delay 4, 5 and 6 is the compensation of this relative delay between them. The time delay necessary are one, two and three time-bit for delay 4, 5 and 6, respectively (e.g. 100, 200 and 300 ps at bit rate of 10 Gbit/s). These delays can be achieved either electrically or optically.

Thanks to four photo-detectors, the synchronous parallelized bits are converted in electrical format. Next, they are transformed into the LVDS (Low Voltage Differential Signalling) format before processing. Most of the recent high speed electronic devices are based on LVDS standard currently standardized by the TIA/EIA (Telecommunications Industry Association/Electronic Industries Association) ANSI/TIA/EIA-644-A (LVDS) Standard. This technology allows products to address high data rates ranging from 100's of Mbps to greater than 2 Gbit/s. LVDS brings many other benefits, which include:

- Low-voltage power supply compatibility
- Low noise generation
- High noise rejection
- Robust transmission signals
- Ability to be integrated into system level ICs.

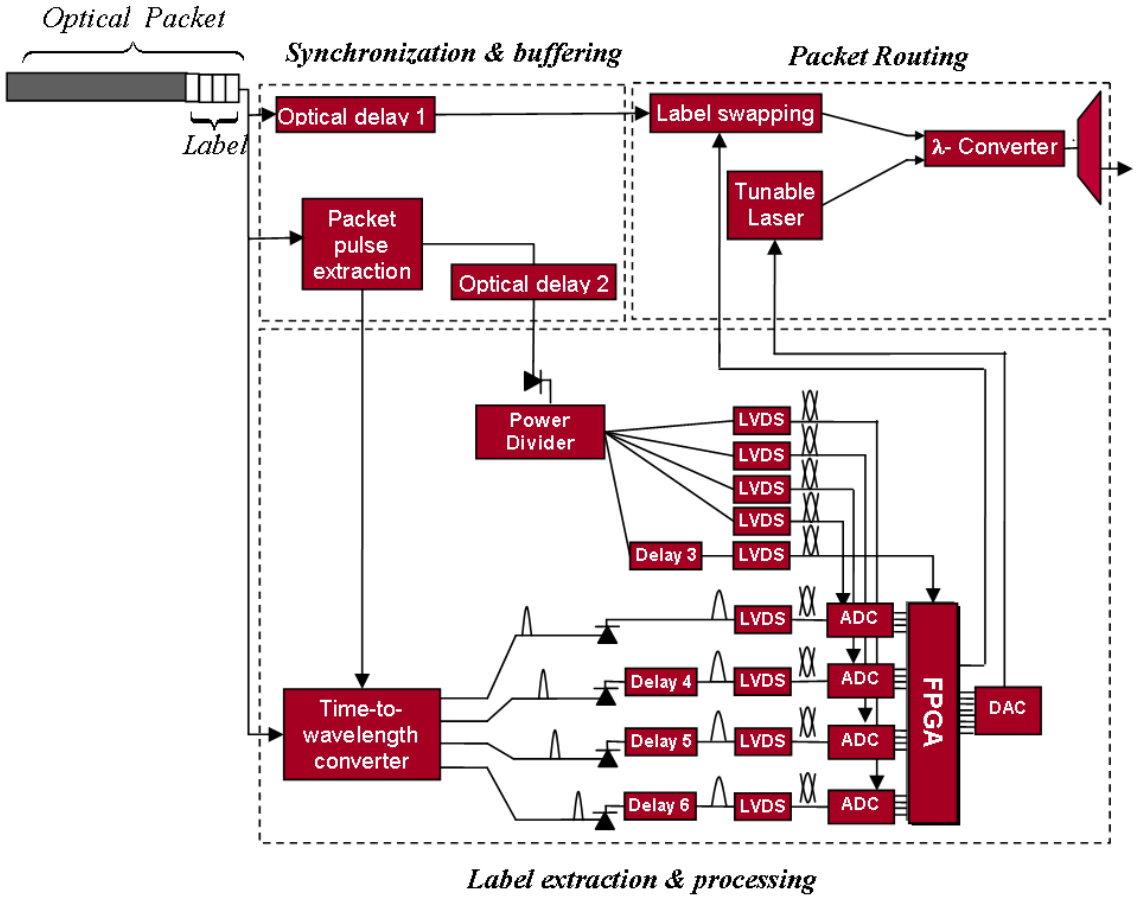


Figure 6.2: Conceptual diagram of time-to-wavelength converter based optical packet label processing

An analog-to-digital converter (ADC) is used for sampling, amplifying and buffering the electrical analog bits as well as producing a variable detecting threshold level. Routing algorithm operations and output command generation can be done in FPGA (field-programmable gate array) sub-system. For the ADCs and the FPGA input chip-enables, the packet pulse extractor signal can be reused after compensating the total time delay in the intermediate components within delay 2 and delay 3, respectively. Here, the electronic sub-sections are considered in details.

6.4.1 Photo-detection

In the present optical networks, the majority of data pre- and post-processing for the packet routing are done electronically relied on the VLSI technology. Therefore, the development of high-speed photo-detectors in the wideband photonic system is important. Sensitivity, dynamic range, quantum efficiency, responsivity, internal gain, bandwidth and noise are some of the key parameters;

- Sensitivity of a photo-detector is defined as the minimum mean optical power

needed to achieve a given bit error rate, BER (CCITT standard requires a BER of 10^{-10}).

- Dynamic range is the range of input power levels over which the BER is acceptable.

- Quantum efficiency, η, and the responsivity, R, are interlinked; the η is essentially the efficiency of converting an incident photon (optical power) into photo current, whereas the R is the amount of photo current obtained for a unit of incident optical power. Responsivity and quantum efficiency are wavelength dependent.

- Photo-detector bandwidth refers to the range of frequencies over which the detector provides useful output at a pre-defined level (e.g. 3 dB).

Photo-detectors can be broadly categorized into two types: those without internal gain such as p-n and p-i-n diodes and those with internal gain such as avalanche photo-diode (APD) and phototransistor. The internal gain of a detector refers to the generation of secondary electron-hole pairs created by the primary photo generated pair as in APDs or the electrical gain of bipolar transistor based photo-detectors.

Quantum (Shot) noise and Dark current noise are the principal noises associated with photodetectors. Quantum (Shot) noise is due to the statistical nature of the production and collection of photo-generated electrons upon optical illumination. It has been shown that the statistics follow a Poisson process. Dark current noise is the current that continues to flow through the bias circuit in the absence of the light. This is the combination of bulk dark current, which is due to thermally generated electron and hole in the p-n junction, and the surface dark current, due to surface defects, bias voltage and surface area. So, in order to calculate the total noise presented in photodetector, we should sum up the root mean square of each noise current by assuming that those are uncorrelated. Signal to noise ratio (SNR) and noise equivalent power (NEP) are the terms often used to quantify the signal and noise ratio in an optoelectronic device.

The basic goal is to achieve the lowest possible noise at a given bandwidth or data rate. There is often a fundamental trade-off between the sensitivity and the bandwidth of a photo-detector. For example, in the case of a p-i-n detector with a FET pre-amplifier, a large resistor may be needed to extract a useful voltage to drive the gate of the FET. However, the RC constant becomes large which limits the bandwidth of the receiver. The p-i-n photo-detectors are designed to provide high speed whereas APDs are essentially high gain devices. Since from a system point of view, the product of the gain and the bandwidth is important, there will a region of overlap where either device may be equally suitable.

In our experience, two photo-detector types (TIA-950 and TIA-525) are used. Table 6.1 summarizes the characteristics of employed photo-detectors. Figure 6.3 represents the electrical converted label pulses (bits) measured within these photo-detectors.

Table 6.1: Characteristics of TIA-950 and TIA-525 photo-detectors

Photo-detector model	TIA-950	TIA-525
Detector type	InGaAs (900-1700 nm range)	InGaAs (900 -1700nm)
Trans-impedance	1.2 K	1.4 K, 14K
Post amplifier gain	×10, ×1	×10, ×1
Maximum input power	0.8 mW	1.2 mW
Bandwidth	750 MHz at gain of 1 250 MHz at gain of 10	125 MHz at 1.4 k trans-impedance 35 MHz at 14 K trans-impedance
Noise level	3 pW/Hz$^{1/2}$	3 pW/Hz$^{1/2}$
Maximum output voltage	2 V p-p, no load, 1 V p-p, 50 Ω load	4 Vp-p, no load, 2 V p-p, with 50 Ω load

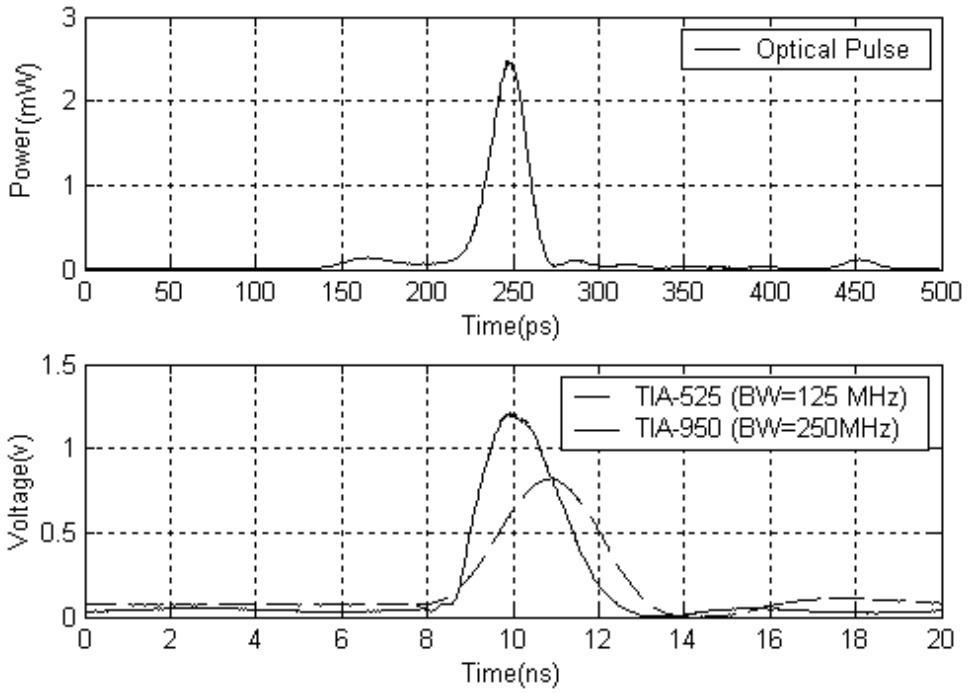


Figure 6.3: The pulse detected within the TIA-950 and TIA-525 photo-detectors

The RZ (return-to-zero) modulated optical label bits have 40 ps time-width. The electrical pulse width (2 ns for TIA-950 and 4 ns for TIA-525) is a limit for the optical packet minimum duration. Otherwise, a guard time between two successive packet labels is useful in order to avoid the interference between them in the electronic circuit. For example guard time of about 2 and 4ns are necessary by using TIA-950 and TIA-525 respectively.

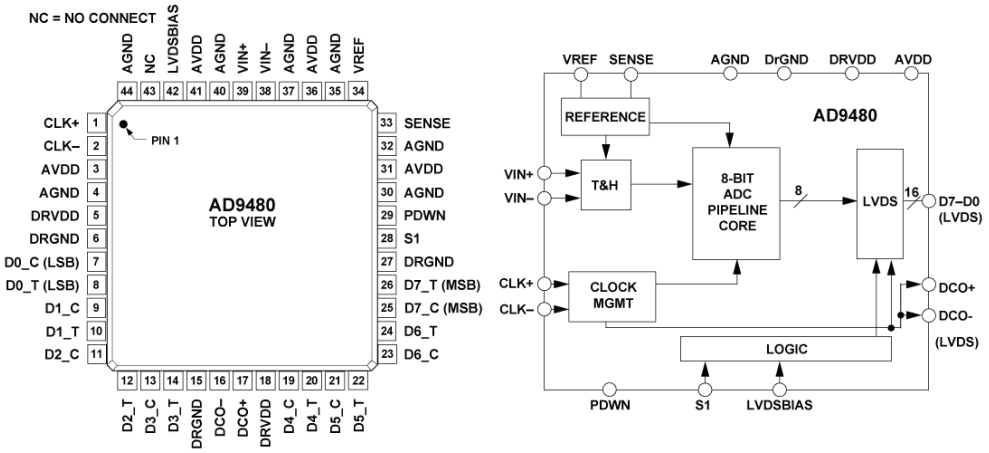


Figure 6.4: Functional block diagram and pin out diagram of ADC converter AD9480

6.4.2 Analog-to-digital converter (ADC)

Typically, an ADC is an electronic device that converts an input analog voltage to a digital number. It sets the receiver's maximum bandwidth, signal-to-noise ratio (SNR), and dynamic range. For a high-speed ADC the sampling speed, SNR, SFNR (Signal-to-Fluctuation Noise Ratio) and THD (Total harmonic distortion) are the basic parameters used to characterize the dynamic performance of the ADC. Here, we employed the AD9480 which is an 8-bit, monolithic analog-to-digital converter optimized for 250 MSPS conversion rate fabricated by Analog Devices Company. Figure 6.4 presents the functional block diagram and pin out diagram of this converter. The Pin function description is shown in table 6.2.

The maximum bandwidth of the ADC is equal to 1/2 of the ADC's sampling rate. But in our label processing scheme (figure 6.2), the ADC is used to transform the electrical photo-detector output pulse into a logic level pulse. So, only one sample per bit is enough in order to bit value detection (i. e. '0' or '1'). Thus, the ADC used in label processing application must have a sampling rate as fast as the paralleled label bit rate.

The dynamic performance of the ADC depends on external and internal factors. The internal factors mainly include design architecture and process which is optimized by the manufacturer. The external factors include signal source, signal input circuit, clock source, output digital load, power supply decoupling.

AD9480 consists of five sections: reference voltage circuitry, clock circuitry, input stage, ADC pipeline core, and the output stage (figure 6.4). The input stage includes a high bandwidth sample & hold (S/H) amplifier accepting the analog input signal and capturing it at either rising or falling edge of the sampling clock. Then the ADC pipeline core converts the analog signal to digital form, sequentially, with the most significant bit (MSB) first and finally, digital output of the ADC is produced. The AD9480 has 8 clock periods of data latency.

The analog input stage requires a common-mode voltage to act as a reference line around which the signal can swing. The common-mode reference voltage is

Table 6.2: Pin function descriptions

Pin No.	Mnemonic	Description	Pin No.	Mnemonic	Description
1	CTK+	Input Clock-True	23	D6-C	Data Output Bit 6-Complement
2	CTK-	Input Clock-complement	24	D6-T	Data Output Bit 6-True
3	AVDD	3.3 V Analog Supply	25	D7-C	Data Output Bit 7-Complement (MSB)
4	AGND	Analog Ground	26	D7-T	Data Output Bit 7-True (MSB)
5	DRVDD	3.3 V Digital Output Supply	27	DRGND	Digital Ground
6	DRGND	Digital Ground	28	S1	Data Format Select and Duty-Cycle Stabilizer Selection
7	D0-C	Data Output Bit 0-Complement (LSB)	29	PDWN	Power-Down Selection (AVDD)
8	D0-T	Data Output Bit 0-True (LSB)	30	PDWN	Analog Ground
9	D1-C	Data Output Bit 1-Complement	31	AVDD	3.3 V Analog Supply
10	D1-T	Data Output Bit 1-True	32	AGND	Analog Ground
11	D2-C	Data Output Bit 2-Complement	33	SENSE	Reference Mode Selection
12	D2-T	Data Output Bit 2-True	34	VREF	Voltage Reference Input/Output
13	D3-C	Data Output Bit 3-Complement	35	AGND	Analog Ground
14	D3-T	Data Output Bit 3-True	36	AVDD	3.3 V Analog Supply
15	DRGND	Digital Ground	37	AGND	Analog Ground
16	DCO-	Data Clock Output-Complement	38	VIN-	Analog Input-Complement
17	DCO+	Data Clock Output-True	39	VIN+	Analog Input-True
18	DRVDD	3.3 V Digital Output Supply	40	AGND	Analog Ground
19	D4-C	Data Output Bit 4-Complement	41	AVDD	3.3 V Analog Supply
20	D4-T	Data Output Bit 4-True	42	LVDSBIAS	LVDS Output Current Adjust
21	D5-C	Data Output Bit 5-Complement	43	NC	No Connect (Leave Floating)
22	D5-T	Data Output Bit 5-True	44	AGND	Analog Ground

typically half of the ADC supply voltage. In the reference circuitry also, a band-gap is integrated to provide a high accuracy internal reference voltage for the ADC core.

The conversion rate of the ADC is determined by the input clock. The AD9480 has an internal clock duty-cycle stabilization circuit that locks to the rising edge of clock and optimizes timing internally for sample rates between 100 MSPS and 250 MSPS. Jitter on the rising edge of the input is still of paramount concern and is not reduced by the internal stabilization circuit. The clock duty-cycle stabilizer can be disabled at Pin 28 (S1).

The ADC input structure is designed to accept both single-ended and LVDS formats. LVDS uses a dual wire system, running 180 degrees of each other. This enables noise to travel at the same level, which in turn can get filtered more easily and effectively. Thus, lower signal voltage swings could be used which means data can be switched very quickly. Table 6.3 presents a comparison between LVDS, TTL/CMOS (Transistor Transistor Logic/ complementary metal oxide semiconductor), GTL/BTL (Gunning Transceiver Logic / backplane Transceiver Logic) and PECL (Positive Emitter Coupled Logic) standards. The optimal performance of AD9480 is obtained when the analog inputs are driven differentially.

A wideband transformer, such as Mini-Circuits ADT1-1WT (0.4-800 MHz), can

Table 6.3: Comparison between addressing standards

Parameter	LVDS	TTL/CMOS	GTL/BTL	PECL
Signaling	Differential	Single ended	Single ended	Diff./Single ended
Output voltage swing	±350 mV	2.4–5.5 V	1V	±800 mV
Receiver threshold	±100 mV	1.2–1.5 V	±200 mV	±200 mV
Maximum Speed	>400 Mbps	<100 Mbps	<100 Mbps	>400 Mbps
Drive current (mA)	3–10 mA	75 mA	40–80 mA	40–60 mA
Noise generation	Low	High	Medium	Medium
Power dissipation	Ultra low	High	Med.- High	Medium

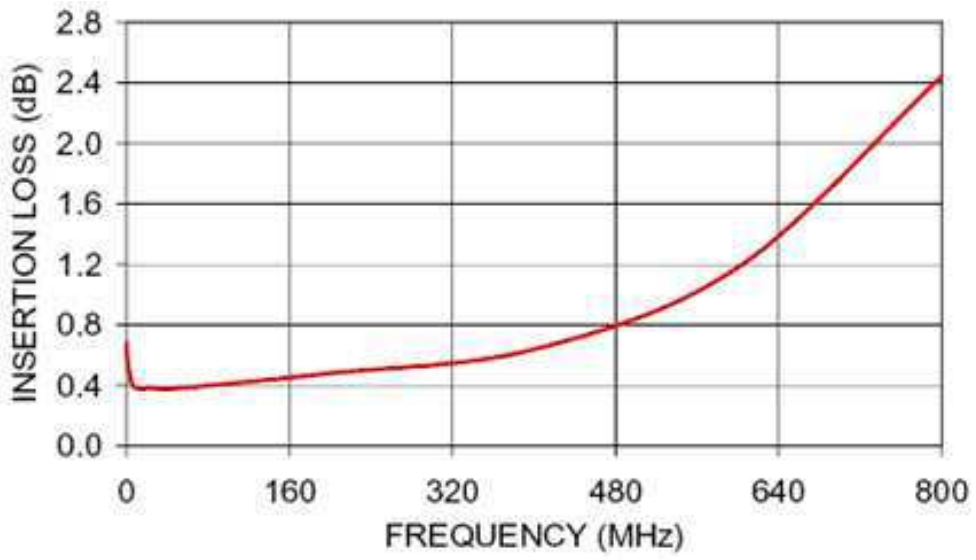


Figure 6.5: ADT1-1WT wideband transformer insertion loss

provide the differential analog inputs for connecting the photo-detector output on the ADC input. Figure 6.5 displays the insertion loss of this transformer.

Figure 6.6 illustrates the schematic setup of the ADC together with LVDS/CMOS converter, logic gate and flip-flop ICs. Analog input and clock pulse signals enter at SMA Connector J1 and J2 respectively. These signals are terminated to ground through a 50 Ω resistance. The input is ac-coupled to a high speed differential receiver (Motorola-MC100LVEL16) which provides the required low jitter and fast edge rates needed for best performance.

The high-speed switching of LVDS signals almost always requires a line impedance matching resistor at the receiving end of the cable or transmission media (100 Ω in AD9480). Linear variable differential transformer (LVDT) products eliminate this external resistor by integrating it with the receiver. The SN75LVDT386 is eight-differential line receivers used for ADC output signals.

Finally, the digital bits can be saved in a buffer to serve in FPGA or other logic circuitry. The LVTH162374 has 16-bit edge-triggered D-type flip-flops with 3-

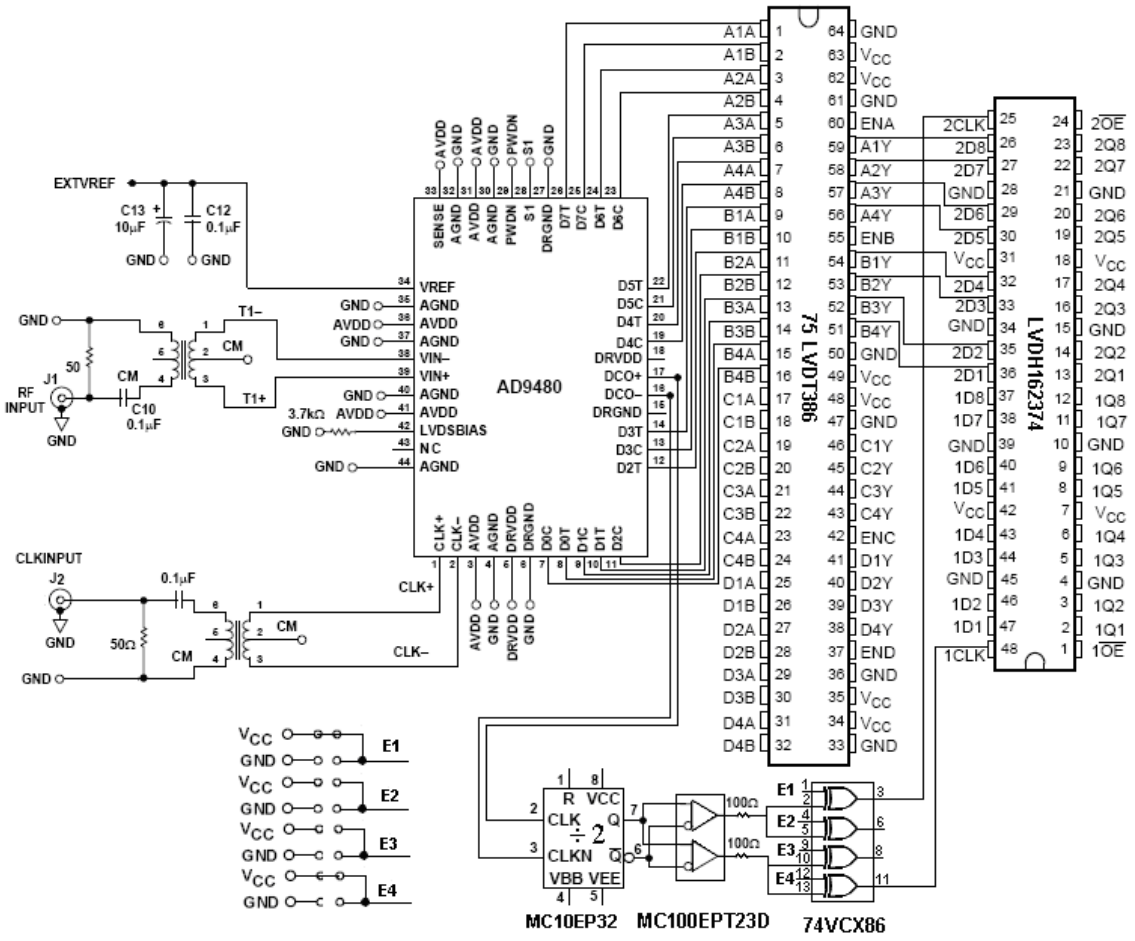


Figure 6.6: Schematic montage of ADC

state outputs designed for low-voltage (3.3-V) operation, but with the capability to provide a TTL interface to a 5-V system environment. They are particularly suitable for implementing buffer registers, I/O ports, bidirectional bus drivers, and working registers. On the positive transition of the clock (CLK), the Q outputs of the flip-flop take on the logic levels set up at the D inputs (figure 6.6).

For the clock of flip-flops (LVTH162374), the output clock of AD9480 (DCO+ and DCO-) are used. An ECL ÷2 divider (MC100EP32) with differential clock inputs together with a dual differential LVPECL to LVTTL translator (MC100EPT23) are employed to product the clock pulses compatible with LVTH162374.

To synchronize the input data with the clock within LVTH162374, the propagation delay on clock and data paths must be equalized. The propagation delay on SN75LVDT386 (data path) is 2.6 ns. The propagation delay within MC100EP32 and MC100EPT23 are 150 ps and 1.5 ns respectively. Therefore the delay on the clock path is 1.65 ns. To compensate the rest of delay between clock and data paths a 74VCX86 integrated circuit is used which includes four 2-input exclusive-OR gates.

Based on the RF analog input pulse amplitude, 2^8 combinations are achieved in ADC output. The ADC most significant bit (MSB) is '1' when analog amplitude is

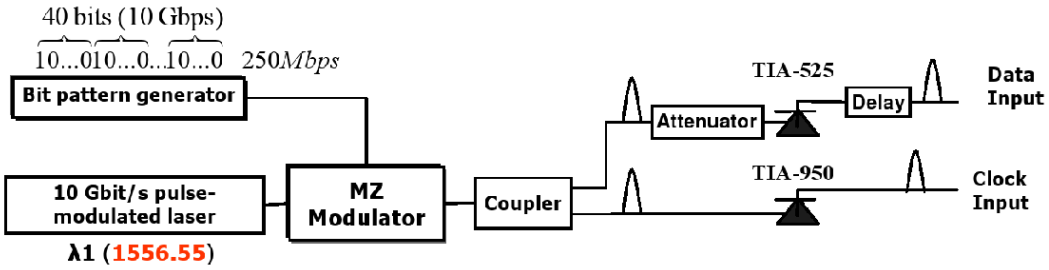


Figure 6.7: ADC test circuit

upper than a threshold voltage ($V_{threshold} = V_{in}(max)/2$). The threshold voltage for AD9480 is 0.35 V. In such way, if clock and analog input are synchronized well in ADC, for each analog pulse ($V_{in} \geq V_{threshold}$) there is a digital pulse available in ADC MSB output (pin 25). Likewise, the other ADC output bits can serve in the place of MSB to decrease the threshold level. But an additional OR logic gate is necessary to combine it with the other more significant bits.

As there were only one pattern generator in our laboratory, the configuration presented in figure 6.7 is used for generating the input and clock pulses to test the ADC circuit (figure 6.6). To generate a sequence with 250 Mbps bit rate with thin width pulses, an Anritsu pulse pattern generator (MP1763B) is employed to produce NRZ sequence at 10 Gbit/s. The periodic data sequence consists of 40-bits subsequences (one '1' and thirty nine '0'). So, a sequence of '1' bits with 250 MHz bit rate is produced. This sequence is utilized in a Mach-Zehnder (MZ) modulator to modulate a distributed feed back (DFB) laser beam (λ= 1556.55nm). To reduce the pulse width more (> 40 ps), the laser beam is pulse-modulated at 10 Gbps before injecting to the MZ modulator. The MZ output is divided in two parts in a 3-dB coupler and is injected into two photo-detectors (TIA-950 and TIA-525). An electrical delay line (Wiltron Co. 3114) is used for compensating the delay between the clock and input bits within the ADC. As the same sequence is used for both of input and clock signals, the output level in MSB is always '1'. So, the output waveform of flip-flop stays at '1'state.

Figure 6.8 and 6.9 show the result of the experiment for two individual sequences. In figure 6.8, the selected sequence consisted of periodic 7-bit subsequences ("1111110') at 250 Mbps. The input data bits are shifted via delay line (about one time-bit in relation to clock sequence). In such way, the three different statuses between clock and input ('0' or '1') can be checked;

- The clock bit and input data bits are present and synchronous: the flip-flop output is always '1'.
- The input data bit is absent but the clock bit is present: in this condition, the ADC will do the sampling and the flip-flop output returns to '0'.
- The input bit is present but there is no more clock pulse: in this situation the ADC operation is suspended and the flip-flop keeps last stored logic state. In this condition the value of analog input signal is not important.

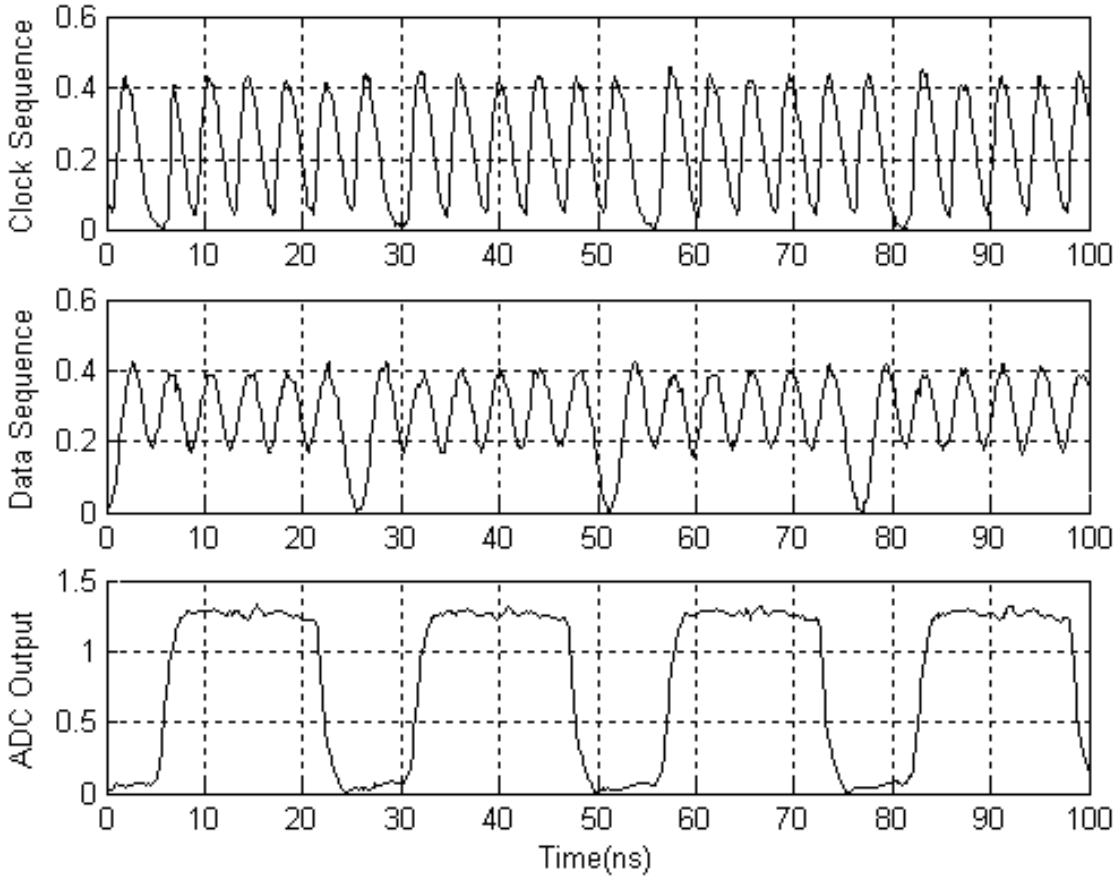


Figure 6.8: ADC functionality test with a periodic 7-bit block sequence

Figure 6.9 shows the same experiment for a sequence consisted of periodic 13-bit blocks ('1111111111110').

6.4.3 Label processing (within FPGA)

As the packet label consists of 4 bits, we need 4 ADC in total (figure 6.2). After being detected the label bits must be utilized to generate the routing commands. The MPLS router computes a new label and wavelength from an internal routing look-up table given the current label, current wavelength, and router output port. Based on forwarding model as unicast, multicast or broadcast, the packet must be distributed into one or more destination. If the routing table is fixed, one can use a logic circuit to realize the command signal.

In the dynamic routing case, an adaptive algorithm must be realized in which the only cost and power efficient solution is FPGA. An FPGA (field programmable gate array) is a semiconductor device containing programmable logic components and programmable interconnects that can be combined to produce functions such as a numerical multiplier, divider, accumulator etc. In a modern FPGA it is possible to program different areas of one chip to perform many hundreds of calculations in

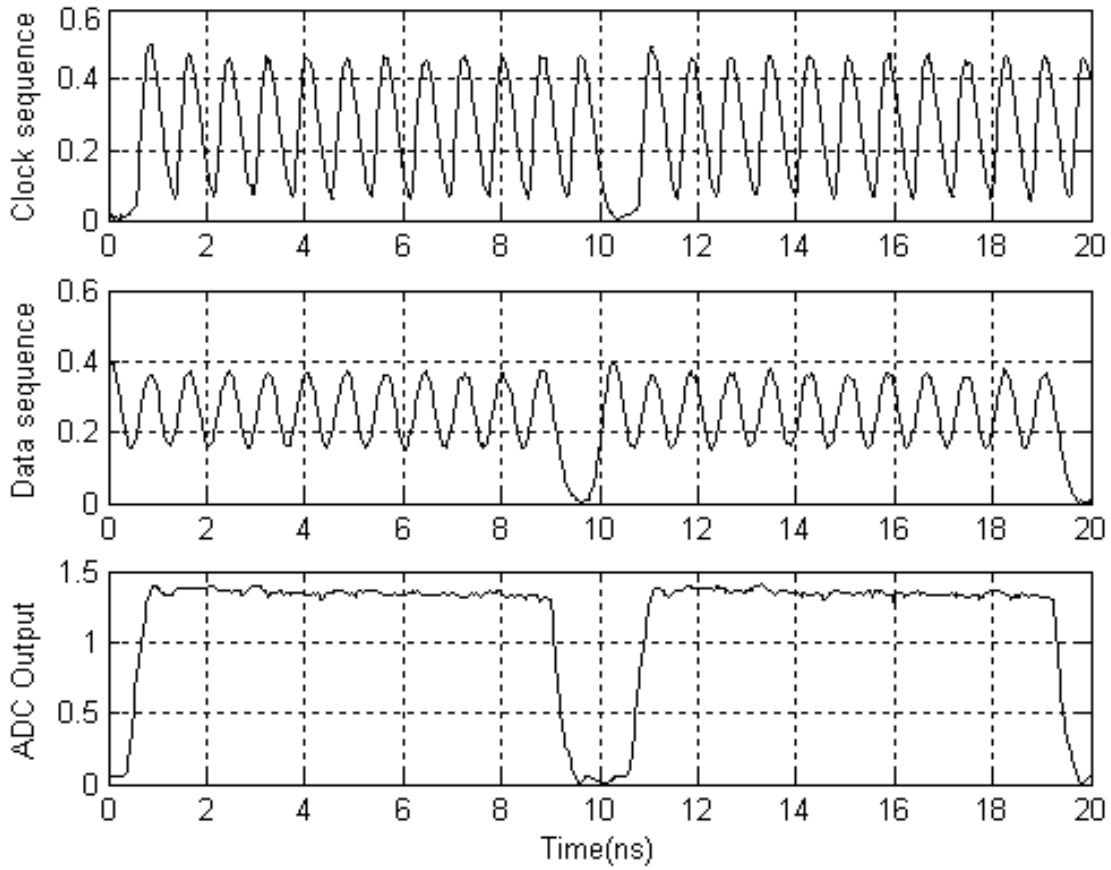


Figure 6.9: ADC functionality test with a periodic 13-bit block sequence

parallel, running at speeds of 200 MHz to 500 MHz. The latest generations of devices contain certain 'hard' functions, such as memories and multipliers built directly out of basic silicon building blocks rather than the logic elements. The use of dedicated components represents a more efficient use of the raw silicon and allows a higher performance in designs where their functions are required. Further information on FPGA devices can be found in the device datasheets from FPGA manufacturers such as Xilinx and Altera.

6.5 Packet forwarding

Packet label swapping together with other switching or buffering mechanisms (space, wavelength, etc.) are configured in the forwarding process;

6.5.1 Label swapping

All-Optical Label Swapping (AOLS) implements routing and packet-by-packet forwarding functions of MPLS directly at the optical domain. The packet label swap-

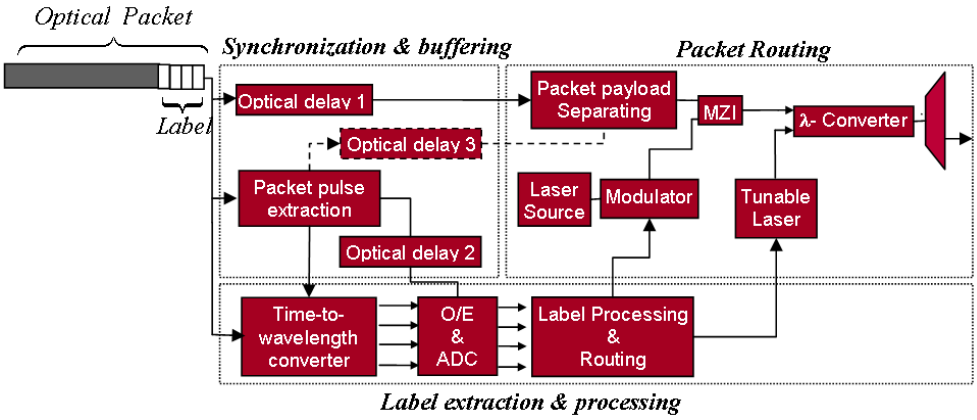


Figure 6.10: Schematic diagram of the packet label swapping

ping function involves swapping the original label with the new label. Thanks to MPLS labels, the local look-up tables in routers are scalable and by using AOLS to make the table lookup procedure, packet forwarding is no longer a critical time-consuming activity [351]. Figure 6.10 illustrates the schematic diagram of the packet label swapping which includes three operations namely, packet payload separating, new label generating and new label re-writing. Similar to the packet-pulse extraction (4.8.2), the label reading/erasing/rewriting operations are critically dependent on the optical label-encoding scheme. The presented scheme (figure 6.10) is compatible with WDM- and TDM-labelling format.

The packet payload separation is performed according to the label-coding format. For SCM coded packet label the label swapping system is already presented (by using electro-absorption modulator, fiber Bragg grating and Mach-Zehnder interferometer) in chapter 4 (part 4.8.4). For bit-serial coded label, the packet pulse extraction can be reused for packet payload separation.

In the all-optical node design proposed in the IST-LASAGNE project, a new label which must be replaced with the packet old label is generated by means of optically splitting, delaying and combining an optical pulse in order to create a label pattern [107]. This method has a potential problem regarding the power budget. At each coupling joint (point) the optical power will be distributed and optical amplifiers need to be used to maintain an even power level of the optical pulses in the label. Furthermore, updating the label pattern requires complete new ODL configurations [352].

According to the label look-up table in the label processing subsystem, the new label can be generated and is used to modulate a laser beam via an optical modulator. The modulator type depends on the label modulation format. The packet label can be encoded at a lower bit rate and different modulation formats from the payload. An integrated electroabsorption modulation laser (EML) is used in label swapping system proposed by Zhu et al. [121]. Hung et al. perform DPSK encoded bit-serial label swapping by using an optical phase modulator [353]. Finally, the cross-phase modulation in the SOA-MZI wavelength converter imprints payload

information onto the optical carrier from the EML while achieving 2R regeneration of the payload.

6.5.2 Optical switching

Optical switching can be performed using different technologies including space-, time-, wavelength-, code-division multiplexing or a combination of them. Optical switches are presented in chapter 4 (part 4.5). Here, the packet forwarding is based on wavelength switching whereby the output wavelength is chosen based on the processed label subset. Obviously, an arrayed-waveguide grating (AWG) wavelength demultiplexer can be used in order to provide spatial switching of the packet at the output of the system.

The electronic command signal delivered by the label processing subsystem is used to control the optical switch subsystem. Different electrical voltage levels can be assigned for different label subset bit combinations. A simple solution for providing the different mentioned voltage levels is the utilization of a digital-to-analog converter. DAC5686 is a 16-bit, 500-MSPS, Dual-channel digital-to-analog converter fabricated by Texas Instrument. It has been specifically designed to allow for low input data rates between the DAC and ASIC, or FPGA, and high output transmit intermediate frequencies (IF).

6.5.3 Tunable laser source

Wavelength based optical switch can be designed in numerous ways. The most straightforward is to incorporate a tunable laser and a wavelength converter. The tunable lasers in the front-end wavelength converters must switch the wavelengths very fast (typically in the nanosecond range). Such a criterion will favor the tunable laser types that are controlled electronically versus the ones that have thermal or mechanical tuning elements. A crucial criterion for the deployment of fast-switching lasers is the guarantee of frequency stability over their lifetime.

A common concept to realize semiconductor tunable laser is based on the counter-directional coupling of two or more combs of longitudinal modes that are defined in separately contacted segments [354]. Increased attention has been paid to solutions utilizing sampled gratings or superstructure gratings with distributed Bragg reflectors (e.g. Rear-sampled grating reflector (GCSR) laser with a grating-assisted codirectional coupler [355], sample grating or super structure grating (SSG) distributed Bragg reflector (DBR) lasers [356], high-speed electroabsorption SSG-DBR lasers [357]). These structures, however, require an additional regrowth step and are, therefore, complicated to fabricate [354]. Designs based on lateral distributed feedback and first concepts introducing photonic crystal sections controlling the intracavity coupling properties have recently been reported [358]. The latter concepts avoid any additional regrowth step. A tutorial on tunable semiconductor lasers is presented in [359].

6.5.4 Wavelength conversion

Optical wavelength converters that utilize nonlinearities in SOAs offer some advantages in terms of integration potential, power consumption, and optical power efficiency. A number of SOA-based wavelength converters have been demonstrated [360]. The major limitation of SOA-based wavelength converters is the slow SOA recovery (typically several tens to hundreds of picoseconds), causing unwanted pattern effects in the converted signal, and limiting the maximum operation speed of the wavelength converters. It has already been theoretically and experimentally clarified that the increase in electrical pumping power, confinement factor, and interaction device length effectively improve the speed performance [361] [362].

Fiber Bragg grating (100 Gbit/s) [363], interferometric configuration (168 Gbit/s) [364], two cascaded SOAs (170.4 Gbit/s) [365], and optical filtering (320 Gbit/s) [360] are some of the proposed technique for improving the SOA-based wavelength converter.

6.5.5 Integrating possibility

The optical integration effort might be valuable in terms of the integrated optics preferences. Different subsystems in the presented scheme in figure 6.1 should be integrated. Obviously, the electronic subsystem can be integrated. As a trial, an example was designed and included on a mask with the help of the COBRA lab of TU-Eindhoven. Figure 6.11-a displays a part of the SOA time-to-wavelength converter (presented in the previous chapter) including a SOA, an Arrayed waveguide grating (AWG) phasar and four photo-detectors. The Mast layout of this circuit is presented in figure 6.11-b.

Moreover, monolithically integrated devices that contain a 40 Gbit/s optical wavelength converter and a sub-nanosecond tunable laser have been realized [366]. Therefore, regarding the efforts in integrated optics, the realization of an almost integrated router system is conceivable as a perspective for future work.

6.6 Discussion

The opto-electronic scheme has some benefits including;

- **Packet rate scalability:** The packet bit rate in an optical network does not vary instantaneously. Even, if it change, the packet label could still be detected and processed. However, the auxiliary modulated lasers must be synchronized with the label bits (see figure 5.1). A bank of variable dispersive elements (e.g. several length of DCFs) can be employed in order to provide the required delay between the auxiliary modulated bits (colored bits). The packet bit rate variation is not possible in FBG based time-to-wavelength converter [341].

- **Asynchronous (burst) mode operation:** As shown in figure 5.1, the proposed time-to-wavelength converter needs only a packet pulse extractor (to detect the

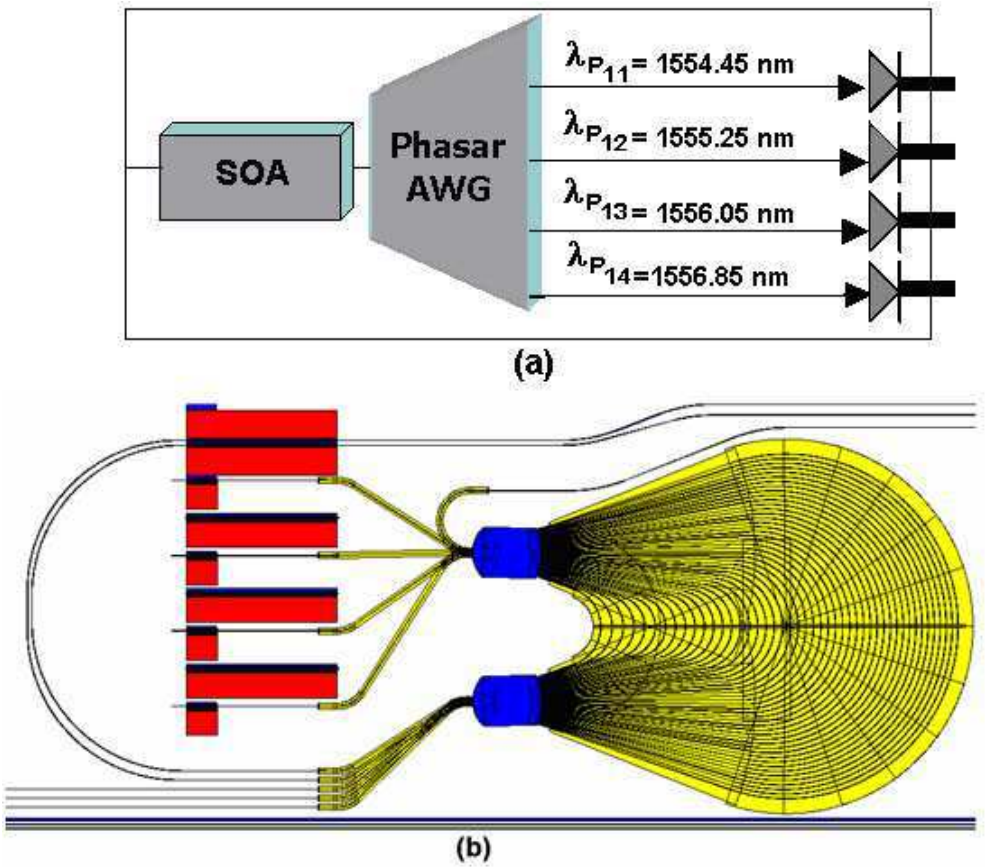


Figure 6.11: (a) First mask schematic proposed, (b) Mask lay out designed by TU/e

packet label subset) in order to separate the label subsets. By compensating the delay between the intermediate components, the packet pulse extractor output can be reused for ADC input enables. In such a way, synchronous or asynchronous operation can be handled in the remaining operations (packet length insensitivity).

- **Modularity:** Every sub-system presented in figure 6.2 could be optimized separately. In other words, the realization and the optimization of each sub-system can be done independently.
- **Flexibility:** By increasing the order of time-to-wavelength converter, the processing length of the label subset may be increased. However, conversion efficiency at larger wavelength spans is a key limit in increasing the order of the presented FWM based time-to-wavelength converter which can be improved by dual pump based methods.
- **Compatibility:** As most of the actual optical network components do the packet processing and forwarding within the opto-electronic sub-systems. In the proposed method, there is the possibility of jointing with the other sub-systems (e.g. different optical switch or routing algorithms).

- **Dynamic bit detection:** As each electrically transformed bit must be processed in digital header processing sub-system, the ADC can reshape the distorted bits. Moreover, by digitizing the photo-detector output signals, different threshold levels for detecting '0' and '1' are available.

6.7 Summary

The design and partially implementation of an opto-electronic optical packet routing system is demonstrated in this chapter. In this architecture, a 4-bit time-to-wavelength converter (presented in detail in chapter 5) is employed as a serial-to-parallel converter for slowing down the packet labet bits. The slowed down parallelized label bits are transformed on electronic signals via photo-detectors. Next, an ADC (analog to digital converet) is used for each label bit in order to digitiz and bit level detection. Finally, the digitized label bits are processed in an FPGA in order to produce the correspounded command signals for the optical switch and label swapping subsystems. The advantages of this architecture are presented in 6.6. Furthermore, a partial or total integration of this scheme can be expected.

CHAPTER

7

Design of an All-optical Packet Forwarding System

7.1 Introduction

All-optical packet forwarding systems allow integration of data and optical networking towards the photonic Internet of the future. The key concept is an efficient and transparent packet forwarding method using an optical-label switching mechanism which can coexist with WDM technologies on the same fiber. In such a way, the allocated time for packet label processing and packet routing can be reduced via all-optical solutions. So, all the label and payload can be modulated at the same bit-rate. This reduces not only the packet format complexity, but also the label duration (leading to a greater data bit-rate).

In order to simplify the requirement in all-optical packet switched networks and to eliminate the need of optical address lookup table, the self-routing address format is proposed which identifies each output port of every node in a network by a different bit in the packet label. Self-routing has been used in packet and ATM switches to reduce the hardware cost and control complexity [367]. The packet routing speed is limited by the hardware speed only. So, it is feasible to build an "all-optical bypass" to accelerate a conventional router.

This chapter addresses an adaptive and scalable self-routing all-optical packet switched network based on time-to-wavelength converter, all-optical decoder and other available functional element technologies. The proposed architecture, which allows multiple addresses for the same node, is similar to the opto-electronic archi-

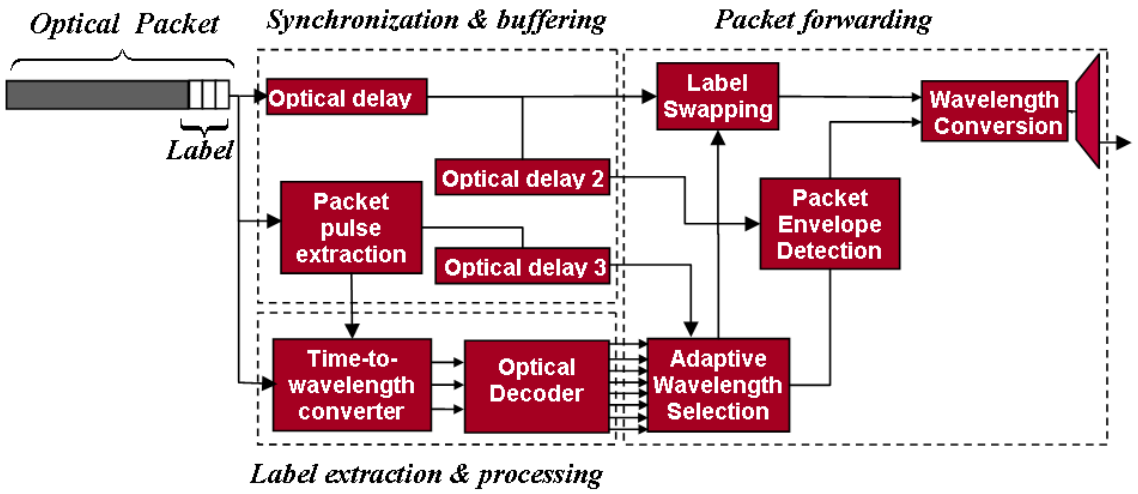


Figure 7.1: Conceptual diagram of time-to-wavelength converter based optical packet label processing

tecture presented in chapter 6 (figure 6.1). However, the objective is to propose a transparent packet routing system where the electronic-domain operation is minimized. Figure 7.1 illustrates a schematic representation of the proposed architecture which includes three main sub-systems, namely, synchronization & buffering, label extraction & processing, and packet forwarding.

The synchronization & buffering subsystem proposed in figure 7.1 is similar to the one presented in chapter 6. In the label extraction sub-system, the time-to-wavelength converter once again is employed in order to parallelize the packet label subset. Next, they are amplified and sent to an optical decoder module which produces an optical command pulse corresponding to each label subset (decoder input) bit combination. Therefore, the label extraction and processing will be done in all-optical modules. Afterwards, the decoder output signal is used for packet wavelength switching. In the next section, the principle of an all-optical 3×8 decoder will be discussed.

7.2 All-optical decoder

A decoder is a multiple-input, multiple-output logic circuit that converts parallel coded inputs into coded outputs, where the input and output codes are different. Decoding is necessary in applications such as data multiplexing and memory address decoding. The simplest decoder circuit would be an AND gate because the output of an AND gate is ON (1) only when all its inputs are ON. A slightly more complex decoder would be the n-to-2^n type binary decoders. They are combinational circuits that convert binary information from n-bit coded inputs to a maximum of 2^n unique outputs. We say a "maximum"of 2^n outputs because there may well be unused bit combinations, within the n-bit input-coded information leading to less than 2^n outputs. This type of decoder can be described through the use of AND and

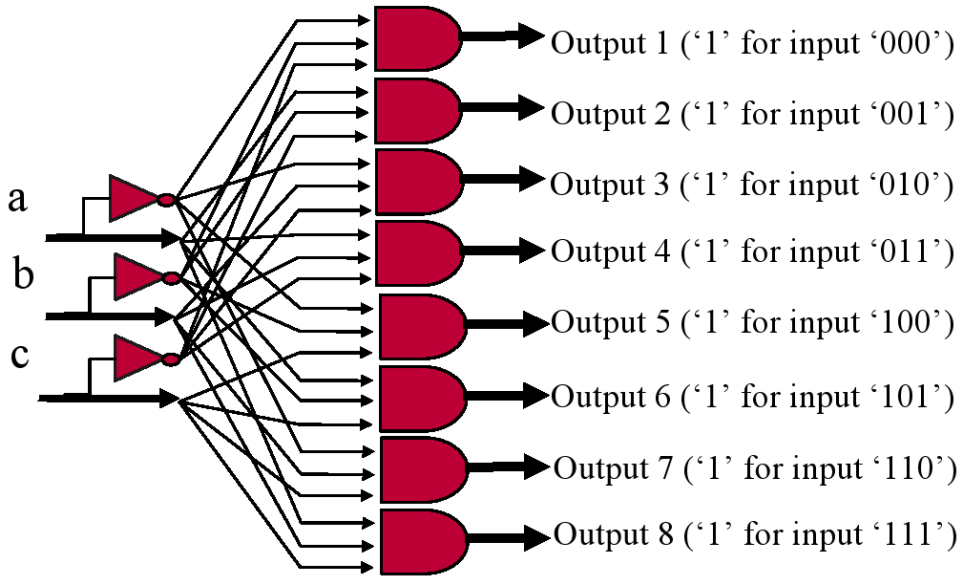


Figure 7.2: Schematic of a 3×8 logic-gate decoder

Table 7.1: Truth table of a 2×4 (in bold part) and 3×8 decoder

Input a	Input **b**	Input **c**	Output **1**	Output **2**	Output **3**	Output **4**	Output 5	Output 6	Output 7	Output 8
0	**0**	**0**	**1**	**0**	**0**	**0**	0	0	0	0
0	**0**	**1**	**0**	**1**	**0**	**0**	0	0	0	0
0	**1**	**0**	**0**	**0**	**1**	**0**	0	0	0	0
0	**1**	**1**	**0**	**0**	**0**	**1**	0	0	0	0
1	0	0	0	0	0	0	1	0	0	0
1	0	1	0	0	0	0	0	1	0	0
1	1	0	0	0	0	0	0	0	1	0
1	1	1	0	0	0	0	0	0	0	1

NOT logic operators. Figure 7.2 illustrates the logic representation of a 3×8 decoder. For each combination of the input bits a command signal is produced.

Table 7.1 shows the truth table of a 3×8 decoder (the bold part is the truth table of a 2×4 decoder relative to *input b* and *input c*). Each output of the decoder is ‘1’for only one input combination and ‘0’, otherwise. The decoder implementation is straightforward in electronics as schematized in figure 7.2. However, for the realization of an all-optical counterpart, the optical logic gate cascading is rather critical. Our objective is to reduce the complexity to a single gate (and a single SOA) per output. For this, we use the cross-polarization modulation (XPolM) effect in SOAs [5].

By comparing the NOT, NOR and AND logic gate truth tables (see figure 3.1) and the decoder truth table (table 7.1), the 3×8 decoder outputs (figure 7.2) can be obtained through 8 logic gates namely:

- A three-input NOR ($\overline{a+b+c}$) for the output 1
- Three AND-NOT (i.j.$\bar{k}$) for output 4, 6 and 7,

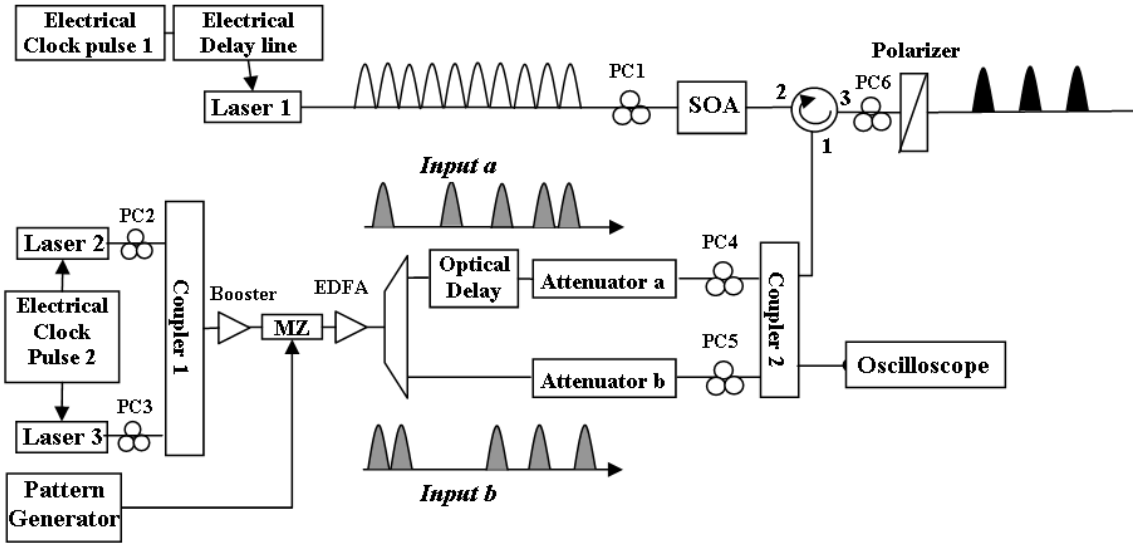


Figure 7.3: All-optical two input NOR gate setup

- Three AND-NOR (i.$\overline{j+k}$) for output 2, 3 and 5,
- A three-input AND ($a.b.c$) for output 8.

where a, b and c are the three decoder input bits, '**.**' and '+' note Boolean symbols for AND and OR logic operations respectively and i, j and $k \in a, b, c$. Here, we discuss the realization of the mentioned logic functions. The experiments use a 1.2 mm long SOA driven with a 300 mA current (with inverse bias polarity). It is fabricated by Alcatel OPTO+. In the following subsections, the realization of logic functions mentioned above.

7.2.1 All-optical NOR gate using XPolM effect in SOA ($\overline{a+b+c}$)

The truth table of a three-input NOR logic gate is shown in table 7.1 (columns 1, 2, 3 and 4). By appending a second or more input in the NOT logic gate (Presented in part 3.3) one can produce a two or more inputs NOR gate. Soto et al. [71] demonstrate a three-input NOR logic function using XPolM in SOA where the NRZ (non return-to-zero) format modulated input logic signals with a bit rate of 2.5 Gbit/s is used. Due to the experimental limitations in our laboratory, it was not the possibility to realize a three-input NOR logic gate (with RZ (return-to-zero) modulation format at 10 Gbit/s). So, we present the experimental result of a two-input NOR logic function with RZ modulation format at 10 Gbit/s. Figure 7.3 displays the experimental setup. Obviously, for three-input NOR logic gate one can add a third input (in counter-propagating) on the figure 7.3.

The 10 Gbit/s (λ=1550.62 nm) pulse-modulated laser 1 (Alcatel 1915-LMM laser module) is used as the co-propagating input. It serves as the output beam, too. The polarization controllers, PC 1 and PC 6, are set so as the laser 1 beam can pass through the SOA in absence of the input a and input b. In the presence of one of

the counter-propagating input beams, the polarization state of the laser 1 beam is rotated in the SOA (due to the XPolM effect) and the light is blocked by the polarizer (when the polarization state rotation is 90^o). In the presence of both of the inputs not only the XPolM but also the cross gain modulation (XGM) effect in the SOA reduces further the laser 1 pulse amplitudes during transmission through the SOA and the polarizer output.

The experiment is done at a bit-rate of 10 Gbit/s. Laser 2 and 3 are DFBs (distributed-feedback lasers) with wavelength of λ=1556.38 nm and 1557.72 nm, respectively. To show the validity of the NOR logic functionality, '1001010110' and '1100010101' sequences are chosen as input a and input b sequences, respectively. They include all input-bit combinations (00, 01, 10 and 11). To provide an RZ modulation format, the electrical current of DFB laser 2 and 3 are biased at 37 and 5 mA, respectively, and directly modulated at 10 Gbit/s in the gain switched conditions. The pulse-modulated laser 2 and 3 are modulated again within a $LiNob_3$ Mach-Zehnder (MZ) modulator with a 16-bit periodic sequence of '1001010110001010' (obtained from an MP1763B Anritsu pulse pattern generator).A booster (with output power of 13 dBm) compensates the power attenuation into the MZ modulator (figure 7.3). Moreover, two polarization controller (PC 2 and PC 3) are employed to optimize the modulation in the MZ. The modulated laser 2 and 3 are separated with a DWDM demultiplexer (Optiwork 100 GHz multi-channel DWDM module). The different optical fiber length together with an optical delay line (for delay adjustment) is used for providing 10-bit specified *input a* and *b* sequences. At bit rate of 10 Gbit/s a time-delay of 700 ps is needed to provide '1001010110' and '1100010101' for *input a* and *b*, respectively. It can be verified by observing the output beam of coupler 2 in an Agilent 83480A oscilloscope.

For synchronization of the co- and counter-propagating signals within the SOA, the attenuator A and B together with the internal electrical delay line of HP70841B pattern generator are used. The attenuator A is set to maximum in order to block the *input a*. It permits us to synchronize *input b* with the co-propagating beam in SOA using the internal electrical delay line of the MP1763B pulse pattern generator. The power of the counter-propagating beam (*input b*) can be changed by attenuator B in order to rotate the co-propagating beam polarization state of 90^o (due to XPolM effect in SOA) in order to be blocked by the polarizer. The result sequence is '0011101010'. Now, both of *input a* and *b* are injected into the SOA, simultaneously. The average input powers for input beams are -6.1 dBm. Figure 7.4 illustrates the experimental result of *a NOR b* logic gate. The output sequence ('0010101000') has 9.2 dB of extinction ratio.

7.2.2 All-optical three-input AND logic gate (*a.b.c*)

The truth table of a three-input AND logic gate is illustrated in table 7.1 (column 1 (*input a*), column 2 (*input b*), column 3 (*input c*) and column 11 (*output*(*a.b.c*)). According to the table 3.1, a number of methods are presented to product the AND logic gate functionality. But most of them are proposed for two-input logic AND (e.g.

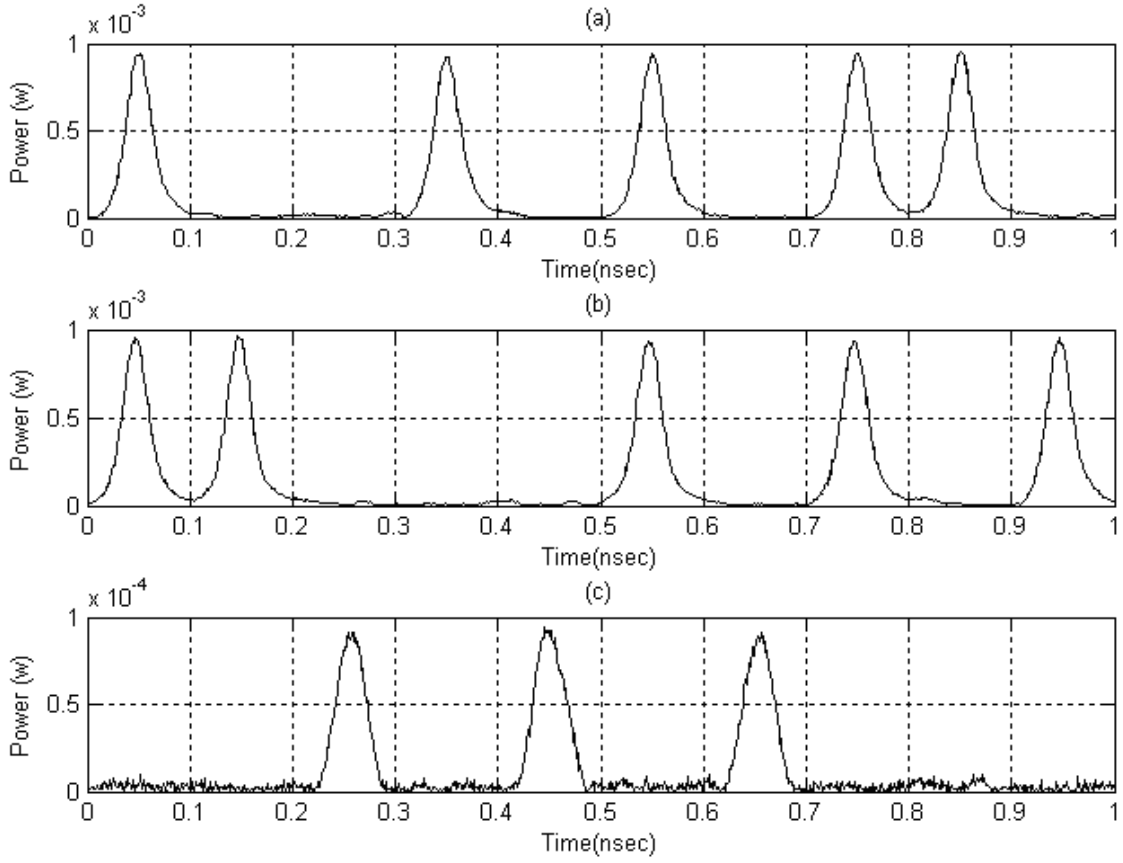


Figure 7.4: Experimental result of two-input NOR gate (based on figure 7.3); (a)*input a*, (b) *input b* and (c) *input a NOR input b*

TOAD, UNI, NOLM, MZI, FWM, and etc.). A three-input AND logic gate with only one active nonlinear element can be realized by XPolM in SOA. The experimental configuration is shown in figure 7.5. Input a serves as the output beam affected with the other two counter-propagating signals corresponding to the other two inputs. The polarizer is set to block the forward propagating beam in absence of input b and input c. The power and polarization state of the two other inputs (*b* and *c*) must be optimized to rotate the polarization state of input a up to 90^o whereby it can pass through the polarizer.

During our experiments, there was only one bit pattern generator working at 10 Gbit/s in our laboratory. But it is evident that in the absence of *input a* (abc; 000, 001, 010 and 011) there is no light left at the SOA output except the SOA spontaneous emission which will be filtered. So, only the possible input combinations, in which the input a is always '1' (abc; 100, 101, 110 and 111), needs to be checked. Therefore, the pattern generator 1 and MZ 1 (shown in figure 7.5) can be omitted. '1100110101' and '0110101001' are chosen as input b and input c sequences, respectively. The synchronization process between input a, b and c are similar to one presented method in 7.2.1.

Figure 7.6 displays the result of three-input AND logic gate implementation

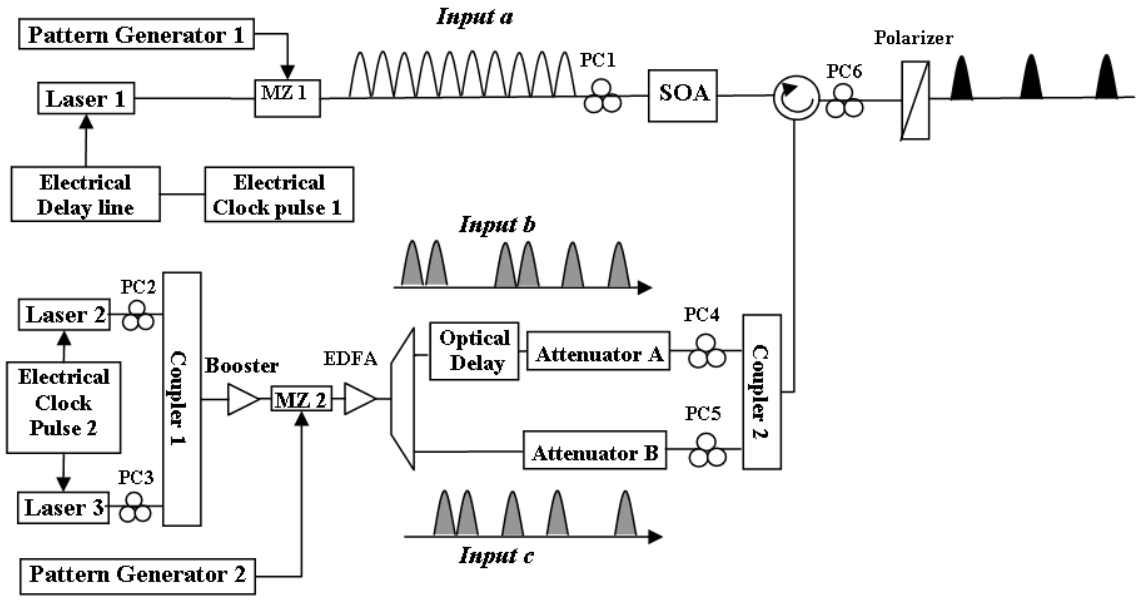


Figure 7.5: All-optical three input AND gate setup using the XPolM effect in SOA

with RZ modulation format at 10 Gbit/s. The average input power for *input a*, *b* and *c* are -6.7, -9.2 and -8.3 dBm, respectively. The measured extinction ratio of the output signal is 7.9 dB. The input wavelengths are 1557.72 nm (counter-propagating), 1556.38 nm (counter propagating) and 1550.62 nm (co-propagating).

7.2.3 All-optical AND-NOT logic gate ($i.j.\bar{k}$)

The truth table of this logic function is shown in table 7.1 (column 1 (*input i*), column 2 (*input j*), column 3 (*input k*) and column 7 (*output* $i.j.\bar{k}$)). This functionality can be realized by injection of a third entrance in a two-input SOA based AND gate in which the presence of the third input degrades the output signal because of the XGM effect in the SOA. The schematic diagram of this functionality using XPolM is shown in figure 7.7. Here, *input i* serves as the output beam. A polarizer is set to block the *input i* in absence of *input j*. The polarization of *input i* is rotated in the presence of *input j* in order to pass through the polarizer. *Input k* is used to degrade *input i* power at the SOA output. An extra filter is centered around *input i* wavelength in order to block *input j*. So, the output is '1' if both of *input i* and *input j* are '1' and *input k* is '0'.

The synchronization is done at first between two co-propagating beams. Next, by using the optical delay line the counter-propagating beam is synchronised with them. Similar to the three-input AND gate, in absence of input i there are no more light beam in the SOA output (*ijk*; 000, 001, 010, 011). So, the other combination possibilities of input signals, in which the input i is always '1' (*ijk*; 100, 101, 110, 111), are checked. '0101101001' and '1001011010' are chosen as input j and input k sequences, respectively. The input wavelengths are 1557.72 nm (counter-

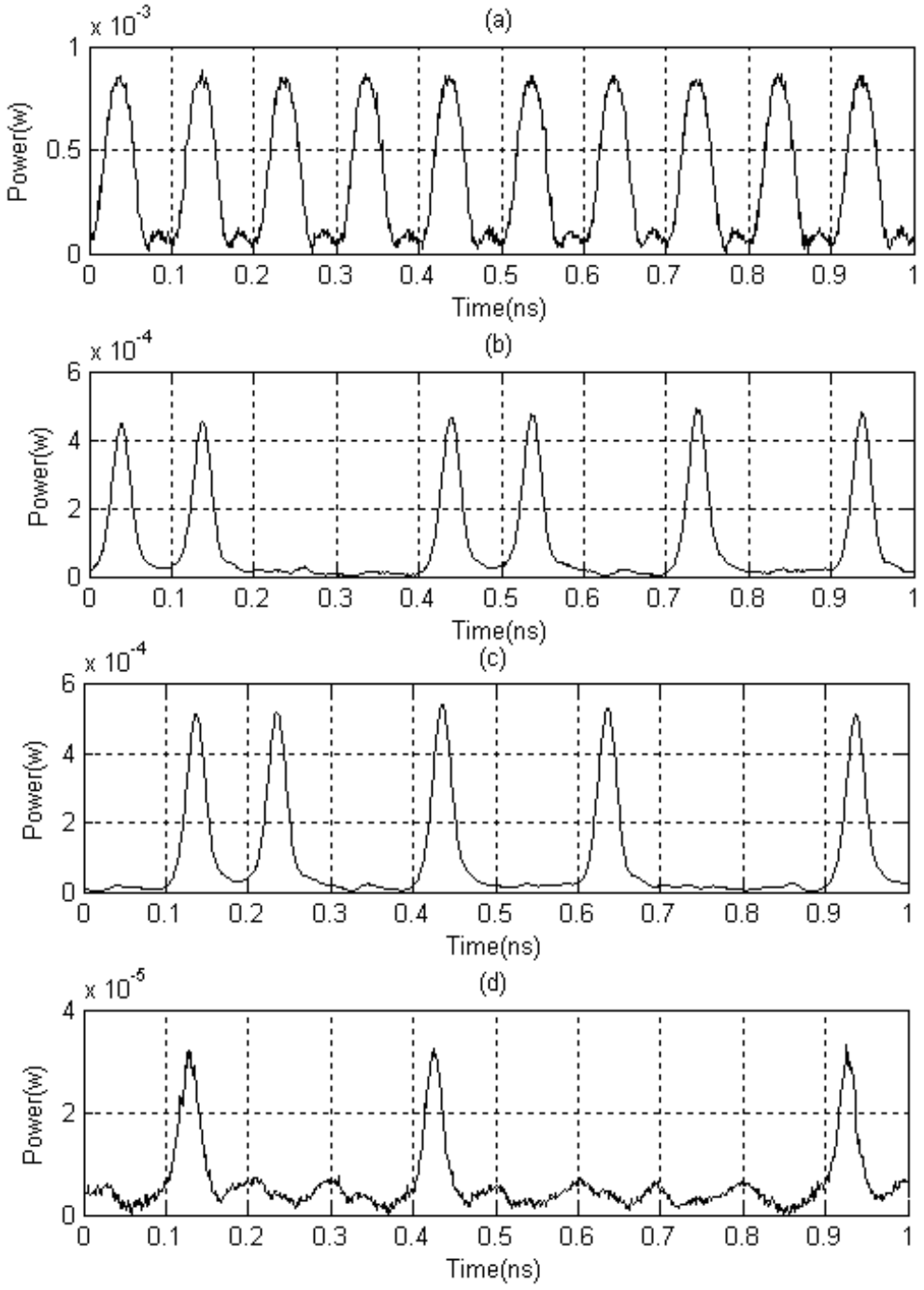


Figure 7.6: Three-input AND logic function based on figure 7.5; (a) *input a* (co-propagating), (b) and (c) are the *input b* and *c* (counter-propagating) and (d) is the output.

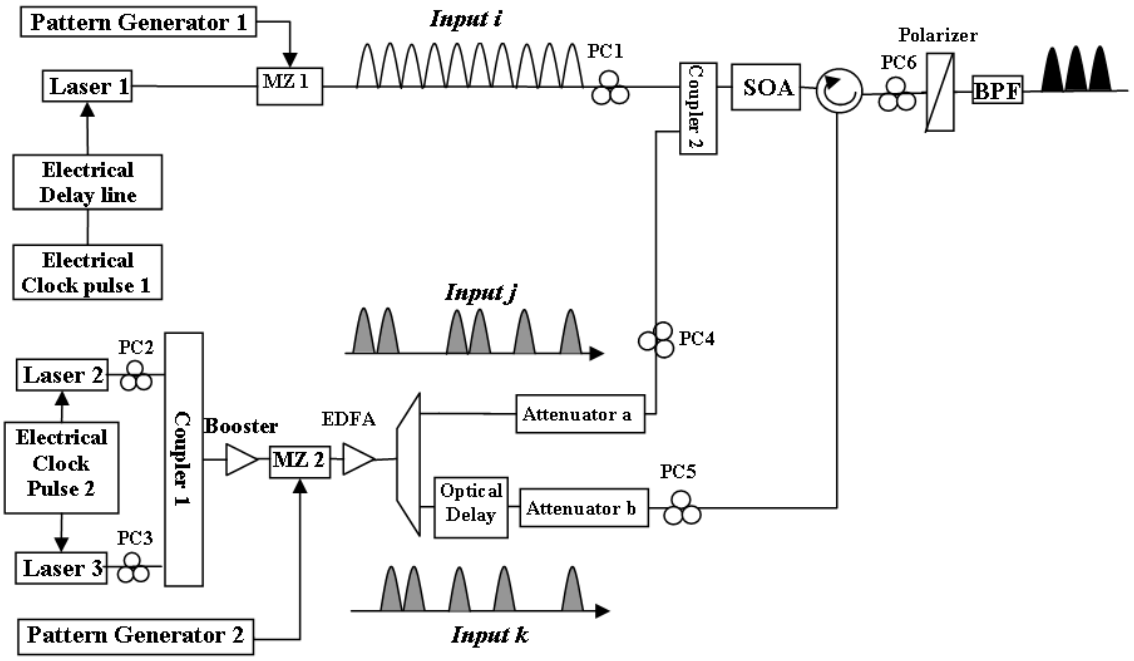


Figure 7.7: All-optical three-input AND-NOT gate function ($i.j.\bar{k}$) setup

propagating), 1556.38 nm (co-propagating) and 1550.62 nm (co-propagating). They have RZ modulation format (10 Gbit/s). The average input powers for inputs i, j and k is -9.5, -12.2 and -11.3 dBm respectively. The output logic function corresponding to the input bit-sequence ('0100100001') is displayed in figure 7.8.

The difference between the configuration utilized for output 4, 6 and 7 is related to the order of the input signal. When $i, j \in b, c$ and $k = a$ the can produce the *output* 4. Likewise, for $i, j \in a, c$ and $k = b$ it generates *output* 6 and finally, $i, j \in a, b$ and $k = c$ represents *output* 7. The measured output signal extinction ratio is 12 dB.

7.2.4 All-optical AND-NOR logic gate ($i.\overline{j+k}$)

This functionality has been reported with using XGM in a SOA [41] with a bit-rate of 1.25 Gbit/s. A configuration such as that of figure 7.3 can also be used to realize this function using XPolM. This case is similar to the NOR function presented in part (7.2.1). The forward propagating beam now consists in one of the logical inputs (e.g. *input i*) whereas the two remaining inputs (j and k) are sent in the counter-propagating direction. Therefore when *input i* is set to '0', the output will remain on '0' and when set to '1', it works as a NOR gate. Figure 7.9 illustrates the $i.\overline{j+k}$ logic function (when *input i* is null (not shown) no light can pass through since there is no other forward propagating beam).

The input wavelengths are 1557.72 nm (counter-propagating), 1556.38 nm (counter-propagating) and 1550.62 nm (co-propagating). The modulation format is always RZ at bit-rate of 10 Gbit/s. The average input power for inputs i, j and k are -5.1, -6.2 and -6.3 dBm respectively. The input bit combination possibilities in which the *inputi*

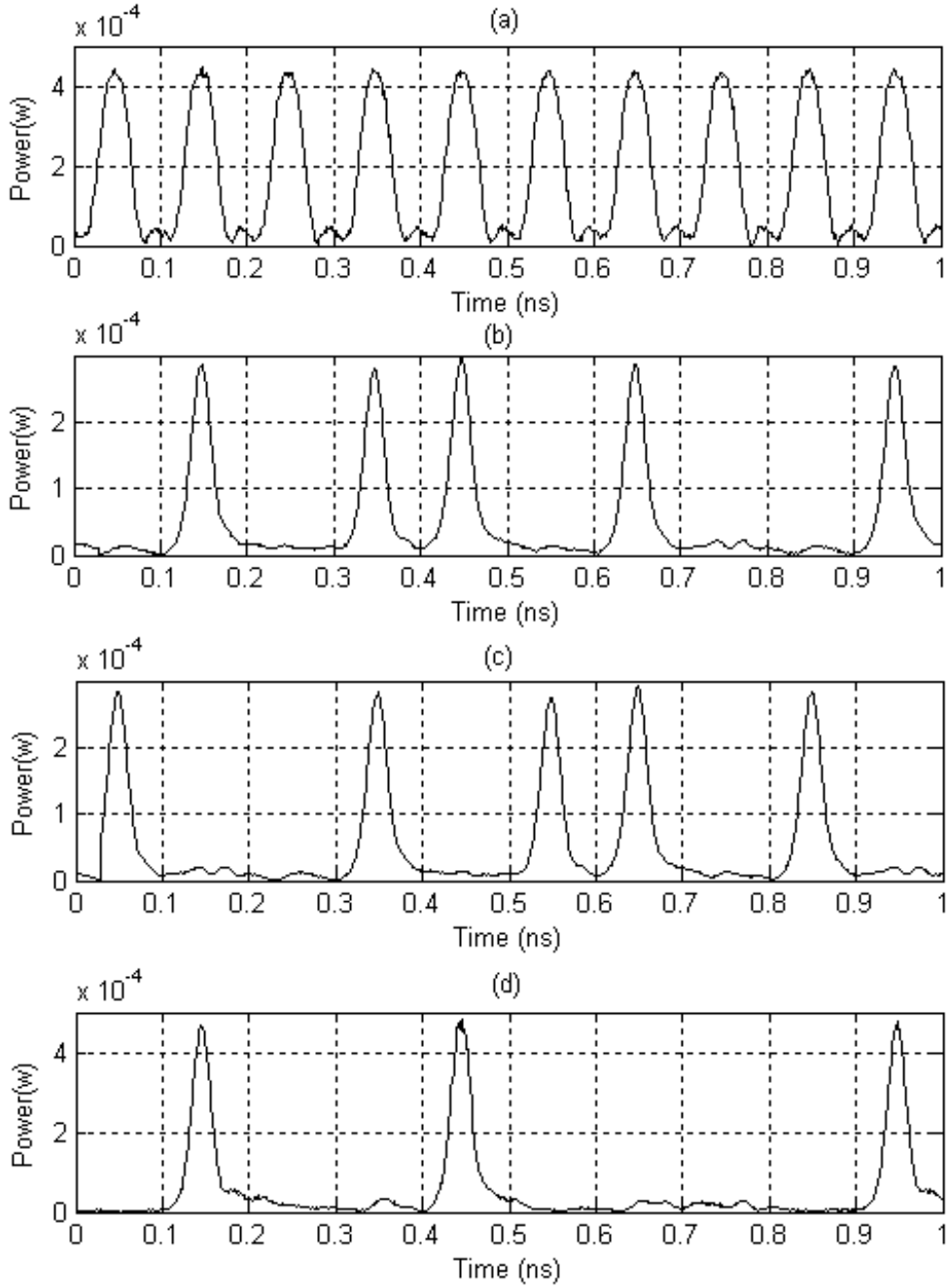


Figure 7.8: AND-NOT logic function ($i.j.\bar{k}$) based on figure 7.7; (a) and (b) are the *inputi* and *j* (co-propagating), (c) is the *input k* (counter-propagating) and (d) is the output.

Table 7.2: Representation of a 4×16 decoder truth table; O_i stands for *output i*

Input	O_1	O_2	O_3	O_4	O_5	O_6	O_7	O_8	O_9	O_{10}	O_{11}	O_{12}	O_{13}	O_{14}	O_{15}	O_{16}
0000	1	0	0	0	0	0	0	0	0	0	0	0	0	0	0	0
0001	0	1	0	0	0	0	0	0	0	0	0	0	0	0	0	0
0010	0	0	1	0	0	0	0	0	0	0	0	0	0	0	0	0
0011	0	0	0	1	0	0	0	0	0	0	0	0	0	0	0	0
0100	0	0	0	0	1	0	0	0	0	0	0	0	0	0	0	0
0101	0	0	0	0	0	1	0	0	0	0	0	0	0	0	0	0
0110	0	0	0	0	0	0	1	0	0	0	0	0	0	0	0	0
0111	0	0	0	0	0	0	0	1	0	0	0	0	0	0	0	0
1000	0	0	0	0	0	0	0	0	1	0	0	0	0	0	0	0
1001	0	0	0	0	0	0	0	0	0	1	0	0	0	0	0	0
1010	0	0	0	0	0	0	0	0	0	0	1	0	0	0	0	0
1011	0	0	0	0	0	0	0	0	0	0	0	1	0	0	0	0
1100	0	0	0	0	0	0	0	0	0	0	0	0	1	0	0	0
1101	0	0	0	0	0	0	0	0	0	0	0	0	0	1	0	0
1110	0	0	0	0	0	0	0	0	0	0	0	0	0	0	1	0
1111	0	0	0	0	0	0	0	0	0	0	0	0	0	0	0	1

is always '1' (*ijk*; 100, 101, 110, 111), are verified. '1001010110' and '1100110100' are chosen as *input j* and *input k* sequences, respectively. The output logic function is shown in figure 7.9. The difference between the configuration utilized for *output*2, 3 and 5 is the order of the input signals ($j, k \in b, c$ and $i = a$ for *output* 2, $j, k \in a, c$ and $i = b$ for *output* 3 and $j, k \in a, b$ and $i = c$ for *output* 5). The measured extinction ratio is 10.4 dB. Figure 7.10 illustrates the measured eye diagram of the logic function. Bit error rate estimated from the Agilent 83480A oscilloscope eye-diagram histogram is 10^{-6} on '1' and 10^{-7} on '0' bits (PRBS $2^{15}-1$ obtained from an MP1763B Anritsu pulse pattern generator). As each decoder output is zero for 7 input bit combinations and one for only one input bit combination, the probability of '0' and '1' bits at each decoder output are $\frac{7}{8}$ and $\frac{1}{8}$, respectively. Therefore, the bit error rate of the decoder can be calculated as follow;

$$BER = \frac{P(1|0) + 7P(0|1)}{8} = 2.2 \times 10^{-7} \tag{7.1}$$

This is the maximum value of BER measured in our experiences.

We have demonstrated in this set of experiments that 8 SOAs are enough to implement the 3×8 decoder shown in figure 7.2 after splitting the inputs into 8 beams.

The all-optical decoder idea may also be represented for 4×16 decoder. Table 7.2 exhibits the truth table of a 4×16 decoder. Similar to the 3×8 decoder, the 4×16 can also be realized by combining the AND and NOT logic function in order to reduce the number of required logic gates.

As shown in table 7.2, the output reproduction signals need the following logic functions:

- A four-input NOR logic functionality for O_1
- Four three-input NOR logic functionalities for O_2, O_3, O_5, and O_9

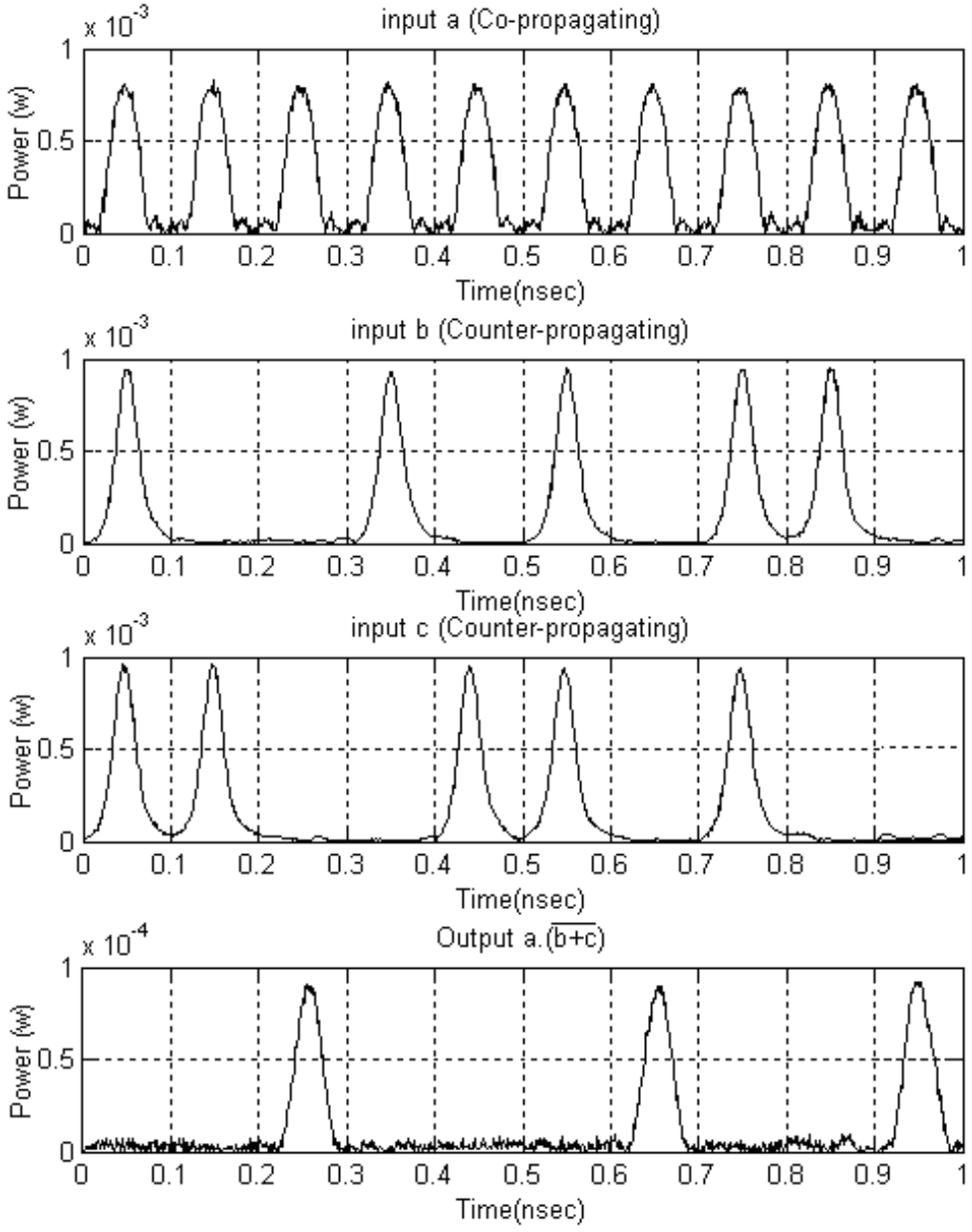


Figure 7.9: AND-NOR logic function ($i.\overline{j+k}$)

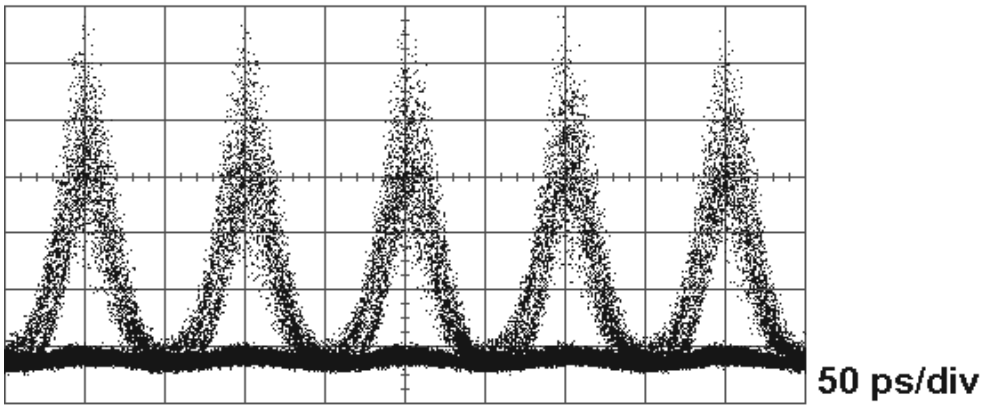


Figure 7.10: Measured eye diagram of $(i.\overline{j+k})$ logic function.

- Six AND-NOR $(i.j.\overline{k+t})$ logic functions for O_4, O_6, O_7, O_{10}, O_{11} and O_{13}
- Four AND-NOT $(i.j.k.\bar{t})$ logic functions for O_8, O_{12}, O_{14} and O_{15}
- A four-input AND logic function for O_{16}.

The two first terms (three- and four-input NOR logic gates), can be realized with the XPolM effect in a SOA with the method presente in 7.2.1. The AND-NOR logic functions $(i.j.\overline{k+t})$ may be produced still with the XPolM effect at the basis of the $i.j.\bar{k}$ gate with the fourth input injected in counter-propagation so as it tends to reduce the output through XGM. The same solution could be proposed for AND-NOT functions (by utilizing the XPolM based three-input AND gate (figure 7.5) and injecting the fourth input in counter-propagation). The four-input AND logic function can not be produced due to the efficiency reduction of XPolM in the presence of four distinct laser beams in the SOA. Besides, other SOA nonlinear effects such as XGM and FWM attenuate the desired output signals. Thus, we must use cascaded AND logic gates producing the four-input AND logic gate. It can be estimated then a minimum 4, 8 and 17 SOAs are required in order to design a 2×4, 3×8 and 4×16 decoders, respectively. Large all-decoders seem to be beyond the current optical technologies. They must be performed electronically (via O/E and E/O converters).

7.3 Packet forwarding

As mentioned in chapter 4, by using optical labels, the IP packets are directed through the core optical network without requiring O/E/O conversions whenever a routing decision is necessary. In a transparent optical network, not only the packet label is extracted and processed optically, but also, the packet forwarding is achieved via all-optical subsystems. The synchronization between the optical subsystems and the timing information of the incoming packet is of crucial importance. Similar to the

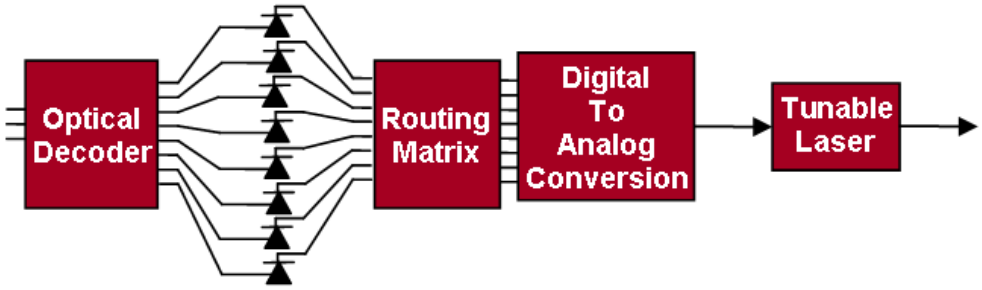


Figure 7.11: Adaptive wavelength generator subsystem.

packet switching architecture presented in chapter 6, here, the packet forwarding idea is based on packet wavelength conversion whereby the output wavelength is chosen based on the processed label subset. As seen in figure 7.1, the packet forwarding system includes 4 subsystems, namely:

- Adaptive wavelength selection
- Packet envelope detection
- Label swapping
- Wavelength conversion.

In following sections these operation are discussed.

7.3.1 Adaptive wavelength selection

Wavelength generating based on the label subset can be performed either opto-electronically or all-optically. In 6.5.3, an opto-electronic method for generating different wavelengths based on the packet label subset is proposed. This architecture can be reused when the packet label is extracted and processed optically via an all-optical decoder. Each of the eight outputs of the 3×8 decoder is transformed to electrics via a photo-detector and is addressed to a specific input bit of an electrical digital-to-analog converter (DAC). Therefore, for each decoder output a distinct voltage level will be provided for controlling different wavelengths of a tunable laser source. oltage level will be provided for controlling different wavelengths of a tunable laser source. Figure 7.11 illustrates the wavelength generating circuit in which the command signals are provided electronically.

The chip-enable of DAC is active for each packet label. Thus, the voltage level of the DAC output remains constant for the entire packet duration. Moreover the electrically transformed decoder output signal must have enough power to pass form the DAC input threshold voltage (e.g. for DAC5686 fabricated by Texas Instruments, the input signal range is [0.1−1.25V]). A similar wavelength channel selection circuit which support 100 wavelength channels spaced by 0.4 nm with measured switching of 100 ns is proposed by Chan et al. in 2001 [106]. Uenohara

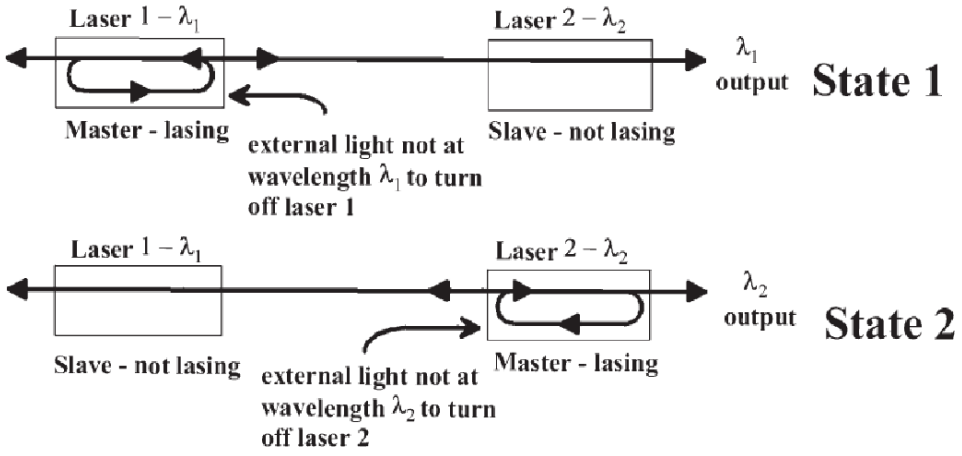


Figure 7.12: Arrangement of two coupled identical lasing cavities showing the possible states, after [107].

et al. report the DAC based wavelength tuning for a label bit-rate of 400 MBit/s in 2004 [97]. In the presented method, the bottleneck is the electronic control circuit speed limitation and switching time of the tunable laser. In order to provide a reconfigurable packet switching system, the routing matrix sub-system is proposed. It consists of a series of interconnected elements controlled by the routing plane and is responsible for mapping the incoming packet address to the appropriate outgoing link (look-up table). The routing matrix containing information does not change dynamically.

A more advanced solution consists of using all-optical flip-flop in order to provide an all-optical wavelength selection system. An optical flip-flop has two stable states and thereby is capable of serving as a one bit memory. A flip-flop is controlled by one or two control signals (called set and reset signals). They have been shown to have useful applications in optical packet routing and switching [107]. Coupled laser diodes [368], nonlinear polarization rotation in SOA [84], coupled Mach-Zehnder interferometers [108], two-coupled mode-locked ring lasers [369], VCSEL [370], Multimode interference bistable laser diodes [371] [372], SOA-based fiber ring laser with an intracavity Lyot filter [373] and SOA/DFB-Laser Diode [374] are some of the techniques proposed before for all-optical flip-flop realization. Switching time, power and length of the set and reset pulses used to switch the device and integration possibilities are the main parameters of realization techniques. A schematic of the flip-flop used in LASAGNE label swapper and packet router project [107] is depicted in figure 7.12.

The system can have two states. In state 1, light from laser 1 suppresses lasing in laser 2. In this state, the optical flip-flop memory emits CW light at wavelength λ_1. Conversely, in state 2, the light from laser 2 suppresses lasing in laser 1. In state 2, the optical flip-flop memory emits CW light at wavelength λ_2. To change states, lasing in the dominant laser can be stopped by injecting an external light at the dominant laser's lasing wavelength. A critical issue is the amount of coupling between the

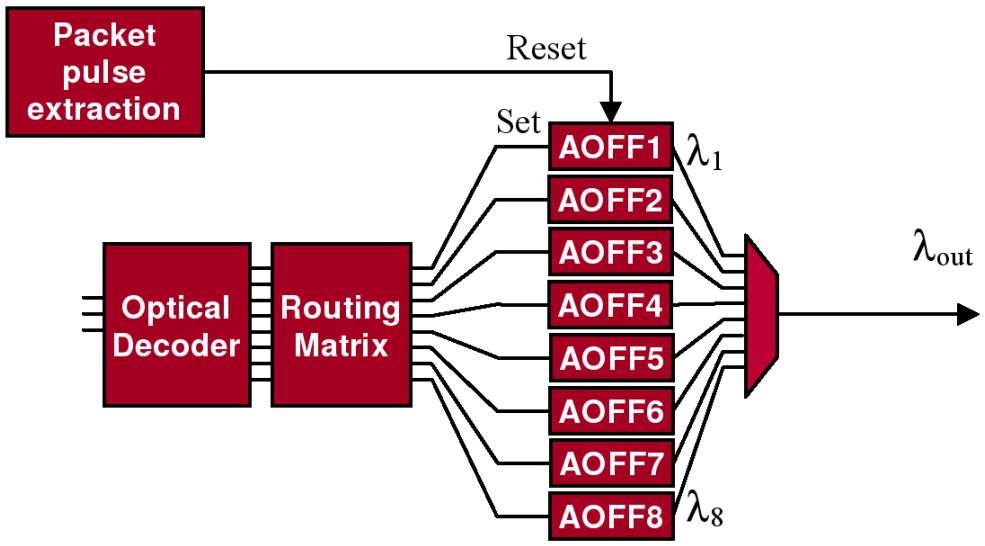


Figure 7.13: All-optical wavelength selection system; AOFF represents all-optical flip-flop

two lasers. The minimum amount of coupling between the lasers that is required to obtain bistable operation depends on the implementation, but the coupling should be strong (typically 40% or larger). Figure 7.13 displays the flip-flop based all-optical adaptive wavelength selecting system.

Each flip flop has two emitting wavelengths namely, λ_{ON} and λ_{OFF}. The λ_{OFF} for all of the flip-flops are chosen the same (e.g. λ_0). It will be filtered by the multiplexer (see figure 7.13). Eight distinct wavelengths ($\lambda_1, \cdots$ and λ_8) are chosen for 8 flip-flops' λ_{ON}. In the first step, all of the flip-flops are reset by the packet pulse extraction. Each output pulse of the decoder passes through routing matrix and sets its associated optical flip-flop. Finally, the selected wavelength (λ_{ON}) is sent into the multiplexer.

Among the methods proposed for realization the optical flip-flops, the wavelength dependent methods (in which the set and reset signal wavelengths are dependent on the emitting wavelengths) such as that presented in figure 7.12 should be eliminated. So, the SOA based methods might be a good candidate for optical flip-flop realizations [108] [84].

The set and reset pulse-widths are important in this design, which depends on the all-optical flip-flop technology. Moreover, when the label bits are modulated in RZ format, the set and reset pulse-widths (for instance, ~10 ps in bit rate of 40 Gbit/s) may be insufficient for driving (switching) the flip-flops. Pulse width conversion [109], RZ to NRZ conversion [110] are some of the techniques proposed for all-optical pulse broadening.

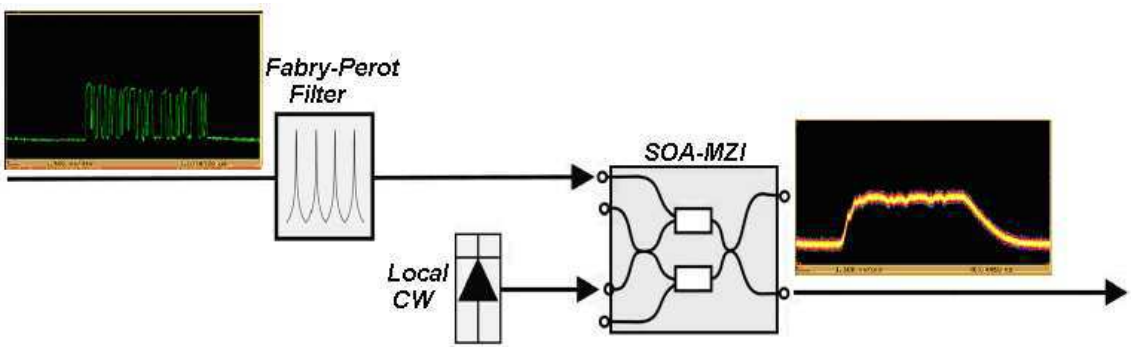


Figure 7.14: 10 Gbit/s packet envelope detector using SOA-MZI technique, after [122]

7.3.2 Packet envelope detection

For serial labelling, the payload-envelope detection (PED) function is used in the label-erase/rewrite process to precisely locate the associated payload without processing its interned content bits. The packet-envelope detector can be constructed using a monolithic, integrated-ring laser or other injection-locked structures [375]. An all-optical PED circuit can potentially reduce the rise and fall times as well as jitter, showing promise to increase channel utilization due to reduced guard band duration. Koch et al. [376] present a PED system for variable length 40-Gb/s return-to-zero payload and 10-Gb/s non-return-to-zero label. The recovered payload envelope has 300-ps rise time. Recently, a new all-optical packet envelope detection based on SOA-Mach-Zehnder interferometric gates was proposed at NTUA (National Technical University of Athens)[122]. Figure 7.14 shows the schematic of this envelope detector.

An optical Q-filter such as a Fabry-Pérot (FP) filter is employed for optical bit-rate filtering to suppress the label using. The Q-factor chosen should optimize the trade-off between the rise/fall time and locking frequency, which affects the label suppression [376]. The filtered packet together with a local CW laser beam is injected into a Mach-Zehnder interferometer in order to recover the payload envelope.

By replacing the local CW beam with the output beam of adaptive wavelength selection subsystem (λ_{out} in figure 7.13), new payload envelope on a packet label-based wavelength will be provided.

7.3.3 Packet label stripping

The forwarding function involves swapping the original label with the new label and physically converting the labelled packet to the new wavelength. The same label swapping mechanism proposed in IST-LAZAGNE project [107] can be used in our scheme whereby, routing matrix output signal (figure 7.17) can be reused for the new label generator subsystem. Recently, new labelling methods have been proposed whereby new label generation for label swapping in every intermediate network node is not required [351] [123]. In these methods, an optical packet is

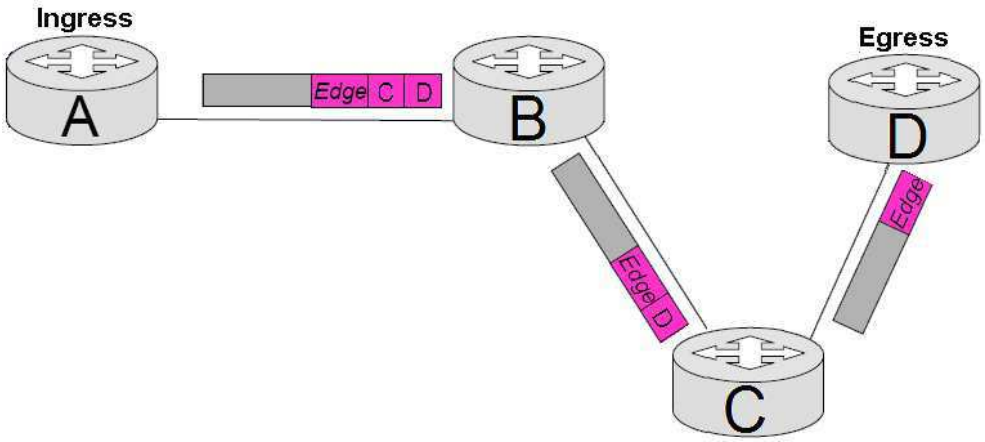


Figure 7.15: Label stripping strategy, after [107]

switched through the network based on an end-to-end label. This label consists of multiple local labels (figure 7.15). In each intermediate node, a part of this label (associated local label) is stripped off and a switching decision is made. This procedure is repeated up to the end of the destination network node [351]. This method can simplify the proposed forwarding architecture presented in this chapter.

7.3.4 Wavelength conversion

The wavelength conversion subsystem is discussed in chapter 6 (6.5.4). The wavelength converter block is responsible for transferring the packet on the λ_{out} (provided by adaptive wavelength selection block and switched by packet envelope detection block).

7.4 Discussion

The optical decoder based packet routing can be categorized among the self-routing methods. The schematic representation of all optical label processing and routing system is shown in figure 7.16. Polarization sensitivity is the main disadvantage of the presented all-optical decoder. As the input packet polarization state is unknown, using the FWM or XPolM in the time-to-wavelength converter or optical decoder may not have enough efficiency.

Polarization insensitive wavelength converters a solution for stabilizing the input packet polarization. In such a way, the input packet passes, firstly, through a polarization insensitive wavelength converter before any other operation. Hatta et al. present full C-band 40-Gbps NRZ operation and polarization insensitive operation of the SOA-MZI wavelength converters [377]. Besides, as using the polarization effect (XPolM) in integrated devices seems difficult, other nonlinear effect might be

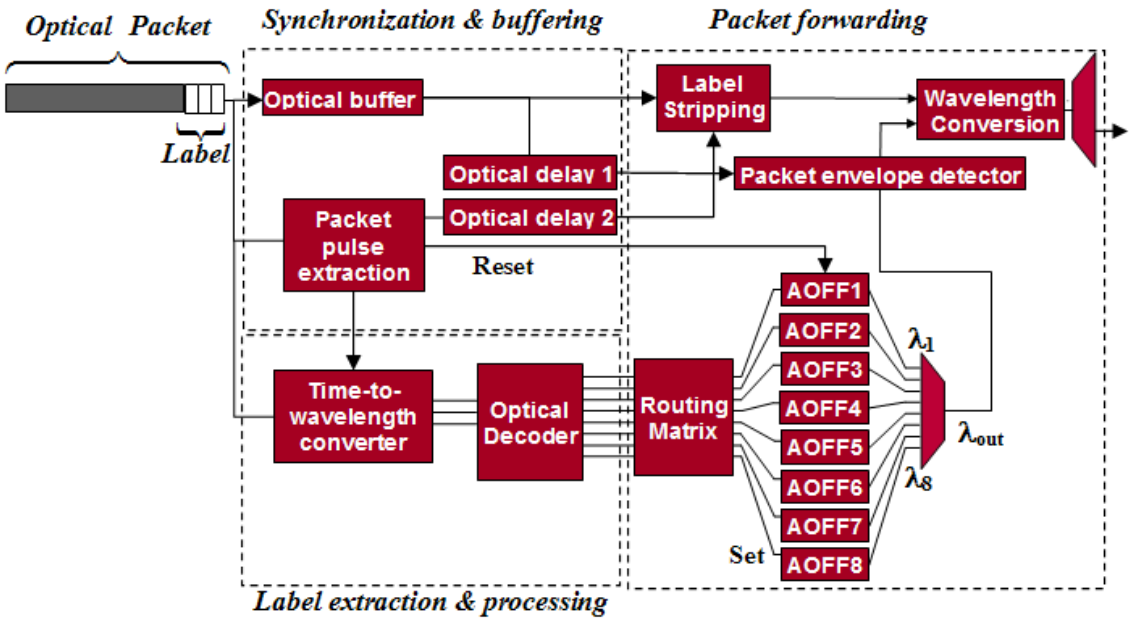


Figure 7.16: Schematic representation of an all optical label processing and routing system

replaced with XPolM effect for reproducing the same logic functionalities (see table 3.1).

Figure 7.17 illustrates the experimental verification of LASAGNE label swapper and packet router. At the entrance, the optical label and payload are separated. The extracted optical label is fed to a bank of XOR auto-correlators (AOLXG) and will compare with a local address word. These local addresses are generated using a network of optical delay lines (ODLs). An ODL is comprised of a set of interconnected fibre delay lines, couplers and splitters, generating a bit sequence out of one pulse. After comparison a high intensity pulse will appear at the output of the AOLXG with the matching address. This pulse feeds a control block that drives a wavelength converter and generates a new optical label (this label is again generated in an ODL). Two switches provide the flexibility to assign different outgoing labels and wavelengths to the same incoming label. After the header and payload are combined again, the packet is sent through an AWG.

However, disadvantages are related to requirements in optical power and fiber length stimulated the research and development of compact semiconductor-based switch. In return in the proposed scheme in figure 7.16 no more packet address regeneration is not required. The case where the routing decisions are made on the basis of a single-bit information in the header is referred to as bit-level packet switching (BLPS) [378]. Packet switching with bit-level processing is also proposed in ARTEMIS (All-optical self-RouTer EMploying bIt and packet-level procesSing) project [123]. Avoiding local address generation, the ARTEMIS system is capable of routing 40 Gbit/s asynchronous packets.

The self-routing-network architecture proposed is shown in figure 7.18 and con-

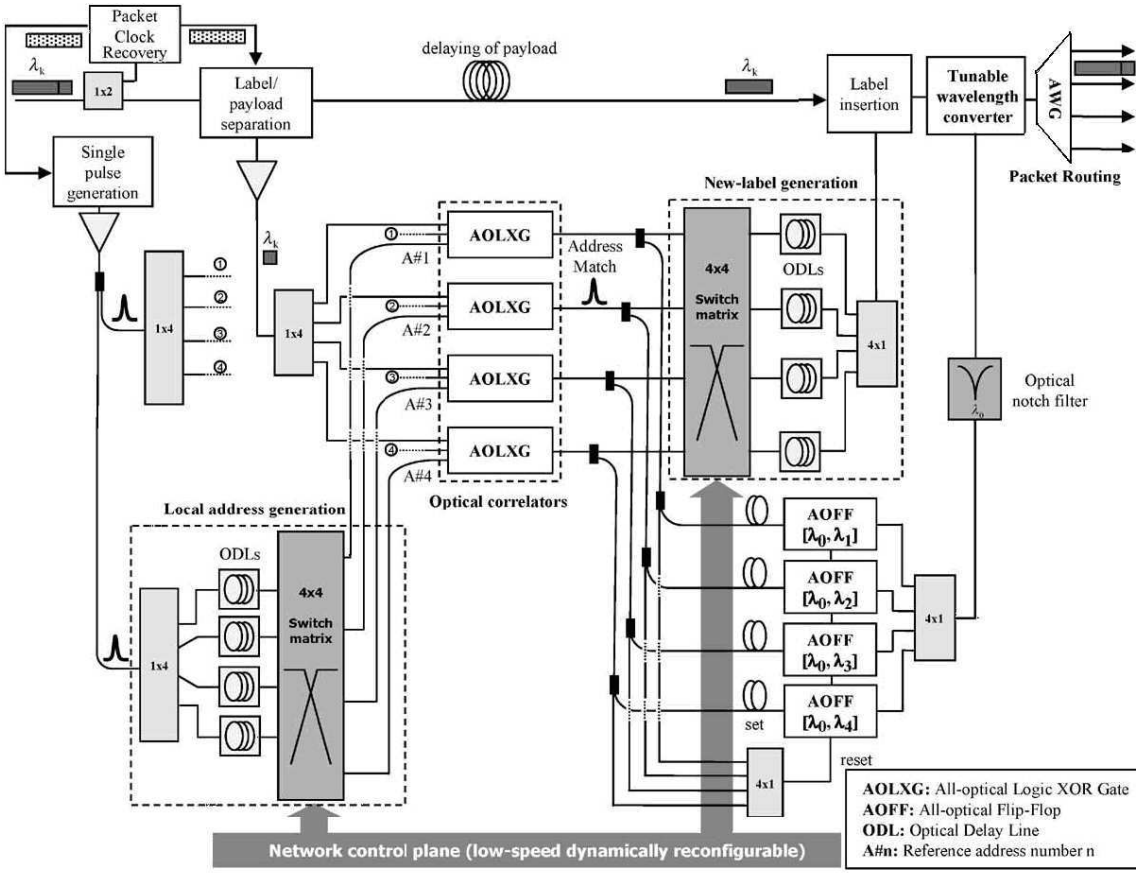


Figure 7.17: Experimental verification of LASAGNE label swapper and packet router, after [107]

sists of two clearly defined layers;

- The optical layer in which all network functionalities associated with transmission, regeneration, and routing are performed.
- The control plane is solely responsible for resources reservation for contention protection.

The transmission of optical packets through the ARTEMIS network is realized using optical headers that contain stacked optical "tags" [153], each corresponding to a specific node. In addition, each optical tag contains bit-level information for optically controlling the switching matrix of the node and thus routing the data packet to the appropriate outgoing link and on to the next hop. The number of stacked tags depends on the number of hops within the network and they are embedded by the control plane after the burst assembly process in the ingress node (IN). Each tag contains a control signal that is a serially encoded binary word, used to set the switches within the node switching matrix. Moreover, each tag has three embedded routing bits responsible for controlling the switching matrix of the node that consists of 1×2 optically controlled optical gates.

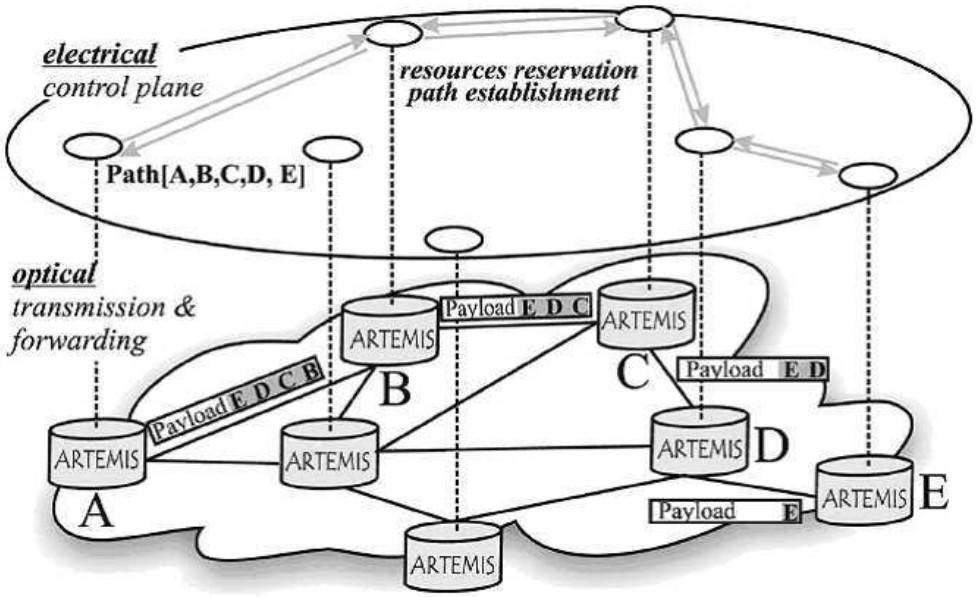


Figure 7.18: ARTEMIS network architecture and all-optical burst forwarding, after [123].

Figure 7.19 presents the schematic diagram of header processing/forwarding plan of the ARTEMIS network. The incoming optical packet and the recovered packet clock stream enter the tag extraction gate that consists of an SOA-MZI gate configured as a Boolean AND gate. The whole payload, including tag#2, are switched, whereas only tag#1 remains unswitched and enter the header processing/ forwarding plane. Tag#1 is then fed into an array of SOA-MZI (performing AND) gates, each responsible for extracting a single routing bit. Finally, each routing bit enters the control-signal-generation block and depending on its binary value, a control signal is generated and forwarded to the switching matrix.

Control signal can be generate via one of the three distinct ways; using an optical flip-flop [368], an optical circuit with finite memory [379], or an electronic pulse generator followed by an optoelectronic conversion [380]. These generated CW signals are used to control the all-optical 1×2 optical elements of the switching matrix described in the next section. Figure 7.20(a) and (b) show how these elementary 1×2 switching elements can be interconnected so as to form 4×4 and 8×8 strictly nonblocking switching matrices.

In our method (see figure 7.16) the separation of label subset bits (so-called "tag" in figure 7.19) is done with only one SOA (in a time-to-wavelength configuration discussed in chapter 5). Moreover, in the ARTEMIS architecture, the number of control signals required for the routing of a packet is equal to the number of stages within an N×N switching fabric, which is in turn equal to $T = log_2 N$. In order to provide an independent optical path to interconnect each one of the inputs to every possible output a passive coupling stage is employed at the output of the Nth stage, consisting of N×1 fiber couplers. Conversely, in our scheme for each packet

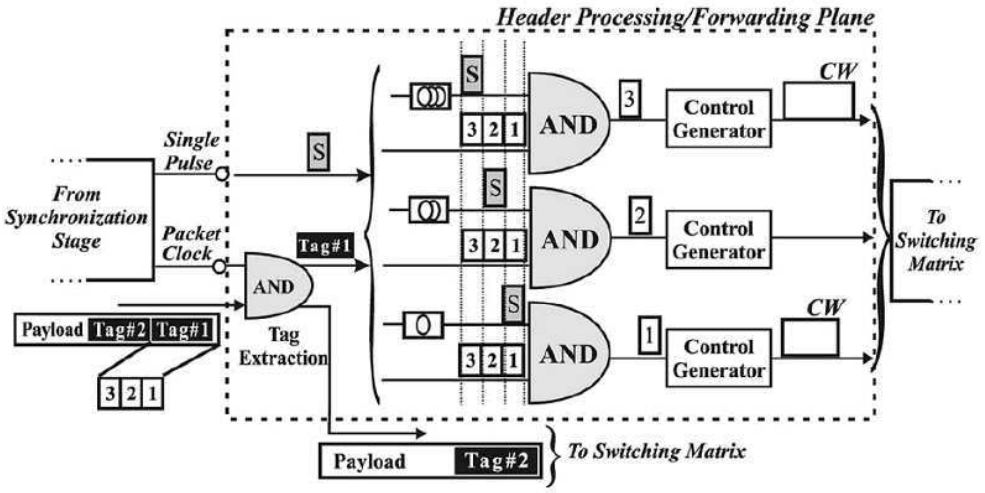


Figure 7.19: Detailed schematic diagram of the header-processing/forwarding plane, after [123].

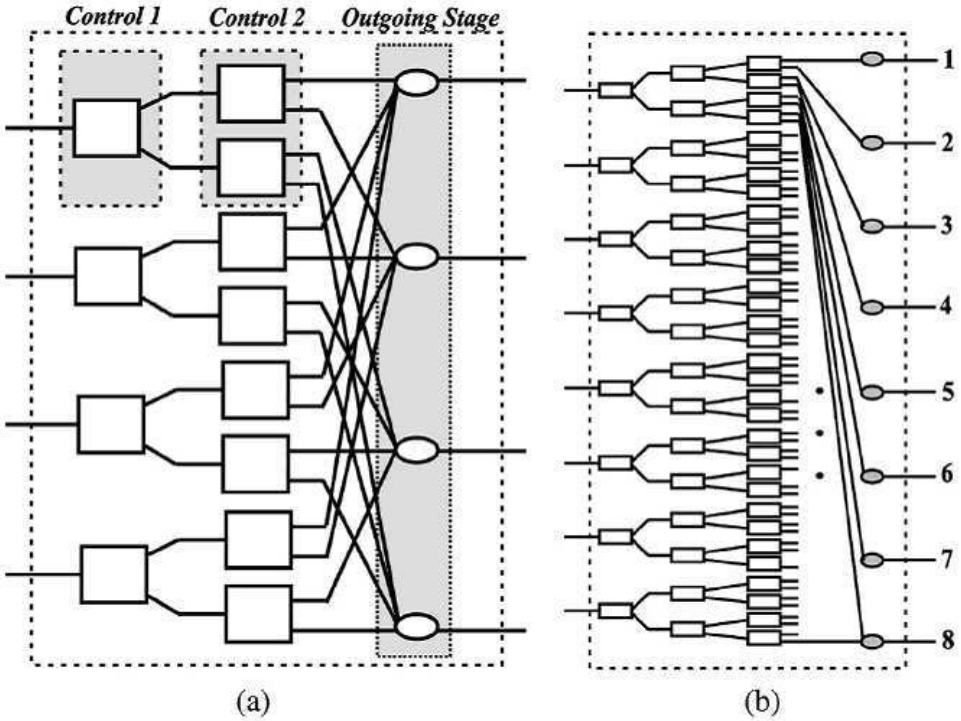


Figure 7.20: ARTEMIS (a) 4×4 and (b) 8×8 switching matrices. In both cases, the elementary 1×2 switching elements are interconnected so as to form a strictly nonblocking switching fabric, after [123].

labet subset (tag) there is only one wavelength produced by the associated flip-flop. Furthermore, the new generated wavelength is used as an input of a wavelength converter. The packet spatial switching is possible with an AWG to deliver the packet in the desired outgoing port. Therefore no switching matrix is required.

Integration of functionalities in such a system environment to perform lossless packet processing and routing in the optical domain still remains an elusive target. Regarding the present integrated optics technology, most of the packet forwarding subsystem presented in figure 7.16 can be realized with integrated optic technologies [381].

7.5 Summary

In this chapter, for the first time in our knowledge, the implementation of an all-optical 3×8 decoder based on XPolM in SOAs at 10 Gbit/s is demonstrated. The design requires only one active optical device per output. The measured extinction ratio of the output signals is between 7.9 and 12 dB. Next, an all-optical solution for optical packet forwarding based on time-to-wavelength converter and all-optical decoder is proposed. The main advantage of this approach is the ability to route the packets or bursts independently of packet length. The optical integration effort might be valuable in terms of the integrated optics preferences.

General Conclusion and Perspectives

The constantly increasing demand for network bandwidth together with progressing in optical technologies accelerates the amount of research in the field of optical networks. Optical communication is a promising choice to fulfill the ever-increasing demand on bandwidth via the vast available capacity of the fiber optics. In particular, a great part of research in optical networks is dedicated to transparency in optical networks in order to bypass the O/E/O conversions in the intermediate nodes (routers) of the network. Thus, a number of network protocols (such as MPLS, GMPLS and etc.) together with switching strategies (circuit- burst- or packet-switching) are proposed for data transparency in the network. Among the switching strategies, the burst switching is more compatible with the current optoelectronic technologies in terms of data transparency and switching speed. The packet switching is more efficient for data communication, but due to the limited speed on electronics (in comparison with the present optical bandwidth in fiber optics) an the insufficient evolution of all-optical signal processing alternatives, the packet based optical networks are not still a practical solution in transparent optical networks.

The objective point of this research work was to propose an all-optical method for packet routing and forwarding in the transparent optical networks. In this thesis we investigate, design and partially implement some optoelectronic and all-optical signal processing systems.

In the first chapter a brief introduction onto the optical network evolution and network node in terms of opaque and transparent architectures are addressed. Moreover, the advantages and disadvantages of layering design of optical network are investigated and finally a review on the packet based network protocols (e.g. OSI, MPLS, $\cdots$) is presented.

As most of the reported optical signal processing operations in this work are based on SOAs, the second chapter deals with the SOA in terms of structure, operation principle, and nonlinear effects. Cross-polarization modulation (XPolM), cross phase modulation (XPM) and four wave mixing (FWM) are the main nonlinear effect used in the succeeding chapters. A new method for improvement polarization sensibility of the FWM effect in SOA is proposed as well. It consists of using a spectrum-sliced incoherent light source in the place of a coherent pump (classic case). Despite a 3 dB efficiency reduction in the best case with respect to an

equivalent coherent light launching, the use of unpolarized, incoherent light allows polarization insensitivity as demonstrated theoretically and experimentally. The accumulated noise due to the incoherent light source in the output FWM signal can be reduced using the non-linear gain compression characteristics of SOA.

All-optical logic gates are frequently employed in optical signal processing and in particular in our packet switching architectures. A abstract of the previous efforts for different optical logic gate realization is addressed in chapter 3. Moreover, a new design of XOR and XNOR logic gates at 10 Gbit/s based on a new configuration of the ultrafast nonlinear interferometer (UNI) system is proposed. The output extinction ratio between 5.5 and 7.5 dB is achieved at 10 Gbit/s data rate. The output signal efficiency can be increased by input signal extinction ratio enhancement. BPM (beam propagation method) simulation shows the possibility of a half-adder realization based on the presented XOR and XNOR logic gates.

A state-of-art about the packet switching subsystems and, in particular, packet label (header) processing is presented in chapter 4. Labelling scheme (bit serial, subcarrier multiplexing, orthogonal modulation, and etc.) has been proposed for MPLS based packets. Among these schemes, bit-serial approach is the least restrictive approach in terms of Packet bit rate and modulation extinction ratio. Interferometric methods, optical bit pattern matching, label slowed down processing and all-optical label processing are the 4 main techniques proposed for packet label recognition. The two former methods have less limitations in terms of label bit combination and simpleness.

A new time-to-wavelength converting (TWC) method is applied for label slowed down processing in which the TWC acts as a serial-to-parallel converter. The major element of the TWC concept is the use of an optical AND logic gate. Each input data bit in the original time domain is transferred onto a specific wavelength. The FWM and XPolM effects in SOA were used for performing an all-optical AND logic gate. The extinction ratio of 8−9 dB (XPolM) and 9 and 12.5 dB (FWM) were achieved.

As most core routers of backbone or metro networks have only four to eight outgoing ports, it may be possible to determine a packet's outgoing port by looking at only a small subset of the label bits in the destination address. Thus, regarding to the experimental results of a 4-bit time-to-wavelength converter, an optoelectronic design for the optical packet switching based on label slowed down processing method is demonstrated and partially realized in chapter 6. In this system, the packet payload remains always in optic during the packet label processing operations. Packet rate scalability, asynchronous (burst) mode operation, modularity, and flexibility (in terms of increasing the processing length of the label subset and packet length) are some of advantages of this architecture. The experience was done at bit rate of 10 Gbit/s for packet labels.

In chapter 7, a new all-optical packet switch design is presented, in which all the packet processing and forwarding operations are performed in optics. The time-to-wavelength conversion technique is reused for separating the three bits of packet label. An all-optical 3×8 decoder based on cross-polarization modulation (XPolM) in SOAs is responsible for detecting the label subset combination and providing the

proper signal to a wavelength selection subsystem. The decoder is demonstrated at 10 Gbit/s. The measured extinction ratio of the output signals is between 7.9 and 12 dB. Besides, by using the packet stripping technique the packet swapping and new label generating operations are not required. Therefore, regarding the packet label subset, the packet will be forwarded onto a new wavelength.

In the presented architecture in chapter 6 and 7, all the label and payload can be modulated at the same bit-rate. Moreover, the allocated time for packet label processing and packet routing can be reduced via all-optical solutions (chapter 7). This not only reduces the packet format complexity, but also reduces the label duration (leading to a greater data bit-rate).

In perspective, the following issues are proposed;

- The optical integration efforts of an all-optical packet switching system
- Investigation of other nonlinear effect in SOA or other optical elements for increasing the efficiency, robustness and polarization sensiblity of the proposed packet switching architectures.
- Repeating the experiments beyond 10 Gbit/s (e.g. 40 Gbit/s)

BIBLIOGRAPHY

[1] K. Morito, S. Tanaka, S. Tomabechi, and A. Kuramata. A broad-band MQW semiconductor optical amplifier with high saturation output power and low noise figure. *IEEE Photonic Technology Letters*, 17(5):974–976, May 2005.

[2] T. Houbavlis, K. Zoiros, A. Hatziefremidis, H. Avramopoulos, L. Occhi, G.Guekos, S.Hansmann, H.Burkhard, and R. Dall'ara. 10 Gbit/s all-optical boolean XOR with SOA fiber sagnac gate. *Electronics Letters*, 35(19):1650–1652, Sep. 1999.

[3] K. L. Hall and K. A. Rauschenbach. All-optical bit pattern generation and matching. *Electronics Letters*, 32(13):1214–1215, Jun. 1996.

[4] A. Poustie, R. Manning, A. Kelly, and K. Blow. All-optical binary counter. *Optics Express*, 6(3):69–74, Jan. 2000.

[5] H. Teimoori, J. D. Topomondzo, C. Ware, and D. Erasme. Optical packet header processing using time-to-wavelength mapping in semiconductor optical amplifiers. *IEEE Journal of Lightwave Technology*, 2007.

[6] A. J. Poustie, K. J. Blow, A. E. Kely, and R. J. Manning. All-optical parity checker using bit differential delay. *Optics Communications*, 162(1-3):37–43, Apr. 1999.

[7] L. Y. Chan, K. K. Qureshi, P. K. A. Wai, B. Moses, L. F. K. Lui, H. Y. Tam, and M. S. Demokan. All-optical bit-error monitoring system using cascaded inverted wavelength converter and optical NOR gate. *IEEE Photonics Technology Letters*, 15(4):593–595, Apr. 2003.

[8] H. Teimoori, J. D. Topomondzo, C. Ware, and D. Erasme. Optical packet header processing using time-to-wavelength mapping in semiconductor optical amplifiers. *IEEE Journal of Lightwave Technology*, 25(8):2149–2158, Aug. 2007.

[9] X. Huang, M. Zhang, L. Wang, and P. Ye. Novel scheme of 40 Gb/s all-optical NOT gate based on SOA-assisted sagnac interferometer. In *International Conference on Communications, Circuits and Systems*, volume 1, pages 621–624, Jun. 2004.

[10] M. Jinno and T. Matsumoto. Ultrafast all-optical logic operations in a nonlinear sagnac interferometer with two control beams. *Optics letters*, 16(4):220–222, Feb. 1991.

[11] K. Zoiros, T. Houbavlis, K. Vlachos, H. Avramopoulos, F. Girardin, G. Guekos, S. Hansmann, and H. Burkhard. 10 ghz boolean XOR with semiconductor optical amplifier fiber sagnac gate. In *CLEO*, pages 379–380, May 1999.

[12] Y. H. Kao, I. V. Goltser, M. N. Islam, and G. Raybon. Ultrafast optical logic gate using a semiconductor laser amplifier operating at transparency in a loop mirror. In *CLEO*, volume 11, pages 94–95, USA, May 1997.

[13] A. J. Poustie, K. J. Blow, A. E. Kelly, and R. J. Manning. All-optical binary half-adder. *Optics communications*, 156(1-3):22–26, Nov. 1998.

[14] A. Frenkel, T. G. Chang, I. Glesk, and P. R. Prucnal. Demonstration of pulse frequency division multiplexing using terahertz optical asymmetric demultiplexer. *IEEE photonics technology letters*, 10(9):1322–1324, Sep. 1998.

[15] H. Dong, H. Sun, Q. Wang, N.K. Dutta, and J. Jaques. 80 Gb/s all-optical logic AND operation using Mach-Zehnder interferometer with differential scheme. *Optics communications*, 265(1):79–83, Sep. 2006.

[16] J. Y. Kim, J. M. Kang, T. Y. Kim, and S. K. Han. 10 Gbit/s all-optical composite logic gates with XOR, NOR, OR and NAND functions using SOA-MZI structures. *Electronics Letters*, 42(5):303–304, Mar. 2006.

[17] T. Fjelde, D. Wolfson, A. Kloch, C. Janz, A. Coquelin, I. Guillemot, F. Gaborit, F. Poingt, B. Dagens, and M. Renaud. 10 Gbit/s all-optical logic OR in monolithically integrated interferometric wavelength converter. *Electronics Letters*, 36(9):813–815, Apr. 2000.

[18] R. P. Webb, R. J. Manning, G. D. Maxwell, and A. J. Poustie. 40 Gbit/s all-optical XOR gate based on hybrid-integrated Mach-Zehnder interferometer. *Electronics Letters*, 39(1):79–81, Jan. 2003.

[19] T. Fjelde, D. Wolfson, A. Kloch, B. Dagens, A. Coquelin, I. Guillemot, F. Gaborit, F. Poingt, and M. Renaud. Demonstration of 20 Gbit/s all-optical logic

XOR in integrated SOA-based interferometric wavelength converter. *Electronics Letters*, 36(22):1863–1864, Oct. 2000.

[20] S. Lee, J. Park, K. Lee, D. Eom, S. Lee, and J. H. Kim. All-optical exclusive NOR logic gate using Mach-Zehnder interferometer. *Japanese Journal of Applied Physics*, 41(10B):L1155–L1157, Oct. 2002.

[21] X. Ye, P. Ye, and M. Zhang. All-optical NAND gate using integrated SOA-based Mach-Zehnder interferometer. *Optical Fiber Technology*, 12(4):312–316, Oct. 2006.

[22] T. Houbavlis, K. E. Zoiros, G. Kanellos, and C. Tsekrekos. Performance analysis of ultrafast all-optical boolean XOR gate using semiconductor optical amplifier-based Mach-Zehnder interferometer. *Optics Communications*, 232:179–199, Mar. 2004.

[23] Y. K. Chen, C. J. Hu, C. C. Lee, K. M. Feng, M. K. Lu, Y. K. Tu, and S. L. Tzeng. All-optical logic XOR using differential scheme and Mach-Zehnder interferometer. *Electronics Letters*, 38(21):1271–1273, Oct. 2002.

[24] Q. Wang, G. Zhu, H. Chen, J. Jaques, J. Leuthold, A. B. Piccirilli, and N. K. Dutta. Study of all-optical XOR using Mach-Zehnder interferometer and differential scheme. *IEEE Journal of Quantum Electronics*, 40(6):703–710, Jun. 2004.

[25] H. Sun, Q. Wang, H. Dong, and N. Dutta. XOR performance of a quantum dot semiconductor optical amplifier based Mach-Zehnder interferometer. *Optics Express*, 13(6):1892–1899, Mar. 2005.

[26] J. M. Martinez, F. Ramos, J. Marti, J. Herrera, and R. Llorente. All optical n-bit XOR gate with feedback for optical packet header processing. In *ECOC*, volume 3, page P4.8, Copenhagen, Denmark, Sep. 2002.

[27] G. Berrettini, A. Malacarne, P. Ghelfi, A. Bogoni, and L. Poti. Ultrafast integrable and reconfigurable XNOR, AND, NOR, and NOT photonic logic gate. *IEEE Photonics Technology Letters*, 18(8):917–919, Apr. 2006.

[28] D. Nesset, M.C. Tatham, L.D. Westbrook, and D. Cotter. Degenerate wavelength operation of an ultrafast all-optical AND gate using four wave mixing in a semiconductor laser amplifier. *Electronics Letters*, 30(23):1938–1940, Nov. 1994.

[29] K. Vahala, R. Paiella, and G. Hunziker. Ultrafast wdm logic. *IEEE Journal of Selected Topics in Quantum Electronics*, 3(2):698–701, Apr. 1997.

[30] K. Chan, C. K. Chhan, L. K. Chen, and F. Ton. 20-Gbit/s all-optical XOR gate by four-wave mixing in semiconductor optical amplifier with RZ-DPSK modulated inputs. In *Optical Fiber Communication*, volume 1, Los Angeles, USA, Feb. 2004.

[31] D. Nesset, M.C. Tatham, and D. Cotter. All-optical AND gate operating on 10 Gbit/s signals at the same wavelength using four-wave mixing in a semiconductor laser amplifier. *Electronics Letters*, 31(11):896–897, May 1995.

[32] N. Deng, C. K. Chan, and L. K. Chen. Demonstration of an all-optical three-input exclusive-OR logic gate for high-speed optical dpsk signals. In *ECOC*, volume 2, pages 227–228, Cannes, France, Sep. 2005.

[33] I. Kang, C. Dorrer, and J. Leuthold. All-optical XOR operation of 40 Gbit/s phase-shift-keyed data using four-wave mixing in semiconductor optical amplifier. *Electronics Letters*, 40(8):496–497, Apr. 2004.

[34] S. Kumar and A. E. Willner. All optical XNOR gate using simultaneous four-wave mixing and cross-gain modulation in an SOA. In *LEOS*, volume 2, pages 913–914, Nov. 2004.

[35] P. O. Hedekvist, A. Bhardwaj, K. Vahala, and H. Andersson. Advanced all-optical logic gates on a spectral bus. *applied optics*, 40(11):1761–1766, Apr. 2001.

[36] S. H. Kim, J. H. Kim, B. G. Yu, Y. T. Byun, Y. M. Jeon, S. Lee, and D. H. Woo. All-optical NAND gate using cross-gain modulation in semiconductor optical amplifiers. *Electronics Letters*, 18(Sep.):1027–1028, Sep. 41.

[37] X. Zhang, Y. Wang, J. Sun, D. Liu, and D. Huang. All-optical AND gate at 10 Gbit/s based on cascaded single-port-couple SOAs. *Optics Express*, 12(3):361–366, Feb. 2004.

[38] Y. T. Byun, K. S. Choi, Y. M. Jhon, D. H. Woo, S. Lee, and S. H. Kim. Realization of high-speed all-optical OR gate using cross-gain modulation. In *Lasers and Electro-Optics Society*, pages 436–437, Oct. 2005.

[39] A. Sharaiha, H. W. Li, F. Marchese, and J. L. Bihan. All-optical logic NOR gate using a semiconductor laser amplifier. *Electronics Letters*, 33(4):323–324, Feb. 1997.

[40] J. H. Kim, Y. M. Jhon, Y. T. Byun, S. Lee, D. H. Woo, and S. H. Kim. All-optical XOR gate using semiconductor optical amplifiers without additional input beam. *IEEE Photonic Technology Letters*, 14(10):1436–1438, Oct. 2002.

[41] A. Sharaiha, J. D. Topomondzo, and P. Morel. All-optical logic AND-NOR gate with three inputs based on cross-gain modulation in a semiconductor optical amplifier. *Journal of Optics communications*, 265(1):322–325, 2006.

[42] A. Hamie, A. Sharaiha, M. Guegan, and B. Pucel. All-optical logic NOR gate using two-cascaded semiconductor optical amplifiers. *IEEE Photonic Technology Letters*, 14(10):1439–1441, Oct. 2002.

[43] C. Zhao, X. Zhang, H. Liu, D. Liu, and D. Huang. Tunable all-optical NOR gate at 10 Gb/s based on SOA fiber ring laser. *Optics express*, 13(8):2793–2798, Mar. 2005.

[44] S. Pereira, P. Chak, and J. E. Sipe. All-optical AND gate by use of a kerr nonlinear microresonator structure. *Optics Letters*, 28(6):444–446, Mar. 2003.

[45] T. A. Ibrahim, R. Grover, L. C. Kuo, S. Kanakaraju, L. C. Calhoun, and P. T. Ho. All-optical AND/NAND logic gates using semiconductor microresonators. *IEEE Photonics Technology Letters*, 15(10):1422–1424, Oct. 2003.

[46] M. Naruse, H. Yoshida, T. Miyazaki, F. Kubota, and H. Ishikawa. Ultrafast all-optical NOR gate based on intersubband and interband transitions. *IEEE Photonic Technology Letters*, 17(8):1701–1703, Aug. 2005.

[47] S. Mikroulis, H. Simos, E. Roditi, A. Chipouras, and D. Syvridis. 40-Gb/s NRZ and RZ operation of an all-optical AND logic gate based on a passive InGaAsP/InP microring resonator. *Journal of Lightwave Technology*, 24(3):1159–1164, Mar. 2006.

[48] T. Fujisawa and M. Koshiba. All-optical logic gates based on nonlinear slot-waveguide couplers. *Journal of Optical Society America B*, 23(4):684–691, Apr. 2006.

[49] W. B. Fraga, J. W. M. Menezes, M. G. da Silva, C. S. Sobrinho, and A. S. B. Sombra. All optical logic gates based on an asymmetric nonlinear directional coupler. *Optics Communications*, 262(1):32–37, Jun. 2006.

[50] Y. Wang and J. Liu. All-fiber logical devices based on the nonlinear directional coupler. *IEEE Photonic Technology Letters*, 11(1):72–74, Jan. 1999.

[51] J. Wang, J. Sun, and Q. Sun. Experimental observation of a 1.5 μm band wavelength conversion and logic NOT gate at 40 Gbit/s based on sum-frequency generation. *Optics Letters*, 31(11):1711–1713, Jun. 2006.

[52] Y. L. Lee, B. A. Yu, T. J. Eom, W. Shin, C. Jung, Y. C. Noh, J. Lee, D. K. Ko, and K. Oh. All-optical AND and NAND gates based on cascaded second-order nonlinear processes in a Ti-diffused periodically poled $LiNbO_3$ waveguide. *Optics Express*, 14(7):2776–2782, Apr. 2006.

[53] T. K. Liang, L. R. Nunes, M. Tsuchiya, K. S. Abedin, T. Miyazaki, D. Van Thourhout, P. Dumon, R. Baets, and H. K. Tsang. All-optical high speed NOR gate based on two photon absorption in silicon wire waveguides. *Optics communications*, 265(1):171–174, 2006.

[54] J. E. McGeehan, M. Giltrelli, and A. E. Willner. All-optical digital 3-input AND gate using sum- and difference-frequency generation in a PPLN waveguide. In *LEOS Summer Topical Meetings*, pages 179–180, Jul. 2005.

[55] J. H. Lee, T. Nagashima, T. Hasegawa, S. Ohara, N. Sugimoto, and K. Kikuchi. 40 Gbit/s XOR and AND gates using polarisation switching within 1 m-long bismuth oxide-based nonlinear fibre. *Electronics Letters*, 41(19):1074–1075, Sep. 2005.

[56] B.-E. Olsson and P. A. Andrekson. Polarization-independent all-optical AND-gate using randomly birefringent fiber in a nonlinear optical loop mirror. In *OFC*, pages 375–376, Feb. 1998.

[57] A. Bogoni, L. Pot, R. Proietti, G. Meloni, F. Ponzini, and P. Ghelfi. Regenerative and reconfigurable all-optical logic gates for ultra-fast applications. *Electronics Letters*, 41(7):435–436, Mar. 2005.

[58] C. Yu, L. Christen, T. Luo, Y. Wang, Z. Pan, L.-S. Yan, and A.E. Willner. All-optical XOR gate based on kerr effect in single highly-nonlinear fiber. In *CLEO*, volume 2, page 3, May 2004.

[59] M. N. Islam. All-optical cascadable NOR gate with gain. *Optics letters*, 15(8):417–419, Apr. 1990.

[60] B. S. Robinson, S. A. Hamilton, S. J. Savage, and E. P. Ippen. 40 Gbit/s all-optical XOR using a fiber-based folded ultrafast nonlinear interferometer. In *OFC*, pages 561–563, Anaheim,USA, Mar. 2002.

[61] D. Taverner, N. G. R. Broderick, D. J. Richardson, M. Ibsen, and R. I. Laming. All-optical AND gate based on coupled gap-soliton formation in a fiber bragg grating. *Optics Letters*, 23(4):259–261, Feb. 1998.

[62] E. S. Awad, P. Cho, and J. Goldhar. High-speed all-optical AND gate using nonlinear transmission of electroabsorption modulator. *IEEE Photonics Technology Letters*, 13(5):472–474, May 2001.

[63] N. E. Dahdah, R. Coquille, B. Charbonnier, E. Pincemin, C. Kazmierski, G. Aubin, and A. Ramdane. All-optical wavelength conversion by EAM with shifted bandpass filter for high bit-rate networks. *IEEE Photonics Technology Letters*, 18(1):61–63, Jan 2006.

[64] N. S. Patel, K. L. Hall, and K. A. Rauschenbach. 40 Gbit/s cascadable optical logic using an ultrafast nonlinear interferometer. *Optics Letters*, 21(18):1466–1468, Sep. 1996.

[65] K. L. Hall and K. A. Rauschenbach. 100 Gbit/s bitwise logic. *Optics letters*, 23(16):1271–1273, Aug. 1998.

[66] C. Bintjas, M. Kalyvas, G. Theophilopoulos, T. Stathopoulos, H. Avramopoulos, L. Occhi, L. Schares, G. Guekos, S. Hansmann, and R. Dall'Ara. 20 Gbps boolean XOR with UNI gate. In *ECOC*, volume 4, pages 61–62, Munich, Sep. 2000.

[67] G. Theophilopoulos, K. Yiannopoulos, M. Kalyvas, C. Bintjas, G. Kalogerakis, and H. Avramopoulos. 40 ghz all-optical XOR with UNI gate. In *Optical Fiber Communication Conference and Exhibit(OFC)*, volume 1, pages MB2–1–MB2–3, 2001.

[68] H. Soto, C.A. Diaz, J. Topomondzo, D. Erasme, L. Schares, and G. Guekos. All-optical AND gate implementation using cross-polarization modulation in a semiconductor optical amplifier. *Photonics Technology Letters*, 14(4):498–500, Apr. 2002.

[69] L. Q. Guo and M. J. Connelly. All-optical AND gate with improved extinction ratio using signal induced nonlinearities in a bulk semiconductor optical amplifier. *Optics Express*, 14(7):2938–2943, Apr. 2006.

[70] L. Han, X. Teng, L. Hu, N. Hua, and H. Zhang. All optical NOR and OR gates using cross polarization modulation in a single SOA. In *Lasers and Electro-Optics Society*, pages 438–439, Oct. 2005.

[71] H. Soto, J. D. Topomondzo, D. Erasme, and M. Castro. All-optical NOR gates with two and three input logic signals based on cross-polarization modulation in a semiconductor optical amplifier. *Optics Communications*, 218(4-6):243–247, Apr. 2003.

[72] H. Soto, D. Erasme, and G. Guekos. 5-Gb/s XOR optical gate based on cross-polarization modulation in semiconductor optical amplifiers. *IEEE Photonic Technology Letters*, 13(4):335–337, Apr. 2001.

[73] H. Soto, E. lvarez, C. A. Daz, J. Topomondzo, D. Erasme, L. Schares, L. Occhi, G. Guekos, and M. Castro. Design of an all-optical NOT XOR gate based on cross-polarization modulation in a semiconductor optical amplifier. *Optics Communications*, 237(1-3):121–131, Jul. 2004.

[74] D. Cotter, J. K. Lucek, M. Shabeer, K. Smith, D. C. Rogers, D. Nesset, and P. Gunning. Self-routing of 100 Gbit/s packets using 6 bit 'keyword 'address recognition. *Electronics Letters*, 31(17):2201–2203, Aug. 1995.

[75] Z. Zhu, V. J. Hernandez, M. Y. Jeon, J. Cao, Z. Pan, and S. J. Ben Yoo. Rf photonics signal processing in subcarrier multiplexed optical-label switching communication systems. *IEEE Journal of lightwave technology*, 21(12):3155–3166, Dec. 2003.

[76] I. Chlamtac, A. Fumagalli, L. G. Kazovsky, P. Melman, W. H. Nelson, P. Poggiolini, M. Cerisola A. N. M. M. Choudhury, T. K. Fong, R. T. Hofmeister, C.-L. Lu, A. Mekkittikul D. J. M. Sabido, I. C. J. Suh, and E.W.M. Wong. CORD: contention resolution by delay lines. *IEEE Journal on Selected Areas in Communications*, 14(5):1014–1029, Jun. 1996.

[77] D. Wonglumsom, I. M. White, S. M. Gemelos, K. Shrikhande, and L. G. Kazovsky. Hornet-a packet-switched WDM network: Optical packet transmission and recovery. *IEEE Photonics Technology Letters*, 11(12):1692–1694, Dec. 1999.

[78] A. Crean, M. D. Vaughn, R. Gaudino, M. Shell, and D. L. Blumenthal. OPERA: An optical packet experimental routing architecture with label swapping capability. *Journal of Lightwave Technology*, 16(12):2135–2145, Dec. 1998.

[79] I. T. Monroy, E. van Breusegem, T. Koonen, J. J. V. Olmos, J. van Berkel, J. Jennen, C. Peucheret, and E. Zouganeli. Optical label switched networks: laboratory trial and network emulator in the IST-STOLAS project. *IEEE Communications Magazin*, 44(8):43–51, Aug. 2006.

[80] P. Gambini, M.Renaud, C. Guillemot, F. Callegati I. Andonovic, B. Bostica, D. Chiaroni, G. Corazza, S. L. Danielsen, P. Gravey, P. B. Hansen, M. Henry, C. Janz, A. Kloch, R. Krahenbuhl, C. Raffaelli, M. Schilling, A. Talneau, and L. Zucchelli. Transparent optical packet switching: Network architecture and demonstrators in the keops project. *IEEE Journal on Selected Areas in Communications*, 16(7):1245–1259, Jul. 1998.

[81] L. Dittmann, C. Develder, D. Chiaroni, F. Neri, F. Callegati, W. Koerber, A. Stavdas, M. Renaud A. Rafel, J. Sole-Pareta, W. Cerroni, N. Leligou, L. Dembeck, B. Mortensen, M. Pickavet, N. Le Sauze, M. Mahony, B. Berde, and G. Eilenberger. The european IST project DAVID: a viable approach toward optical packet switching. *IEEE Journal on Selected Areas in Communications*, 21(7):1026–1040, Sep. 2003.

[82] G. K. Chang, J. Yu, Y. K. Yeo, A. Chowdhury, and Z. Jia. Enabling technologies for next-generation optical packet-switching networks. In *IEEE*, volume 94, pages 892–910, May 2006.

[83] J. P. Sokoloff, P. R. Prucnal, I. Glesk, and M. Kane. A terahertz optical asymmetric demultiplexer (TOAD). *IEEE Photonic Technology Letters*, 5(7):787–790, Jul. 1993.

[84] H. J. S. Dorren, M. T. Hill, Y. Liu, N. Calabretta, A. Srivatsa, F. M. Huijskens, H. de Waardt, and G. D. Khoe. Optical packet switching and buffering by using all-optical signal processing methods. *Journal of Lightwave Technology*, 21(1):2–12, Jan. 2003.

[85] M. Eiselt, W. Pieper, and H. G. Weber. SLALOM: Semiconductor laser amplifier in a loop mirror. *IEEE Journal of Lightwave Technology*, 13(10):2099–2112, Oct. 1995.

[86] X. Shen and R. Kachru. Optical header recognition by spectroholographic filtering. *Optics Letters*, 20(24):2508–2510, Dec. 1995.

[87] J. Widjaja, N. Wada, Y. Ishii, and W. Chujo. Photonic packet address processor using holographic correlator. *Electronics Letters*, 37(11):703–704, May 2001.

[88] J. Shin, M. Jeon, and C. Kang. Fiber-optic matched filters with metal films deposited on fiber delay-line ends for optical packet address detection. *IEEE Photonics Technology Letters*, 8(7):941–943, Jul. 1996.

[89] J. E. McGeehan, M. C. Hauer, A. B. Sahin, and A. E. Willner. Multiwavelength -channel header recognition for reconfigurable WDM networks using optical correlators based on sampled fiber bragg gratings. *IEEE Photonics Technology Letters*, 15(10):1464–1466, Oct. 2003.

[90] M. C. Hauer, J. E. McGeehan, S. Kumar, J. D. Touch, J. Bannister, E. R. Lyons, C. H. Lin, A. A. Au, H. P. Lee, D. S. Starodubov, and A. E. Willner. Optically assisted internet routing using arrays of novel dynamically reconfigurable FBG-based correlators. *IEEE Journal of Lightwave Technology*, 21(11):2765–2778, Nov. 2003.

[91] X. Shilin, Z. Qingji, W. Jianxin, X. Jie, and W. Yun. Realization of multi-wavelength label optical packet switching. *IEEE Photonics Technology Letters*, 15(4):605–607, Apr. 2003.

[92] L. Y. Chan, P. K. A. Wai, L. F. K. Lui, L. Xu, H. Y. Tam, and M. S. Demokan. All-optical header processing using an injection-locked fabry-prot laser diode. *Microwave and Optical Technology Letters*, 44(4):342345, Apr. 2005.

[93] B. Hoanca, S. Dubovitsky, D. X. Zhu, A. A. Sawchuk, W. H. Steier, and P. D. Dapkus. All-optical routing using wavelength recognizing switches. *IEEE Journal of Lightwave Technology*, 16(12):2243–2254, Dec. 1998.

[94] H. L. Minh, Z. Ghassemlooy, and W. P. Ng. Ultrafast header processing in all-optical packet switched-network. In *7th Intern. Conf. on Transparent Optical Networks ICTON*, pages 50–53, Barcelona, Spain, Jul. 2005.

[95] J. M. Martinez, F. Ramos, and J. Marti. All-optical packet header processor based on cascaded SOA-MZIs. *Electronics Letters*, 40(8):894, Jul. 2004.

[96] S. A. Hamilton and B. S. Robinson. 40-Gb/s all-optical packet synchronization and address comparison for OTDM networks. *IEEE Photonics Technology Letters*, 14(2):209–211, Feb. 2002.

[97] H. Uenohara, T. Seki, and K. Kobayashi. Novel header processing technique and wavelength routing performance of an optical packet switch with a multi-bit optical digital-to-analog conversion-type header processor. In *OFC*, volume 2, pages 340–342, Feb. 2004.

[98] O. Boyraz, Han Yan, and B. Jalali. Optical header extraction and recognition by discrete time stretch technique. In *IEEE International Topical Meeting on Microwave Photonics(MNP04)*, pages 63–65, Oct. 2004.

[99] C. Kit, F. Tong, C. K. Chan, L. K. Chen, and H. Wai. An all-optical packet header recognition scheme for self-routing packet networks. In *Optical Fiber Communication Conference (OFC)*, pages 284–285, Mar. 2002.

[100] M. C. Cardakli, S. Lee, A. E. Willner, V. Grubsky, D. Starodubov, and J. Feinberg. Reconfigurable optical packet header recognition and routing using time-to-wavelength mapping and tunable fiber bragg gratings for correlation decoding. *IEEE Photonic Technology Letters*, 12(5):552–554, May 2000.

[101] H. Harai and M. Murata. Optical fiber-delay-line buffer management in output-buffered photonic packet switch to support service differentiation. *IEEE Journal on Selected Areas in Communications*, 24(8):108–116, Aug. 2006.

[102] Y. Shimazu and M. Tsukada. Ultrafast photonic ATM switch with optical output buffers. *IEEE Journal of Lightwave Technology*, 10(2):265–272, Feb. 1992.

[103] I. Glesk, J. P. Solokoff, and P. R. Prucnal. All-optical address recognition and self routing in a 250 Gbit/s packet-switched network. *Electronic Letters*, 30(16):1322–1323, Aug. 1994.

[104] K.-L. Deng, I. Glesk, K. I. Kang, and P. R. Prucnal. Unbalanced TOAD for optical data and clock separation in self-clocked transparent OTDM networks. *IEEE Photonics Technology Letters*, 9(6):830832, Jun. 1997.

[105] H. Soto, D. Erasme, and G. Guekos. Cross-polarization modulation in semiconductor optical amplifiers. *IEEE Photonics Technology Letters*, 11(8):970–972, Aug. 1999.

[106] C.-K. Chan, K. L. Sherman, and M. Zirngib. A fast 100-channel wavelength-tunable transmitter for optical packet switching. *IEEE Photonic Technology Letters*, 13(7):729–731, Jul. 2001.

[107] F. Ramos, E. Kehayas, J. M. Martinez, R. Clavero, J. Marti, L. Stampoulidis, D. Tsiokos, H. Avramopoulos, J. Zhang, P. V. Holm-Nielsen, N. Chi, P. Jeppesen, N. Yan, I. T. Monroy, A. M. J. Koonen, M. T. Hill, Y. Liu, H. J. S. Dorren, R. Van Caenegem, D. Colle, M. Pickavet, and B. Riposati. Ist-lasagne: towards all-optical label swapping employing optical logic gates and optical flip-flops. *IEEE Journal of Lightwave Technology*, 23(10):2993–3011, Oct. 2005.

[108] M. T. Hill, H. J. S. Dorren, X. J. M. Leijtens, J. H. den Besten, T. de Vries, J. H. C. van Zantvoort, E. Smalbrugge, Y. S. Oei, J. J. M. Binsma, G. D. Khoe, and M. K. Smit. Coupled mach-zehnder interferometer memory element. *Optics Letters*, 30(13):1710–1712, Jul. 2005.

[109] G. A. Rauschenbach, K. L. Hall, J. C. Livas, and G. Raybon. All-optical pulse width and wavelength conversion at 10 Gb/s using a nonlinear optical loop mirror. *IEEE Photonic Technology Letters*, 6(9):1130–1132, Sep. 1994.

[110] T. G. Silveira, A. Teixeira, G. T. Beleffi, D. Forin, P. Monteiro, H. Furukawa, and N. Wada. All-optical conversion from RZ to NRZ using gain-clamped SOA. *IEEE Photonic Technology Letters*, 19(6):357–359, Mar. 2007.

[111] T. Hatta, T. Miyahara, Y. Miyazaki, K. Takagi, K. Matsumoto, T. Aoyagi, K. Motoshima, K. Mishina, A. Maruta, and K. Kitayama. Polarization insensitive monolithic 40 Gbit/s SOA-MZI wavelength converter with narrow active waveguides. *IEEE Journal of Selected Topics in Quantum Electronics*, 13(1):32–39, Jan.-Feb. 2007.

[112] F. Chang. *Introduction to optical networks*. Technical report, Nortel Institute, University of Waterloo, OPTera, Nov. 1999.

[113] J. P. Jue and V. M. Vokkarane. *Optical burst switched networks*. Springer, 2005.

[114] C. Qiao. Labeled optical burst switching for IP-over-WDM integration. *IEEE Communications Magazine*, 38(9):104–114, Sep. 2000.

[115] M. Ilyas and H. T. Mouftah. *The handbook of optical communication networks*. CRC press, 2003.

[116] C. Schubert, R. Ludwig, and H. G. Weber. High-speed optical signal processing using semiconductor optical amplifiers. *Journal of Optical and Fiber Communications Reports*, 2(2):171–208, Jun. 2005.

[117] H. Buchta. Analysis of physical constraints in an optical burst switching network. *PhD thesis,Technical University of Berlin*, http://edocs.tu-berlin.de/diss/2005/buchta_hao.pdf, 2005.

[118] D. Benhaddou and G. Chaudhry. Photonic switching techniques and architecture for next generation optical networks. *Cluster Computing*, 7(3):281–291, Jul. 2004.

[119] H. P. Nolting. All-optical 3R-regeneration for photonic networks. In *ONDM*, Budapest, Hungary, Feb. 2003.

[120] N. Calabretta, Y. Liu, H. de Waardt, G.D. Khoe, and H.J.S. Dorren. All-optical header processor for packet switched networks. *IEE Proceedings in Optoelectronics*, 150(3):219–223, Jun. 2003.

[121] Z. Zhu, Z. Pan, and S. J. B. Yoo. A compact all-optical subcarrier label-swapping system using an integrated EML for 10-Gb/s optical label-switching networks. *IEEE Photonics Technology Letters*, 17(2):426–428, Feb. 2005.

[122] L. Stampoulidis, E. Kehayas, D. Apostolopoulos, P. Bakopoulos, K. Vyrsokinos, and H. Avramopoulos. On-the-fly all-optical contention resolution for NRZ and RZ data formats using packet envelope detection and integrated optical switches. *IEEE Photonics Technology Letters*, 19(8):538–540, Apr. 2007.

[123] E. Kehayas, K. Vyrsokinos, L. Stampoulidis, K. Christodoulopoulos, K. Vlachos, and H. Avramopoulos. Artemis: 40-Gb/s all-optical self-routing node and network architecture employing asynchronous bit and packet-level optical signal processing. *IEEE Journal of Lightwave Technology*, 24(8):2996–2977, Aug. 2006.

[124] K. G. Coffman and A. M. Odlyzko. *"Internet growth: Is there a "Moore's Law "for data traffic? "*. Handbook of Massive Data Sets, J. Abello, P. M. Pardalos, and M. G. C. Resende, eds. Kluwer, 2002.

[125] G. Kramer and G. Pesavento. Ethernet passive optical networks (EPON): building a next-generation optical access network. *IEEE Communications Magazine*, 40(2):66–73, Feb. 2002.

[126] M. A. Bourouha, M. Bataineh, and M. Guizani. Advances in optical switching and networking: past, present, and future. In *Proceedings IEEE South east Con*, pages 405 – 413, London, UK, 5-7 Apr. 2002.

[127] S. K. Liaw, K. P. Ho, Y. K. Chen, and C. C. Lee. Reconfigurable WDM add/drop multiplexer based on optical switches and fibre bragg gratings. *Journal of Optical and Quantum Electronics, Springer Netherlands*, 31(1):77–83, Jan. 1999.

[128] J. J. O. Pires, O. O'Mahony, N. Parnis, and E. Jones. Scaling limitations in full-mesh WDM ring networks using arrayed-waveguide grating OADMs. *Electronics Letters*, 35(1):73–75, Jan. 1999.

[129] S. Sumriddetchkajorn and K. Chaitavon. A thin-film filter-based 1×2 reconfigurable fiber-optic add-drop module with a quadruple fiber-optic collimator. *IEEE Photonics Technology Letters*, 18(5):676–678, Mar. 2006.

[130] K. Okamoto, K. Takiguchi, and Y. Ohmori. 16-channel optical add/drop multiplexer using silica-based arrayed-waveguide gratings. *Electronics Letters*, 31(9):723–724, Apr. 1995.

[131] J. Ertel, R. Helbing, C. Hoke, O. Landolt, K. Nishimura, P. Robrish, and R. Trutna. Design and performance of a reconfigurable liquid-crystal-based optical add/drop multiplexer. *IEEE Journal of Lightwave Technology*, 24(4):1674–1680, Apr. 2006.

[132] T. Pingsheng, O. Eknoyan, and H. F. Taylor. Rapidly tunable polarisation independent optical add drop multiplexer in ti:linbo3. *Electronics Letters*, 38(5):242–244, Feb. 2002.

[133] M. Raburn, L. Bin, Y. Okuno, and J. E. Bowers. InP-InGaAsP wafer-bonded vertically coupled X-crossing multiple channel optical add-drop multiplexer. *IEEE Photonics Technology Letters*, 13(6):579–581, Jun. 2001.

[134] D. Gauden, E. Goyat, C. Vaudry, P. Yvernault, and D. Pureur. Tunable mach-zehnder-based add-drop multiplexer. *Electronics Letters*, 40(21):1374–1375, Oct. 2004.

[135] P. K. A. Wai, L. Y. Chan, L. F. K. Lui, and H. Y. Tam. Intelligent all-optical add-drop node for packet switched networks using two-stage injection-locked laser diodes. In *30th European Conference on Optical Communication*, volume 2, pages 154–155, Stockholm, Sweden, 5-9 Sept. 2004.

[136] F. Arecco, D. Scarano, S. Schmid, D. J. Blumenthal, and R. Gaudino. Acousto optic devices in add/drop multiplexer nodes. In *24th European Conference on Optical Communication*, volume 1, pages 117–118, Madrid, Spain, 20-24 Sep. 1998.

[137] L. Y. Lin and E. L. Goldstein. Opportunities and challenges for MEMS in lightwave communications. *IEEE Journal of Selected Topics in Quantum Electronics*, 8(1):163–172, Jan.-Feb. 2002.

[138] P. H. H. Ernest, G. Mohan, and V. Bharadwaj. An efficient algorithm for virtual topology reconfiguration in WDM optical ring networks. In *Proceedings of the tenth international conference on computer communications and Networks*, pages 55–60, 2001.

[139] B. Mukherjee. WDM optical communication networks: progress and challenges. *IEEE Journal on Selected Areas in Communications*, 18(10):1810–1824, Oct. 2000.

[140] M. Tabiani and M. Kavehrad. Theory of an efficient n×n passive optical star coupler. *IEEE Journal of Lightwave Technology*, 9(4):448–455, Apr. 1991.

[141] C. Feng, D. H. C. Du, and A. Pavan. Topological embedding into WDM optical passive star networks with tunable transmitters of limited tuning range. *IEEE Transactions on Computers*, 47(12):1404–1413, Dec. 1998.

[142] H. S. Yang, M. Herzog, M. Maier, and M. Reisslein. Metro WDM networks: Performance comparison of slotted ring and awg star networks. *IEEE Journal of Selected Areas in Communication*, 22(8):1460–1473, Oct. 2004.

[143] N. Kamiyama. A large-scale awg-based single-hop WDM network using couplers with collision avoidance. *IEEE Journal of Lightwave Technology*, 23(7):2194–2205, Jul. 2005.

[144] Y. W. Leung. Multipassive-star-coupler hub for metro WDM networks. *IEEE Photonics technology letters*, 18(15):1261–1263, Aug. 2006.

[145] J. D. Bainbridge, A. R. Sharafi, I. H. White, M. A. Cowin, M. F. C. Stephens, M. Owen, R. V. Penty, K. M. Guild, A. Tzanakaki, M. J. O'Mahony, G. H. B. Thompson, S. J. Clements, and C. B. Rogers. All-optical routing using a 12×12

passive InP wavelength selective router and tuneable wavelength conversion. In *IEE Colloquium on Multiwavelength Optical Networks: Devices, Systems and Network Implementations*, pages 8/1–8/5, 1998.

[146] R. A. Barry and P. A. Humblet. Latin routers, design and implementation. *IEEE Journal of Lightwave Technology*, 11(5):891–899, May-June 1993.

[147] Z. Zhang and Y. Yang. Low-loss switching fabric design for recirculating buffer in WDM optical packet switching networks using arrayed waveguide grating routers. *IEEE Transactions on Communications*, 54(8):1469–1472, Aug. 2006.

[148] L. Fenghai, C. J. Rasmussen, and R. L. S. Pedersen. Experimental verification of a new model describing the influence of incomplete signal extinction ratio on the sensitivity degradation due to multiple interferometric crosstalk. *IEEE Photonics Technology Letters*, 11(1):137–139, Jan. 1999.

[149] L. Xu, H. G. Perros, and G. Rouskas. Techniques for optical packet switching and optical burst switching. *IEEE Communications Magazine*, 39(1):136–142, Jan. 2001.

[150] G. Retvari and T. Cinkler. Practical OSPF traffic engineering. *IEEE Communications Letters*, 8(11):689–691, Nov. 2004.

[151] H. Zang, J. P. Jue, and B. Mukherjee. A review of routing and wavelength assignment approaches for wavelength-routed optical WDM networks. *Optical Networks Magazine*, 1(1):47–60, Jan. 2000.

[152] H. Zang, J. P. Jue, L. Sahasrabuddhe, R. Ramamurthy, and B. Mukherjee. Dynamic light-path establishment in wavelength-routed WDM networks. *IEEE Communications Magazine*, 39(9):100 – 108, Sep. 2001.

[153] S. Yao, B. Mukherjee, and S. Dixit. Advances in photonic packet switching: an overview. *IEEE Communications Magazine*, 38(2):84–94, Feb. 2000.

[154] M. Tabiani and M. Kavehrad. Recent progress in optical packet processing technologies for optical packet-switched networks. *NTT technical review*, 2(7):12–22, Jul. 2004.

[155] V. M. Vokkarane and J. P. Jue. Prioritized burst segmentation and composite burst-assembly techniques for QoS support in optical burst-switched networks. *IEEE Journal on Selected Areas in Communications*, 21(7):1198–1209, Sep. 2003.

[156] A. Bononi, G. A. Castanon, and O. K. Tonguz. Analysis of hot-potato optical networks with wavelength conversion. *IEEE Journal of Lightwave Technology*, 17(4):525–534, Apr. 1999.

[157] J. Xu, C. Qiao, J. Li, and G. Xu. Efficient channel scheduling algorithms in optical burst switched networks. In *INFOCOM*, volume 2, pages 2268–2278, Stockholm, Sweden, 30 Mar.-3 Apr. 2003.

[158] R. Ramaswami and K.N. Sivarajan. Routing and wavelength assignment in all-optical networks. *IEEE/ACM Transactions on Networking*, 3(5):489–500, Oct. 1995.

[159] V. M. Vokkarane and J. P. Jue. Burst segmentation: An approach for reducing packet loss in optical burst switched networks. *SPIE Optical Networks Magazine*, 4(6):81–89, Nov.-Dec. 2003.

[160] S. Sengupta and R. Ramamurthy. From network design to dynamic provisioning and restoration in optical cross-connect mesh networks: an architectural and algorithmic overview. *IEEE Network*, 15(4):46–54, Jul.-Aug. 2001.

[161] K. Bala, R. R. Cordell, and E. L. Goldstein. The case for opaque multiwavelength optical networks. In *Digest of the LEOS Summer Topical Meetings*, pages 58–59, 1995.

[162] A. Tzanakaki, I. Zacharopoulos, and I. Tomkos. Near and longer term architectural designs for OXCs/OADMs network topologies. In *Photonics in Switching*, pages 271–273, 2003.

[163] G. Ellinas, J. Labourdette, J. Walker, S. Chaudhuri, L. Lin, E. Goldstein, and K. Bala. Network control and management challenges in opaque networks utilizing transparent optical switches. *IEEE Communications Magazine*, 42(2):S16–S24, Feb. 2004.

[164] V. Kaman, X. Zheng, O. Jerphagnon, C. Pusarla, R. J. Helkey, and J. E. Bowers. A cyclic MUX-DMUX photonic cross-connect architecture for transparent waveband optical networks. *IEEE Photonics Technology Letters*, 16(2):638–640, Feb. 2004.

[165] X. Zheng, V. Kaman, S. Yuan, Y. Xu, O. Jerphagnon, A. Keating, R. C. Anderson, H. N. Poulsen, B. Liu, J. R. Sechrist, C. Pusarla, R. Helkey, D. J. Blumenthal, and J. E. Bowers. Three-dimensional MEMS photonic cross-connect switch design and performance. *IEEE Journal of Selected Topics in Quantum Electronics*, 9(2):571–578, Mar.-Apr. 2003.

[166] N. A. Riza and S. Yuan. Low optical interchannel crosstalk, fast switching speed, polarization independent 2×2 fiber optic switch using ferroelectric liquid crystals. *Electronic Letters*, 34(13):1341–1342, Jun. 1998.

[167] S. Venkatesh, R. Haven, D. Chen, H. L. Reynolds, G. Harkins, S. Close, M. Troll, J. E. Fouquet, D. Schroeder, and P. McGuire. Recent advances in bubble-actuated cross-connect switches. In *CLEO/Pacific Rim*, volume 1, pages I–414–I–415, Chiba, Japan, Jul. 2001.

[168] J. L. Ramsey, R. Shankar, and T. J. Hall. Improved methods for generating dynamic computer generated holograms for realising adaptive optical cross connects. In *CLEO/Europe*, page 506, 2005.

[169] G. Shen, W. Grover, T. Cheng, and S. Bose. Sparse placement of electronic switching nodes for low blocking in translucent optical networks. *Journal of Optical Networking*, 1(12):424–441, Nov. 2002.

[170] B. Ramamurthy, D. Datta, H. Feng, J. P. Heritage, and B. Mukherjee. Transparent vs. opaque vs. translucent wavelength-routed optical networks. In *OFC 1999*, volume 1, pages 59–61, Oct. 1999.

[171] H. Zimmermann. OSI reference model-the ISO model of architecture for open systems interconnection. *IEEE Transactions on Communications*, 28(4):425–432, Apr. 1980.

[172] A. Gladisch, R. P. Braun, D. Breuer, A. Ehrhardt, H. M. Foisel, M. Jaeger, R. Leppla, M. Schneiders, S. Vorbeck, W. Weiershausen, and F. J. Westphal. Evolution of terrestrial optical system and core network architecture. *Proceedings of the IEEE*, 94(5):869–891, May 2006.

[173] R. Nagarajan, M. Kato, J. Pleumeekers, P. Evans, D. Lambert, A. Chen, V. Dominic, A. Mathur, P. Chavarkar, M. Missey, A. Dentai, S. Hurtt, J. Back, R. Muthiah, S. Murthy, R. Salvatore, S. Grubb, C. Joyner, J. Rossi, R. Schneider, M. Ziari, F. Kish, , and D. Welch. Single-chip 40-channel InP transmitter photonic integrated circuit capable of aggregate data rate of 1.6 tbit/s. *Electronics Letters*, 42(13):771–773, Jun. 2006.

[174] R. Slavik and S. LaRochelle. Large-band periodic filters for DWDM using multiple-superimposed fiber bragg gratings. *IEEE Photonics Technology Letters*, 14(12):1704–1706, Dec. 2002.

[175] M. J. O'Mahony, D. Simeonidou, D. K. Hunter, and A. Tzanakaki. The application of optical packet switching in future communication networks. *IEEE Communications Magazine*, 39(3):128–135, Mar. 2001.

[176] T. Li. MPLS and the evolving internet architecture. *IEEE Communications Magazine*, 37(12):38–41, Dec. 1999.

[177] G. Armitage. MPLS: the magic behind the myths. *IEEE Communications Magazine*, 38(1):124–131, Jan. 2000.

[178] J. Lawrence. Designing multiprotocol label switching networks. *IEEE Communications Magazine*, 39(7):134–142, Jul. 2001.

[179] A. Viswanathan, N. Feldman, Z. Wang, and R. Callon. Evolution of multiprotocol label switching. *IEEE Communications Magazine*, 36(5):165–173, May 1998.

[180] G. Hagard and M. Wolf. Multiprotocol label switching in ATM networks. *Ericsson Rev.*, 75(1):32–39, Jan. 1998.

[181] D. Awduche. MPLS and traffic engineering in IP networks. *IEEE Communications Magazine*, 37(12):42–47, Dec. 1999.

[182] M. Ali, D. Elie-Dit-Cosaque, and L. Tancevski. Enhancements to multiprotocol lambda switching (MPλS) to accommodate transmission impairments. In *IEEE Global Telecommunications Conference*, volume 1 of *GLOBECOM '01*, pages 70–75, 25-29 Nov. 2001.

[183] D. Awduche and Y. Rekhter. Multiprotocol lambda switching: combining MPLS traffic engineering control with optical crossconnects. *IEEE Communications Magazine*, 39(3):111–116, Mar. 2001.

[184] K. Bergman. Photonic networks for intra-chip, inter-chip, and box-to-box interconnects in high-performance computing. In *ECOC*, page Tu1.2.1, 2006.

[185] M. Smit, S. Oei, F. Karouta, R. Ntzel, J. Wolter, E. Bente, X. Leijtens, J. van der Tol, M. Hill, H. Dorren, D. Khoe, and H. Binsma. Photonic integrated circuits: where are the limits? In *IPRA/NPIS*, page IWB1, San Diego, USA, Apr. 2005.

[186] T. Fjelde, D. Wolfson, A. Kloch, M. L. Nielsen, and H. Wessing. SOA-based functional devices. In *SPIE*, volume 4532, pages 114–126, Jul. 2001.

[187] K. Inoue. Waveform distortion in a gain-saturated semiconductor optical amplifier for NRZ and manchester formats. *IEE Proceedings Optoelectronics*, 144(6):433–437, Dec. 1997.

[188] M. J. Connelly. *Semiconductor Optical Amplifiers*. Kluwer Academic Publishers, Boston, 2002.

[189] T. Saitoh, T. Mikai, and O. Mikami. Theoretical analysis and fabrication of antireflection coatings on laser diode facets. *IEEE Journal of Lightwave Technology*, 3(2):288–293, Feb. 1985.

[190] C. E. Zah, R. Bhat, S. G. Menocal, N. Andreadakis, F. Favire, C. Caneau, M.A. Koza, and T. P. Lee. 1.5μm GaInAsP angled-facet flared-waveguide travelling-wave laser amplifiers. *IEEE Photonics Technology Letters*, 2(1):990–992, Nov. 1990.

[191] M. S. Lin, A. B. Piccirilli, Y. TWU, and N. K. Dutta. Fabrication and gain measurements for burried facet optical amplifier. *Electronics Letters*, 5(20):1378–1379, Sep. 1989.

[192] A. E. Kelly, I. F. Lealman, L. J. Rivers, S. D. Perrin, and M. Silver. Polarisation insensitive, 25 dB gain semiconductor laser amplifier without antireflection coatings. *Electronics Letters*, 32(19):1835–1836, Sep. 1996.

[193] T. Ito, N. Yoshimoto, K. Magari, and H. Sugiura. Wide-band polarization-independent tensile-strained InGaAs MQW-SOA gate. *IEEE Photonics Technology Letters*, 10(5):657–659, May 1998.

[194] O. Qasaimeh. Optical gain and saturation characteristics of quantum-dot semiconductor optical amplifiers. *IEEE Journal of Quantum Electronics*, 39(6):793–798, Jun. 2003.

[195] P. Brosson. Semiconductor lasers and integrated devices. Website, 2007. http://www.bibsciences.org/bibsup/opt-coll/pub/2000/pdf/brosson.pdf.

[196] L. Labdonde, I. Valiente, P. Lamouler, E. Delevaque, S. Boj, and J. C. Simon. Experimental and theoretical investigation of a gain clamped semiconductor optical amplifier. In *ECOC*, pages 2.715–2.718, 1994.

[197] N. Buldawoo, S. Mottet, F. Le Gall, D. Sigogne, D. Meichenin, and S. Chelles. A semiconductor laser amplifier-reflector for the future FTTH applications. In *ECOC*, volume 2, pages 196–199, Edinburgh, Scotland, Sep. 1997.

[198] J. Prat, C. Arellano, V. Polo, and C. Bock. Optical network unit based on a bidirectional reflective semiconductor optical amplifier for fiber-to-the-home networks. *IEEE Photonics Technology Letters*, 17(1):250–252, Jan. 2005.

[199] R. J. Manning and D. A. O. Davies. Three-wavelength device for all-optical signal processing. *Optics letters*, 19(12):889–891, Jun. 1994.

[200] M. Sugawara, N. Hatori, T. Akiyama, Y. Nakata, and H. Ishikawa. Quantum-dot semiconductor optical amplifiers for high bit-rate signal processing over 40 Gbit/s. In *CLEO/Pacific Rim*, volume 1, pages I–260 – I–261, Jul. 2001.

[201] T. W. Berg and J. Mork. Ultrafast optical signal processing using semiconductor quantum dot amplifiers. In *The 15th Annual Meeting of the IEEE Lasers and Electro-Optics Society*, volume 1, pages 321–322, 10-14 Nov. 2002.

[202] J.-Y. Emery, T. Ducellier, N. Bachmann, P. Doussihe, F. Pommereau, R. Ngo, F. Gaborit, L. Goldstein, G. Laube, and J. Barrau. High performance 1550 nm polarisation-insensitive semiconductor optical amplifier based on low-tensile-strainedbulk galnaspd. *Electronics Letters*, 33(12):1083–1084, Jun. 1997.

[203] A. Borghesani, N. Fensom, A. Scott, G. Crow, L. Johnston, J. King, L. Rivers, S. Cole, S. Perrin, D. Scrase, G. Bonfrate, A. Ellis, I. Lealman, G. Crouzel, L. H. K. Chun, A. Lupu, E. Mahe, and P. Maigne. High saturation power (>16.5 dBm) and low noise figure (<6 dB) semiconductor optical amplifier for C-band operation. In *IEEE Optical Fiber Communications Conference*, volume 2, pages 534–536, 23-28 Mar. 2003.

[204] A. Ougazzaden, D. Sigogne, A. Mircea, E. V. K. Rao, A. Ramdane, and L. Silvestre. Atmospheric pressure MOVPE growth of high performance polarisation insensitive strain compensated MQW InGaAsP/InGaAs optical amplifier. *Electronics Letters*, 31(15):1242–1244, Jul. 1995.

[205] A. E. Kelly, I. F. Lealman, L. J. Rivers, S. D. Perrin, and M. Silver. Low noise figure (7.2 dB) and high gain (29 dB) semiconductor optical amplifier with a single layer ar coating. *Electronics Letters*, 33(6):536–538, Mar. 1997.

[206] Fujitsu Laboratories Ltd. Fujitsu develops world's first semiconductor optical amplifier with signal waveform re-shaping function at 40 Gbps. *http://www.fujitsu.com/global/news/pr/archives/month/2005/20050304-01.html*, 2007.

[207] T. Akiyama, M. Ekawa, M. Sugawara, H. Sudo, K. Kawaguchi, A. Kuramata, H. Ebe, and K. Morito. An ultrawide-band (120 nm) semiconductor optical amplifier having an extremely-high penalty-free output power of 23 dBm realized with quantum-dot active layers. In *Optical Fiber Communication Conference*, volume 2, page PDP. 12., 23-27 Feb. 2004.

[208] P. Doussiere, F. Pommereau, J. Y. Emery, R. Ngo, J. L. Lafragette, P. Aubert, L. Goldstein, G. Soulage, T. Ducellier, M. Bachmann, and G. Laube. 1550 nm polarization independent DBR gain clamped SOA with high dynamic input power range. In *ECOC*, volume 3, pages 169–172, Oslo, Norway, Sep. 1996.

[209] D. A. Francis, S. P. DiJaili, and J. D. Walker. A single-chip linear optical amplifier. In *OFC*, volume 4, pages PD13–1 – PD13–3, Anaheim, USA, 2001.

[210] Kamelian products & services. *http://www.kamelian.com/*, 2007.

[211] G. P. Agrawal. *Nonlinear Fiber Optics, 3rd ed*. Academic Press, 2001.

[212] G. P. Agrawal and N. K. Dutta. *Long-Wavelength Semiconductor Laser*. van Nostrand Reinhold Company Inc., 1986.

[213] R. Manning, A. Ellis, A. Poustie, and K. Blow. Semiconductor laser amplifier for ultrafast all-optical signal processing. *Journal of optical Society America B*, 14(11):3204–3216, Nov. 1997.

[214] M. Willatzen, A. Uskov, J. Mrk, H. Olesen, B. Tromborg, and A. P. Jauho. Nonlinear gain suppression in semiconductor lasers due to carrier heating. *IEEE Photonics Technology Letters*, 3(7):606–609, Jul. 1991.

[215] J. Zhou, N. Park, J. W. Dawson, K. J. Vahala, M. A. Newkirk, and B. I. Miller. Terahertz four-wave mixing spectroscopy for study of ultrafast dynamics in a semiconductor optical amplifier. *Applied Physics Letters*, 63(9):1179–1181, Aug. 1993.

[216] R. Ludwig, S. Diez, and H. G. Weber. A novel all-optical switch for demultiplexing in OTDM-systems demonstrated in a 640 Gbit/s WDM/TDM experiment. In *OFC*, page PDP 22, 1998.

[217] S. Diez. *All-Optical Signal Processing by Gain-Transparent Semiconductor Switches*. PhD thesis, Fachbereich 4 (Physik) der TU Berlin, 2000.

[218] G. P. Agrawal and N. A. Olsson. Self-phase modulation and spectral broadening of optical pulses in semiconductor laser amplifiers. *IEEE Journal of Quantum Electronics*, 25(11):2297–2306, Nov. 1989.

[219] M. L. Nielsen, B. E. Olsson, and D. J. Blumenthal. Pulse extinction ratio improvement using SPM in an SOA for OTDM systems applications. *IEEE Photonic Technology Letters*, 14(2):245–247, Feb. 2002.

[220] C. Yan, Y. Su, L. Yi, L. Leng, X. Tian, X. Xu, and Y. Tian. All-optical format conversion from NRZ to BPSK using a single saturated SOA. *IEEE Photonics Technology Letters*, 18(22):2368–2370, Nov. 2006.

[221] H. J. Lee, H. G. Kim, J. Y. Choi, and H. K. Lee. All-optical clock recovery from NRZ data with simple NRZ-to-PRZ converter based on self-phase modulation of semiconductor optical amplifier. *Electronics Letters*, 35(12):989–990, Jun. 1999.

[222] T. Watanabe, H. Yasaka, N. Sakaida, and M. Koga. Waveform shaping of chirp-controlled signal by semiconductor optical amplifier using Mach-Zehnder frequency discriminator. *IEEE Photonics Technology Letters*, 10(10):1422–1424, Oct. 1998.

[223] N. Calabretta, Y. Liu, H. de Waardt, G. D. Khoe, and H. J. S. Dorren. All-optical header-payload separator. In *ECOC*, volume 1, pages 1–2, Copenhague, Danemark, Sep. 2002.

[224] J. H. Kim, K. R. Oh, H. S. Kim, and K. Cho. All-optical switching by counterpropagating operation in cascaded semiconductor optical amplifiers. *IEEE Photonics Technology Letters*, 12(5):513–515, May 2000.

[225] K. Inoue. Technique to compensate waveform distortion in a gain-saturated semiconductor optical amplifer using a semiconductor saturable absorber. *Electronics Letters*, 34(4):376–378, Feb. 1998.

[226] Y. Ueno, S. Nakamura, and K. Tajima. Nonlinear phase shifts induced by semiconductor optical amplifiers with control pulses at repetition frequencies in the 40-160 GHz range for use in ultrahigh-speed all-optical signal processing. *Journal of Optical Society America B*, 19(11):2573–2589, Nov. 2002.

[227] M. L. Masanovic, V. Lal, E. J. Skogen, J. S. Barton, J. A. Summers, J. A. Raring, L. A. Coldren, and D. J. Blumenthal. Cross-phase modulation efficiency in

offset quantum-well and centered quantum-well semiconductor optical amplifiers. *IEEE Photonic Technology Letters*, 17(11):2364–2366, Nov. 2005.

[228] A. Teixeira, T. Silveira, P. Andr, R Nogueira, G. Tosi-Bellefi, P. Monteiro, and J. Da Rocha. All-optical switching with SOA based devices. In *CAOL*, pages 52–55, 2005.

[229] K. Suzuki, K. Iwatsuki, S. Nishi, and M. Suruwatari. Error-free demultiplexing of 160 Gbit/s pulse signal using loop mirror including semiconductor laser amplifier. *Electronics Letters*, 30(18):1501–1503, Sep. 1994.

[230] R. Schreieck. Ultrafast dynamics in ingaasp/inp optical amplifiers and mode locked laser diodes. *PhD thesis, Swiss Federal Institute of Technology,Zurich, Diss. ETH No. 14337*, 3(2):288–293, Feb. 2001.

[231] C. Schubert, S. Diez, J. Berger, R. Ludwig, U. Feiste, H. G. Weber, G. Toptchiyski, K. Petermann, and V. Krajinovic. 160-Gb/s all-optical demultiplexing using a gain-transparent ultrafast-nonlinear interferometer (GT-UNI). *IEEE Photonics Technology Letters*, 13(5):475–477, May 2001.

[232] S. Fischer, M. Dlk, E. Gamper, W. Vogt, W. Hunziker, E. Gini, H. Melchior, A. Buxens, H. N. Poulsen, and A. T. Clausen. All-optical regenerative OTDM add/drop multiplexer at 40 Gbit/s using monolithic InP Mach-Zehnder interferometer. *IEEE Photonics Technology Letters*, 12(3):335–337, Mar. 2000.

[233] C. Schubert, C. Schmidt, C. Brner, E. Dietrich, S. Ferber, R. Ludwig, and H. G. Weber. A gain-transparent ultrafast-nonlinear interferometer (GTUNI) in a 160 Gb/s optical sampling system. In *Optical Amplifiers and Applications (OAA)*, page OTuD5, 2002.

[234] J. Leuthold, C. H. Joyner, B. Mikkelsen, G. Raybon, J. L. Pleumeekers, B. I. Miller, K. Dreyer, and C. A. Burrus. 100 Gbit/s all-optical wavelength conversion with integrated SOA delayed-interference convguration. *Electronics Letters*, 36(13):1129–1130, Jun. 2000.

[235] T. Yamamoto, U. Feiste, J. Berger, C. Schubert, C. Schmidt, R. Ludwig, and H. G. Weber. 160 Gbit/s demultiplexer with clock recovery using SOA-based interferometric switches and its application to 120 km fiber transmission. In *ECOC*, volume 2, pages 192–193, Amsterdam- Netherlands, Oct. 2001.

[236] Y. Ueno, S. Nakamura, and K. Tajima. Penalty-free error-free all-optical data pulse regeneration at 84 Gb/s by using a symmetric-Mach-Zehnder-type semiconductor regenerator. *IEEE Photonics Technology Letters*, 13(5):469–471, May 2001.

[237] D. Pastor, A. Martinez, J. Capmany, S. Sales, B. Ortega, and P. Munoz. Experimental characterization of XGM-SOA-based wavelength converted SCM systems. *IEEE Photonics Technology Letters*, 15(1):114–116, Jan. 2003.

[238] D. Norte and A. E. Willner. All-optical data format conversions and reconversions between the wavelength and time domains for dynamically reconfigurablewdm networks. *Journal of Lightwave Technology*, 14(6):1170–1182, Jun. 1996.

[239] D. J. Blumenthal, A. Carena, L. Rau, V. Curri, and S. Humphries. All-optical label swapping with wavelength conversion for WDM-IP networks with subcarrier multiplexed addressing. *IEEE Photonics Technology Letters*, 11(11):1497–1499, Nov. 1999.

[240] D. Norte and A. E. Willner. Multistage all-optical WDM-to-TDM-to-WDM and TDM-to-WDM-to-TDM data-format conversion and reconversion through 80 km of fiber and three EDFAs. *IEEE Photonic Technology Letters*, 7(11):1354–1356, Nov. 1995.

[241] T. Silveira, A. Teixeira, and P. Monteiro. Cross-gain modulation bandwidth enhancement in semiconductor optical amplifiers by means of detuned optical filter. *Electronics Letters*, 41(13):53–54, Jun. 2005.

[242] N. Calabretta, Y. Liu, F. M. Huijskens, M. T. Hill, H. de Waardt, G.D. Khoe, and H. J. S. Dorren. Optical signal processing based on self-induced polarization rotation in a semiconductor optical amplifier. *Journal of Lightwave Technology*, 22(2):372–381, Feb. 2004.

[243] J. J. V. Olmos, I. T. Monroy, J. P. Turkiewicz, N. Calabretta, H. J. S. Dorren, and A. M. J. Koonen. Asynchronous all-optical label extraction in a time-serial IM/DPSK scheme supporting variable packet-length operation. *Microwave and optical technology letters*, 46(5):453–454, Sep. 2005.

[244] I. White, R. Penty, M. Webster, Y. J. Chai, A. Wonfor, and S. Shahkooh. Wavelength switching components for future photonic networks. *IEEE Communications Magazine*, 40(9):74–82, Sep 2002.

[245] P.-M. Gong, J.-T. Hsieh, S.-L. Lee, and J. Wu. Theoretical analysis of wavelength conversion based on four-wave mixing in light-holding SOAs. *IEEE Journal of Quantum Electronics*, 40(1):31–40, Jan. 2004.

[246] N. K. Das, Y. Yamayoshi, and H. Kawaguchi. Analysis of basic four-wave mixing characteristics in a semiconductor optical amplifier by the finite-difference beam propagation method. *IEEE Journal of Quantum electronics*, 36(10):1184–1192, Oct. 2000.

[247] G. P. Agrawal. Population pulsations and nondegenerate four-wave mixing in semiconductor lasers and amplifiers. *Journal of Optical Society Am. B*, 5(1):147–159, Jan. 1988.

[248] A. Uskov, J. Mrk, J. Mark, M. C. Tatham, and G. Sherlock. Terahertz four-wave mixing in semiconductor optical amplifiers: Experiment and theory. *Applied Physics Letters*, 65(8):944–946, Aug. 1994.

[249] A. Uskov, J. Mork, and J. Mark. Wave mixing in semiconductor laser amplifiers due to carrier heating and spectral-hole burning. *IEEE Journal of Quantum Electronics*, 30(8):1769–1781, Aug. 1994.

[250] A. E. Kelly, A. D. Ellis, D. Nesset, R. Kashyap, and D. G. Moodie. 100 Gbit/s wavelength conversion using FWM in an MQW semiconductor optical amplifier. *Electronics Letters*, 34(20):1955–1956, Oct. 1998.

[251] C. Ware and D. Erasme. 30 GHz sub-clock recovery using an opto-electronic phase-locked loop based on four-wave mixing in a semiconductor optical amplifier. In *CLEO/Europe*, page 487, 2005.

[252] O. Kamatani and S. Kawanishi. Prescaled timing extraction from 400 Gb/s optical signal using a phase lock loop based on four-wave mixing in a laser diode amplifier. *IEEE Photonics Technology Letters*, 8(8):1094–1096, Aug. 1996.

[253] J. P. R. Lacey, M. A. Summerfield, and S. J. Madden. Tunablility of polarization-insensitive wavelength converters based on four wave mixing in semiconductor optical amplifiers. *Journal of lightwave technology*, 16(12):2419–2427, Dec. 1998.

[254] J. S. Lee, Y. C. Chung, and D. J. DiGiovanni. Spectrum-sliced fiber amplifier light source for multichannel WDM applications. *IEEE Photonics Technology Letters*, 5(12):1458–1461, Dec. 1993.

[255] Y. S. Jang and Y. C. Chung. Four-wave mixing of incoherent light in a dispersion-shifted fiber using a spectrum-sliced fiber amplifier light source. *IEEE Photonics Technology Letters*, 10(2):218–220, Feb. 1998.

[256] D. Forsyth and M. Connelly. Spectrum-sliced wavelength conversion using four-wave mixing from a semiconductor optical amplifier. In *in Optical Amplifiers and Their Applications Topical Meeting*, page TuC3, 2005.

[257] J. Zhou, N. Park, K. J. Vahala, M. A. Newkirk, and B. I. Miller. Four-wave mixing wavelength conversion efficiency in semiconductor travelling-wave amplifiers measured to 65 nm of wavelength shift. *Applied Physics Letters*, 6(8):984–987, Aug. 1994.

[258] J. W. Goodman. *Statistical Optics*. New York: Wiley, 2000.

[259] K. E. Stubkjaer. Semiconductor optical amplifier-based all-optical gates for high-speed optical processing. *IEEE Journal of Selected Topics in Quantum Electronics*, 6(6):1428–1438, Jun. 2000.

[260] G. R. Collecutt and P. D. Drummond. Digital response in an all optical AND gate using parametric (χ^2) solitons. In *CLEO*, page 194, San Fransisco, USA, May 2000.

[261] X. Chen, M. Yao, J. Zhang, L. Xu, M. Chen, and Y. Gao. Performances of switching window of ultrafast nonlinear interferometer (UNI) demultiplexer. *International Journal of Infrared and Millimeter Waves*, 21(9):1503–1516, Sep. 2000.

[262] C. Xingzhong, Y. Minyu, C. Minghua, Z. Jianfeng, X. Lei, G. Yizhi, and C. H. Chen. Demonstration of optical switch operation of an ultrafast nonlinear interferometer (UNI) with counter-propagating control pulse. In *Fourth Optoelectronics and Communications Conference Communications*, volume 1, pages 475–476, Oct. 1999.

[263] H. Teimoori, J. D. Topomondzo, C. Ware, H. Soto, and D. Erasme. All-optical half-adder using a single UNI gate. *Journal of Optical communications*, 27(6):301–304, Dec. 2006.

[264] S. Kumar, D. Gurkan, and A. E. Willner. All-optical half adder using a PPLN waveguide and an SOA. In *OFC*, volume 1, Feb. 2004.

[265] E. Kehayas, D. Tsiokos, K. Vrysokinos, L. Stampoulidis, G. T. Kanellos, C. Bintjas, G. Guekos, and H. Avramopoulos. All-optical half adder using two cascaded UNI gates. In *IEEE Lasers and Electro-Optics Society*, volume 1, pages 228–229, Oct. 2003.

[266] D. Tsiokos, E. Kehayas, K. Vyrsokinos, T. Houbavlis, L. Stampoulidis, G. T. Kanellos, N. Pleros, G. Guekos, and H. Avramopoulos. 10-Gb/s all-optical half-adder with interferometric SOA gates. *IEEE Photonics Technology Letters*, 16(1):284–286, Jan. 2004.

[267] S. Kim, S. Lee, B. Kang, S. Lee, and J. Park. All-optical binary half adder using slaloms. In *CLEO/Pacific Rim*, volume 2, pages II–254 – II–255, Jul. 2001.

[268] T. Byun, Y. M. Jhon, S. Lee, D. H. Woo, and Sun Ho Kim. All-optical half adder using cross gain modulation in semiconductor optical amplifiers. *Optics Express*, 14(22):10693–10698, Oct. 2006.

[269] J. Dong, S. Fu, X. Zhang, P. Shum, L. Zhang, J. Xu, and D. Huang. Single SOA based all-optical adder assisted by optical bandpass filter: Theoretical analysis and performance optimization. *Optics Communications*, 270(2):238–246, Feb. 2007.

[270] T. Izuhara, R. Roth, R. M. Osgood, S. Bakhru, and H. Bakhru. Low-voltage tunable TE/TM converter on ion-sliced lithium niobate thin film. *Electronics Letters*, 39(15):1118–1119, Jul. 2003.

[271] A. Hirano, T. Kataoka, S. Kuwahara, M. Asobe, and Y. Yamabayashi. All-optical limiter circuit based on four-wave mixing in optical fibres. *Electronics Letters*, 34(14):1410–1411, Jul. 1998.

[272] A. Rostami and G. Rostami. Integrated optical limiter using kerr-like nonlinear bragg grating. In *Asia-Pacific Conference*, volume 1, pages 38–41, 2003.

[273] C. Guillemot, M. Henry, F. Clerot, A. Le Corre, J. Kervaree, A. Dupas, and P. Gravey. Keops optical packet switch demonstrator: architecture and testbed performance. In *Optical Fiber Communication Conference*, volume 3, pages 204–206, 2000.

[274] A. Okada. All-optical packet routing in AWG-based wavelength routing networks using an out-of-band optical label. In *OFC*, volume 1, pages 213–215, Washington and DC, 2002.

[275] N. Wada, H. Harai, W. Chujo, and F. Kubota. Multi-hop and 40 Gbit/s variable length photonic packet routing based on multi-wavelength label switching and waveband routing and label swapping. In *OFC*, volume 1, pages 216–217, Washington, DC, 2002.

[276] D. Hunter, M. Nizam, M. Chia, I. Andanovic, K. Guild, A. Tzanakaki, M. O'Mahony, J. Bainbridge, M. Stephens, R. Penty, and I. White. WASP-NET: A wavelength switched packet network. *IEEE Communications Magazine*, 37(3):120–129, Mar. 1999.

[277] M. Hickey and L. Kazovsky. The STARNET coherent WDM computer communication network: Experimental transceiver employing a novel modulation format. *IEEE Journal of Lightwave Technology*, 6(5):876–884, May 1994.

[278] E. N. Lallas, N. Skarmoutsos, and D. Syvridis. An optical FSK-based label coding technique for the realization of the all-optical label swapping. *IEEE Photonic Technology Letters*, 14(10):1472–1474, Oct. 2002.

[279] N. Chi, L. Xu, L. Christiansen, K. Yvind, J. Zhang, P. Holm-Nielsen, C. Peucheret, C. Zhang, and P. Jeppesen. Optical label swapping and packet transmission based on ASK/DPSK orthogonal modulation format in IP-over-WDM networks. In *Optical Fiber Communication Conference*, pages 792–794, Mar. 2003.

[280] Y. M. Lin, M. C. Yuang, S. L. Lee, and W. I. Way. Using superimposed ASK label in a 10 Gbit/s multi hop all-optical label swapping system. *IEEE Journal of Lightwave Technology*, 22(2):351–361, Feb. 2004.

[281] N. Deng, Y. Yang, C. K. Chan, W. Hung, and L. K. Chen. Intensity- modulated labelling and all-optical label swapping on angle-modulated optical packets. *IEEE Photonics Technology Letters*, 16(4):1218–1220, Apr. 2004.

[282] C. Chow and H. K. Tsang. Optical packet label using polarization shift keying (PolSK) label and amplitude shift keying (ASK) payload. In *Optical Fiber Communication Conference (OFC)*, page Paper OME73, 2005.

[283] I. T. Monroy, A. M. J Koonen, J. Zhang, N. Chi, P. V. Holm-Nielsen, C. Peucheret, J. J. V. Olmos, and G-D Khoe. Techniques for labeling of optical signals in burst switched networks. In *First International Workshop on Optical Burst Switching*, Dallas, Texas, U.S.A., Oct. 2003.

[284] T. Saito, Y. Yano, and N. Henmi. Optical TDM 20 Gb/s-105 Km transmission employing newly proposed optical PLL timing extraction. *IEEE Photonic Technology Letters*, 6(4):555–557, Apr. 1994.

[285] E. Awad, P. S. Cho, N. Moulton, and J. Goldhar. Subharmonic optical clock recovery from 160 Gb/s using time-dependent loss saturation inside a single electroabsorption modulator. *IEEE Photonics Technology Letters*, 15(12):1764–1766, Dec. 2003.

[286] R. Salem and T. E. Murphy. Broadband optical clock recovery system using two-photon absorption. *IEEE Photonic Technology Letters*, 16(9):2141–2143, Sep. 2004.

[287] F. G. Agis, C. Ware, D. Erasme, R. Ricken, V. Quiring, and W. Sohler. 10-GHz clock recovery using an optoelectronic phase-locked loop based on three-wave mixing in periodically poled lithium niobate. *IEEE Photonics Technology Letters*, 18(13):1460–1462, Jul. 2006.

[288] Z. Hu, K. Nishimura, C. Hsu-Feng L. Rau, M. Usami, J. E. Bowers, and D. J. Blumenthal. 40-Gb/s optical packet clock recovery with simultaneous reshaping using a traveling-wave electroabsorption modulator based ring oscillator. *IEEE Photonics Technology Letters*, 16(12):2640–2642, Dec. 2004.

[289] J. Renaudier, B. Lavigne, M. Jourdran, P. Gallion, F. Lelarge, B. Dagens, A. Accard, O. Legouezigou, and G.-H. Duan. First demonstration of all-optical clock recovery at 40 GHz with standard-compliant jitter characteristics based on a quantum-dots self-pulsating semiconductor laser. In *ECOC*, volume 6, pages 31–32, Sep. 2005.

[290] J. Yu, C. Gee-Kung, and A. Chowdhury. Detecting burst-mode optical label or payload generated by OCSS technique using conventional receivers. *IEEE Photonics Technology Letters*, 17(7):1567–1569, Jul. 2005.

[291] P. J. Duthie and M. J. Wale. Rearrangeably nonblocking 8×8 guided wave optical switch. *Electronics Letters*, 24(10):594–596, May 1988.

[292] C. Zhou and Y. Yang. Wide-sense non-blocking multicast in a class of regular optical WDM networks. *IEEE Transactions on Communications*, 50(1):126–134, Jan. 2002.

[293] H. S. Hamza and J. S. Deogun. Design and analysis of strictly nonblocking WDM optical-switching networks. *Journal of Optical Networking*, 6(4):322–340, Apr. 2007.

[294] A. Stok and E. H. Sargent. Lighting the local area: Optical code-division multiple access and quality of service provisioning. *IEEE Networks*, 14(6):42–46, Nov.-Dec. 2000.

[295] A. Teixeira, P. Andr, R. Nogueira, P. Monteiro, and J. da Rocha. All-optical routing limitations due to semiconductor optical amplifiers dynamics. *Lecture Notes in Computer Science (Lect. notes comput. sci.) ISSN0302-9743, Springer Berlin/Heidelberg*, 3124:766–771, 2004.

[296] B. Ramamurthy and B. Mukherjee. Wavelength conversion in WDM networking. *IEEE Journal of Selected Areas in Communication*, 16(7):1061–1073, Sep. 1998.

[297] X. Ma and G. S. Kuo. Optical switching technology comparison: optical MEMS vs. other technologies. *IEEE Communications Magazine*, 41(11):S16–S23, Nov. 2003.

[298] B. Pesach, G. Bartal, E. Refaeli, A. J. Agranat, J. Krupnik, and D. Sadot. Free-space optical cross-connect switch by use of electroholography. *Applied Optics*, 39(5):746–758, Feb. 2000.

[299] R. P. Schreieck, M. H. Kwakernaak, H. Jackel, and H. Melchior. All-optical switching at multi-100-Gb/s data rates with Mach-Zehnder interferometer switches. *IEEE Journal of Quantum Electronics*, 38(8):1053–1061, Aug. 2002.

[300] J. M. Tang, P. S. Spencer, P. Rees, and K. A. Shore. Enhanced TOAD performance by negative frequency-detuned signal and control picosecond optical pulses. *IEEE Journal of Quantum Electronics*, 36(5):574–582, May 2000.

[301] R. J. Runser, P. Toliver, I. Glesk, and P. R. Prucnal. Experimental demonstration of a 1.5 ps demultiplexing window for high speed optical networks using a forward-pumped Mach-Zehnder TOAD. In *34th Annual Conference on Information Sciences and Systems*, Princeton University, Mar. 2000.

[302] R. Kasahara, M. Yanagisawa, T. Goh, A. Sugita, A. Himeno, M. Yasu, and S. Matsui. New structure of silica-based planar lightwave circuits for low-power thermooptic switch and its application to 8 8 optical matrix switch. *IEEE Journal of Lightwave Technology*, 20(6):993–1000, Jun. 2002.

[303] T. Sakata, H. Togo, M. Makihara, F. Shimokawa, and K. Kaneko. Improvement of switching time in a thermocapillarity optical switch. *IEEE Journal of Lightwave Technology*, 19(7):1023–1027, Jul. 2001.

[304] H. C. Tapalian, J.-P. Laine, and P. A. Lane. Thermooptical switches using coated microsphere resonators. *IEEE Photonics Technology Letters*, 14(8):1118–1120, Aug. 2002.

[305] R. Krahenbuhl, M. M. Howerton, J. Dubinger, and A. S. Greenblatt. Performance and modeling of advanced Ti:$LiNbO_3$ digital optical switches. *IEEE Journal of Lightwave Technology*, 20(1):92–99, Jan. 2002.

[306] C. M. Gallep and E. Conforti. Reduction of semiconductor optical amplifier switching times by preimpulse step-injected current technique. *IEEE Photonics Technology Letters*, 14(7):902–904, Jul. 2002.

[307] A. Fratalocchi, R. Asquini, and G. Assanto. Integrated electro-optic switch in liquid crystals. *Optics express*, 13(1):32–37, Jan. 2005.

[308] J. Diao and P. L. Chu. Analysis of partially shared buffering for WDM optical packet switching. *Journal of Lightwave Technology*, 17(12):2461–2469, Dec. 1999.

[309] K. Vlachos, K. Seklou, and E. Varvarigos. Performance evaluation of an optical packet scheduling switch. In *IEEE Global Telecommunications Conference (GLOBECOM)*, volume 3, pages 1857–1861, Nov.-dec. 2004.

[310] C. J. C. Hasnain, K. Pei cheng K. Jungho, and C. Shun-lien. Variable optical buffer using slow light in semiconductor nanostructures. *Proceedings of the IEEE*, 91(11):1884–1897, Nov. 2003.

[311] R. S. Tucker, K. P. Cheng, and C. J. C. Hasnain. Slow-light optical buffers: capabilities and fundamental limitations. *IEEE Journal of Lightwave Technology*, 23(12):4046–4066, Dec. 2005.

[312] S. Rangarajan, Z. Hu, L. Rau, and D. J. Blumenthal. All-optical contention resolution with wavelength conversion for asynchronous variable-length 40 Gb/s optical packets. *IEEE Photonics Technology Letters*, 16(2):689–691, Feb. 2004.

[313] C. M. Gauger. Optimized combination of converter pools and fdl buffers for contention resolution in optical burst switching. *Journal of Photonic Network Communications and Springer Netherlands*, 8(2):139–148, Sep. 2004.

[314] V. M. Vokkarane, J. P. Jue, and S. Sitaraman. Burst segmentation: an approach for reducing packet loss in optical burst-switched networks. In *IEEE International Conference on Communications (ICC)*, volume 5, pages 2673–2677, New York, USA, Apr. 2002.

[315] C. Su, L.-K. Chen, and K.-W. Cheung. Theory of burst-mode receiver and its applications in optical multi-access networks. *IEEE Journal of Lightwave Technology*, 15(4):590–606, Apr. 1997.

[316] G. T. Kanellos, D. Petrantonakis, D. Tsiokos, P. Bakopoulos, P. Zakynthinos, N. Pleros, D. Apostolopoulos, G. Maxwell, A. Poustie, and H. Avramopoulos. All-optical 3R burst-mode reception at 40 Gb/s using four integrated MZI switches. *IEEE Journal of Lightwave Technology*, 25(1):184–192, Jan. 2007.

[317] O. Leclerc, B. Lavigne, E. Balmefrezol, P. Brindel, L. Pierre, D. Rouvillain, and F. Seguineau. Optical regeneration at 40 Gb/s and beyond. *IEEE Journal of Lightwave Technology*, 21(11):2779–2790, Nov. 2003.

[318] K. Chan, F. Tong, C. K. Chan, L. K. Chen, and W. Hung. An all-optical packet header recognition scheme for self-routing packet networks. In *Optical Fiber Communication Conference*, pages 284–285, Mar. 2002.

[319] K.-H. Park, T. Mizumoto, A. Matsuura, and Y. Naito. All-optical address extraction for optical routing. *IEEE Journal of Lightwave Technology*, 16(7):1129–1136, Jul. 1998.

[320] C. Bintjas, K. Yiannopoulos, N. Pleros, G. Theophilopoulos, M. Kalyvas, H. Avramopoulos, and G. Guekos. Clock recovery circuit for optical packets. *IEEE Photonics Technology Letters*, 14(9):1363–1365, Sep. 2002.

[321] T. J. Xia, Y.-H. Kao, Y. Liang, J. W. Lou, K. H. Ahn, O. Boyraz, G. A. Nowak, A. A. Said, and M. N. Islam. Novel self-synchronization scheme for high-speed packet TDM networks. *IEEE Photonics Technology Letters*, 11(2):269–271, Feb. 1999.

[322] Z. Yongpeng and Y. Peida. Simple self-synchronization scheme for OTDM packet networks. In *The 15th Annual Meeting of the IEEE on Lasers and Electro-Optics*, volume 2, pages 373–374, 2002.

[323] D. Petrantonakis, D. Apostolopoulos, O. Zouraraki, D. Tsiokos, P. Bakopoulos, and H. Avramopoulos. Packet-level synchronization scheme for optical packet switched network nodes. *Optics Express*, 14(26):12665–12669, Dec. 2006.

[324] S. Diez, R. Ludwig, and H. G. Weber. All-optical switch for TDM and WDM/TDM systems demonstrated in a 640 Gbit/s demultiplexing experiment. *Electronic letters*, 34(8):803805, Apr. 1998.

[325] P. K. Hwan and T. Mizumoto. A packet header recognition assigning the position of a signal in the time axis and its application to all-optical self-routing. *IEEE Journal of Lightwave Technology*, 19(8):1076–1084, Aug. 2001.

[326] D. Gurkan, M. C. Hauer, A. B. Sahin, Z. Pan, S. Lee, A. E. Willner, K. R. Parameswaran, and M. M. Fejer. Demonstration of multi-wavelength all-optical header recognition using a ppln and optical correlators. In *European Conference on Optical Communication*, volume 3, pages 312–313, Oct. 2001.

[327] N. Wada and K.-I. Kitayama. A 10 Gb/s optical code division multiplexing using 8-chip optical bipolar code and coherent detection. *IEEE Journal of Lightwave Technology*, 17(10):1758–1765, Oct. 1999.

[328] S. A. Hamilton and B. S. Robinson. > 100 Gbit/s time-domain processing techniques optical packet switching. In *Optical Fiber Communication Conference*, volume 1, pages 23–27, Feb. 2004.

[329] H. Teimoori, J. D. Topomondzo, C. Ware, and D. Erasme. All-optical packet-switching decoder design and demonstration at 10 Gbit/s. *IEEE Photonics Technology Letters*, 19(10):738–740, May. 2007.

[330] D. J. Blumenthal, B. E. Olsson, G. Rossi, T. E. Dimmick, L. Rau, M. Masanovic, O. Lavrova, R. Doshi, O. Jerphagnon, J. E. Bowers, V. Kaman, L. A. Coldren, and J. Barton. All-optical label swapping networks and technologies. *IEEE Journal of Lightwave Technology*, 18(12):2058–2075, Dec. 2000.

[331] L. Rau, G. Rossi, O. Jerphagnon, R. Doshi, D. S. Humphries, D.J. Blumenthal, V. Kaman, and J.E. Bowers. Wavelength routing of 40 Gbit/s packets with 2.5 Gbit/s header erasure/rewriting using all-fiber wavelength converter. *Electronics Letters*, 36(4):345–347, Feb. 2000.

[332] J. Zhang, N. Chi, P.V. Holm-Nielsen, C. Peucheret, and P. Jeppesen. Performance of manchester-coded payload in an optical FSK labeling scheme. *IEEE Photonics Technology Letters*, 15(8):1174–1176, Aug. 2003.

[333] Y. M. Lin, W. I. Way, and G. K. Chang. A novel optical label swapping technique using erasable optical single-sideband subcarrier label. *IEEE Photonics Technology Letters*, 12(8):1088–1090, Aug. 2000.

[334] H. J. Lee, S. J. B. Yoo, V. K. Tsui, and S. K. H. Fong. A simple all-optical label detection and swapping technique incorporating a fiber bragg grating filter. *IEEE Photonics Technology Letters*, 13(6):635–637, Jun. 2001.

[335] M. Y. Jeon, Z. Pan, J. Cao, and S. J. B. Yoo. All-optical sub-carrier label-swapping with 2R regeneration. In *OFC*, pages 277–279, Paper TuQ4, Mar. 2003.

[336] Z. Zhu, Z. Pan, J. Cao, and S.J.B. Yoo. Integrated electro-absorption modulation DFB laser based all-optical subcarrier label swapping. In *OFC*, page WF5, Los Angeles, USA, Mar. 2004.

[337] S. Fischer, M. Duelk, M. Puleo, R. Girardi, E. Gamper, W. Vogt, W. Hunziker, E. Gini, and H. Melchior. 40-Gb/s OTDM to 4×10 Gb/s WDM conversion in monolithic InP Mach-Zehnder interferometer module. *IEEE Photonic Technology Letters*, 11(10):1262–1264, Oct. 1999.

[338] A. Buxens, H. N. Poulsen, A. T. Clausen, and P. Jeppesen. All-optical OTDM-to-WDM signal-format translation and OTDM add-drop functionality using bidirectional four wave mixing in semiconductor optical amplifier. *Electronics Letters*, 36(2):156–158, Jan. 2000.

[339] K. L. Lee, A. W. L. Chan, C. Shu, A. Nirmalathas, and C. Lim. Optical label processing by multiwavelength sampling using a switching-wavelength pulsed carrier in an interferometric wavelength converter configuration. In *IEEE LEOS*, volume 2, pages 849–850, Nov. 2004.

[340] Y. Han, O. Boyraz, A. Nuruzzaman, and B. Jalali. Optical header recognition using time stretch preprocessing. *Optics Communications*, 237(4-6):333–340, Jul. 2004.

[341] N. Calabretta, G. Contestabile, and E. Ciaramella. Exploiting time-to-wavelength conversion for all-optical label processing. *IEEE Photonic Technology Letters*, 18(1):436–438, Jan. 2006.

[342] G. Contestabile, N. Calabretta, M. Presi, and E. Ciaramella. Single and multicast wavelength conversion at 40 Gb/s by means of fast nonlinear polarization switching in an SOA. *IEEE Photonic Technology Letters*, 17(12):2652–2655, Dec. 2005.

[343] S. Jansen, G. Khoe, H. de Waardt, M. Heid, S. Spalter, E. Meissner, C. Weiske, and A. Schoepflin. Optimizing the wavelength configuration for FWM-based demultiplexing in a SOA. In *Optical Fiber Communications Conference (OFC)*, volume 2, pages 539–541, Mar. 2003.

[344] O. Leclerc, P. Brindel, D. Rouvillain, E. Pincemin, B. Dany, E. Desurvire, C. Duchet, E.Boucherez, and S. Bouchoule. 40 Gbit/s polarization-insensitive and wavelength-independent InP Mach-Zehnder modulator for all-optical regeneration. *Electronics Letters*, 35(9):730–731, Apr. 1999.

[345] I. Tomkos, I. Zacharopoulos, E. Roditi, D. Syvridis, and A. Uskov. On the polarisation sensitivity and performance optimisation of a dual pump four wave mixing based wavelength converter. *Journal of Optical and Quantum Electronics, Springer Netherlands*, 32(1):97–113, Jan. 2000.

[346] M. Zhao, G. Morthier, and R. Baets. Analysis and optimization of intensity noise reduction in spectrum-sliced WDM systems using a saturated semiconductor optical amplifier. *Photonic Technology Letters*, 14(3):390–392, Feb. 2002.

[347] S. J. Kim, J. H. Han, J. S. Lee, and C. S. Park. Suppression of intensity noise in 10 Gbit/s spectrum-sliced incoherent light channel using gain-saturated semiconductor optical amplifiers. *Electronics Letters*, 35(12):1000–1001, Jun. 1999.

[348] R.Takahashi and H. Suzuki. 1-Tb/s 16-b all-optical serial-to-parallel conversion using a surface-reflection optical switch. *IEEE Photonic Technology Letters*, 15(2):287–289, Feb. 2003.

[349] R. K. Tan, C. M. Verber, and A. J. S. Thorpe. Self-timed integrated-optical serial-to-parallel converter for 100 Gbit/s time demultiplexing. *IEEE Photonic Technology Letters*, 6(10):1228–1231, Oct. 1994.

[350] M. L. Dennis, W. Kaechele, W. K. Burns, T. F. Carruthers, and L. N. Duling. Photonic serial-parallel conversion of high-speed otdm data. *IEEE Photonics Technology Letters*, 12(11):1561–1563, Nov. 2000.

[351] R. V. Caenegem, D. Colle, M. Pickavet, and P. Demeester. Benefits of label stripping compared to label swapping from the point of node dimensioning.

Journal of Photonic Network Communications, Springer Netherlands, 12(3):227–244, Dec. 2006.

[352] N. Yan, I. T. Monroy, and T. Koonen. All-optical label swapping node architectures and contention resolution. In *9th Conference on Optical Network Design and Modelling (ONDM)*, pages 115–123, Feb. 2005.

[353] W. Hung, C.-K. Chan, L.-K. Chen, and F. Tong. Pbit-serial optical packet label-swapping scheme using DPSK encoded labels. *IEEE Photonics Technology Letters*, 15(11):1630–1632, Nov. 2003.

[354] S. Mahnkopf, M. Kamp, M. Arlt, R. Mrz, F. Lelarge, G.-H. Duan, and A. Forchel. Widely tunable complex-coupled distributed feedback laser with photonic crystal mirrors and integrated optical amplifier. *EEE Photonic Technology Letters*, 16(3):729–731, Mar. 2004.

[355] Y. Fukashir, K. Shrikhande, M. Avenarius, M. S. Rogge, I. M. White, D. Wonglumsom, and L. G. Kazovsky. Fast and fine wavelength tuning of a GCSR laser using a digitally controlled driver. In *Optical Fiber Communications (OFC 2000)*, volume 2, pages 338–340, 2000.

[356] H. Ishii, H. Tanobe, F. Kano, Y. Tohmori, Y. Kondo, and Y. Yoshikuni. Broad-range wavelength converage (62.4 nm) with superstructure- grating DBR laser. *Electronic Letters*, 32(5):454–455, Mar. 1996.

[357] G. Alibert, F. Delorme, P. Boulet, J. Landreau, and H. Nakajima. Subnanosecond tunable laser using a single electroabsorption tuning super structure grating. *IEEE Photonic Technology Letters*, 9(7):895–897, Jul. 1997.

[358] M. Mller, M. Kamp, A. Forchel, and J.-L. Gentner. Wide-range-tunable laterally coupled distributed feedback lasers based on ingaaspinp. *Applied Physics Letters*, 79(17):2684–2686, Oct. 2001.

[359] L. A. Coldren, G. A. Fish, Y. Akulova, J. S. Barton, L. Johansson, and C. W. Coldren. Tunable semiconductor lasers: A tutorial. *IEEE Journal of Lightwave Technology*, 22(1):193–202, Jan. 2004.

[360] Y. Liu, E. Tangdiongga, Z. Li, H. de Waardt, A. M. J. Koonen, G. D. Khoe, X. Shu, I. Bennion, and H. J. S. Dorren. Error-free 320-Gb/s all-optical wavelength conversion using a single semiconductor optical amplifier. *IEEE Journal of Lightwave Technology*, 25(1):103–108, Jan. 2007.

[361] T. Durhuus, B. Mikkelsen, C. Joergensen, S. L. Danielsen, and K. E. Stubkjaer. All-optical wavelength conversion by semiconductor optical amplifiers. *IEEE Journal of Lightwave Technology*, 14(6):942–954, Jun. 1996.

[362] C. Joergensen, S. L. Danielsen, K. E. Stubkjaer, M. Schilling, K. Daub, P. Doussiere, F. Pommerau, P. B. Hansen, H. N. Poulsen, A. Kloch, M. Vaa,

B. Mikkelsen, E. Lach, G. Laube, W. Idler, and K. Wunstel. All-optical wavelength conversion at bit rates above 10 Gb/s using semiconductor optical amplifiers. *IEEE Journal of Selected Topics in Quantum Electronics*, 3(5):1168–1180, Oct. 1997.

[363] A. D. Ellis, A. E. Kelly, D. Nesset, D. Pitcher, D. G. Moodie, and R. Kashyap. Error free 100 Gb/s wavelength conversion using grating assisted cross-gain modulation in 2 mm long semiconductor amplifier. *Electronic Letters*, 34(20):1958–1959, Oct. 1998.

[364] S. Nakamura, Y. Ueno, and K. Tajima. 168-Gb/s all-optical wavelength conversion with a symmetric Mach-Zehnder-type switch. *IEEE Photonic Technology Letters*, 13(10):1091–1093, Oct. 2001.

[365] R. J. Manning, X. Yang, R. P. Webb, R. Giller, F. C. Garcia Gunning, and A. D. Ellis. The "turbo-switch"a novel technique to increase the high-speed response of SOAs for wavelength conversion. In *OFC/NFOEC*, page Paper OWS8, Anaheim, USA, Mar. 2006.

[366] P. Bernasconi, L. Zhang, W. Yang, N. Sauer, L. L. Buhl, J. H. Sinsky, I. Kang, S. Chandrasekhar, and D. T. Neilson. Monolithically integrated 40-Gb/s switchable wavelength converter. *IEEE Journal of Lightwave Technology*, 24(1):71–75, Jan. 2006.

[367] Y. Oie, T. Suda, M. Murata, D. Kolson, and H. Miyahara. Survey of switching techniques in high speed networks and their performance. In *IEEE INFOCOM-90*, pages 1242–1251, jun. 1990.

[368] M. T. Hill, H. de Waardt, G. D. Khoe, and H. J. S. Dorren. All-optical flip-flop based on coupled laser diodes. *IEEE Journal of Quantum Electronics*, 37(3):405–413, Mar. 2001.

[369] E. Tangdiongga, X. Yang, Z. Li, Y. Liu, D. Lenstra, G.-D. Khoe, and H.J.S. Dorren. Optical flip-flop based on two-coupled mode-locked ring lasers. *IEEE Photonics Technology Letters*, 17(1):208–210, Jan. 2005.

[370] H. Kawaguchi. ll-optical signal processing using polarization bistable vcsels. In *7th International Conference Transparent Optical Networks*, volume 2, pages 87–90, Jul. 2005.

[371] M. Takenaka, K. Takeda, Y. Kanema, Y. Nakano, M. Raburn, and T. Miyahara. All-optical switching of 40 Gb/s packets by mmi-bld optical label memory. *Optics Express*, 14(22):10785–10789, Oct. 2006.

[372] M. Raburn, M. Takenaka, K. Takeda, X. Song, J. S. Barton, and Y. Nakano. Integrable multimode interference distributed bragg reflector laser all-optical flip-flops. *IEEE Photonics Technology Letters*, 18(13):1421–1423, Jul. 2006.

[373] P. D. Kumavor, E. Donkor, and B. C. Wang. All-optical lyot-filter-assisted flip-flop operation using a semiconductor optical amplifier. *IEEE Journal of Selected Topics in Quantum Electronics*, 12(4):697–701, Jul.-Aug. 2006.

[374] W. D'Oosterlinck, J. Buron, F. Ohman, G. Morthier, and R. Baets. All-optical flip-flop based on an SOA/DFB-laser diode optical feedback scheme. *IEEE Photonic Technology Letters*, 19(7):489–491, Apr. 2007.

[375] Z. Hu, R. Doshi, H.-F. Chou, H. N. Poulsen, D. Wolfson, J. E. Bowers, and D. J. Blumenthal. Optical label swapping using payload envelope detection circuits. *IEEE Photonic Technology Letters*, 17(7):1537–1539, Jul. 2005.

[376] B. R. Koch, Z. Hu, J. E. Bowers, and D. J. Blumenthal. All-optical payload envelope detection for variable length 40-Gb/s optically labeled packets. *IEEE Photonic Technology Letters*, 18(17):1846–1848, Sep. 2006.

[377] T. Hatta, T. Miyahara, Y. Miyazaki, K. Takagi, K. Matsumoto, T. Aoyagi, K. Motoshima, K. Mishina, A. Maruta, and K. Kitayama. Polarization-insensitive monolithic 40-Gbps SOA-MZI wavelength converter with narrow active waveguides. *IEEE Journal of Selected Topics in Quantum Electronics*, 13(1):32–39, Jan.-feb. 2007.

[378] B. Y. Yu, R. Runser, P. Toliver, K.-L. Deng, D. Zhou, T. Chang, S. W. Seo, K. I. Kang, I. Glesk, and P. R. Prucnal. Network demonstration of 100 Gb/s optical packet switching with self-routing. *Electronics Letters*, 33(16):1401–1402, Jul. 1997.

[379] K. Yiannopoulos, L. Stampoulidis, T. Houbavlis, and H. Avramopoulos. Generation of 40-ghz control signals from flag pulses for switching all optical gates for use with optical packets. *Optics letters*, 29(3):241–243, Feb. 2004.

[380] T. Nakahara, R. Takahashi, H. Takenouchi, K. Takahata, and H. Suzuki. Time-domain 16-bit label swapping and self-routing of 40-Gb/s burst optical packets. *IEEE Photonics Technology Letters*, 16(9):2153–2155, Sep. 2004.

[381] E. Kehayas, D. Tsiokos, P. Bakopoulos, D. Apostolopoulos, D. Petrantonakis, L. Stampoulidis, A. Poustie, R. McDougall, G. Maxwell, Y. Liu, S. Zhang, H. J. S. Dorren, J. Seoane, P. V. Holm-Nielsen, P. Jeppesen, and H. Avramopoulos. 40-Gb/s all-optical processing systems using hybrid photonic integration technology. *IEEE Journal of Lightwave Technology*, 24(12):4903–4911, Dec. 2006.

List of Publications

1. H. Teimoori, J. D. Topomondzo, C. Ware, H. Soto, and D. Erasme. "All-optical half-adder using a single UNI-gate", Journal of Optical Communications, 27(6):301-304, Dec. 2006.

2. H. Teimoori, J. D. Topomondzo, C. Ware, and D. Erasme, "Optical packet header processing using time-to-wavelength mapping in semiconductor optical amplifiers", IEEE Journal of Lightwave Technology, Aug. 2007.

3. H. Teimoori, J. D. Topomondzo, C. Ware, R. Gabet and D. Erasme, "All-Optical Packet-Switching Decoder Design and Demonstration at 10 Gbit/s". IEEE Photonics Technology Letters, 19(10):738-740, May 2007.

4. H. Teimoori, J. D. Topomondzo, C. Ware, and D. Erasme, "All-Optical 3×8 SOA-based Decoder Design and Demonstration at 10 Gbit/s for Packet-Switching Applications", Broadband Europe'06, Geneva, Switzerland, Dec. 2006.

5. H. Teimoori, C. Ware, and D. Erasme, "Application du mélange à quatre ondes à la conversion série / parallèle", Journées Nationales d'Optique Guidée JNOG'05, Chambery, France, Nov. 2005.

6. H. Teimoori, C. Ware, J. D. Topomondzo and D. Erasme, "Traitement du label de paquets optiques pour les réseaux optiques de communications", Journées Nationales d'Optique Guidée JNOG'07, Grenoble, France, Jul. 2007.

7. J. D. Topomondzo, H. Teimoori, D. Erasme and H. Soto, "Novel scheme for all-optical XOR and NOTXOR implementation based on an ultrafast non linear interferometer". 5th International Conference on Photonics Devices and Systems, Prague, Jun. 2005.